PPAR-γ Regulatory Networks in Bone Metabolism And Mineralization

PPAR-γ regulerende netwerken in bot metabolisme en mineralisatie

The research described in this thesis was performed at the Department of Internal Medicine of Erasmus Medical Center, Rotterdam, The Netherlands, and supported by *NucSys*, a Marie Curie Research Training Program funded by the European Union (contract number MRTN-CT-019496).

ISBN: 978-94-6299-104-0

Cover: Photograph of Cathedral Gorge, Kimberley WA, Australia

The printing of this thesis was financially supported by Erasmus Medical Center, Rotterdam.

Printed by Ridderprint BV, 2984 AX Ridderkerk, The Netherlands

PPAR-γ Regulatory Networks in Bone Metabolism And Mineralization

Thesis

to obtain the degree of Doctor from the Erasmus University Rotterdam by command of the rector magnificus

Prof. dr. H.A.P. Pols

and in accordance with the decision of the Doctorate Board

The public defence shall be held on

Tuesday 16 June 2015 at 11:30 hours

by

Claudia Bruedigam

born in Schwerin, Germany

Promotor:	Prof. dr. J.P.T.M. van Leeuwen
Other members:	Prof. dr. G.J.V.M. van Osch
	Prof. dr. D.F.E. Huylebroeck
	Prof. dr. S. Kersten
Copromotor:	Dr. H.J. van de Peppel

Für meine Eltern / For my parents

Contents

1 General introduction

1.1 Bone remodeling

Bone is a highly dynamic tissue that is permanently remodeled as an intrinsic mechanism to regenerate bone during life, to accomplish longitudinal growth, and to generate new bone during fracture repair. As bone formation must match closely the amount of bone that is resorbed at each site, bone remodeling is controlled by the coupled actions of osteoclasts and osteoblasts [1–3]. Osteoblasts control the formation and activity of osteoclasts that are responsible for the initiation and execution of resorption at remodeling sites. The bone resorbed by osteoclasts is replaced through the differentiation and activity of osteoblasts. This coupling of the two processes is essential for bone balance. Due to age, sex hormone status, cancer and a variety of diseases associated with an activation of the immune system, the balance between bone resorption and formation can be shifted leading to local or systemic bone loss that ultimately results in osteoporosis [4]. Osteoporosis is a prevalent skeletal disorder in the elderly that is characterized by impaired bone strength and increased fracture risk. It is associated with reduced life quality and increased mortality [5, 6]. On the other hand, excessive bone formation can give rise to sclerosing bone disorders that include many rare and often hereditary osteochondrodysplasias (e.g. osteopetrosis, Van Buchem disease and sclerosteosis), but can also be caused by a variety of dietary, metabolic, endocrine, hematologic, infectious or neoplastic disorders [7–9].

1.2 Extracellular matrix mineralization

Bone quality is determined by its material composition. Extracellular matrix proteins provide bone its flexibility, whereas the mineral content is responsible for its mechanical strength [10, 11]. Variations in the amount of mineral and collagen affect the properties and quality of bone. Bone with a low mineral content may not provide sufficient supportive function, whereas a very high mineral content may result in micro cracks and eventually a complete fracture due to impaired flexibility of the bone. Osteoblasts as bone forming cells are primarily responsible for the mineralization process. They first produce a non-mineralized extracellular matrix that predominantly consists of collagen type 1. Mineralization of this matrix then occurs by the deposition of hydroxyapatite that eventually forms hydroxyapatite crystals. The osteogenic differentiation marker alkaline phosphatase (ALPL) hydrolyses organic phosphate substrate to release free inorganic phosphate [12]. ALPL is highly expressed in matrix vesicles together with several phosphate and calcium transporters that increase local phosphate and calcium concentrations and thereby initiate the mineralization process [13–15]. For mineral deposition to proceed, a tight balance is required between the levels of free inorganic phosphate and pyrophosphate. Inorganic pyrophosphate antagonizes the ability of free inorganic phosphate to crystallize with calcium to form hydroxyapatite and thereby suppresses hydroxyapatite crystal propagation. Three molecules have been identified as central coordinate regulators of extracellular free pyrophosphate and phosphate levels: tissue-nonspecific alkaline phosphatase (TNAP) that hydrolyzes pyrophosphate, nucleotide pyrophosphatase phosphodiesterase 1 (NPP1) that generates pyrophosphate from nucleoside triphosphates, and the multiple-pass transmembrane protein ANK that mediates intracellular to extracellular channeling of pyrophosphate [16]. Therefore, the currently held doctrine posits that ANK and NPP1 function to suppress mineralization by increasing the extracellular concentration of pyrophosphate while TNAP promotes the mineralization process by

reducing pyrophosphate levels and increasing the concentration of the mineralization stimulator inorganic phosphate [16]. Mineralization of the extracellular matrix is not unique for bone tissue as demonstrated by ectopic calcification in pathological conditions [17]. Vascular mineralization (pathological mineralization) is a prominent feature of advanced atherosclerosis [18]. Although atherosclerosis and vascular mineralization are currently considered to form separate genetic entities, mineralization contributes to the overall morbidity of atherosclerosis by causing an increased risk for myocardial infarction [19–22]. The latter is caused by, at least in part, a decreased elasticity of the vessels [23, 24]. Bone-associated proteins such as osteonectin, osteocalcin, and matrix Gla protein have been detected in mineralized vascular tissues. Vascular mineralization has been considered to be an organized and highly regulated process that is similar to mineralization in bone tissue. Vascular smooth muscle cells (VSMCs) are currently considered as being responsible for the formation of vascular mineralization *in vivo*. In more detail, mechanical and inflammatory redox signals from the aortic vasculature have emerged as secretagogues for BMP that leads to activation of endothelial NADPH oxidases and subsequent generation of reactive oxygen species (ROS) [25–27]. These paracrine signals augment aortic myofibroblast Msx2-Wnt signaling and matrix turnover and promote osteoblast-like differentiation of VSMCs [28–33]. Furthermore, oxidation of vascular LDL cholesterol generates oxysterols that trigger Runx2 activity via hedgehog pathways [32]. Interestingly, apoptosis of VSMCs appears to be an additional key factor in vascular mineralization [34–36]. After an extracellular matrix has been formed, VSMC apoptosis is sufficient to accelerate atherosclerosis, to promote plaque mineralization and medial degeneration, to prevent expansive remodeling and to promote stenosis in atherosclerosis [37–39].

1.3 Mesenchymal stem cell lineage skewing as burden for osteoblast differentiation

Bone strength is negatively correlated with bone marrow adipogenesis in aging and patients with osteoporosis. Furthermore, the recently observed reduced bone mass and increased risk of peripheral fractures in thiazolidinedione (TZD)-treated patients are suggested to result from bone marrow adipogenesis that is caused by a switch of mesenchymal stem cells (MSC) into the adipogenic lineage [40, 41]. Pluripotent MSCs in the bone marrow surround trabecular elements of the skeleton. They can enter amongst others the osteoblastic and adipocytic lineages upon regulation through specific endocrine, paracrine or autocrine signals. It is currently hypothesized that there is a competitive balance between osteoblasts and adipocytes that underlies a cross-talk between complex signaling mechanisms inducing one's cell fate and ultimately suppressing the alternative lineage (recently reviewed in [42]). At least partially, MSC lineage commitment is regulated at the transcriptional level [43]. Herein, runx2 and osterix are considered as important osteoblast-specific transcription factors whereas activation of peroxisome proliferator-activated receptor γ (PPAR-γ) is suggested to cause the entry of MSCs into the fat lineage that leads indirectly to suppression of osteogenesis [44–50].

1.4 Signal transduction networks controlling osteoblast differentiation

The differentiation from mesenchymal stem cells towards the osteogenic lineage is controlled by several endocrine and paracrine factors (e.g. Hedgehogs, bone morphogenic proteins, TGF-β, PTH, WNTs, and interleukins) that regulate the expression of cell lineage-specific sets of transcription factors [51–60].

1.4.1 Peroxisome proliferator - activated receptor γ (PPAR-γ)

PPAR-γ belongs to the nuclear receptor superfamily of transcription factors [61]. Its main function is to regulate fatty acid uptake and storage (reviewed in [62–64]). Activation of PPAR-γ occurs upon binding to a variety of ligands which can be nutritionally derived endogenous polyunsaturated fatty acids and eicosanoids [65–67] or synthetic compounds including thiazolidinediones (reviewed in [68]). The latter are pharmaceutical compounds with insulin-sensitizing function. The single PPARG gene undergoes alternative splicing and promoter usage giving rise to two proteins: PPAR-γ1 and PPAR-γ2. The latter contains an additional N-terminal exon that results in a higher ligand-independent transactivation capacity when compared to PPAR-γ1 [69]. Expression of PPAR-γ2 is mainly limited to adipocytes whereas PPAR-γ1 is found ubiquitously expressed [70, 71].

Rosiglitazone (trade name Avandia, GlaxoSmithKline) is a synthetic PPAR-γ agonist belonging to the thiazolidinedione class of compounds. It improves insulin sensitivity and lowers blood glucose and lipid levels. Despite these beneficial metabolic actions, serious cardiovascular side effects have been reported for rosiglitazone in recent epidemiological studies [40, 72–75]. In more detail, rosiglitazone treatment has been linked to an increased risk for myocardial infarction [72, 73]. Rosiglitazone and other PPAR-γ agonists have been shown earlier to induce apoptosis of human and rodent VSMCs via PPAR-γ - dependent and - independent mechanisms [76–80]. Also unwanted skeletal side-effects have been documented. A vast number of recent studies have revealed an increased risk of peripheral fractures in TZD-treated patients [40, 81–85]. Currently proposed mechanisms include a direct suppression of bone formation and a stimulation of bone resorption resulting in reduced bone mass and quality. Putative underlying mechanisms include rosiglitazone - mediated suppression of bone formation and stimulation of bone resorption caused by: a) a stimulation of osteoclast differentiation from hematopoietic precursor cells [86]; b) a preferential

differentiation of mesenchymal stem cells into adipocytes at the expense of osteoblasts in the bone marrow [41, 45, 87, 88]; or c) the modulation of hormone levels and/or sensitivity that are important for bone metabolism, e.g. leptin [89], insulin [90, 91], insulin-like growth factor I [92], or estrogen [93]. Following the reported side-effects of rosiglitazone, its use has decreased dramatically since it was first released in 1999. Adverse effects alleged to be caused by rosiglitazone were the subject of over 13,000 lawsuits against GSK, and as of July 2010, GSK has agreed to settlements of more than 11,500 suits [94]. In Europe, the European Medicines Agency (EMA) recommended in September 2012 that rosiglitazone be suspended from European market because the benefits of rosiglitazone no longer outweighed the risks [95]. Rosiglitazone was withdrawn from the market in the UK and India in 2010, and in New Zealand and South Africa in 2011 [96].

1.4.2 Vitamin D receptor

By being one of the major factors in calcium homeostasis vitamin D is essential for the development and maintenance of healthy bones. 1α,25-dihydroxyvitamin D3 (1,25D3), the biologically most active vitamin D receptor (VDR) agonist, is produced by subsequent vitamin D 25-hydroxylase (CYP2R1) and 25-hydroxyvitamin D-1α-hydroxylase (CYP27B1) hydroxylation steps in the liver and kidney, respectively [97]. The main function of 1,25D3 is to maintain calcium homeostasis. It is of crucial importance for proper physiology that serum calcium is maintained within a narrow range. Bone formation is indirectly influenced by 1,25D3 since it controls calcium uptake in the intestine and reabsorbs calcium in the kidneys. Also direct effects of 1,25D3 on osteoblasts are established: *in vitro* 1,25D3 stimulates mineralization of osteoblast cultures [98, 99] and 1,25D3-mediated gene expression modifications of various osteoblast differentiation and mineralization-related genes such as alkaline phosphatase (ALPL), osteocalcin (BGLAP) and osteopontin (SPP1) has been re-

ported [98, 100, 101]. 1,25D3 also enhances matrix vesicle maturation [102]. To prevent excessive mineralization and consequential pathologies such as bone marble disease, 1,25D3 is associated to several control systems. For example, 1,25D3 stimulates its own degradation by up-regulating the expression of 1,25-hydroxyvitamin-D3-24-hydroxylase (CYP24A1), an enzyme catalyzing the initial step for 1,25D3 degradation [98, 103]. Both VDR and PPAR-γ are nuclear receptors and both form a heterodimer with retinoid X receptors. Moreover, recent studies have revealed evidence for a molecular cross-talk between VDR and PPAR-γ involving a stimulatory effect of 1,25D3 on PPAR expression that is dependent on VDR [104, 105].

1.5 Aim of this thesis

The PPAR-γ activators of the thiazolidinedione (TZD) class have recently been identified as risk factors for osteoporosis and cardiovascular disease [40, 72–75]. In order to better understand the underlying mechanisms that may facilitate the development of strategies to prevent the actions of these risk factors in the future, this thesis has aimed to characterize the cell intrinsic functional roles and consequences of perturbed PPAR-γ signaling in bone metabolism and pathological mineralization. Human mesenchymal stem cells, various human osteoblast cell lines, and human vascular smooth muscle cells served as model systems to study cell-intrinsic mechanisms controlled by PPAR-γ signaling. The latter was perturbed in these models by using both genetic and pharmacological approaches. The fact that the cell models used follow a well-characterized differentiation program with robust molecular markers being available allowed to study the influence of perturbed PPAR-γ signaling on the precise dynamics of the differentiation processes. The data obtained from biochemical, microscopic, and gene expression studies were always complemented with the information regarding the differentiation process. The experimental work of this thesis is divided into the

following chapters: In Chapter 2, the expression and regulation mechanisms of PPAR-γ were investigated in all models described above. This work was then followed by the functional characterization of the consequences of perturbed PPAR-γ signaling in mesenchymal stem cells differentiating into either osteoblasts or adipocytes in Chapter 3. A potential cross-talk between PPAR-γ and VDR signaling in differentiating osteoblasts was investigated in Chapter 4. And finally, the last two results sections in Chapters 5 and 6 studied the impact of PPAR-γ signaling on pathological mineralization using combined biochemical and bioinformatics approaches. Comprehensive integrated analyses of the obtained data and additional publicly available datasets have revealed new concepts underlying the detrimental effects of thiazolidinedione - activated PPAR-γ signaling on bone and vascular health that provide promising strategies to prevent thiazolidinedione-induced bone loss and cardiovascular complications in the future.

2 Evidence for multiple Peroxisome proliferator-activated receptor γ transcripts in bone

2.1 Abstract

The expression, regulation and functional significance of multiple Peroxisome proliferator-activated receptor γ transcript variants in bone were studied. PPARG transcripts giving rise to PPAR-γ1 protein were expressed in human osteoblasts, whereas PPARG-2 transcript and protein remained virtually absent. PPARG expression underwent homologous regulation, was upregulated during differentiation and directly induced by the osteogenic hormone dexamethasone, suggesting a role of PPAR-γ1 for osteogenesis. Differences between the stabilities of PPARG-1, -3 and -4 were observed. We hypothesize that cell-specific expression patterns of multiple PPARG transcript variants encoding for the same protein but differing in mRNA stabilities enable a fine-tuning of PPARG action, which eventually supports a well-

Claudia Bruedigam, Marijke Koedam, Marco Eijken, Johannes P.T.M. van Leeuwen: *Evidence for multiple Peroxisome proliferator-activated receptor γ transcripts in bone: fine-tuning by hormonal regulation and mRNA stability*; 2008; 582(11):1618-24; FEBS Letters

adjusted signal transduction between the cell and its environment.

2.2 Introduction

Peroxisome proliferator-activated receptor γ (PPARG) is a nuclear transcription factor that plays roles in the control of proliferation, differentiation and survival of various cell types (reviewed in [106]). The single *PPARG* gene undergoes alternative splicing and promoter usage giving rise to two proteins: PPARγ-1 and PPAR-γ2 (Figure 2.1; [107]. PPAR-γ2 contains an additional N-terminal exon that results in a higher trans-activation capacity compared to PPAR-γ1 [69]. Besides this functional difference at protein level, there is an additional complexity at its transcript level. Interestingly, PPAR-γ1 protein can be translated from the three PPARG transcripts PPARG-1, -3 and -4 that only differ in their 5'-untranslated region [108]. The existence of multiple transcript variants encoding for the same protein has been reported for other genes as well [109], but its functional significance has not been revealed yet. PPAR-γ1 protein is expressed in many cell types, whereas the expression of PPAR-γ2 is mainly limited to adipocytes [70, 71, 110]. Also, it has been reported that PPAR-γ1 is expressed in a murine pre-osteoblastic cell line [88, 111].

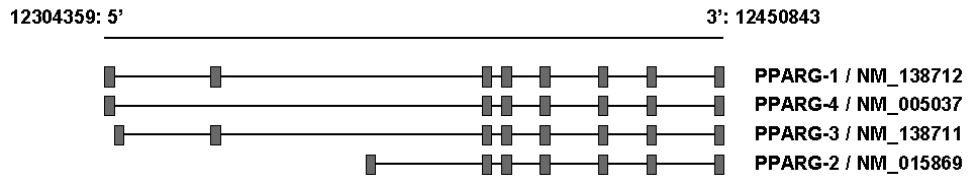

Figure 2.1
Exon - intron structures of multiple PPARG transcripts. Exons are depicted as grey squares and separated from each other by intronic sequences (black lines). The positions and sizes do not match real scale. Sequences underlying this figure were received from the NCBI database (received on 05, 05, 2015 from the NCBI on-line database/Entrez Gene, http://www.ncbi.nlm.nih.gov).

In this study we investigated the differential expression of the four PPARG transcript variants in human pre-osteoblast and osteoblast-like cells, and in human mesenchymal stem cells (MSCs) that were driven to differentiate towards the osteoblastic lineage. Furthermore the effect of the osteoblast differentiation - inducing hormone dexamethasone (DEX) and the PPAR-γ agonist rosiglitazone (ROSI) on PPARG expression in human osteoblasts were investigated.

2.3 Materials and methods

2.3.1 Cell culture

SV-HFO cells [112], normal human osteoblasts (NHOST, Cambrex Bio Science CC-2538, East Rutherford, NJ, USA), human vascular smooth muscle cells (VSMC, Cambrex Bio Science, CC-2583) and human mesenchymal stem cells (MSC, Cambrex Bio Science) were cultured as described previously [113].

2.3.2 Short-term incubation studies with dexamethasone, RU-486 or rosiglitazone

Medium was supplemented with 10 μM ROSI (Cayman Europe, Tallin, Estonia), 100 nM DEX in the absence or presence of 2 μM of the glucocorticoid receptor antagonist RU-486 (Sigma) at specific time points (3, 6, 12, 24 and 48 h) before harvest at day 7 of culture. For short-term ROSI incubations, SV-HFO cells were grown in medium as described above. For short-term DEX and RU-486 incubations, SV-HFO cells were grown in the medium as described above with the exception that DEX was not continuously added.

2.3.3 Quantification of PPARG transcript expression

RNA isolation and cDNA synthesis have been carried out as described recently [114] except that the total amount of RNA was quantified spectrophotometrically using NanoDrop technology (Bancroft Building Wilmington, DE 19810, USA) according to the manufacturer's instructions. Quantitative real time-PCR (Q-RT-PCR) was either based on FAM/TAMRA or SYBR Green detection. FAM/TAMRA - based Q-RT-PCR was performed as described previously [114] with the exception that reaction mixes contained 8 instead of 20 ng cDNA. SYBR Green - based Q-RT-PCR was carried out using an ABI 7700 sequence detection system (Applied Biosystems, Foster City, CA). Reactions were performed in 25 μl volumes using qPCR core kit for SYBR Green I (Eurogentec, Seraing, Belgium). Reaction mixes contained 8 ng cDNA, 3.5 mM MgCl2, 200 μM dNTPs, and 0.025 U/μl Hot GoldStar enzyme. Primer and probe sequences as well as their concentrations are listed in Table 2.1.

2.3.4 Actinomycin D treatment

SV-HFO cells were cultured as described above until day 7 of culture. At 6, 12, 24 and 48 hours before harvesting, actinomycin D (2 μg / ml; Sigma) was added to the cultures. Then RNA was isolated and Q-RT-PCR was performed as described above.

2.3.5 Western blotting

Cells were solubilized in lysis buffer (M-PER Mammalian extraction kit, Pierce Rockford, IL 61105, USA). Total protein concentrations were quantified using BCA protein assay kit (Pierce). 50 μg of total protein extract were loaded on an SDS-polyacrylamide gel consisting of a 5% (w/v) stacking and a 10% (w/v) running gel. After electrophoretic separation, samples were transferred to Nitrocellulose blotting membrane (Hybond, Amersham Pharmacia, UK). Unspecific binding sites were blocked using 4% skim milk in TBS without Tween for

Table 2.1
Primer and probe concentrations and sequences

GAPDH		
300 nM	Forward	5'-ATGGGGAAGGTGAAGGTCG-3'
300 nM	Reverse	5'-TAAAAGCAGCCCTGGTGACC-3'
150 nM	Probe	5'-FAM-CGCCCAATACGACCAAATCCGTTGAC-TAMRA-3'
PPARG 1 (NM 138712)		
50 nM	Forward	5'-GTGGCCGCAGATTTGAAAGAAG-3'
50 nM	Reverse	5'-TGTCAACCATGGTCATTTCG-30-3'
PPARG 2 (NM 015869)		
50 nM	Forward	5'-CAAACCCCTATTCCATGCTGTT-3'
50 nM	Reverse	5'-AATGGCATCTCTGTGTCAACC-3'
PPARG 3 (NM 138711)		
50 nM	Forward	5'-AGAAGCCTGCATTTCTGCAT-3'
50 nM	Reverse	5'-TGGCCTTGTTGTATATTTGTGGTT-3'
PPARG 4 (NM 005037)		
50 nM	Forward	5'-GTGGCCGCAGAAATGACCATG-3'
50 nM	Reverse	5'-GAGAGATCCACGGAGCTGAT-3'
ANGPTL4		
50 nM	Forward	5'-GACAAGAACTGCGCCAAGAG-3'
50 nM	Reverse	5'-AGTACTGGCCGTTGAGGTTG-3'
FABP4		
50 nM	Forward	5'-TACTGGGCCAGGAATTTGAC-3'
50 nM	Reverse	5'-GGACACCCCCATCTAAGGTT-3'
ADFP		
50 nM	Forward	5'-CAGAAGCTAGAGCCGCAAAT-3'
50 nM	Reverse	5'-AGCCCCTTACAGGCATAGGT-3'

over-night at 4°C. Then, the membrane was incubated in primary antibody solution (primary antibody diluted in TBS with 0.1% TBS-Tween and 1% skim milk) for 1 h at room temperature on a roller bank. The dilution for rabbit polyclonal antibody against PPARG was 1:1,000 (Cat. 600-401-419, Rockland Gilbertsville, PA 19525 USA). Mouse monoclonal antibody against GAPDH (Cat. MAB374; Millipore) was used as an internal calibrator in a dilution of 1:20,000 and incubated for 30 min at room temperature. The membrane was washed four times in 0.1% (v/v) TBS-Tween and incubated in a diluted secondary antibody solution (secondary antibody diluted in TBS with 0.1% TBS-Tween and 1% skim milk) for 1 h at room temperature. The secondary antibodies, anti-rabbit IgG conjugated with IRDye

800CW (Cat. 17122; Rockland) and anti-mouse IgG conjugated with Alexa Fluor 680 (Cat. A21057, Invitrogen) were used in a 1:10,000 dilution for 1 h at room temperature to detect the respective primary antibody. After washing the membrane four times in 0.1% (v/v) TBS-Tween and having removed residual Tween by washing in TBS only, fluorescence was detected and analyzed using LI-COR Infrared Imaging System (Odyssey Lincoln, NE USA).

2.3.6 Statistics

Data presented are the results of at least two independent experiments performed in at least triplicate. Values are the means ± S.E. Significance was calculated using the Students t-test.

2.4 Results

2.4.1 Expression of PPARG and its primary target genes

The cell models used all proceed through a differentiation process resulting in the production of a mineralized extracellular matrix in a 2 - 3 week period [113]. PPARG expression was demonstrated during the differentiation of the two human pre-osteoblast cell lines SV-HFO, NHOST and MSCs that were differentiated towards the osteoblast lineage (Figure 2.2). In addition, PPARG expression was demonstrated in mineralizing VSMC that are an experimental model of arthrosclerosis (Figure 2.2). The expression levels of the four PPARG transcript variants PPARG-1,-2, -3 and -4 at various time points during culture were quantified by Q-RT-PCR. Expression levels of PPARG-1, -3 and -4 were significantly increased during differentiation and mineralization of all the four cell models. PPARG-2 expression, however, was virtually absent in SV-HFO, NHOST and VSMC and significantly lower compared to PPARG-1 in MSCs (Figure 2.2). Interestingly, PPARG expression levels were virtually absent and did not increase in the non-mineralizing condition, i.e. when cells were not

stimulated with DEX to differentiate towards a mineralized matrix - producing osteoblast (Figure 2.2). Finally, the presence of PPAR-γ1 protein and its increase during differentiation (from day 3 to 14 of SV-HFO culture) was confirmed by western blotting (Figure 2.2). In addition, expression levels of the confirmed primary PPAR-γ targets ANGPTL4, ADFP and FABP4 [115, 116] increased during differentiation of SV-HFO (Figure 2.3).

2.4.2 Direct regulation of PPARG expression by DEX

Short-term treatment with the synthetic cortisol analog DEX during early differentiation of SV-HFO (day 12) showed already after 3 h significant increases in expression levels of PPARG transcripts-1, -3 and -4 (Figure 2.4). The expression further increased when DEX was added to the medium for 6, 24 and 48 h before harvest. Induction of PPARG-1, -3 and -4 expression levels was completely blocked by the glucocorticoid receptor antagonist RU-486 (Figure 2.4). In addition, blocking *de novo* protein biosynthesis using cycloheximide did not affect the stimulatory action of DEX on PPARG-1, -3 and -4 expression (Figure 2.5).

2.4.3 Homologous regulation of PPARG

ROSI is a well-studied PPARG agonist and stimulates PPARG signalling in several target tissues (reviewed in [117]). We found that, after short-term treatment with ROSI, PPARG-1, -3 and -4 transcript levels were significantly increased (Figure 2.6). PPARG-4 transcript was already significantly induced after 3 h of treatment compared to control, and increases in PPARG-3 and -1 expression levels reached significance after 6 or 12 h, respectively. However, PPARG-2 expression was not induced upon ROSI-treatment (data not shown).

2.4.4 Differential dynamics for expression of PPARG splice variants

By analyzing the stabilities of the PPARG transcripts using the RNA polymerase II blocker actinomycin D in a timecourse experiment, we observed that the stabilities surprisingly differed between the PPARG transcripts 3 and 1/4 (Figure 2.7). The half-life of the PPARG transcripts-1 and -4 was about 24 h. The PPARG-3 transcript had about a 6-fold shorter half-life of 4 h.

2.5 Discussion

The aim of the current study was to assess the expression and regulation of PPARG in human osteoblasts. They are bone-forming cells and have the unique function to produce and mineralize an extracellular protein matrix. Osteoblasts undergo several developmental phases through their lifetime: early commitment to organic-matrix production, mineralization and apoptosis or terminal differentiation into an osteocyte. The complex developmental process is orchestrated by the timely activation of specific transcription factors that regulate the expression of their target genes and thus define the osteoblast phenotype (reviewed in [118]). The current study demonstrates increasing expression of the three PPARG transcripts-1, -3 and -4 giving rise to PPAR-γ1 protein but not PPARG-2 encoding for PPAR-γ2 protein during differentiation of the two human pre-osteoblast cell lines SV-HFO and NHOST. We furthermore found that PPARG expression was increased during mesenchymal stem cell differentiation towards the osteoblastic lineage. And, finally the observations in the osteoblasts were confirmed in a VSMC-based model for artherosclerosis that mimics matrix formation and mineralization by the osteoblasts. In the absence of differentiation towards matrix producing and mineralizing cells, the PPARG transcript levels are virtually absent and do not

increase during culture time. Together these data show a clear coupling between PPAR-γ1 expression and extracellular matrix synthesis and mineralization indicating a role for PPAR-γ1 signalling in these processes.

Presence of DEX is crucial for all cell models examined to develop into a mineralizing condition [119]. Our short-term DEX incubation studies demonstrated that PPARG expression is directly stimulated by DEX. Inhibition by the glucocorticoid receptor antagonist RU-486 suggests that *PPARG* is a direct glucocorticoid receptor target gene. Our hypothesis is underlined by *in silico* searches for putative glucocorticoid receptor response elements (GRE) in the promoter region of the *PPARG* gene, which revealed several hits closed to the transcription start sites (Tatjana Degenhardt, personal communication). However, the identification of functional GRE in the *PPARG* gene is necessary to better understand *PPARG* regulation at chromatin level. In addition, our data do not exclude an indirect osteoblast differentiation - driven expression of *PPARG* because PPARG-1 expression also increases in a DEX-independent differentiating murine osteoblast cell model [111].

We demonstrate for the first time in human osteoblasts the presence and regulation of the two additional PPARG transcripts 3 and 4. Moreover, we show that these transcripts as well as PPARG-1 are homologously upregulated. Interestingly, the magnitude of transcriptional regulation by both rosiglitazone and DEX is different between PPARG-1, -3, and -4. This points to a high order of complexity in promoter usage and transcriptional control for these transcripts. An even higher order of control of transcript levels of these PPARG transcripts is demonstrated by the mRNA stability analyses. Both at transcriptional control and stability, the PPARG-3 transcript is the most sensitive. Overall these data support the significance of a precise fine-tuning of *PPARG* expression in the cell for an optimal function in metabolism. Finally, the differences in stabilities for the three PPARG transcripts -1, -3 and -4 are mechanistically intriguing and yet unexplained. Transcript stability is usually dedicated to the 3'-, but not the 5'-UTR in which these transcripts differ. Thereby the current data suggest also a

role for this part of the transcript in stability control.

In conclusion, the current study demonstrates that 1) PPARG-1, -3 and -4 transcript levels encoding for PPAR-γ1 protein increase during differentiation of all four cell models that were used in this study, 2) PPARG expression is directly regulated by DEX, and 3) PPARG regulates its expression itself by an auto-regulatory mechanism. We suggest from this that cell-specific PPARG transcript variant ratios, due to their specific transcriptional regulation and stabilities, enable a fine-tuning of PPARG receptor-level regulation supporting a well-adjusted signal transduction between the cell and its environment.

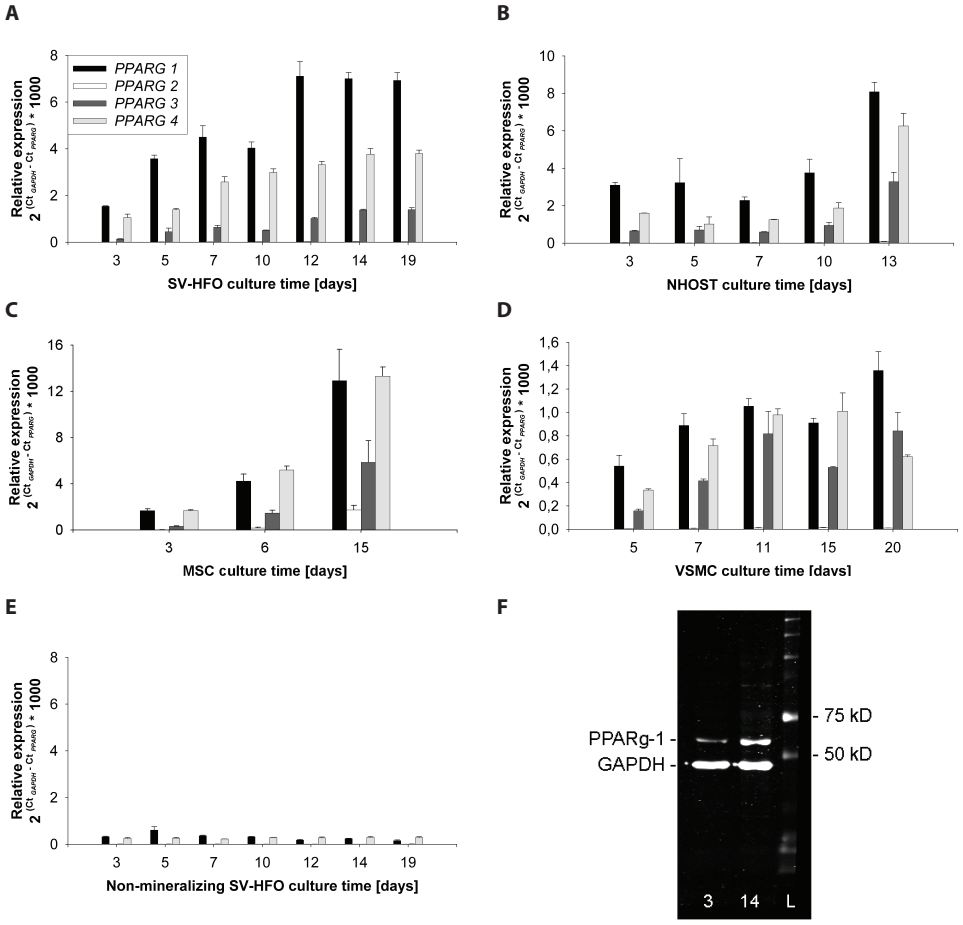

Figure 2.2
Expression levels of multiple PPARG transcripts encoding for PPAR-γ1 protein increase during differentiation of human osteoblasts and osteoblast-like cells. Q-RT-PCR of PPARG transcripts 1 - 4 in the human pre-osteoblast cell lines SV-HFO (A) and NHOST (B), human bone marrow - derived mesenchymal stem cells differentiated towards osteoblasts MSC (C), human vascular smooth muscle cells VSMC (D) and SV-HFO grown on medium lacking the osteogenic differentiation factor DEX (E). Expression levels are relative to the housekeeping gene GAPDH. Values are the mean of at least three biological replicates $\pm$ S.E. Western blotting of PPAR-γ1 (upper band) in SV-HFO at day 3 and 14 of culture (F). GAPDH (lower band) was used as loading control. 3, 14: SV-HFO culture days 3 and 14, respectively; L: protein standard.

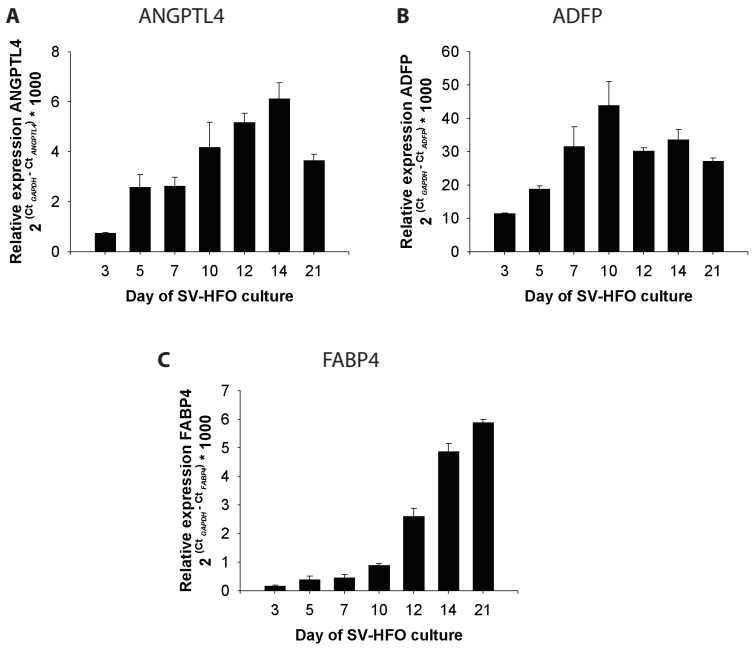

Figure 2.3
Expression levels of primary PPAR-γ target genes increase during osteoblast differentiation. Q-RT-PCR of ANGPTL4 (A), ADFP (B) and FABP4 (C) in the human osteoblast cell line SV-HFO at multiple time points during differentiation. Expression levels are relative to the housekeeping gene GAPDH. Values are the mean of at least three biological replicates ± S.E.

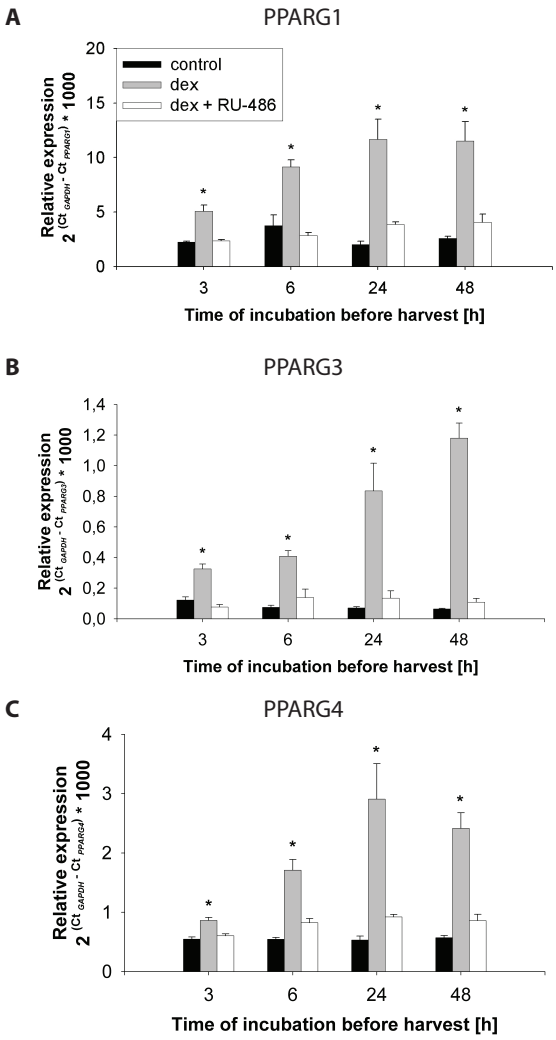

Figure 2.4
Glucocorticoid receptor-regulated expression of PPARG. SV-HFO cells were short-term incubated with the cortisol analog DEX and/or the glucocorticoid receptor antagonist RU-486 at day 12 of culture. Transcript levels were measured using Q-RT-PCR. Values are relative to the housekeeping gene GAPDH and the mean of at least three biological replicates $\pm$ S.E. Asterisks (*) denote values that were determined to be significantly ($P \leq 0.05$) different from those of control.

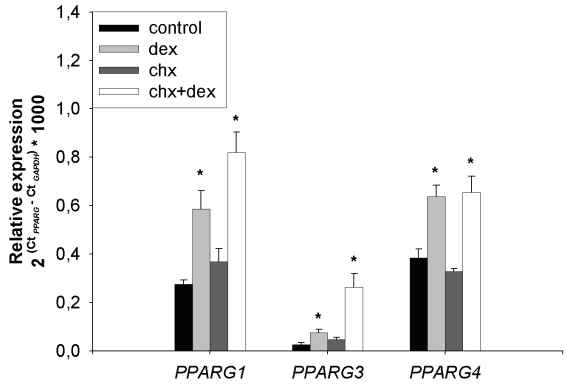

Figure 2.5
De novo protein biosynthesis is not required for induction of PPARG expression by dexamethasone. SV-HFO cells were short-term incubated with the DEX and/or the protein synthesis inhibitor cycloheximide. Transcript levels were measured using Q-RT-PCR. Values are relative to the housekeeping gene GAPDH and the mean of at least three biological replicates ± S.E. Asterisks (*) denote values that were determined to be significantly ($P \leq 0.05$) different from those of control.

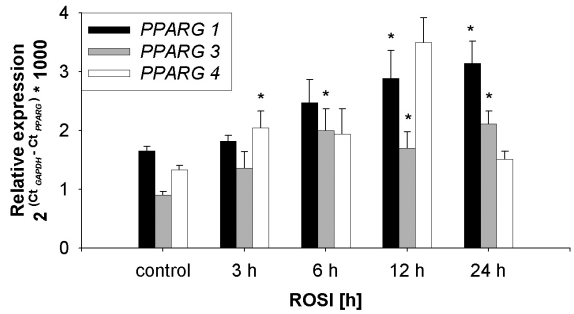

Figure 2.6
Homologous regulation of PPARG. Rosiglitazone was added to the SV-HFO cultures at distinct time points before harvest at day 7. Transcript levels were measured using Q-RT-PCR. Values are relative to the housekeeping gene GAPDH and the mean of at least three biological replicates ± S.E. Asterisks (*) denote values that were determined to be significantly ($P \leq 0.05$) different from those of control.

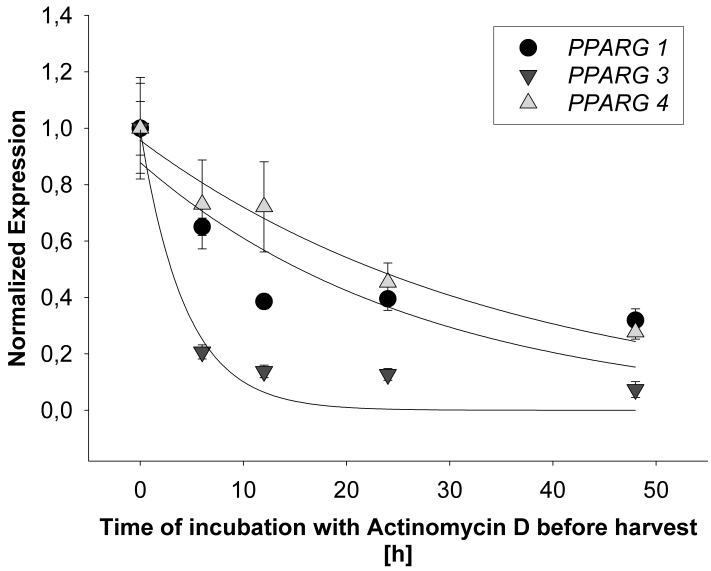

Figure 2.7
Differential stabilities of the three PPARG transcripts PPARG-1, -3 and -4 encoding for PPAR-γ1 protein. The polymerase II inhibitor actinomycin D was added at 6, 12, 24 and 48 h before harvest at day 7. Data have been obtained by Q-RT-PCR. Values are expression levels relative to GAPDH and normalized to control.

3 A new concept underlying mesenchymal stem cell lineage skewing

3.1 Abstract

Bone-marrow adipogenesis is an aging-related phenomenon and is correlated with osteoporosis. The latter is a prevalent bone disease in the elderly leading to increased fracture risk and mortality. It is widely hypothesized that the underlying molecular mechanism includes a shift in the commitment of mesenchymal stem cells (MSCs) from the osteogenic lineage to the adipogenic lineage. Lineage skewing is at least partially a result of transcriptional changes. The nuclear transcription factor peroxisome proliferator - activated receptor γ (PPAR-γ) has been proposed as a major decision factor in MSC lineage commitment, promoting adipogenesis at the expense of osteogenesis. Here we found that PPAR-γ acted unexpectedly to stimulate osteoblast differentiation from human bone marrow - de-

Claudia Bruedigam, Marco Eijken, Marijke Koedam, Jeroen van de Peppel, Ksenja Drabek, Hideki Chiba, Johannes P.T.M. van Leeuwen: *A new concept underlying stem cell lineage skewing that explains the detrimental effects of thiazolidinediones on bone*; 2010; 28:916-927; Stem Cells

rived MSCs. Both rosiglitazone - mediated activation and overexpression of PPAR-γ caused acceleration of osteoblast differentiation. Conversely, shRNAi-mediated PPAR-γ knockdown diminished osteoblast differentiation. MSCs that were treated with rosiglitazone did not preferentially differentiate into adipocytes. However, the rosiglitazone - mediated acceleration of osteoblast differentiation was followed by increased accumulation of oxygen species and apoptosis. In contrast to the osteogenic lineage, cells of the adipogenic lineage were protected from this. Our data support a new concept on bone health that adds to the explanation of the clinically observed suppressive action of activated PPAR-γ on bone and the associated phenomenon of bone marrow adipogenesis. This concept is based on a higher susceptibility of the osteogenic than the adipogenic lineage to oxidative stress and apoptosis that is preferentially triggered in the osteoblasts by activated PPAR-γ.

3.2 Introduction

Osteoporosis is a prevalent skeletal disorder in the elderly that is characterized by impaired bone strength and increased fracture risk. It is associated with reduced life quality and increased mortality [5,6,120]. Bone strength is negatively correlated with bone marrow adipogenesis in aging and patients with osteoporosis. Furthermore, the recently observed reduced bone mass and increased risk of peripheral fractures in thiazolidinedione (TZD) - treated patients are suggested to result from bone marrow adipogenesis that is caused by a switch of mesenchymal stem cells (MSCs) into the adipogenic lineage [40,41].

Pluripotent MSCs in the bone marrow surround trabecular elements of the skeleton. They can enter, among others, the osteoblastic and adipocytic lineages upon regulation through specific endocrine, paracrine, or autocrine signals. It is currently hypothesized that there is a competitive balance between osteoblasts and adipocytes that underlies a cross-talk between complex signaling mechanisms inducing one's cell fate and ultimately suppressing the al-

ternative lineage (recently reviewed in [42]). At least partially, MSC lineage commitment is regulated at the transcriptional level [43]. Herein, runx2 and osterix are considered as important osteoblast- specific transcription factors, whereas activation of peroxisome proliferator-activated receptor γ (PPAR-γ) is suggested to cause the entry of MSCs into the fat lineage that leads indirectly to suppression of osteogenesis [44–50].

PPAR-γ belongs to the nuclear receptor superfamily of transcription factors. Its main function is to regulate fatty acid uptake and storage (reviewed in [62–64]). Activation of PPAR-γ occurs upon binding to a variety of ligands that can be nutritionally derived endogenous polyunsaturated fatty acids and eicosanoids [65–67] or synthetic compounds including TZDs (reviewed in [68]). The latter are pharmaceutical compounds with insulin - sensitizing function that are frequently prescribed to type II diabetic patients. The single *PPARG* gene undergoes alternative splicing and promoter usage, giving rise to two proteins: PPAR-γ1 and PPAR-γ2. The latter contains an additional N-terminal exon that results in a higher ligand-independent transactivation capacity when compared to PPAR-γ1 [69]. Expression of PPAR-γ2 is mainly limited to adipocytes, whereas PPAR-γ1 is found to be ubiquitously abundant [70, 71]. We have recently demonstrated dynamic expression patterns of PPAR-γ1 protein variant in osteoblasts and osteogenic hMSCs. Expression levels increase during the differentiation process and reach a plateau during the late phase that is defined by the onset of extracellular matrix mineralization [121]. This has suggested a role of PPAR-γ in osteogenesis besides the reported role in adipogenic MSC commitment.

In the current study, we investigated the impact and identity of PPAR-γ - regulated processes in osteoblast differentiation. We used both direct and indirect approaches to perturb PPAR-γ signaling in various human MSC and osteoblast models and analyzed the long-term osteoblastic phenotype outcome. In a condition of increased PPAR-γ activity, a first phase of accelerated differentiation was followed by a second phase of increased accumulation of reactive oxygen species (ROS) and apoptosis. Cells from the adipogenic lineage were pro-

tected from rosiglitazone - induced ROS accumulation and apoptosis and revealed a stronger expressed oxidative stress response network when compared to the osteogenic lineage. The results of the current study lead to a new concept of PPAR-γ action that challenges the role of PPAR-γ as MSC lineage decision maker and direct suppressor of osteoblast differentiation. This new concept is based on (1) evidence for a stimulatory role of PPAR-γ in both osteoblast and adipocyte differentiation from MSCs and (2) the revealed differential susceptibilities of osteogenic and adipogenic lineages to PPAR-γ ligand - induced ROS stress and apoptosis. Resistance of adipocytes but not osteoblasts to TZD - induced ROS and apoptosis builds the molecular basis for the new concept that adds to the explanation of clinically observed bone marrow adipogenesis, diminished bone formation, and increased fracture rate in TZD-treated patients.

3.3 Materials and methods

3.3.1 Cell culture

SV-HFO preosteoblasts [112], normal human osteoblasts (NHOst; Lonza, Basel, Switzerland, http://www.lonza.com), and human bone marrow-derived mesenchymal stem cells (hMSC; Lonza) were cultured as described previously [119]. MSCs were derived from two different donors, and passages 6 and 7 were used for the experiments. Adipogenic differentiation was induced by culturing confluent hMSCs in differentiation medium that was supplemented with 100 nM dexamethasone, 500 μM 3-isobutyl-1-methylxanthine (IBMX), and 60 μM indomethacin.

3.3.2 Human tissues

The tissues used in this publication were provided by Erasmus MC Tissue Bank (Dr. Riegman, Erasmus MC, Rotterdam, The Netherlands, http://www.tubafrost.org). Total RNA was isolated as described below.

3.3.3 Constructs

PPAR-γ1 expression construct containing PPAR-γ1 open reading frame in pCMV6-XL4 vector was purchased from Origene (Rockville, MD, http://www.origene.com), and PPAR-γ2 expression construct was kindly provided by Prof. J. Auwerx (Institut Clinique de la Souris, Strasbourg, France, http://www.ics-mci.fr). Sh-RNAi constructs targeting PPAR-γ were obtained from TRC library TRC-Hs1.0 (human) via OpenBiosystems.

3.3.4 Transfection studies

SV-HFO and hMSC were cultured as described above until 60% confluency was reached. Transfection was achieved by electroporation using the appropriate Amaxa nucleofector kit according to the manufacturer's recommendations (Lonza).

3.3.5 Quantification of mRNA expression

RNA isolation, cDNA synthesis, and quantitative real-time polymerase chain reaction (Q-RT-PCR) were carried out as described recently [121]. Primer and probe sequences and concentrations are shown in Table 3.1. QRT- PCR efficiencies were similar and about 100% for all reactions.

3.3.6 DNA, protein, alkaline phosphatase activity, and mineralization assays

Alkaline phosphatase (ALPL), DNA, protein, and calcium measurements were performed as described previously [119].

3.3.7 Quantification of lipid vesicle formation

Cells were fixed in 10% formaline/phosphate-buffered saline (PBS), washed with 60% (v/v) isopropanol, and subsequently incubated with Oil red O working solution (Sigma, St. Louis, http://www.sigmaaldrich.com; 60% (v/v) Oil red O in deionized water). Staining solution was removed by washing with deionized water. Then culture plates were dried and remaining stain was dissolved in igepal working solution (Sigma; 4% (w/v) igepal in isopropanol). Absorbance was measured photometrically at 490 nm.

3.3.8 Measurement of reactive oxygen species

Total reactive oxygen species were measured using the cell-permeable non-fluourescent probe 20-70-dichlorofluorescin diacetate (DCF-DA; Sigma), which is de-esterified intracellularly and turns into highly fluorescent 20,70-dichlorofluorescin upon oxidation. Culture medium was replaced with 10 μM DCF-DA in modified ringer buffer (125 mM NaCl, 5 mM KCl, 1.2 mM KH2PO4, 25 mM Hepes, 6 mM glucose, 1.2 mM MgSO4, and 1 mM CaCl2; pH 7.4) and incubated for 1 hour at 37°C in the dark. Cultures were washed with PBS and supplemented with differentiation medium, and the fluorescence signal was subsequently quantified. Superoxide radicals were measured using Mitosox red mitochondrial superoxide indicator (Molecular Probes Inc., Eugene, http://probes.invitrogen.com) according to the manufacturer's instructions. Microscopic images were processed using Cell profiler software (http://www.cellprofiler.org).

3.3.9 Apoptosis measurement

Apoptotic cells were counted by fluorescent-activating cell sorting using FacsCanto II apparatus (BD Biosciences, San Diego) after staining with 1 μg/ml FITC-labeled annexin-V (IQ-Products, Groningen, The Netherlands) and 0.25 μg/ml propidium iodide (Nexins Research, Netherlands) according to the manufacturers' instructions.

3.3.10 Statistics

Data presented are the results of at least two independent experiments performed in at least triplicate. Values are the means $\pm$ S.E. Significance was calculated using the Student's t-test.

3.4 Results

3.4.1 PPAR-γ1 is the predominant expressed isoform in osteoblasts

The three PPAR isoforms, α, β/δ, and γ, share high structural and physiological homology. We investigated expression levels of PPAR-α, β/δ, and γ in osteoblasts and adipocytes. Primer pairs were designed to detect all mRNA molecules that encode the ligand-binding domain of each PPAR isoform. Because the *PPARG* gene gives rise to PPAR-γ1 and PPAR-γ2 splice variants that differ only in their N-terminal region but contain identical ligand-binding domains, an additional primer pair was designed to detect the PPARG2-specific exon. Total PPAR-γ was between 2- and 500-fold higher expressed than PPAR-α or -β/δ in human osteoblasts, osteogenic hMSCs, and human bone tissue samples (Figure 3.1 A and B). PPAR-γ was the predominant expressed isoform in human adipocytes and human fat tissue as well (Figure 3.1 C). The splice variant PPAR-γ1 accounted for more than 99% of total expressed PPAR-γ in bone (Figure 3.1 A and B). In fat, both PPAR-γ variants were expressed, which

is consistent with the data reported by others (Figure 3.1 C) [71, 122]. We had shown earlier that PPAR-γ1 expression level was dynamically regulated during osteogenic differentiation [121]. Functionality of endogenous PPAR-γ signaling in osteoblasts and osteogenic hMSCs was shown by dose-dependent induction of expression of the primary PPAR target gene ANGPTL4 within 3 hours after treatment with the specific PPAR-γ agonist rosiglitazone in SV-HFO and hMSCs at day 3 of differentiation (Figure 3.1 D).

3.4.2 Activated PPAR-γ stimulates both adipocyte and osteoblast differentiation from human mesenchymal stem cells

To test whether activation of PPAR-γ results in a switch from osteoblastic towards adipocytic lineage commitment, hMSC cultures were grown in rosiglitazone - supplemented osteogenic

Figure 3.1 (following page)
PPAR isoform expression in human bone and fat. Expression levels of PPAR isoforms PPAR-α, β/δ, and γ were determined by quantitative real-time polymerase chain reaction (Q-RT-PCR). To discriminate between both PPAR-γ splice variants, a PPARG2-specific primer pair was used (red bars). (A): Human pre-osteoblast model SV-HFO and osteogenic hMSCs, (B) human bone tissue from sternum and crista supraepicondylaris, and (C) adipogenic hMSCs and human fat tissue. (D): Functionality of PPAR-γ in SV-HFO and osteogenic hMSC. Expression levels of the primary PPAR target gene ANGPTL4 were analyzed by Q-RT-PCR in SV-HFO and osteogenic hMSC at day 3 of differentiation that were incubated for 3 hours with control, 1, or 10 μM rosiglitazone. SV-HFO and hMSC experiments were independently repeated. Data points represent means of three biological replicates $\pm$ S.E. Asterisks (*) denote values that were determined to be significantly different ($p \leq 0.05$) from those of controls. Q-RT-PCR data from bone and fat tissue are the mean of two technical replicates. To provide an idea about absolute expression levels of the three PPAR isoforms in cells, Ct values of osteogenic hMSCs at day 3 are provided: Ct (PPARA) = 26.18 $\pm$ 0.38; Ct (total PPARG) = 23.69 $\pm$ 0.04; Ct (PPARG2) = not detected; Ct (PPARD) = 26.63 $\pm$ 0.25. The following Ct values were detected in adipogenic hMSC at day 3 of differentiation: Ct (PPARA) = 27.81 $\pm$ 0.18; Ct (total PPARG) = 22.06 $\pm$ 0.22; Ct (PPARG2) = 28.23 $\pm$ 6 0.26; Ct (PPARD) = 28.19 $\pm$ 0.23. Abbreviations: hMSC, human mesenchymal stem cell; PPAR, peroxisome proliferator-activated receptor.

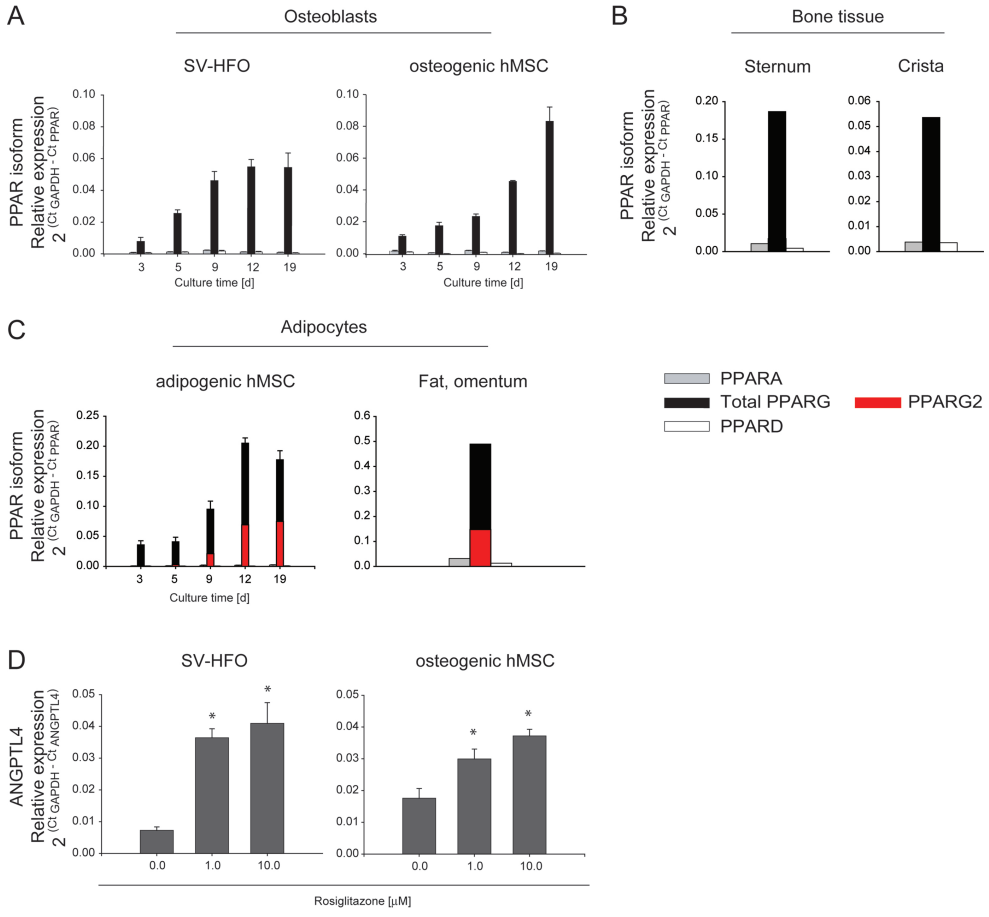
A
Osteoblasts
SV-HFO
osteogenic hMSC
PPAR isoform
Relative expression
2 (Ct GAPDH - Ct PPAR)
Culture time [d]
B
Bone tissue
Sternum
Crista
C
Adipocytes
adipogenic hMSC
Fat, omentum
PPARA
Total PPARG
PPARG2
PPARD
D
SV-HFO
osteogenic hMSC
ANGPTL4
Relative expression
2 (Ct GAPDH - Ct ANGPTL4)
Rosiglitazone [µM]

[h]

or adipogenic medium. Rosiglitazone stimulated mineralization in osteogenic hMSCs (Figure 3.2 A) as well as in SV-HFO and NHOst osteoblast cultures (data not shown). In adipogenic hMSCs, extensive formation of adipocytes was detected that was enhanced by rosiglitazone (Figure 3.2 B).

3.4.3 Rosiglitazone stimulates osteoblast differentiation in a PPAR-γ - dependent manner

To further elucidate the role of PPAR-γ in osteoblast differentiation, the effects of continuous rosiglitazone supplementation on expression levels of osteoblast differentiation markers RUNX2, collagen type IA1 (COL1A1), osteopontin (SPP1), osteocalcin (BGLAP), activating transcription factor 4 (ATF4), and FOS-like antigen 1 (FOSL1 or FRA1) and alkaline phosphatase (ALP) activity were analyzed in osteogenic hMSC cultures. Expression levels of all osteoblast differentiation markers were elevated in rosiglitazone - supplemented cultures in a differentiation stage - dependent manner. RUNX2 and COL1A1 expression levels were significantly higher in rosiglitazone - treated hMSCs when compared to respec-

Figure 3.2 (following page)
Effect of rosiglitazone on adipocyte and osteoblast differentiation from human mesenchymal stem cells (hMSCs). MSC cultures were differentiated with dexamethasone and β-glycerophosphate into the osteogenic or with dexamethasone, indomethacin, and 3-isobutyl-1-methylxanthine into the adipogenic lineage and continuously supplemented with control, 0.1, 1, or 10 μM rosiglitazone and analyzed at day 15 for (A) extracellular matrix mineralization by Alizarin red staining and (B) lipid vesicle formation by Oil red O staining. In panel A in the Alizarin red staining of the adipo + control and adipo + 10 μM rosi condition, light pink aspecific staining can be observed. This is not mineralization but adipocytes, as can be clearly seen from the accumulation of lipid droplets. The experiment was repeated with a second sample of MSCs from the same donor, and data were confirmed in a second MSC donor as well. Data points from staining semiquantification plots below represent the mean of four biological replicates $\pm$ S.E. Asterisks (*) denote values that were determined to be significantly different ($p \leq 0.05$) when compared to respective controls. Abbreviations: adipo, adipogenic; osteo, osteogenic.

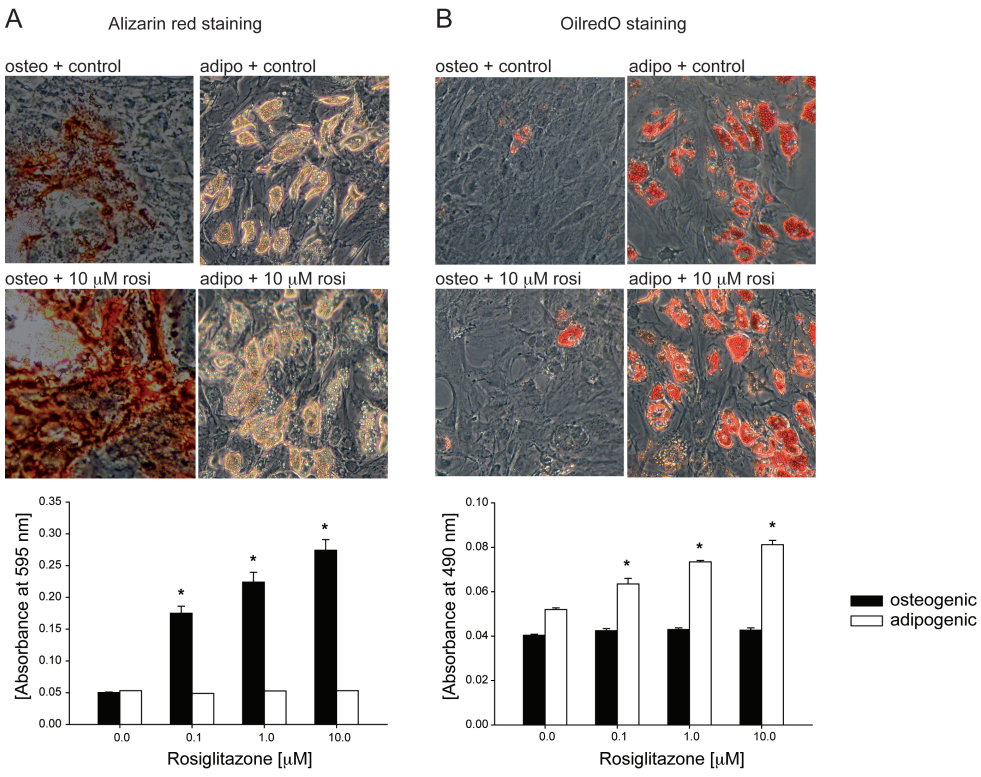
A
Alizarin red staining
B
OilredO staining
osteo + control
adipo + control
osteo + 10 μM rosi
adipo + 10 μM rosi
[Absorbance at 595 nm]
[Absorbance at 490 nm]
Rosiglitazone [μM]
0.0
0.1
1.0
10.0
osteogenic
adipogenic

[h]

tive controls during the early phase of differentiation (day 3; Figure 3.3 A). Expression levels of ATF4, FOSL1, BGLAP, and SPP1 were significantly elevated by rosiglitazone in hMSCs at day 15 (Figure 3.3 A). ALP activity was dynamically regulated in control condition and reached its peak at day 15 of culture. Treatment with rosiglitazone caused an accelerated ALP activity pattern (Figure 3.3 B) and resulted in increased mineralization (Figure 3.3 C). Rosiglitazone had similar effects on the differentiation of the human pre-osteoblast cell line SV-HFO and NHOst (data not shown). Rosiglitazone treatment resulted in a significant upregulation of the primary PPAR target gene ANGPTL4 (Figure 3.3 A) and a significant increase in PPARG1 expression levels, whereas PPARG2 expression remained absent (data not shown).

In order to assess the involvement of PPAR-γ, hMSCs were transfected with shRNAi constructs targeting mRNA sequences that encode the ligand-binding domain of PPAR-γ. Expression of PPARG was significantly downregulated and ALPL expression was significantly reduced in PPAR-γ-shRNA cultures when compared to controls five days after transfection (Figure 3.3 D). Interestingly, PPARA expression levels were higher in both PPAR-γ-shRNA cultures when compared to controls (Figure 3.3 D). A similar observation in regard to the inversed relationship between PPARA and PPARG expression was described earlier by Patel et al. [123]. However, it is unlikely that this PPARA expression will compensate for the knockdown of PPARG because the expression of the primary PPAR target gene ANGPTL4 was diminished in PPAR-γ-shRNA cultures (Figure 3.3 D). To investigate the impact of increased PPAR-γ expression, hMSC cultures were transfected with PPAR-γ expression constructs under the control of pCMV promoter. ALP activity levels were significantly higher in PPAR-γ overexpressing cells (Figure 3.3 E). Interestingly, both PPAR-γ1 and PPAR-γ2 overexpression resulted in higher ALP activity when compared to empty vector controls (Figure 3.3 E).

3.4.4 The pro-differentiative effect of rosiglitazone is followed by enhanced PPAR-γ - dependent apoptosis and ROS accumulation

We investigated the effect of rosiglitazone on osteoblast apoptosis, ROS accumulation, and expression of genes involved in mitochondrial dysfunction. The chosen concentration of 10 μM rosiglitazone is well within the range measured in TZD treated patients [124–127]. DNA content was significantly lower in rosiglitazone - treated osteogenic hMSC cultures when compared to control during the late differentiation phase (Figure 3.4 A). The reduction in DNA content was paralleled by increased apoptosis (Figure 3.4 B). Similar effects of rosiglitazone treatment on DNA and apoptosis were confirmed in SV-HFO and NHOst

Figure 3.3 (following page)
Role of rosiglitazone - activated PPAR-γ in osteoblast differentiation. (A): Expression levels of osteogenic differentiation marker genes RUNX2, COL1A1, ATF4, FOSL1, BGLAP, and SPP1 and primary PPAR target gene ANGPTL4 were quantified in continuously 10 μM rosiglitazone- or control-treated hMSC cultures at multiple time points during osteoblast differentiation (induced by dexamethasone and β-glycerophosphate) by quantitative real-time polymerase chain reaction (Q-RT-PCR). (B): ALP activity and (C) extracellular matrix mineralization was quantified in hMSC cultures that were continuously supplemented with 10 μM rosiglitazone- or control-treated hMSC cultures at multiple time points during culture. (D): hMSC cultures were transfected with shRNAi constructs targeting PPARG ligand-binding domain or scrambled control. Total PPARG, PPARG2, PPARA, PPARD, ANGPTL4, and ALPL expression levels were quantified 5 days after transfection by Q-RT-PCR. (E): hMSC cultures were transfected with PPARG1 of PPARG2 expression constructs or empty vector control. Total PPARG, PPARG2, and ALPL expression levels were quantified 3 days after transfection by Q-RT-PCR. Data from panels (A) - (C) were reproduced in an independent experiment with a second sample of cells from the same MSC donor. The experiment of panels (D) and (E) was repeated independently in a second MSC donor. Data points represent means of four biological replicates $\pm$ s.e.m. Asterisks (*) denote values that were determined to be significantly different ($p \leq 0.05$) when compared to respective controls. Abbreviations: ALP, alkaline phosphatase; ATF4, activating transcription factor 4; BGLAP, osteocalcin; COL1A1, collagen type IA1; FOSL1, FOS-like antigen 1; hMSC, human mesenchymal stem cell; PPAR, peroxisome proliferator-activated receptor; SPP1, osteopontin.

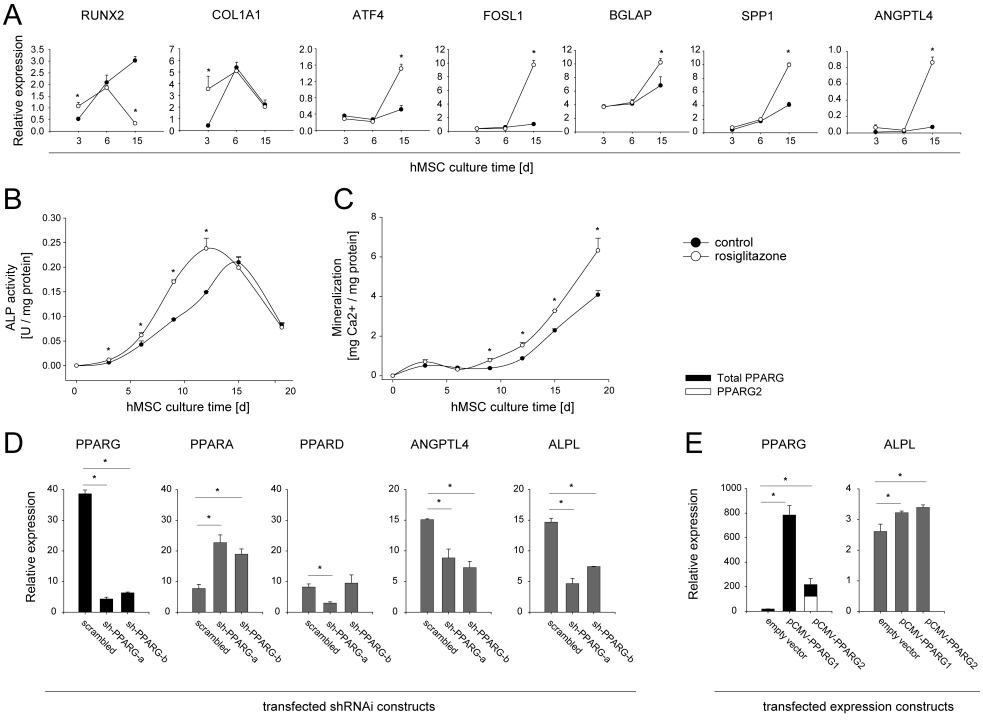
A
RUNX2
COL1A1
ATF4
FOSL1
BGLAP
SPP1
ANGPTL4
Relative expression
hMSC culture time [d]
B
ALP activity [U / mg protein]
hMSC culture time [d]
C
Mineralization [mg Ca2+ / mg protein]
hMSC culture time [d]
control
rosiglitazone
Total PPARG
PPARG2
D
PPARG
PPARA
PPARD
ANGPTL4
ALPL
Relative expression
scrambled
sh-PPARG-a
sh-PPARG-b
transfected shRNAi constructs
E
PPARG
ALPL
Relative expression
empty vector
pCMV-PPARG2
pCMV-PPARG1
transfected expression constructs

[h]

(data not shown). Overexpression of PPAR-γ1 or PPAR-γ2 resulted in increased apoptosis that was further enhanced by supplementation with rosiglitazone (Figure 3.4 C). Conversely, the pro-apoptotic effect of rosiglitazone was reduced in hMSCs that were transfected with PPAR-γ-shRNAi constructs (Figure 3.4 D). To assess whether expression of genes involved in apoptosis is affected by rosiglitazone, mRNA levels of apoptosis-related cysteine peptidases caspase 3 (CASP3) and caspase 6 (CASP6) were quantified. Expression levels of both genes showed a tendency to increase or were stable during osteogenic differentiation of hMSCs, and continuous rosiglitazone treatment significantly increased expression levels in a differentiation-dependent manner (Figure 3.4 E). Superoxide radical levels were significantly elevated in rosiglitazone - treated cultures during late differentiation phase (Figure 3.4 F). We further investigated the expression of genes involved in mitochondrial dysfunction. Bcl2-associated X protein (BAX), cytochrome C (CYCS), apoptotic peptidase activating factor 1 (APAF1), voltage-dependent anion channel 1 (VDAC1), and mitochondrial solute carrier family 25 member 4 (SLC25A4) were quantified. Expression levels of all genes were elevated in rosiglitazone - supplemented hMSC cultures at the onset of mineralization when compared to respective controls (Figure 3.4 G). We investigated the role of PPAR-γ in mitochondria - dependent apoptosis by overexpression and knockdown studies and subsequent analysis of CYCS and BAX expression. PPAR-γ overexpression revealed modest increases in CYCS and BAX expression levels (Figure 3.4 H), whereas downregulation of PPAR-γ resulted in significantly reduced CYCS and BAX transcript levels (Figure 3.4 I).

3.4.5 Differential robustness of adipocytes and osteoblasts to rosiglitazone - induced oxidative stress and apoptosis

Taken together so far, the data above provide evidence for an involvement of PPAR-γ in osteogenic differentiation from hMSCs. The lack of evidence for a direct lineage switch

towards the adipogenic lineage away from the osteogenic lineage gives rise to the question of how the commonly reported reduced number of osteoblasts and increased number of adipocytes is caused in models of stimulated PPAR-γ activity. Alternatively to a direct suppressive action of PPAR-γ on osteoblast differentiation, age-related shifts in stem cell commitment may be secondary to lineage-specific differences in susceptibility to oxidative stress and apoptosis, as has been hypothesized by Warren and Rossi for the hematopoietic system [128].

In order to test this hypothesis, we measured the percentage of apoptotic cells in os-

Figure 3.4 (following page)
Role of rosiglitazone - activated peroxisome proliferator-activated receptor γ (PPAR-γ) in osteoblast apoptosis and mitochondrial dysfunction. (A): DNA content and (B) apoptosis measured as a percentage of annexinV-FITC-positive cells in hMSC cultures that were continuously supplemented with 10 μM rosiglitazone or control. Apoptosis was quantified in a similar manner in (C) hMSC cultures transfected with PPARG1 or PPARG2 expression constructs at day 15 of culture and in (D) hMSC cultures transfected with shRNAi constructs targeting PPARG ligand-binding domain at day 5 of culture. (E): Expression levels of CASP3 and CASP6 were determined by quantitative real-time polymerase chain reaction (Q-RT-PCR) at multiple time points in hMSC cultures that were supplemented continuously with 10 μM rosiglitazone or control. (F) Levels of superoxide radicals were determined by Mitosox staining (white spots in top panels), and data displayed are from mineralization onset at day 15 of culture. Total reactive oxygen species were semi-quantified at culture days 1, 7, and 14. (G) Expression levels of markers of mitochondrial dysfunction BAX, CYCS, APAF1, VDAC1, and SLC25A4 were measured by Q-RT-PCR in hMSC cultures supplemented with 10 μM rosiglitazone or controls at multiple time points. Q-RT-PCR based analysis of BAX and CYCS expression in hMSC cultures that were transfected with PPARG1 or PPARG2 expression constructs (H) or shRNAi constructs targeting PPARG ligand-binding domain (I). Data from panels (A), (B), (G), (E), and (F) were reproduced in an independent experiment with cells from the same MSC donor. The experiments of panel (C), (D), (H), and (I) were repeated independently in MSCs from a second donor. Data points represent means of at least three biological replicates $\pm$ S.E. Asterisks (*) denote values that were determined to be significantly ($p \leq 0.05$) different when compared to respective controls. Abbreviations: APAF1, apoptotic peptidase activating factor 1; BAX, Bcl2-associated X protein; CASP, caspase; CYCS, cytochrome C; DCFDA, 20-70-dichlorofluorescin diacetate; hMSC, human mesenchymal stem cell; rosi, rosiglitazone; SLC25A4, mitochondrial solute carrier family 25 member 4; VDAC1, voltage-dependent anion channel 1.

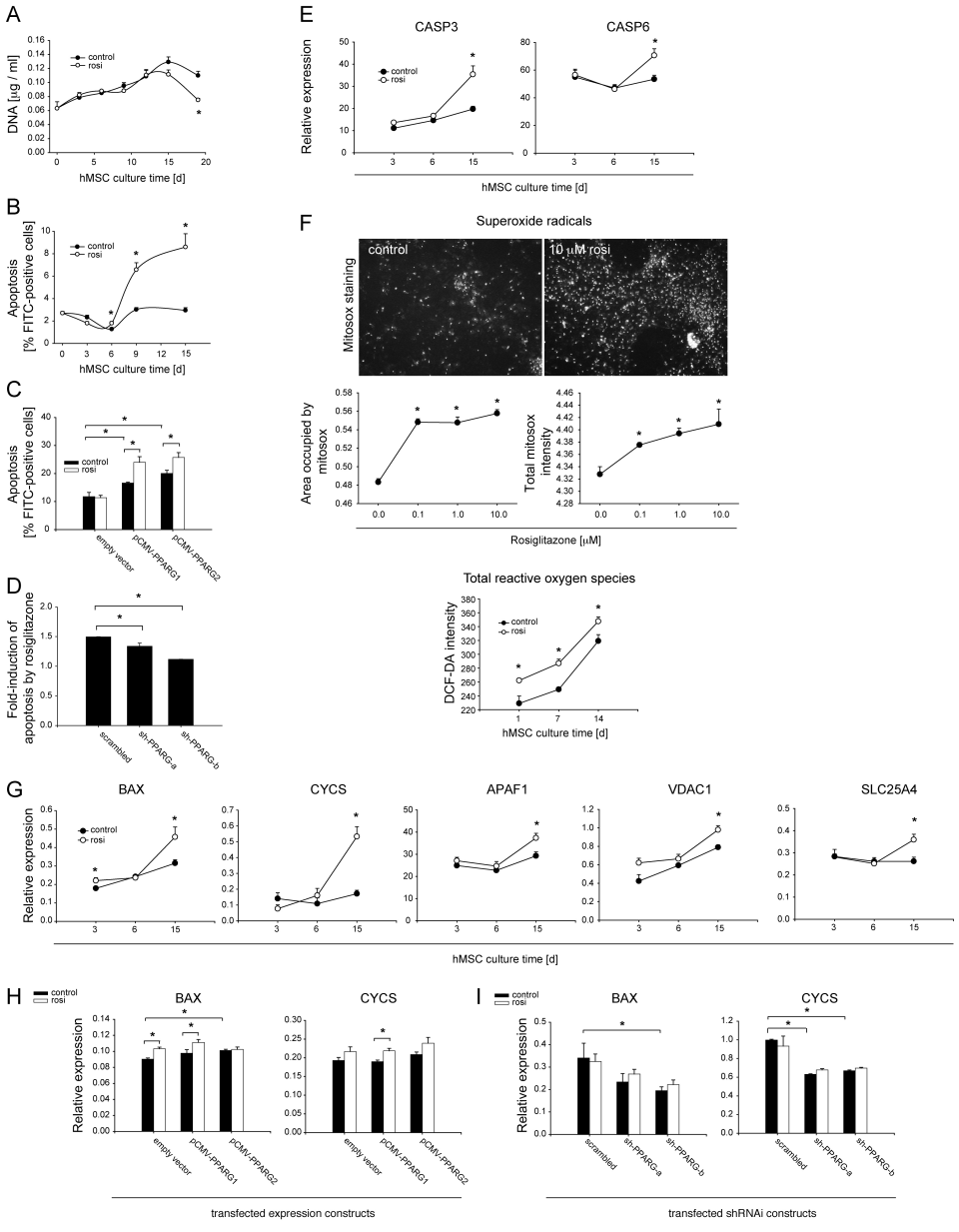
A
DNA [µg / ml]
control
rosi
hMSC culture time [d]
B
Apoptosis [% FITC-positive cells]
hMSC culture time [d]
C
Apoptosis [% FITC-positive cells]
empty vector
pCMV-PPARG1
pCMV-PPARG2
D
Fold-induction of apoptosis by rosiglitazone
scrambled
sh-PPARG-a
sh-PPARG-b
E
CASP3
CASP6
Relative expression
hMSC culture time [d]
F
Superoxide radicals
control
10 µM rosi
Mitosox staining
Area occupied by mitosox
Total mitosox intensity
Rosiglitazone [µM]
Total reactive oxygen species
DCF-DA intensity
hMSC culture time [d]
G
BAX
CYCS
APAF1
VDAC1
SLC25A4
Relative expression
hMSC culture time [d]
H
BAX
CYCS
Relative expression
transfected expression constructs
I
BAX
CYCS
Relative expression
transfected shRNAi constructs

[h]

teogenic and adipogenic cultures that were continuously supplemented with increasing concentrations of rosiglitazone during several time points of differentiation. Interestingly, only the osteogenic but not the adipogenic lineage revealed dose-dependent increases in apoptosis upon stimulation with rosiglitazone (Figure 3.5 A). Also, the amount of superoxide radicals was increased only in the osteogenic lineage upon rosiglitazone treatment, whereas the adipogenic lineage was protected from this (Figure 3.5 B). To further investigate whether the observed difference in rosiglitazone - induced apoptosis between both lineages is a result of transcriptional differences in oxidative stress response genes, we compared mRNA levels of well characterized genes involved in oxidative stress response, in particular, genes encoding proteins with antioxidant capacity, phase I and II metabolizing enzymes, and components of the nuclear factor (erythroid-derived 2)-like 2 (NFE2L2)-mediated oxidative stress response signaling pathway, in osteogenic and adipogenic cultures at several time points during differentiation. Interestingly, genes encoding the antioxidant proteins catalase (CAT), heme oxygenase 1 (HMOX1), and mitochondrial superoxide dismutase 2 (SOD2) were significantly higher expressed in adipocytes (Figure 3.5 C). Also transcripts encoding the phase I and II metabolizing enzymes epoxide hydrolase 1 (EPHX1), microsomal glutathione S-transferase 1 (MGST1), and glutamate cysteine ligase, modifier subunit (GCLM) were more strongly expressed in adipocytes than in osteoblasts throughout the differentiation process (Figure 3.5 C). On the other hand, glutathione S-transferase alpha 4 (GSTA4), glutathione S-transferase kappa 1 (GSTK1), and NAD(P)H dehydrogenase, quinone 2 (NQO2) transcript levels were only significantly higher expressed in adipocytes at later time points during culture but did not reveal any differences during early differentiation (Figure 3.5 C). Smooth muscle gamma 2 subunit of actin (ACTG2) and protein kinase C, alpha (PRKCA) are components of the nuclear factor NFE2L2- mediated oxidative stress response signaling pathway and were significantly higher expressed in the adipogenic compared to the osteogenic lineage (Figure 3.5 C). Interestingly, mitogen-activated protein kinase kinase kinase 5 that is

also known as apoptosis signal regulating kinase 1 (MAP3K5) was more strongly expressed in the osteogenic compared to the adipogenic lineage. This observation is in line with the findings above, because activation of MAP3K5 has been shown to mediate activation of mitogen-activated protein kinase 14, also known as p38 MAPK (MAPK14), which would lead to inhibition of phosphorylated NFE2L2 [129]. In summary, the NFE2L2-mediated oxidative stress response signaling network was more strongly expressed in the adipogenic compared to the osteogenic lineage, suggesting that the osteogenic lineage is more susceptible to oxidative stress and apoptosis. These data support a role for DNA damage and genomic maintenance in lineage skewing of hMSCs in aging and aging-related diseases that are associated with suppressed osteogenesis, in particular in TZD-induced bone loss.

Figure 3.5 (following page)
Differential analysis of apoptosis, superoxide levels, and oxidative stress response gene expression in osteogenic and adipogenic lineages. (A): Apoptosis measured as a percentage of annexinV-FITC-positive cells in hMSC cultures that were differentiated towards the osteogenic or adipogenic lineage and continuously supplemented with control, 0.1, 1, or 10 μM rosiglitazone. (B): Superoxide levels were quantified by Mitosox staining and subsequent Cell profiler image analysis software in hMSC cultures that were differentiated towards the osteogenic or adipogenic lineage and continuously supplemented with control, 0.1, 1, or 10 μM rosiglitazone. (C): Expression levels of oxidative stress response genes were determined in hMSC cultures that were differentiated towards osteogenic or adipogenic lineage and continuously supplemented with control, 0.1, 1, or 10 μM rosiglitazone by quantitative real-time polymerase chain reaction analysis at multiple time points during culture. Data from panels (A) and (B) were independently repeated in an experiment with a second sample of cells from the same MSC donor. The experiment from panel (C) was repeated with MSCs from a different donor. Data points are means of at least three biological replicates $\pm$ S.E. Asterisks (*) denote values that were determined to be significantly different ($p \leq 0.05$) when compared to respective controls. Abbreviations: ACTG2, smooth muscle gamma 2 subunit of actin; adipo, adipogenic; CAT, catalase; EPHX1, epoxide hydrolase 1; GCLM, glutamate cysteine ligase, modifier subunit; GSTA4, glutathione S-transferase alpha 4; GSTK1, glutathione S-transferase kappa 1; HMOX1, heme oxygenase 1; MAP3K5, apoptosis signal regulating kinase 1; MGST1, microsomal glutathione S-transferase 1; NFE2L2, nuclear factor (erythroid-derived 2)-like 2; NQO2, NAD(P)H dehydrogenase, quinone 2; osteo, osteogenic; PRKCA, protein kinase C, alpha; SOD2, superoxide dismutase 2.

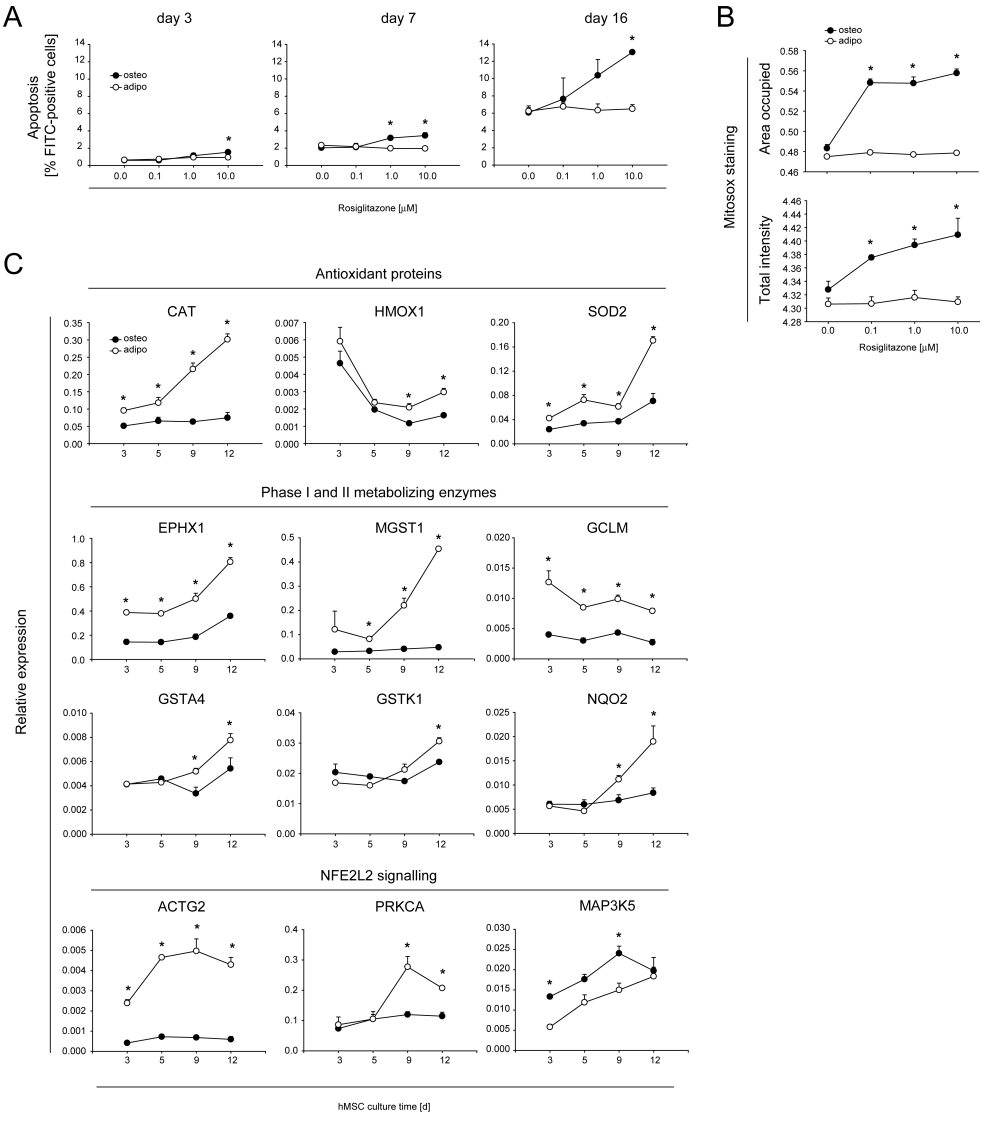
A
day 3
day 7
day 16
Apoptosis
[% FITC-positive cells]
osteo
adipo
Rosiglitazone [µM]
B
Mitosox staining
Area occupied
Total intensity
C
Antioxidant proteins
CAT
HMOX1
SOD2
Phase I and II metabolizing enzymes
EPHX1
MGST1
GCLM
GSTA4
GSTK1
NQO2
NFE2L2 signalling
ACTG2
PRKCA
MAP3K5
Relative expression
hMSC culture time [d]

[h]

3.5 Discussion

The current study has revealed three major findings. First, we have shown that activation of PPAR-γ unexpectedly accelerates human osteoblast differentiation by using a variety of direct and indirect perturbation studies in several osteoblast cell models. The finding that knockdown of PPAR-γ diminishes osteoblast differentiation is particularly significant as many studies to date approach the improvement of osteogenesis by blocking PPAR-γ action. The second major finding is that the observed acceleration of osteoblast differentiation by activated PPAR-γ is ultimately followed by mitochondrial dysfunction, oxidative stress, and apoptosis. This shows that well-balanced PPAR-γ expression and ligand concentrations are important for proper osteoblast differentiation and thereby optimal bone formation. Our third major finding is the observed differential susceptibility of adipocytes and osteoblasts to PPAR-γ-induced oxidative stress that favors osteoblast apoptosis but does not derogate adipocyte survival. On the basis of these findings, we propose a new concept of TZD-mediated mesenchymal stem cell lineage skewing that is shown in Figure 3.6. This new concept adds to the explanation of the reciprocal relationship between osteogenic and adipogenic lineages that is associated with bone loss in a variety of disease and aging models (recently reviewed by [130]).

A vast number of mechanistic studies have provided insight into TZD action on bone. Putative mechanisms include suppression of bone formation and stimulation of bone resorption that are caused by (a) preferential differentiation of MSCs into adipocytes at the expense of osteoblasts in the bone marrow [41, 45, 87, 88], (b) modulation of hormone levels that are important for bone metabolism, such as, leptin [89], insulin [90, 91], insulin-like growth factor I [92], or estrogen [93], and (c) stimulation of osteoclastogenesis by regulation of c-fos expression [86].

The evidence for a preferential differentiation of MSCs into adipocytes at the expense of

osteoblasts is, to date, based on mechanistic studies in murine osteoblastic cells that report a suppression of runx2 expression and promoter activity [41, 45, 87, 88]. The observed stimulation of RUNX2 expression by activated PPAR-γ in human MSCs and osteoblasts in the current study is, therefore, in contrast to the reported data in murine osteoblastic cells at first sight. But interestingly, we have found that RUNX2 expression is time-dependently affected by rosiglitazone. During early osteogenesis, expression levels are elevated in rosiglitazone - supplemented hMSCs and SV-HFO when compared to respective controls. However, during later differentiation stage, RUNX2 expression is diminished by rosiglitazone and PPAR-γ expression is increased in parallel. At first glance, this observation may be interpreted as transdifferentiation from the osteogenic towards the adipogenic lineage. However, it is well established that RUNX2 possesses a dual role in osteogenic differentiation with a positive role in osteogenic lineage commitment and a suppressive action on osteoblast maturation [131, 132]. The fact that expression levels of two well-known osteoblast maturation factors FOSL1 and ATF4 are upregulated at the same time point while RUNX2 levels are decreased suggests that rosiglitazone treatment causes stimulation of osteoblast maturation but not necessarily a transdifferentiation from an osteoblastic towards an adipocytic cell phenotype.

The involvement of PPAR-γ in adipogenesis is well established [122, 133, 134]. We have confirmed a dose-dependent pro-adipogenic effect of rosiglitazone in human MSCs that have been supplemented with dexamethasone, IBMX, and indomethacin to differentiate into the adipogenic lineage. However, supplementation of osteogenic medium (dexamethasone and β-glycerophosphate) with rosiglitazone is not sufficient to induce adipogenesis in hMSC cultures, as we have shown in two different donors.

We have described earlier that endogenous PPAR-γ1 expression is dynamically regulated during the differentiation process of human osteoblasts and osteogenic hMSCs whereas PPAR-γ2 expression is limited to adipocytes [121]. Rosiglitazone treatment results in homol-

ogous upregulation of PPAR-γ1 expression levels, but PPAR-γ2 expression remains virtually absent in the human osteoblast models SV-HFO [121], NHOst, and osteogenic hMSCs (data not shown). Therefore, the supplementation of osteoblast and osteogenic hMSC cultures with rosiglitazone is likely to reflect a condition of increased PPAR-γ1 activity. However, we have not observed any differences between PPAR-γ1- and PPAR-γ2 - overexpressing cells in regard to their osteoblastic phenotype. Therefore, these data do not provide unambiguous evidence for a PPAR-γ variant-specific effect. Future detailed analysis of PPAR-γ variant-specific interactions with the transcription initiation machinery as well as primary PPAR-γ variant-specific target genes in osteoblasts will be necessary to definitively clarify this aspect.

Our finding that rosiglitazone supplementation stimulates osteogenic differentiation from hMSCs, osteoblast maturation, and extracellular matrix mineralization reveals an unexpected role of PPAR-γ in osteogenic differentiation. Detailed analysis of the osteoblastic phenotype at multiple time points shows an acceleration of osteoblast development by activated PPAR-γ as shown by the early stimulation of RUNX2 and COL1A1 expression, ALP activity, and mineralization. We speculate here about a role of PPAR-γ as energy sensor and signaling component for the osteoblastic developmental process. This view is supported by the differentiation phase - dependent upregulation of PPAR-γ reaching the highest expression levels during mineralization onset [121]. The osteoblast differentiation process consists of several highly energy-demanding phases including matrix production, maturation, and mineralization [135], which is coordinated by a switch from glycolysis to respiration that involves increased mitochondrial biogenesis [136]. A role of PPARs in mitochondrial energetics has been demonstrated recently in a mouse model of mitochondrial myopathy [137] and T-cells [138]. Mitochondrial function of T-cells is improved when the concentrations of PPAR-γ agonists used are just in the sufficient range to induce transcriptional activity of PPAR-γ, whereas higher concentrations result in T-cell death [138]. In addition, high con-

centrations of PPAR-γ ligands induce mitochondrial dysfunction in human hepatocarcinoma cells [139] and astrocytes [140]. Mitochondrial dysfunction leads to partial reduction of oxygen that causes the formation of reactive oxygen species [141]. The latter activate signaling cascades, resulting in apoptosis [142].

Alternatively to a direct suppression of transcriptional networks involved in osteoblast differentiation, age-related shifts in mesenchymal stem cell commitment may be secondary to lineage - specific differences in susceptibility to oxidative stress and apoptosis, as has been hypothesized by Warren and Rossi for the hematopoietic system [128]. Our findings that rosiglitazone - stimulated PPAR-γ results in increased expression levels of genes involved in mitochondrial dysfunction, the generation of reactive oxygen species, and apoptosis of the osteogenic lineage but not the adipogenic lineage may explain the reduced number of fully differentiated osteoblasts *in vivo*. This reduction of mature osteoblasts due to premature death is likely to cause an immature or non-optimal bone matrix with lower quality. Further evidence for an apoptotic mechanism in PPAR-γ - mediated bone loss has been provided recently by Elbaz and co-workers. The authors have shown that fatty acids, which are natural PPAR-γ agonists, are released by adipocytes and cause osteoblast lipotoxicity by an apoptotic mechanism in a co-culture system consisting of normal human osteoblasts and pre-adipocytes [143]. In addition, Jung *et al.* have reported a caspase-dependent mechanism of troglitazone- induced apoptosis that is associated with downregulation of ERK and upregulation of p38 in the murine osteoblastic cell model MC3T3-E1 [144]. Kim and co-workers have published earlier the involvement of a MAPK signaling pathway upstream of mitochondria - dependent mechanism in ciglitazone-induced MC3T3 apoptosis [144]. Our data are also supported by the *in vivo* work of Soroceanu and co-workers, who have found decreased osteoblast number and activity due to increased apoptotic death of osteoblasts and osteocytes in five-week-old male non-diabetic C57BL/6 mice that have been treated an additional 90 days with rosiglitazone [145]. Furthermore, bone of these mice is histologically

characterized by decreased trabecular bone volume and increased marrow space with no significant change in bone marrow adipocity [145]. In contrast to this, Ali *et al.* have described bone loss associated with an increase in marrow adipocytes with no significant change in osteoblast lifespan in five-month-old Swiss Webster mice that have been treated with rosiglitazone for 28 days [47]. Divergent skeletal responses to rosiglitazone treatment have been observed more recently in a study with adult female mice from four different inbred strains (C3H/HeJ, DBA/2J, C57BL/6J, and A/J) [146]. It is, therefore, likely that multiple mechanisms contribute to TZD - induced bone loss and that, in mice studies, those are strongly dependent on the genetic background.

The new concept that derives from this study and explains TZD-induced bone loss stresses the importance of mitochondrial dysfunction, oxidative stress, and apoptosis in mesenchymal stem cell lineage skewing and bone loss. The involvement of oxidative stress in osteoblast apoptosis and bone loss has been shown in C57BL/6 mice with advancing age [147]. In these mice, an increase in the prevalence of apoptotic osteoblasts and a corresponding decrease in osteoblast number and bone-formation rate are accompanied by increased oxidative stress and diminished Wnt signaling, a critical regulator of bone formation [147]. A β-catenin-dependent mechanism of oxidative stress - induced PPAR-γ expression and suppressed Wnt3a signaling has been described recently by the same group [148]. Interestingly, despite increased PPAR-γ expression, oxidative stress, diminished Wnt signaling, and reduced osteoblast number in vertebrae of aged C57BL/6 mice, marrow adipocytes are not increased at this site [148]. Therefore, the diversion of MSCs to adipocytes may not be an obligatory part of the oxidative stress - induced anti-osteogenic cascade.

Human osteoblast cell models require glucocorticoids for proper initiation of differentiation and extracellular matrix (ECM) mineralization [119]. However, glucocorticoid - treated male Swiss Webster mice exhibit an increase in osteoblast apoptosis in vertebrae and show apoptosis in 28% of the osteocytes in metaphyseal cortical bone [149]. Increased osteoblast

and osteocyte apoptosis is also found in patients with glucocorticoid - induced osteoporosis [149]. Taken together, the actions of glucocorticoids and TZDs appear to have similarities, and it is conceivable that both nuclear receptors (glucocorticoid receptor and PPAR-γ) interact on common transcriptional networks that play a role in osteoblast apoptosis. In support of this, we have shown recently that PPAR-γ expression is directly induced by the synthetic glucocorticoid dexamethasone in human osteoblasts [121]. This suggests that PPAR-γ is a component of the glucocorticoid-mediated apoptosis pathway in bone.

In conclusion, our findings provide a new concept for TZD-induced bone loss and bone marrow adipogenesis. This concept is based on differences between osteogenic and adipogenic lineages in the susceptibility to oxidative stress, mitochondrial dysfunction, and apoptosis that is triggered by activated PPAR-γ. Therefore, improving mitochondrial function may be a successful strategy to prevent aging-related and TZD-induced bone loss.

Table 3.1
Primer and probe concentrations and sequences

Gene	Concentration (pmol/rct)		Sequence (5'-3')
ALPL	7.5	Forward	GACCCTTGACCCCCACAAT
	7.5	Reverse	GCTCGTACTGCATGTCCCCT
	1.25	Probe	TGGACTACCTATTGGGTCTCTTCGAGCCA
COL1A1	2.5	Forward	CAGCCGCTTCACCTACAGC
	2.5	Reverse	TTTTGTATTCAATCACTGTCTTGCC
	7.5	Probe	CCGGTGTGACTCGTGCAGCCATC
RUNX2	6.25	Forward	ACGTCCCCGTCCATCCA
	6.25	Reverse	TGGCAGTGTCATCATCTGAAATG
	2.5	Probe	ACTGGGCTTCCTGCCATCACCGA
BGLAP	25	Forward	CAGGAGGGCAGCGAGGTA
	25	Reverse	TGGGGCTCCCAGCCA
	5	Probe	TGATACAGGTAGCGCCTG
SSP1	12.5	Forward	CTCAGGCCAGTTGCAGCC
	12.5	Reverse	CAAAAGCAAATCACTGCAATTCTC
	5	Probe	AAACGCCGACCAAGGAAAACTCACTACC
ATF4	1.25	Forward	GTCCCTCCAACAACAGCAAG
	1.25	Reverse	TCCATTTTCTCCAACATCCA
FOSL1	1.25	Forward	AACCGGAGGAAGGAACTGAC
	1.25	Reverse	CTGCAGCCCAGATTTCTCAT
CYCS	1.25	Forward	GTCAGGCCCCTGGATACTCT
	1.25	Reverse	CTCCCCAGATGATGCCTTT
BAX	1.25	Forward	CTGAGCAGATCATGAAGACAGG
	1.25	Reverse	CTGCTCGATCCTGGATGAAA
CASP3	1.25	Forward	TGGAATTGATGCGTGATGTT
	1.25	Reverse	TGGCTCAGAAGCACACAAAC
CASP6	1.25	Forward	TGATGTGCAGCAATACAACAAG
	1.25	Reverse	CGCCTGTTTCAGGGATTCT
VDAC1	1.25	Forward	AAGTGAACAACTCCAGCCTGA
	1.25	Reverse	CACCAGCATTGACGTTCTTG
SLC25A4	1.25	Forward	CTGGTGTCCTACCCCTTTGA
	1.25	Reverse	CAGTCAACTGTCCCCGTGTA
SOD2	1.25	Forward	CAAATTGCTGCTTGTCCAAA
	1.25	Reverse	ACACATCAATCCCCAGCAGT
APAF1	1.25	Forward	TGATGGCATTCCTGTTGTCT
	1.25	Reverse	GGTACTCCACCTTCACACAGG
PPARA	1.25	Forward	GAAGCTGTCCTGGCTCAGAT
	1.25	Reverse	GAAGCTGGTGAAAGCGTGTC

Total PPARG	1.25	Forward	AGGCGAGGGCGATCTTG
	1.25	Reverse	CCCATCATTAAGGAATTCATGTCAT
PPARG2	1.25	Forward	CAAACCCCTATTCCATGCTGTT
	1.25	Reverse	AATGGCATCTCTGTGTCAACC
PPARD	1.25	Forward	GAAGACAGATGCACCAACGA
	1.25	Reverse	GTCTGAACGCAGATGGACCT
ANGPTL4	1.25	Forward	GACAAGAACTGCGCCAAGAG
	1.25	Reverse	AGTACTGGCCGTTGAGGTTG
FABP4	1.25	Forward	TACTGGGCCAGGAATTTGAC
	1.25	Reverse	GGACACCCCCATCTAAGGTT
CAT	1.25	Forward	GGAGCACAGCATCCAATATTCTG
	1.25	Reverse	AATGCCCGCACCTGAGTAAC
HMOX1	1.25	Forward	AGACTGCGTTCCTGCTCAAC
	1.25	Reverse	GCTCTGGTCCTTGGTGTCAT
EPHX1	1.25	Forward	CACCTGGACCAATACGGAAT
	1.25	Reverse	CCAGGGAGAACTTCCTTTCC
MGST1	1.25	Forward	CGAACAGATGACAGAGTAGAACG
	1.25	Reverse	AATATTTTCAAGGTCATTCAGGTG
GCLM	1.25	Forward	AGCTGTTGACTCACAATGATCC
	1.25	Reverse	TCCTGAAGAGCTTCTTGGAAA
GSTA4	1.25	Forward	CATGGCCCAGAAGGCTATAA
	1.25	Reverse	GCAAGGCTCAGCTGATTACC
GSTK1	1.25	Forward	TCCAGATTCCCATCCACTTC
	1.25	Reverse	GCATGGCAGACAAACTTCCT
NQO2	1.25	Forward	GAGGGCCACAGACAAAGATA
	1.25	Reverse	TTGTAGGCTTCGTGGGTTTC
ACTG2	1.25	Forward	CTGCCCTGAGACCCTCTTC
	1.25	Reverse	TCATGAATTCCAGCGGACTC
PRKCA	1.25	Forward	AGATCCAGCCACCATTCAAG
	1.25	Reverse	TGTTAAGACGGGCTGTCCTC
MAP3K5	1.25	Forward	TGGGAAACTCGACTTTGGAG
	1.25	Reverse	ATCTCCACCACCGCAATATC

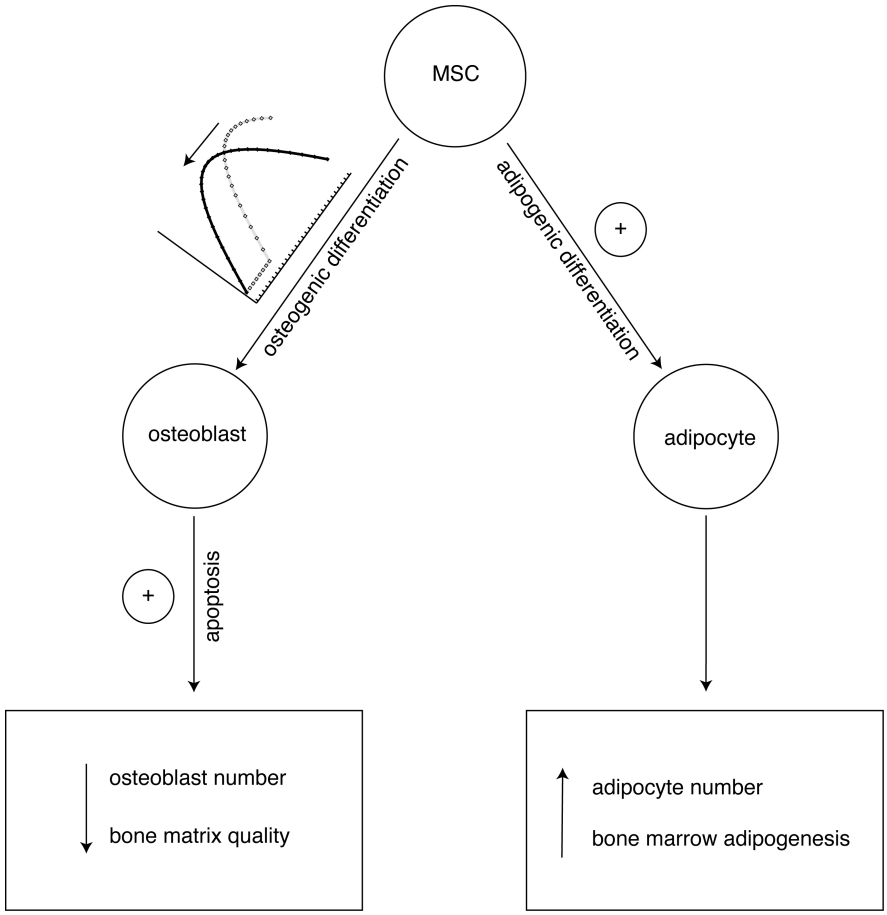

Figure 3.6
Schematic representation of the new concept derived from this study that adds to the explanation of thiazolidinedione (TZD)- induced bone loss. TZD-mediated activation of peroxisome proliferator- activated receptor γ (PPAR-γ) accelerates osteoblast differentiation as indicated by the line graph illustrating the shift in time. Concomitantly there is a stimulation of adipogenesis from MSCs. The phase of accelerated osteoblast differentiation, energy expenditure, and reactive oxygen species production is ultimately followed by increased osteoblast apoptosis, whereas the survival of adipocytes is not affected by TZDs. Therefore, osteogenic and adipogenic lineages reveal differential susceptibilities to TZD-induced apoptosis. This concept builds the molecular basis for the clinically observed bone marrow adipogenesis, diminished bone formation, and increased fracture rate in TZD-treated patients. Abbreviations: MSC, mesenchymal stem cell.

4 Physiological interactions of 1α,25-dihydroxyvitamin D3 and rosiglitazone

4.1 Abstract

Both vitamin D receptor (VDR) and peroxisome proliferator-activated receptor γ (PPAR-γ) are ligand - activated nuclear transcription factors that are instrumental for bone health. While 1α,25-dihydroxyvitamin D3 (1,25D3), the ligand for VDR, is essential for the development and maintenance of healthy bone, PPAR-γ agonists cause detrimental skeletal effects. Recent studies have revealed evidence for a cross-talk between 1,25D3- and PPAR-α/δ ligand - mediated signaling but there is a current lack of knowledge regarding cross-talk between signaling of 1,25D3 and the PPAR-γ ligand - mediated signaling. In this study, we investigated the cross-talk between 1,25D3- and PPAR-γ agonist rosiglitazone - mediated signaling in human osteoblasts. 1,25D3 slightly but significantly induced expression of

Viola J. Woeckel, Claudia Bruedigam, Marijke Koedam, Hideki Chiba, Bram C.J. van der Eerden, Johannes P.T.M. van Leeuwen: *1α25-dihydroxyvitamin D3 and rosiglitazone synergistically enhance osteoblast-mediated mineralization*; 2013; 512:438-443; Gene

the primary PPAR-γ target gene ANGPTL4 but did not influence FABP4. 1,25D3 did not change rosiglitazone regulation of ANGPTL4 and FABP4. The other way around, rosiglitazone reduced CYP24A1 gene expression but this did not change CYP24A1 induction by 1,25D3. The findings regarding CYP24A1 gene expression are in line with the observation that 1,25D3 levels in medium were not affected by rosiglitazone. Furthermore, rosiglitazone significantly inhibited 1,25D3-induction of BGLAP while rosiglitazone alone did not change BGLAP. Additionally, 1,25D3 and rosiglitazone increased osteoblast alkaline phosphatase activity and synergistically stimulated extracellular matrix mineralization. In conclusion, these data provide evidence for a cross-talk between rosiglitazone- and 1,25D3-mediated signaling leading to an acceleration of extracellular matrix mineralization. The data suggest that the reduction of the mineralization inhibitor BGLAP and the increased differentiation status underlie the increased mineralization.

4.2 Introduction

Being one of the major factors in calcium homeostasis, vitamin D is essential for the development and maintenance of healthy bones. 1α,25-dihydroxyvitamin D3 (1,25D3), the biologically most active vitamin D receptor (VDR) agonist, is synthesized by subsequent vitamin D 25-hydroxylase (CYP2R1) and 25-hydroxyvitamin D-1α-hydroxylase (CYP27B1) activity in the liver and kidney, respectively [97]. Bone formation is indirectly influenced by 1,25D3 since it promotes calcium uptake in the intestine and promotes calcium reabsorption in the kidneys. Also direct effects of 1,25D3 on osteoblasts have been established. 1,25D3 stimulates mineralization of human osteoblast cultures [99,150] and modulates gene expression of various osteoblast differentiation - and mineralization - related genes such as alkaline phosphatase (ALPL), osteocalcin (BGLAP) and osteopontin (SPP1) [97, 98, 100, 101]. 1,25D3 also enhances osteoblast-produced matrix vesicle maturation [102]. To prevent uncontrolled

1,25D3 action and potentially hypercalcemia, 1,25D3 stimulates its own degradation by up-regulating the expression of 24,25D3-hydroxylase (CYP24A1) [98, 103].

The synthetic peroxisome proliferator-activated receptor γ (PPAR-γ) agonist rosiglitazone belongs to the thiazolidinediones (TZD) and is an insulin sensitizer. Recent clinical studies have revealed detrimental effects of rosiglitazone on the aging skeleton [40]. Underlying mechanisms include rosiglitazone - mediated suppression of bone formation and stimulation of bone resorption caused by a) stimulation of osteoclast differentiation from hematopoietic precursor cells [86], b) increased osteoblast and osteocyte apoptosis [143–145,151,152], c) preferential differentiation of mesenchymal stem cells into adipocytes at the expense of osteoblasts in the bone marrow [41, 45, 87, 88], or d) modulation of hormones important for bone metabolism, e.g. leptin [89], insulin [90, 91], insulin-like growth factor I [92], or estrogen [93]. Recently, we published a pro-apoptotic effect of rosiglitazone causing a premature onset of mineralization in human osteoblasts and vascular smooth muscle cells [151].

Both VDR and PPAR-γ are nuclear receptors that form heterodimers with the retinoid X receptor (RXR). Moreover, recent studies have revealed evidence for a cross-talk between 1,25D3- and PPAR-α/-δ- ligand - mediated signaling involving a stimulatory effect of 1,25D3 on PPAR expression that is dependent on VDR [104, 105]. However, there is a current lack of knowledge regarding cross-talk between 1,25D3- and PPAR-γ-ligand - mediated signaling. In this study, we therefore investigated the interaction between 1,25D3- and PPAR-γ-ligand - mediated signaling in the context of osteoblast differentiation and mineralization.

4.3 Materials and Methods

4.3.1 Cell culture

The human pre-osteoblast cell line SV-HFO [112] was cultured as described previously [113]. To induce osteoblast differentiation, medium (αMEM; Gibco BRL, Life Technologies) was supplemented with freshly added 10 mM β-glycerophosphate (Sigma-Aldrich) and 100 nM dexamethasone (Sigma-Aldrich) and replaced every 2 or 3 days. As supplements 10 nM 1,25D3 (Leo Pharmaceuticals), 100 nM rosiglitazone (Cayman Chemicals) or a combination of both were used. Cells were harvested at different time points during culture.

4.3.2 Quantification of mRNA expression

Cultures continuously treated with control, 10 nM 1,25D3, 100 nM rosiglitazone or a combination were harvested during the pre-mineralization period (day 5 or 7) and at the onset of mineralization (day 9 or 12, depending on the experiment). RNA isolation, cDNA synthesis and PCR reactions were performed as described previously [102, 121]. Oligonucleotide primer pairs, all being either on exon boundaries or spanning at least one intron, were purchased from Sigma-Aldrich. Sequences and concentrations used are displayed in Table 4.1 Gene names and symbols were used as provided by the HUGO Gene Nomenclature Committee [153].

4.3.3 Quantification of 1,25D3 levels

SV-HFO conditioned medium samples from the cultures at the onset of mineralization (day 9 or 12, respectively of experiment) were analyzed for 1,25D3 concentration by using 1,25-dihydroxyvitamin D RIA (IDS; immunodiagnostic systems) according to the manufacturer's

Table 4.1
Primer and probe concentrations and sequences

		Sequence (5'-3')	Concentration (pmol/rct)
GAPDH	Forward	ATGGGGAAGGTGAAGGTCG	3.75
	Reverse	TAAAAGCAGCCCTGGTGACC	3.75
	Probe	CGCCCAATACGACCAAATCCGTTGAC	3.75
CYP24A1	Forward	CAAACCGTGGAAGGCCTATC	15
	Reverse	AGTCTTCCCCTTCCAGGATCA	15
	Probe	ACTACCGCAAAGAAGGCTACGGGCTG	7.5
BGLAP	Forward	CAGGAGGGCAGCGAGGTA	25
	Reverse	TGGGGCTCCCAGCCA	25
	Probe	TGATACAGGTAGCGCCTG	5
SPP1	Forward	CTCAGGCCAGTTGCAGCC	12.5
	Reverse	CAAAAGCAAATCACTGCAATTCTC	12.5
	Probe	AAACGCCGACCAAGGAAAACTCACTACC	5
COL1A1	Forward	CAGCCGCTTCACCTACAGC	2.5
	Reverse	TTTTGTATTCAATCACTGTCTTGCC	2.5
	Probe	CCGGTGTGACTCGTGCAGCCATC	7.5
ALPL	Forward	GACCCTTGACCCCCACAAT	7.5
	Reverse	GCTCGTACTGCATGTCCCCT	7.5
	Probe	TGGACTACCTATTGGGTCTCTTCGAGCCA	1.25
PPARG	Forward	AGGCGAGGGCGATCTTG	1.25
	Reverse	CCCATCATTAAGGAATTCATGTCAT	1.25
ANGPTL4	Forward	GACAAGAACTGCGCCAAGAG	1.25
	Reverse	AGTACTGGCCGTTGAGGTTG	1.25
FABP4	Forward	TACTGGGCCAGGAATTTGAC	1.25
	Reverse	GGACACCCCCATCTAAGGTT	1.25

instructions.

4.3.4 Statistics

The data provided are based on multiple independent experiments derived from four independent cultures. Values are means $\pm$ S.E. Significance was calculated using the Student's t-test and 2-way ANOVA. P-values ≤ 0.05 were considered as statistically significant.

4.4 Results

4.4.1 1,25D3 effects on primary PPAR-γ target genes

We investigated the effects of 1,25D3 on endogenous osteoblastic PPAR-γ signaling by measuring transcript levels of established primary PPAR-γ target genes in rosiglitazone, 1,25D3 and 1,25D3 / rosiglitazone co-treated human osteoblasts during the pre-mineralization period and at the onset of mineralization. At both time points, rosiglitazone increased expression levels of the primary PPAR-γ target genes angiopoietin-like 4 (ANGPTL4; Figure 4.1 A and C) and fatty acid binding protein 4 (FABP4; Figure 4.1 B and D). 1,25D3 induced ANGPTL4 expression during the pre-mineralization period and during the onset of mineralization (Figure 4.1 A and C). Treatment with 1,25D3 did not change expression levels of FABP4 (Figure 4.1 B and D) and co-treatment with rosiglitazone did not reveal any significant interactions on both PPAR-γ targets (Figure 4.1 A - D).

4.4.2 Rosiglitazone effects on CYP24A1 expression and activity

To investigate the effects of rosiglitazone on endogenous osteoblastic 1,25D3 signaling, we measured the transcript levels of the well-established primary 1,25D3 target gene CYP24A1 in SV-HFO cultures treated with rosiglitazone, 1,25D3 or a combination of rosiglitazone / 1,25D3 during the pre-mineralization period and at the onset of mineralization. CYP24A1 expression was significantly increased by 1,25D3 at both time points (Figure 4.2 A and B). Interestingly, rosiglitazone reduced basal but not 1,25D3-induced CYP24A1 expression during pre-mineralization (Figure 4.2 A) but not at the onset of mineralization (Figure 4.2 B). To determine whether rosiglitazone affects 1,25D3 levels as has been reported before *in vitro* and *in vivo* [105, 154], we analyzed conditioned medium collected at the onset of mineralization from cultures treated with rosiglitazone, 1,25D3 and the combination thereof.

We found the expected increase in 1,25D3 levels in cultures treated with 1,25D3 but the presence of rosiglitazone didn't affect these levels (Figure 4.2 C).

4.4.3 Rosiglitazone effects on BGLAP, SPP1 and COL1A1 expression

BGLAP and SPP1 are well-established 1,25D3 target genes, which have been reported as inhibitors of mineralization [155–158]. We investigated the rosiglitazone and 1,25D3 effects on BGLAP and SPP1. BGLAP expression was increased by 1,25D3 during pre-mineralization and mineralization (Figure 4.3 A and B). Rosiglitazone did not affect BGLAP expression during the pre-mineralization period (Figure 4.3 A) but significantly reduced the 1,25D3-induced BGLAP expression at the onset of mineralization (Figure 4.3 B). SPP1 expression was increased in the pre-mineralization phase only in 1,25D3 / rosiglitazone treated osteoblasts, whereas during mineralization SPP1 expression was increased in all conditions, being 2-fold up-regulated by 1,25D3 and rosiglitazone and 4-fold up-regulated by co-treatment of both agents (data not shown). We also studied the effects of 1,25D3 and rosiglitazone on COL1A1. Rosiglitazone reduced COL1A1 expression in the pre-mineralization phase but during mineralization neither 1,25D3 nor rosiglitazone affected COL1A1 expression (data not shown).

4.4.4 Rosiglitazone and 1,25D3 enhance ALPL activity and synergistically enhance mineralization of human osteoblast cultures

We investigated the effects of rosiglitazone and 1,25D3 and their combination on the phenotype of human pre-osteoblasts. DNA content was similar between 1,25D3 - treated cultures and controls and was significantly reduced in all cultures treated with rosiglitazone (Figure

4.4 A). Both 1,25D3 and rosiglitazone increased ALPL activity and combination treatment showed an additive effect on ALPL activity (Figure 4.4 B), which was confirmed by gene expression (data not shown). Finally, 1,25D3 as well as rosiglitazone increased mineralization in SV-HFO cultures (Figure 4.4 C). Furthermore, the combination of both compounds showed a synergistic stimulation of mineralization (Figure 4.4 C).

4.5 Discussion

The current study demonstrates for the first time that the PPAR-γ agonist rosiglitazone and the VDR ligand 1,25D3 synergistically stimulate extracellular matrix mineralization by human osteoblasts. Although rosiglitazone is a known inhibitor of mineralization, it also causes pro-apoptotic effects leading to a premature onset of mineralization in human osteoblasts [151, 159]. Thereby, both rosiglitazone and 1,25D3 enhance mineralization in human SV-HFO [99, 150]. The current observations demonstrating synergism suggest that VDR and PPAR-γ - mediated stimulation of mineralization share common mechanisms. It is likely that these compounds target common transcriptional networks underlying these physiological processes. VDR and PPAR-γ share the retinoid X receptor (RXR) as a common heterodimeric partner. RXR could have been a limiting factor in case of concomitant activation of VDR and PPAR-γ but the observed synergism suggests that RXR is not a limiting factor.

The precise mechanisms shared by VDR and PPAR-γ to stimulate mineralization remain yet to be delineated. However, an interesting gene and potential mechanism for the regulation of mineralization by 1,25D3 and rosiglitazone is BGLAP. In humans, 1,25D3 strongly induces BGLAP expression [160], which inhibits *de novo* mineralization by delaying nucleation of hydroxyapatite [157, 158]. In addition, BGLAP deficient mice have a bone mineral maturation defect [161]. A reduction of BGLAP activity increases the 1,25D3 potency to

stimulate mineralization (Woeckel et al., in preparation). Here we show that rosiglitazone reduces 1,25D3-induced BGLAP expression during the onset of mineralization but not during the pre-mineralization period which is expected considering the role of BGLAP during the process of mineralization. This is also in line with studies reporting inhibitory effects of PPAR signaling on BGLAP expression. For example, TZD treatment of bone marrow stromal cells which stably express PPAR-γ showed suppression of BGLAP expression [41]. Additionally, murine bone marrow cells from PPAR-γ-deficient heterozygous mice exhibited increased BGLAP expression and a reintroduction of PPAR-γ suppressed BGLAP expression [49]. In contrast to BGLAP, SPP1 gene expression, encoding osteopontin as another inhibitor of mineralization [155, 156], was increased in 1,25D3 / rosiglitazone treated osteoblasts. This is not in line with our observation that mineralization is increased in 1,25D3 / rosiglitazone - treated osteoblasts. However, it appears that SPP1- mediated inhibition of mineralization is strongly related to the phosphorylation status of osteopontin [54] indicating that increased SPP1 gene expression does not directly implicate increased inhibition of mineralization.

Based on literature and our osteoblast mineralization studies, it is tempting to speculate that the synergistic stimulation of 1,25D3-induced mineralization by rosiglitazone is partly based on the reduction of 1,25D3-induced BGLAP expression. Additionally, the enhanced differentiation status of co-treated osteoblasts, as assessed by ALPL activity, could play a role in the observed enhanced mineralization. Furthermore, it has been shown that apoptosis is actively involved in mineralization [34]. We have recently shown in osteoblasts that low oxygen (2%) led to reduced apoptosis and decreased mineralization [162]. In line with this we have also demonstrated that rosiglitazone increased apoptosis in osteoblasts which was accompanied by enhanced mineralization [151]. Both rosiglitazone and 1,25D3 induce apoptosis and can have anti-proliferative effects [151,163,164], which can be another shared mechanism with regard to enhanced mineralization. Unraveling potential interactions at the

level of apoptosis are subject to further studies.

We also studied regulation of CYP24A1 expression as a potential level of interaction. CYP24A1 encodes for the enzyme 24-hydroxylase, the rate limiting step in 1,25D3 degradation and thereby limiting the 1,25D3 activity [165]. 1,25D3 is the most potent inducer of CYP24A1 but we found that in the absence of 1,25D3 rosiglitazone is also able to reduce CYP24A1 expression in human osteoblasts during the pre-mineralization phase, which is a crucial period for 1,25D3-stimulated mineralization [102]. Observations regarding CYP24A1 expression have been reported in melanoma cells, in which the non-specific PPAR ligands bezafibrate and alpha-linolenic acid reduced the 1,25D3-mediated elevation of CYP24A1 [105]. We noted that the inhibitory effect of rosiglitazone was minute compared to the strong induction by 1,25D3, which was confirmed by unaltered 1,25D3 levels. Nevertheless, these data suggest that rosiglitazone is able to modify 1,25D3 metabolism. This was demonstrated by Chakreeyarat *et al.* who recently reported increased circulating levels of 25-hydroxyvitamin D3 in postmenopausal women treated with TZDs [154]. Whether the observed elevated 25-hydroxyvitamin D3 also led to increased levels of 1,25D3 was not investigated. Taken together, further studies have to be completed to identify mechanisms of rosiglitazone - mediated modification of 1,25D3 metabolism in osteoblasts. However, although rosiglitazone can affect CYP24A1 mRNA expression the current data exclude that reduced 1,25D3 metabolism explains the increased mineralization.

Finally, we demonstrate that 1,25D3 can regulate primary PPAR-γ target gene ANGPTL4 suggesting that PPAR-γ signaling is targeted by 1,25D3. This small effect of 1,25D3 on PPAR-γ signaling is in line with recent studies that showed no or minor effects of 1,25D3 treatment on PPAR-γ expression and signaling in various melanoma cell lines and other cell lines not derived from the skin [105, 166]. Whether the regulation of ANGPTL4 plays a role in the synergistically enhanced mineralization, seems unlikely as in the combination treatment the effect of PPAR-γ activation by rosiglitazone is dominant. Nevertheless, the

1,25D3 effect on ANGPTL4 together with the rosiglitazone effect on CYP24A2 expression further points to cross-regulation of PPAR-γ - and VDR transcriptional cascades. In summary, we show that rosiglitazone and 1,25D3 synergistically increase mineralization by human osteoblasts. In these osteoblasts we observed an advanced differentiation status, reduced BGLAP and increased SPP1 expression. These data demonstrate interplay between two nuclear hormone receptor signaling cascades that share at least dimerization with RXR in the control of osteoblast activity.

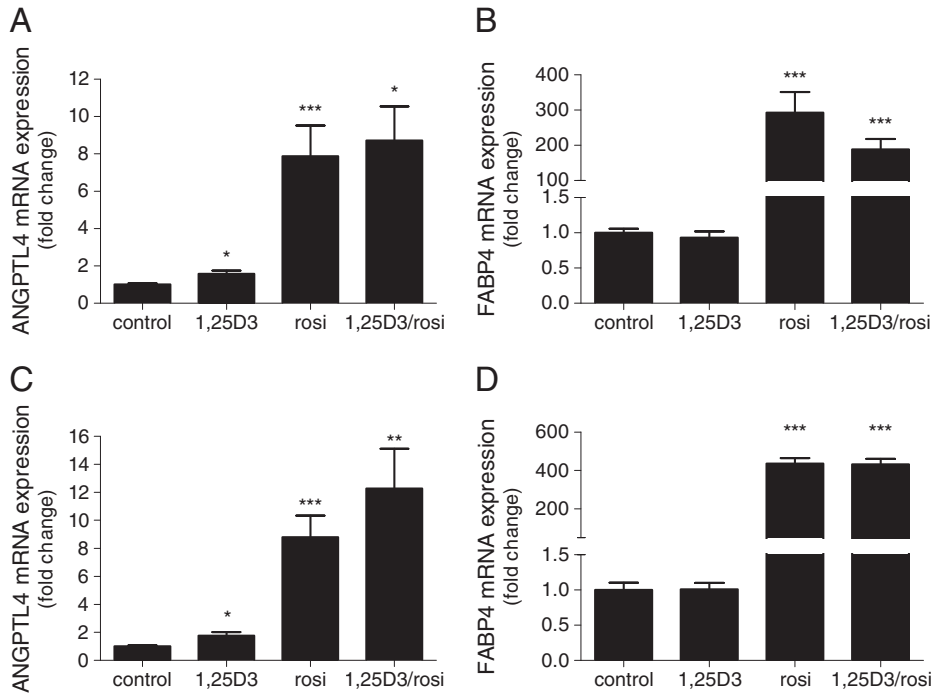

Figure 4.1
The effects of 1,25D3 on primary PPAR-γ target genes in human osteoblasts. SV-HFO cells were harvested in the 1st week of differentiation (A and B) and at the onset of mineralization (C and D) to isolate RNA. mRNA expression of ANGPTL4 (A and C) and FABP4 (B and D) cells were determined by q-RT-PCR. Expression is relative to GAPDH and depicted in fold change to control. *$p \leq 0.05$, **$p \leq 0.01$, and ***$p \leq 0.001$ significantly different from control cultures.

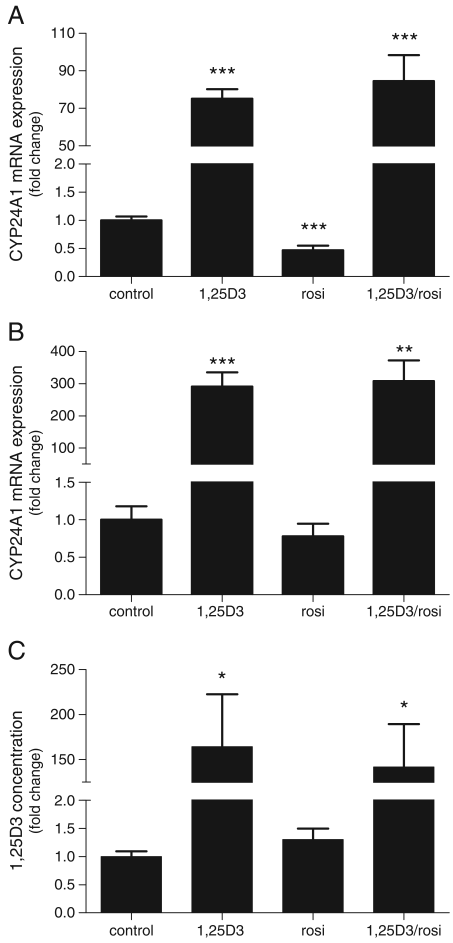

Figure 4.2
Rosiglitazone effects on CYP24A1 expression and activity. SV-HFO cells were harvested in the 1st week of differentiation (A) and at the onset of mineralization (B) and RNA was isolated. mRNA expression of CYP24A1 was determined by q-RT-PCR. Expression is relative to GAPDH and depicted in fold change to control. C) SV-HFO cells were cultured until the onset of mineralization with control, 1,25D3, rosiglitazone or a co-treatment of rosiglitazone / 1,25D3. At this time point medium was collected and 1,25D3 levels were quantified by 1,25-dihydroxyvitamin D3 RIA. *$p \leq 0.05$, **$p \leq 0.01$, and ***$p \leq 0.001$ significantly different from control cultures.

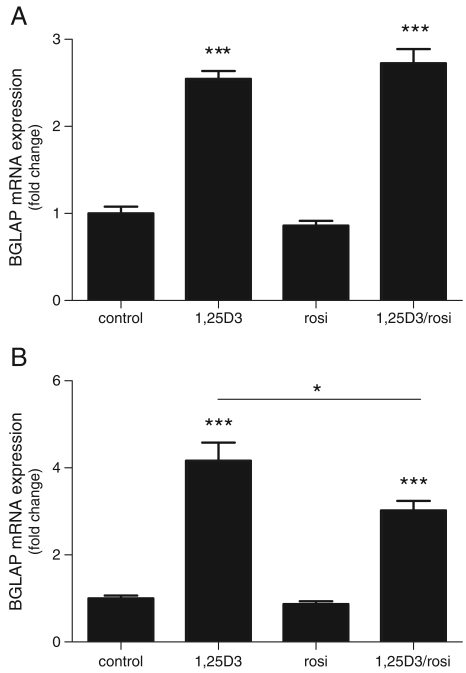

Figure 4.3
Rosiglitazone effects on BGLAP expression. SV-HFO cells were harvested in the 1st week of differentiation (A) and at the onset of mineralization (B) and RNA was isolated. mRNA expression of BGLAP was determined by q-RT-PCR. Expression is relative to GAPDH and depicted in fold change to control. *p $\leq$ 0.05, **p $\leq$ 0.01, and ***p $\leq$ 0.001 significantly different from control cultures. Interaction effects determined by 2-way ANOVA resulted in a p-value of 0.058.

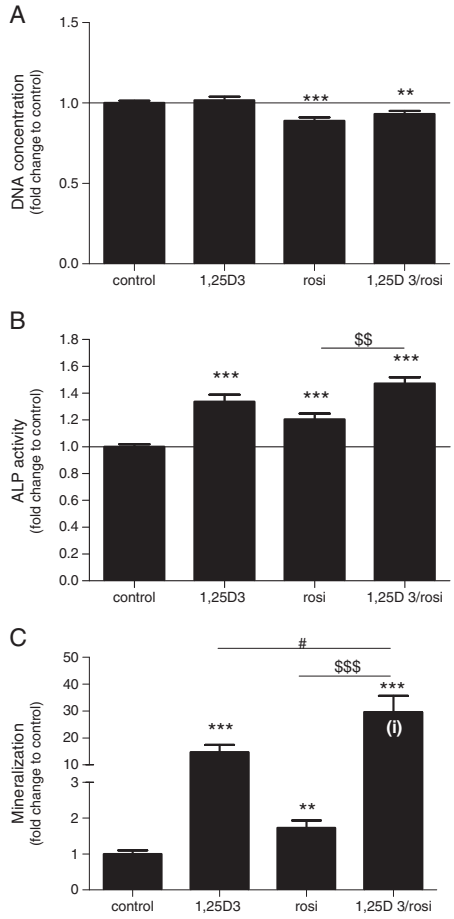

Figure 4.4
Rosiglitazone and 1,25D3 increase osteoblast differentiation and synergistically enhance mineralization. SV-HFO osteoblasts were cultured until the onset of mineralization followed by analyses of A) DNA content as a measure of cell growth, B) ALPL activity as read-out for differentiation and C) calcium measurement reflecting mineralization. Values represent fold-changes to respective controls from two independent experiments. **p $\leq$ 0.01 and ***p $\leq$ 0.001 significantly different from control cultures. #: p $\leq$ 0.05 significantly different from 1,25D3 cultures. $$: p $\leq$ 0.01 and $$$: p $\leq$ 0.001 significantly different from rosiglitazone cultures. i: p $\leq$ 0.05 for 2-way ANOVA significance of interaction.

5 Opposing actions of rosiglitazone and resveratrol on mineralization

5.1 Abstract

Arteriosclerotic vascular disease is a major cardiac health problem in westernized countries and the primary cause of mortality in diabetic patients. Recent data have raised serious safety concerns with the antidiabetic rosiglitazone, a thiazolidinedione with peroxisome proliferator-activated receptor γ (PPAR-γ) agonistic activity, in regard to cardiovascular risks. A common feature of atherosclerosis is vascular mineralization. The latter is formed by vascular smooth muscle cells (VSMC) through complex processes that are similar to mineralization in bone. The aim of the current study was to investigate the effect of rosiglitazone on mineralization in cultured human VSMCs. We found that rosiglitazone stimulated mineralization by, at least in part, induction of caspase-dependent apoptosis. Furthermore, rosiglitazone-induced oxidative stress was correlated with stimulated osteoblast-like differentiation of VSMCs. Treatment of rosiglitazone-supplemented VSMC cultures with the

Claudia Bruedigam, Marco Eijken, Marijke Koedam, Hideki Chiba, Johannes P.T.M. van Leeuwen: *Opposing actions of rosiglitazone and resveratrol on mineralization in human vascular smooth muscle cells*; 2011; 51(5):862-71; Journal of Molecular and Cellular Cardiology

caloric restriction mimetic and antioxidant resveratrol diminished rosiglitazone-induced oxidative stress, osteoblast-like differentiation and mineralization. In conclusion, this study reveals novel insights into the relationship of rosiglitazone and cardiovascular events by providing a model that links rosiglitazone-induced osteoblast-like differentiation, oxidative stress and apoptosis with mineralization in VSMCs. In addition, we position resveratrol in this model acting to reduce rosiglitazone-induced oxidative stress, osteoblast-like VSMC differentiation and mineralization.

5.2 Introduction

Vascular mineralization is a prominent feature of advanced atherosclerosis. Although atherosclerosis and vascular mineralization are currently considered to form separate genetic entities, mineralization contributes to the overall morbidity of atherosclerosis by causing an increased risk for myocardial infarction [19–22]. The latter is caused by, at least in part, a decreased elasticity of the vessels [23,24]. Bone-associated proteins such as osteonectin, osteocalcin, and matrix Gla protein have been detected in mineralized vascular tissues. Therefore, vascular mineralization has been considered to be an organized and highly regulated process that is similar to mineralization in bone tissue. Vascular smooth muscle cells (VSMCs) are currently considered as being responsible for the formation of vascular mineralization *in vivo*. In more detail, mechanical and inflammatory redox signals from the aortic vasculature have emerged as secretagogues for BMP that leads to activation of endothelial NADPH oxidases and subsequent generation of reactive oxygen species (ROS) [25–27]. These paracrine signals augment aortic myofibroblast Msx2-Wnt signaling and matrix turnover and promote osteoblast-like differentiation of VSMCs [28–31, 33]. Furthermore, oxidation of vascular LDL cholesterol generates oxysterols that trigger RUNX2 activity via hedgehog pathways [32]. Interestingly, apoptosis of VSMCs appears to be an additional key factor in

vascular mineralization [34–36]. VSMC apoptosis is sufficient to accelerate atherosclerosis, to promote plaque mineralization and medial degeneration, to prevent expansive remodeling and to promote stenosis in atherosclerosis [38, 39, 167]. Rosiglitazone is a synthetic peroxisome proliferator-activated receptor γ (PPAR-γ) agonist belonging to the thiazolidinedione class of compounds and is currently prescribed as an antidiabetic drug. It improves insulin sensitivity and lowers blood glucose and lipid levels. Despite these beneficial metabolic actions, serious cardiovascular side effects have been reported for rosiglitazone in recent epidemiological studies [72–75, 168]. Most interestingly for this study, rosiglitazone treatment has been linked to an increased risk for myocardial infarction [72, 73]. Rosiglitazone and other PPAR agonists have been shown earlier to induce apoptosis of human and rodent VSMCs via PPAR- dependent and - independent mechanisms [76–80]. However, despite this evidence for rosiglitazone - induced VSMC apoptosis and the established key role of apoptosis in VSMC mineralization, there is a current lack of knowledge in regard to the direct role of rosiglitazone in VSMC-mediated vascular mineralization.

In the current study, we investigated the effect of rosiglitazone on mineralization in human VSMCs. We found that rosiglitazone increased mineralization by combined stimulatory actions on osteoblast-like differentiation, oxidative stress and caspase-mediated apoptosis of human VSMCs. The caloric restriction mimetic and antioxidant resveratrol counteracted this by reducing rosiglitazone-induced oxidative stress, apoptosis and osteoblast-like VSMC differentiation.

5.3 Materials and Methods

5.3.1 Cell culture

Human coronary artery smooth muscle cells (VSMC; Lonza CC-2583) were cultured as described in [113]. Culture conditions were chosen based on those standard conditions for optimal osteoblast-like differentiation of human VSMCs [169]. In more detail, the differentiation medium contained DMEM with high glucose (25 mM D-glucose), 10% heat-inactivated FCS, 0.1 μM dexamethasone and 10 mM β-glycerophosphate.

The human pre-osteoblast cell line SV-HFO was cultured as described previously [113]. The differentiation medium contained α-MEM with 2% charcoal-stripped FCS, 0.1μM dexamethasone and 10 mM β-glycerophosphate.

Rosiglitazone (Cayman Europe) was added to the cultures every 2-3 days when medium was refreshed. At time of medium refreshment, caspase inhbitor Z-VAD-FMK (Promega) and resveratrol (Sigma Aldrich) were added to the cultures in order to block apoptosis and scavenge radicals, respectively.

5.3.2 DNA, protein, alkaline phosphatase activity and mineralization assays

ALPL, DNA, protein and calcium measurements were performed as described previously [113]. In addition, extracellular calcium and hydroxyapatite were stained using calcein (Sigma-Aldrich). Culture medium was replaced with calcein solution (1.7 μM calcein, 1 mM KOH) in osteogenic differentiation medium and incubated for 2 h at 37°C. Cultures were washed with PBS and supplemented with differentiation medium. Microscopic images were acquired immediately and processed using Cell profiler software (http://www.cellprofiler.org).

5.3.3 Measurement of reactive oxygen species

Superoxide radicals were measured using Mitosox red mitochondrial superoxide indicator (Molecular Probes, Invitrogen) according to the manufacturer's instructions. Microscopic images were processed using Cell profiler software (http://www.cellprofiler.org). Total reactive oxygen species were measured using the cell-permeable non-fluorescent probe 2'-7'- dichlorofluorescin diacetate (DCF-DA; Sigma) which is de-esterified intracellularly and turns into highly fluorescent 2',7'-dichlorofluorescin upon oxidation. Culture medium was replaced with 10 μM DCF-DA in modified ringer buffer (125 mM NaCl, 5 mM KCl, 1.2 mM KH2PO4, 25 mM Hepes, 6 mM glucose, 1.2 mM MgSO4 and 1 mM CaCl2, pH 7.4) and incubated for 1 h at 37°C. Cultures were washed with PBS, supplemented with differentiation medium and the fluorescence signal was quantified using Victor2 1420 multilabel counter (Wallac, MA).

5.3.4 Apoptosis measurement

Apoptotic cells were counted by fluorescent-activating cell sorting using FacsCanto II apparatus (BD Biosciences) after staining with 1 μg/ml FITC-labelled annexin-V (IQ-Products) and 0.25 μg/ml propidium iodide (Nexins research) according to the manufacturer's instructions.

5.3.5 Quantification of mRNA expression

RNA isolation, cDNA synthesis and quantitative RT-PCR (QPCR) have been carried out as described recently [121]. Primer and probe sequences and concentrations are displayed in Table 5.1

5.3.6 Statistics

Data presented are the results of at least two independent experiments performed in at least triplicate. Values are the means ± S.E. Significance ($p \leq 0.05$) was calculated using the Student's T-test and displayed in the Figures with asterisks (*). Two-way ANOVA were carried out using SPSS statistics software. Significant interaction effects ($p \leq 0.05$) were displayed in the Figures with hash symbols (#).

5.4 Results

5.4.1 Rosiglitazone induces mitochondrial dysfunction and apoptosis in VSMC cultures

Human vascular smooth muscle cells were induced with dexamethasone and β-glycerophosphate to differentiate in an osteoblast-like manner and to produce and mineralize an extracellular matrix formed in a three-week time period [170]. Using this model of vascular mineralization, we showed that treatment with rosiglitazone resulted in a significant higher percentage of apoptotic cells in a time window that started three days prior to the onset of ECM mineralization (Figure 5.1 A). The chosen concentration of 10 μM for rosiglitazone is well within the range measured in the serum of rosiglitazone-treated patients (i.e. rosiglitazone at 8 mg yields a maximum serum concentration of 598 ± 117 ng / ml or 1.67 μM; Avandia package insert). In addition, rosiglitazone-supplemented cultures contained significantly higher ROS levels during that period (Figure 5.1 B). To investigate whether this was correlated with increased mitochondrial dysfunction, we measured the expression of marker genes in control and rosiglitazone - supplemented conditions. Interestingly, expression of all mitochondrial dysfunction marker genes analyzed was increased in rosiglitazone - supplemented VSMC cultures (Figure 5.1 C). These changes were correlated with increased

PPAR-γ signaling as shown by increased PPAR-γ expression and transcription of its well-confirmed primary target gene ANGPTL4 (Figure 5.1 D).

5.4.2 Rosiglitazone stimulates extracellular matrix mineralization of VSMCs

VSMCs were cultured in the continuous presence of 10 μM rosiglitazone and the mineralization process was subsequently investigated and compared to control cultures. As shown in Figure 5.2 A, rosiglitazone stimulated ECM mineralization, and this effect was dose-dependent (Figure 5.2 B). The osteoblast-like differentiation process leading to mineralizing VSMCs was characterized by changes in cell patterns (Figure 5.2 B). Interestingly, Garfinkel and co-workers had described earlier such VSMC pattern changes in mineralizing VSMC cultures mathematically using a reaction-diffusion model based on the known kinetics of BMP2 and matrix carboxyglutamic acid protein (MGP), an inhibitor of BMP2 [171].

5.4.3 Rosiglitazone - mediated induction of mineralization partly depends on apoptosis

We studied the localization of mineralization spots and areas containing accumulated superoxide anion radicals microscopically. Interestingly, spots with accumulated superoxide anion

Figure 5.1 (following page)
Rosiglitazone induces ROS and apoptosis in VSMCs. A) Apoptosis was quantified by fluorescence - activated cell sorting (FACS) of annexin-V-FITC - labeled cells from 10 μM rosiglitazone - supplemented VSMC cultures (white bars) and controls (black bars) at different timepoints of culture. B) Superoxide anion radicals were quantified by Mitosox staining at day 18 of culture. Q-RT-PCR based analysis of expression of marker genes for C) mitochondrial dysfunction at day 18 of VSMC culture and of D) PPAR target gene ANGPTL4 at multiple timepoints of VSMC culture. Expression levels are relative to GAPDH. Asterisks (*) denote values that were determined to be significantly different from respective controls ($p \leq 0.05$).

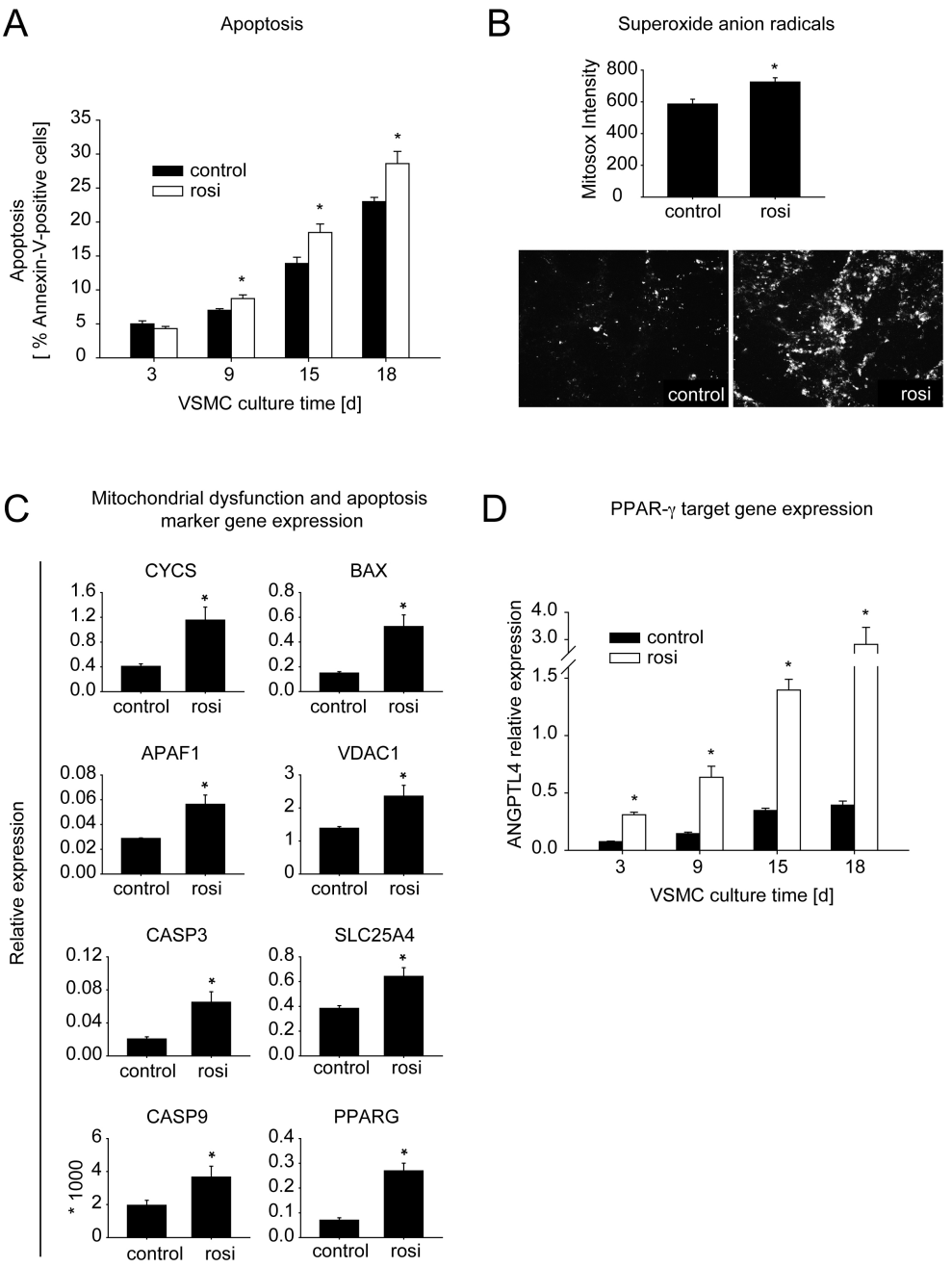
A
Apoptosis
Apoptosis
[% Annexin-V-positive cells]
control
rosi
VSMC culture time [d]
B
Superoxide anion radicals
Mitosox Intensity
control
rosi
C
Mitochondrial dysfunction and apoptosis
marker gene expression
Relative expression
CYCS
BAX
APAF1
VDAC1
CASP3
SLC25A4
CASP9
PPARG
* 1000
D
PPAR-γ target gene expression
ANGPTL4 relative expression
VSMC culture time [d]

[h]

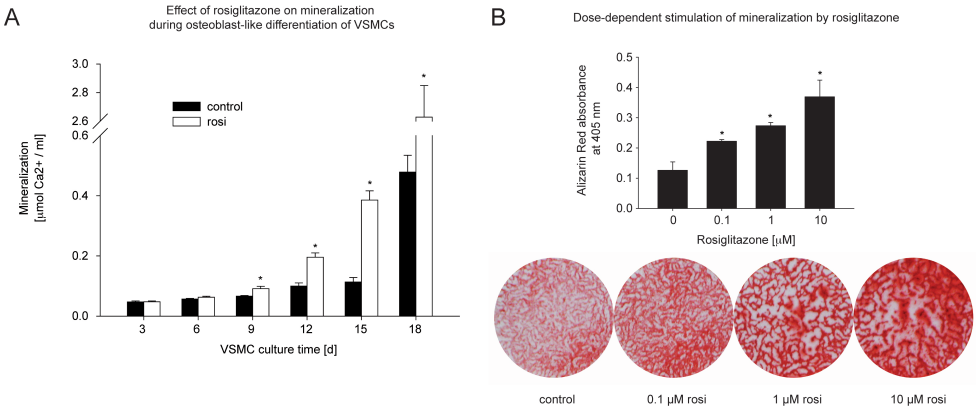

Figure 5.2
Rosiglitazone stimulates extracellular matrix mineralization. A) Mineralization was quantified in control (black bars) and 10 μM rosiglitazone - supplemented (white bars) VSMC cultures during several timepoints of culture. B) Mineralization was determined and semi-quantified by Alizarin red staining in VSMC cultures treated with different concentrations of rosiglitazone or control at day 18 of culture. Asterisks (*) denote values that were determined to be significantly different from respective controls ($p \leq 0.05$).

radicals were found in overlay or in close proximity to mineralization sites in VSMC culture dishes. In more detail, we found after automatic image processing that 93 percent of the identified calcifying spots co-localized with mitosox - stained spots (Figure 5.3 A). To investigate whether apoptosis plays a functional role in the observed rosiglitazone-stimulated mineralization, we perturbed the apoptotic pathway using caspase inhibitor V-ZAD-FMK. The compound significantly reduced basal apoptosis and virtually abolished the pro-apoptotic effect of rosiglitazone (Figure 5.3 B). Mineralization was reduced in cultures that were supplemented with caspase inhibitor alone (Figure 5.3 C). Furthermore, inhibition of apoptosis diminished the stimulatory effect of rosiglitazone on mineralization (Figure 5.3 C). We observed similar effects using the human pre-osteoblast differentiation model SV-HFO (data not shown). Interestingly, mineralization in the cultures treated with both rosiglitazone and caspase inhibitor was not completely abolished suggesting that a) rosiglitazone - mediated

stimulation of mineralization is only partly dependent on apoptosis and b) rosiglitazone affects multiple pathways rather than apoptosis alone resulting in increased mineralization.

5.4.4 Resveratrol diminishes rosiglitazone - mediated stimulation of mineralization, apoptosis and expression of mitochondrial dysfunction marker genes

We aimed to further investigate whether oxidative stress plays a direct role in the observed rosiglitazone - mediated stimulation of mineralization. Oxidative stress can cause mitochondria - dependent apoptosis and has been suggested as pro-mineralizing signal in the development of atherosclerosis [28, 29, 36, 172–174]. We aimed to perturb oxidative stress signaling with the phytoalexin resveratrol. The latter possesses antioxidant activity and confers a diversity of health benefits [175–177]. We assessed the effects of resveratrol on oxidative stress, apoptosis and mineralization in control and rosiglitazone - treated VSMC cultures. The resveratrol concentrations used approximate physiological concentrations present in natural

Figure 5.3 (following page)
Rosiglitazone-mediated induction of mineralization is partly dependent on apoptosis. A) Co-localization of superoxide anion radical and mineralization spots. VSMC were cultured until day 18 of culture. Accumulation of superoxide anions was visualized using mitosox staining (upper left Panel). Mineralized extracellular matrix (ECM) was stained with calcein (lower left Panel). Stained spots were automatically identified using Cell Profiler software. Then spots with dual staining were identified automatically (right Panel). The overlay was quantified in 20 different pictures demonstrating $93.4 \pm 4.0\%$ of calcifying spots co-localized with mitosox spots. Arrows indicate an example of overlapping mitosox and calcein spots. B) Blocking endogenous apoptosis diminishes the stimulatory effect of rosiglitazone on mineralization. VSMC cultures were supplemented with rosiglitazone, caspase inhibitor V-ZAD-FMK (fmk) or both. The percentage of apoptotic cells was quantified by annexin-V-FITC - based FACS at day 18 of VSMC culture. C) Mineralization was determined quantitatively at day 18 of VSMC culture. Asterisks (*) denote values that were determined statistically significant according to Student's T-test, $p \leq 0.05$. Hash symbols (#) designate significant interaction effects according to two-way ANOVA, $p \leq 0.05$.

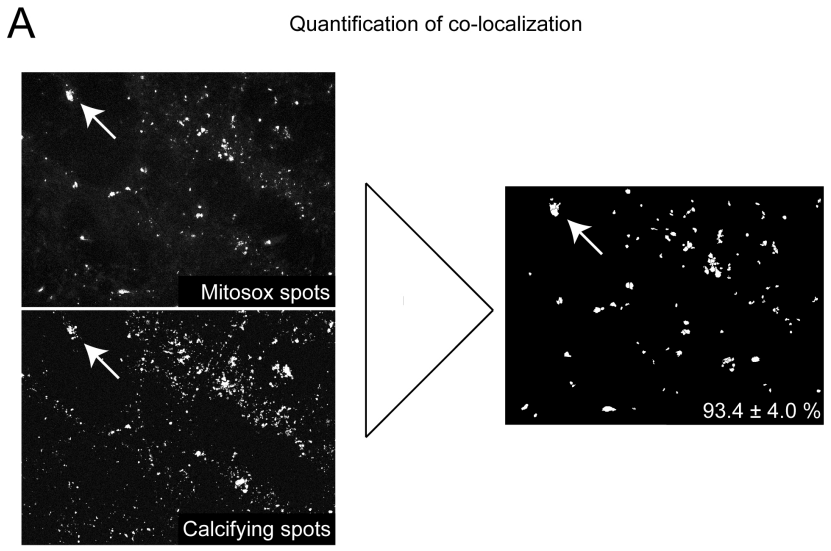
A
Quantification of co-localization
Mitosox spots
Calcifying spots
93.4 ± 4.0 %

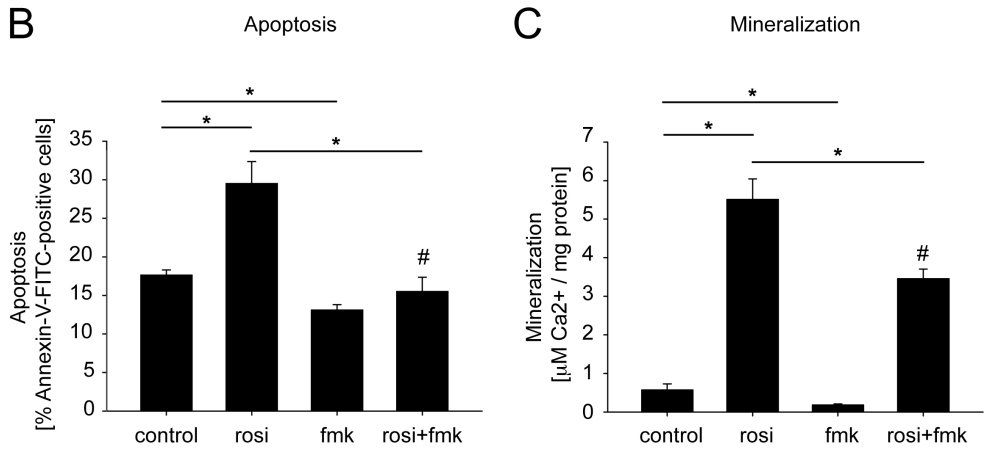
B
Apoptosis
[% Annexin-V-FITC-positive cells]
0
5
10
15
20
25
30
35
control
rosi
fmk
rosi+fmk
*
*
*
#
C
Mineralization
[µM Ca2+ / mg protein]
0
1
2
3
4
5
6
7
control
rosi
fmk
rosi+fmk
*
*
*
#

[h]

products [178, 179]. We found that treatment with resveratrol did not affect basal mineralization in VSMC cultures, however, resveratrol diminished the stimulatory effect of rosiglitazone on mineralization in a dose-dependent manner (Figure 5.4 A). Moreover, resveratrol did not affect basal apoptosis, but the addition of resveratrol to rosiglitazone - supplemented VSMC cultures diminished the stimulatory effect of rosiglitazone on apoptosis (Figure 5.4 B). Similar results were obtained for the expression of mitochondrial dysfunction marker genes cytochrome C (CYCS) and caspase 9 (CASP9; Figure 5.4 C). Interestingly, resveratrol treatment revealed a significant reduction in superoxide anion radicals in VSMCs (Figure 5.4 D). These changes were, however, independent of rosiglitazone treatment, i.e. two-way ANOVA analysis did not reveal any significant interaction effect between rosiglitazone and resveratrol conditions (Figure 5.4 D).

Figure 5.4 (following page)
Resveratrol diminishes rosiglitazone - mediated stimulation of mineralization, apoptosis and expression of mitochondrial dysfunction marker genes. A) VSMC were cultured in the continuous presence of rosiglitazone or control and continuously supplemented with different concentrations of resveratrol or control. Mineralization was quantified spectrophotometrically. B - D) VSMC were supplemented continuously with control, 10 μM rosiglitazone, 10 μM resveratrol or both 10 μM rosiglitazone and 10 μM resveratrol. Apoptosis was measured as percentage of annexin-V-FITC positive cells (B), expression of mitochondrial dysfunction marker genes CYCS and CASP9 were determined by quantitative RT-PCR (C), and superoxide anion radical levels were determined by mitosox staining (D) at day 18 of culture. Asterisks (*) denote values that were determined statistically significant between two groups linked by a line according to Student's T-test, $p \leq 0.05$. When not connected by a line, asterisks designate values determined statistically different from controls (no rosiglitazone and no resveratrol) according to Student's T-test, $p \leq 0.05$. Dollar symbols ($) denote values that were determined statistically significantly different from rosiglitazone conditions (no resveratrol) according to Student's T-test, $p \leq 0.05$. Hash symbols (#) designate significant interaction effects according to two-way ANOVA calculations, $p \leq 0.05$.

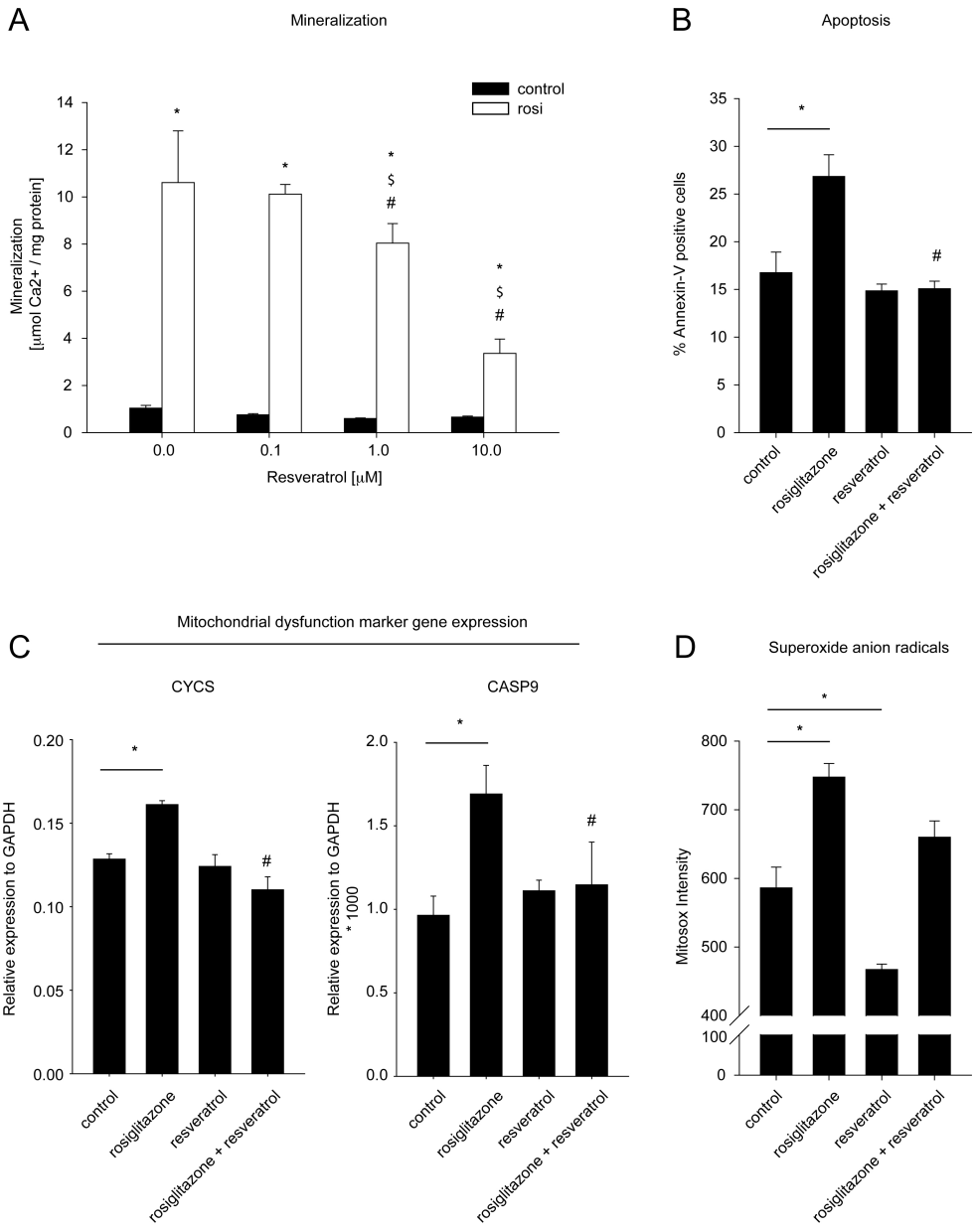
A
Mineralization
control
rosi
Mineralization [µmol Ca2+ / mg protein]
Resveratrol [µM]
0.0
0.1
1.0
10.0
B
Apoptosis
% Annexin-V positive cells
control
rosiglitazone
resveratrol
rosiglitazone + resveratrol
C
Mitochondrial dysfunction marker gene expression
CYCS
CASP9
Relative expression to GAPDH
Relative expression to GAPDH * 1000
D
Superoxide anion radicals
Mitosox Intensity

[h]

5.4.5 Resveratrol interferes with rosiglitazone - modulated osteoblast-like differentiation of VSMCs and BMP signaling

In order to investigate whether rosiglitazone and resveratrol affect osteoblast-like differentiation of VSMCs, we studied the activity and expression of confirmed osteoblast differentiation marker genes in cultures supplemented with rosiglitazone and resveratrol. We found that the activity of alkaline phosphatase, an enzyme important for the initiation of mineralization, was significantly enhanced in rosiglitazone - treated VSMCs (Figure 5.5 A). This increase in ALP activity was independent of apoptosis because supplementation with caspase inhibitor did not show any effects (data not shown). Resveratrol did not affect ALP activity (Figure 5.5 A), but addition of resveratrol to rosiglitazone - supplemented cultures decreased ALP activity in a dose-dependent manner (Figure 5.5 A). Interestingly, the expression of the well-characterized osteogenic differentiation marker gene runt related transcription factor 2 (RUNX2) was significantly increased by rosiglitazone (Figure 5.5 B). Resveratrol treatment alone did not show any effects, but addition of resveratrol to rosiglitazone - treated cultures blocked the stimulatory effect of rosiglitazone on RUNX2 expression (Figure 5.5 B). In order to investigate potential underlying mechanisms linking oxidative stress with the observed osteoblast-like differentiation phenotype, we studied the effects of rosiglitazone on bone morphogenic protein (BMP) pathway. Both bone morphogenic protein 2 (BMP2) and bone morphogenic protein 4 (BMP4) expression are regulated by oxidative stress [180, 181]. We found that BMP2 expression was significantly increased upon treatment with rosiglitazone (Figure 5.5 C). Mono-treatment with resveratrol did not affect BMP2 expression, but the addition of resveratrol to rosiglitazone-treated cultures blocked the stimulatory effect of rosiglitazone on BMP2 expression (Figure 5.5 C). Interestingly, BMP4 expression was lower in rosiglitazone - supplemented cultures compared to controls (Figure 5.5 C). In oppo-

site to the observed rosiglitazone effects, resveratrol treatment stimulated BMP4 expression (Figure 5.5 C). Moreover, expression of the BMP signaling inhibitor SMAD family member 6 (SMAD6) was increased by resveratrol alone (Figure 5.5 C), and in combination with rosiglitazone the increase in SMAD6 expression was even stronger (Figure 5.5 C). The expression of another BMP inhibitor, SMAD family member 7 (SMAD7), was not affected by rosiglitazone or resveratrol (Figure 5.5 C).

5.5 Discussion

The current study has revealed three novel findings. First, rosiglitazone directly stimulated mineralization in cultured human VSMCs, an *in vitro* model for vascular mineralization. This effect was at least partly caused by induction of caspase - dependent apoptosis. Second, rosiglitazone induced oxidative stress that was correlated with increased osteoblast-like differentiation and mineralization of VSMCs. And third, the caloric restriction mimetic and antioxidant resveratrol diminished rosiglitazone - induced oxidative stress, apoptosis, osteoblast-like differentiation and mineralization. These findings are summarized in a model depicted in Figure 5.6.

The identified rosiglitazone / apoptosis / mineralization cascade envisions a novel mechanism that may serve as a new explanatory model for the clinically observed increased risk for myocardial infarction in rosiglitazone-treated diabetic type 2 patients [72, 73]. In support of this, Pro12Ala and C161T loss of function mutations of *PPARG* in humans are associated with a lower incidence of myocardial infarction and angiographically documented atherosclerotic heart disease [182, 183]. However, studies with PPAR-γ ligand - treated transgenic animals and type 2 diabetic patients indicate an antiatherogenic role of PPAR-γ based on morphometric analyses of plaque area from tissue sections and carotid wall thickness [152, 184–189]. Although plaque area and carotid wall thickness are considered as

being good markers of atherosclerosis burden, several other factors contribute to determine the state of this disease, e.g. elasticity of vessels or plaque stability. Importantly, vascular calcification is considered to contribute to the overall morbidity of atherosclerosis including an increased risk for myocardial infarction by, at least in part, decreasing the elasticity of the vessels [23, 24, 190–193]. While calcification is a common feature of advanced atherosclerosis, the formation of atherosclerotic plaque and its calcification are likely to be regulated independently from each other since they form separate genetic entities [194]. We speculate here that activated PPAR-γ may exert opposing effects on these two distinct entities / hallmarks of atherosclerosis, i.e. plaque formation and vascular mineralization. This may place different patients treated with rosiglitazone into groups with highly distinct cardiovascular risks. Future more detailed clinical and experimental studies are necessary to verify this. Amongst those, it will be crucial to analyze the mineralization status of VSMCs in rosiglitazone *versus* sulfonylurea- or metformin-treated type 2 diabetic *in vivo* models.

The finding of the current study that rosiglitazone induced mitochondrial dysfunction and ROS in human hyperglycaemic VSMCs is novel but supported by several studies in other cell types including N1S1 rat hepatoma cells [195], preadipocytes [196], mouse myoblasts [197] and osteoblasts [151]. In contrast to this, rosiglitazone was shown in various *in vivo* studies to exert antioxidant activities in the vasculature [198, 199]. This may be due to beneficial systemic metabolic effects. However, it remains to be studied in the future whether rosiglitazone is capable to exert antioxidant activities as well in late stage type 2 Diabetes when antioxidant capacity is generally declined [200–202]. Whether rosiglitazone stimulated oxidative stress is mediated by activated PPAR-γ signaling or a result of mitochondrial dysfunction that is triggered independently of PPAR-γ is still under debate [203]. Most *in vitro* studies including the current work have used concentrations of rosiglitazone that exceed the Kd for PPAR-γ. Interestingly, these high concentrations are within the range measured in the serum of rosiglitazone - treated patients (i.e. rosiglitazone at 8 mg yields a

maximum serum concentration of 598 $\pm$ 117 ng / ml or 1.67 μM; Avandia package insert).

In addition to the observed stimulatory role of rosiglitazone in apoptosis - mediated mineralization that is correlated with increased oxidative stress, the current data show a second mechanism that is a direct stimulation of osteoblast-like differentiation of VSMCs. In support of this, our group has shown recently that rosiglitazone - activated PPAR-γ accelerates osteogenic differentiation from human mesenchymal stem cells that is ultimately followed by increased oxidative stress and mitochondria - dependent apoptosis leading to a premature onset of extracellular matrix mineralization and a reduced number of osteoblasts [151]. The apoptotic effect of rosiglitazone is not limited to the osteoblasts but also affects osteocytes that are important mediators of bone turnover through various mechanosensory mechanisms [145, 204]. As bone is continuously remodeled throughout life by the action of bone-forming osteoblasts and bone-resorbing osteoclasts, rosiglitazone treatment shifts the balance towards bone resorption leading to a reduced bone mass *in vivo* [40]. In comparison to the mineralization of bone tissue, atherosclerotic plaque mineralization is likely to underlie less sophisticated regulatory mechanisms. Although recent work by Tseng and coworkers has revealed a stimulatory effect of VSMCs on osteoclast differentiation from the monocytic preosteoclast cell line RAW264.7 in a PKA - dependent manner [205], osteoclastic cells may be rare in the vasculature [206]. Therefore, the rosiglitazone - mediated shift in the balance of bone turnover towards increased resorption leading to a reduced amount of mineralized tissue may not apply to vascular mineralization. Taken together, the data of the current study suggest that, once atherosclerotic plaque has been formed, rosiglitazone accelerates the mineralization process leading to an increase in calcified vascular lesions. Because of the suggested dual effect of rosiglitazone on vascular health (i.e. pro-calcifying but anti-atherogenic), detailed future studies are necessary to verify these observations *in vivo*.

The observed resveratrol - mediated inhibition of rosiglitazone - stimulated osteoblast-

like differentiation of VSMCs as shown by a reduction in the activity of the well-characterized osteogenic differentiation marker enzyme alkaline phosphatase (ALP) and expression of RUNX2 is novel. In addition, we found that resveratrol decreased basal ALP activity. The latter is in contrast to the data reported from studies in the murine pluripotent mesenchymal cell line ST2 [207], murine induced pluripotent stem cells [208], human bone marrow-derived mesenchymal stem cells [209] and murine osteoblastic MC3T3-E1 cells [210]. The observed opposing effects of resveratol on ALP activity from pre-osteoblastic cells or mesenchymal stem cells *versus* VSMCs differentiating in an osteoblast-like manner may result from divergent effects of resveratrol due to the osteoblast differentiation stage. In support of this, osteoblast differentiation - dependent effects have been documented for RUNX2 and WNT signaling [131, 132, 211]. Whereas the latter stimulate pre-osteoblast differentiation from mesenchymal progenitors, they inhibit osteoblast maturation and osteocyte differentiation. However, the detailed molecular mechanism underlying this differences in resveratrol effects needs to be identified in future studies.

The stimulatory effect of rosiglitazone-activated PPAR-γ on BMP2 expression in osteogenic VSMCs reported in this study is novel but supported by observations in osteoblasts. In more detail, Siddhivarn *et al.* found that delta-12-prostaglandin J2 which is a precursor of an endogenous PPAR-γ ligand, 15-deoxy-delta-12,14-prostaglandin J2, induces BMP2 expression and bone nodule formation in the murine osteoblast cell line MC3T3-E1 [212]. The diminishing effect of rosiglitazone on BMP4 expression observed in this study is novel as well. Interestingly, Zhou and co-workers have shown recently that BMP4 expression is reduced in cardiomyocytes subjected to nicotine-induced oxidative stress suggesting a diminishing effect of oxidative stress on BMP4 expression [213]. The stimulatory effects of the antioxidant resveratrol on expression of BMP4 and the BMP inhibitor SMAD6 observed in this study are in line with these findings suggesting BMP2 signaling is induced whereas BMP4 signaling is diminished by oxidative stress.

In which manner the reported resveratrol - mediated effects exactly translate into an *in vivo* situation is still under debate and may depend on additional determinants like nutritional conditions and possibly metabolic status. In support of this, resveratrol supresses atherosclerosis in hypercholesterolemic mice (lacking both apolipoprotein E and LDL receptor) on a high fat diet [214] and exerts beneficial effects in male Wistar rats on high-fat diet but not on standard diet (e.g. ox-LDL, decreased serum and hepatic oxidative stress) [215]. The concentrations of resveratrol used in this study approximate physiological concentrations present in natural products [178, 179]. However, resveratrol is rapidly metabolized *in vivo* [216, 217]. Despite the relatively low concentrations of un-metabolized resveratrol found in plasma, it has remained unknown so far whether some tissues are capable of converting resveratrol metabolites back to resveratrol, and possible biological actions of resveratrol metabolites have not been investigated yet. Therefore, a possible application of resveratrol as antioxidant and anti-calcifying compound *in vivo* needs to be tested in future studies.

In conclusion, the current study provides new insights into the relationship of rosiglitazone and cardiovascular events by providing a model that links rosiglitazone - induced oxidative stress, apoptosis and osteoblast-like differentiation of VSMCs with mineralization. These data are particularly interesting in regard to the clinically observed increased risk for myocardial infarction in rosiglitazone - treated diabetic type 2 patients [72, 73]. Finally, we position resveratrol in this model acting to reduce osteoblast-like VSMC differentiation, rosiglitazone - induced oxidative stress and mineralization.

Table 5.1
Primer and probe concentrations and sequences

Gene		Sequence (5'-3')	Concentration (pmol/rct)
GAPDH	Forward	ATGGGGAAGGTGAAGGTCG	3.75
	Reverse	TAAAAGCAGCCCTGGTGACC	3.75
	Probe	CGCCCAATACGACCAAATCCGTTGAC	3.75
CYCS	Forward	GTCAGGCCCCTGGATACTCT	1.25
	Reverse	CTCCCCAGATGATGCCTTT	1.25
BAX	Forward	CTGAGCAGATCATGAAGACAGG	1.25
	Reverse	CTGCTCGATCCTGGATGAAA	1.25
CASP3	Forward	TGGAATTGATGCGTGATGTT	1.25
	Reverse	TGGCTCAGAAGCACACAAAC	1.25
CASP9	Forward	TTACCCCAGTGGTGCTCAGACCA	10
	Reverse	GGTCTTTCTGCTCGACATCACCAA	10
VDAC1	Forward	AAGTGAACAACTCCAGCCTGA	1.25
	Reverse	CACCAGCATTGACGTTCTTG	1.25
SLC25A4	Forward	CTGGTGTCCTACCCCTTTGA	1.25
	Reverse	CAGTCAACTGTCCCCGTGTA	1.25
APAF1	Forward	TGATGGCATTCCTGTTGTCT	1.25
	Reverse	GGTACTCCACCTTCACACAGG	1.25
PPARG	Forward	AGGCGAGGGCGATCTTG	1.25
	Reverse	CCCATCATTAAGGAATTCATGTCAT	1.25
ANGPTL4	Forward	GACAAGAACTGCGCCAAGAG	1.25
	Reverse	AGTACTGGCCGTTGAGGTTG	1.25
RUNX2	Forward	ACGTCCCCGTCCATCCA	6.25
	Reverse	TGGCAGTGTCATCATCTGAAATG	6.25
	Probe	ACTGGGCTTCCTGCCATCACCGA	2.5
COL1A1	Forward	CAGCCGCTTCACCTACAGC	2.5
	Reverse	TTTTGTATTCAATCACTGTCTTGCC	2.5
	Probe	CCGGTGTGACTCGTGCAGCCATC	7.5
BMP2	Forward	ACGGACTGCGGTCTCCTAA	1.25
	Reverse	GGAAGCAGCAACGCTAGAAG	1.25
BMP4	Forward	GCTTCCACCACGAAGAACAT	1.25
	Reverse	AAAGAGGAAACGAAAAGCAGA	1.25
SMAD6	Forward	ACAAGCCACTGGATCTGTCC	1.25
	Reverse	TGATGAGGGAGTTGGTAGCC	1.25
SMAD7	Forward	CTTAGCCGACTCTGCGAACT	1.25
	Reverse	AAATCCATCGGGTATCTGGA	1.25

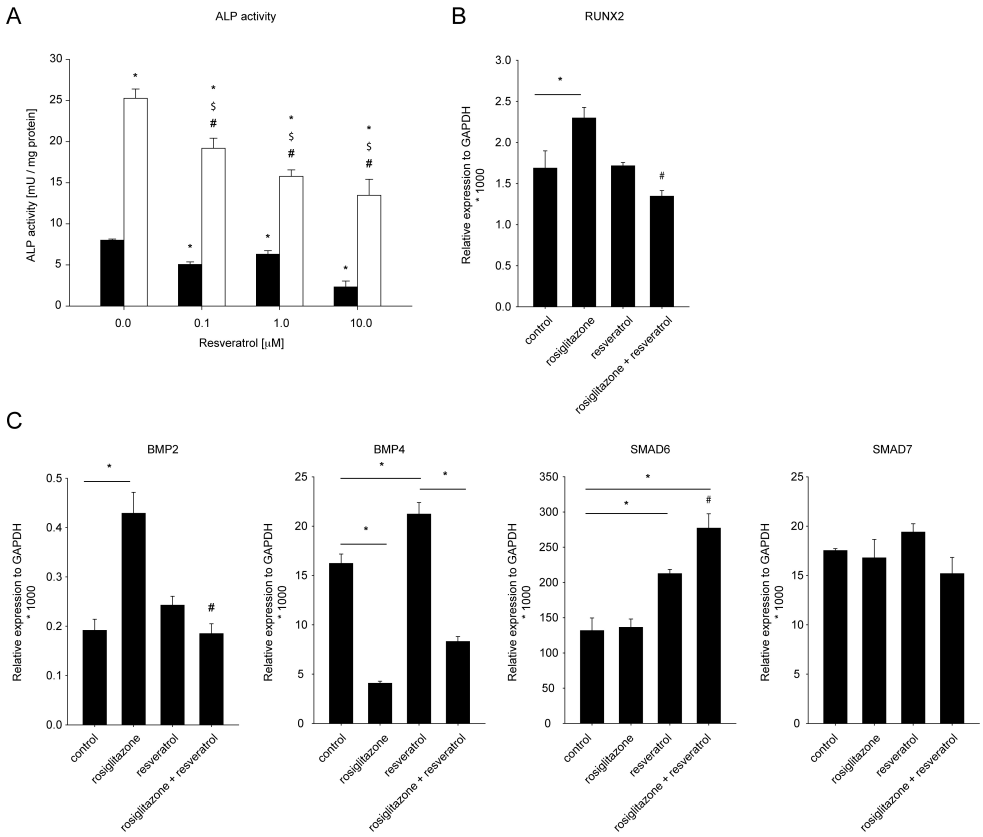

Figure 5.5
Resveratrol interferes with rosiglitazone - modulated osteoblast-like differentiation of VSMCs and BMP signaling. A) VSMC were cultured in the continuous presence of rosiglitazone or control and continuously supplemented with different concentrations of resveratrol or control. ALP activity was measured at day 18 of culture. B and C) VSMC were supplemented continuously with control, 10 μM rosiglitazone, 10 μM resveratrol or both 10 μM rosiglitazone and 10 μM resveratrol. The expression of the osteogenic differentiation marker gene RUNX2 (B) and of BMP signaling components BMP2, BMP4, SMAD6 and SMAD7 (C) were quantified by q-RT-PCR at day 18. Asterisks (*) denote values that were determined statistically significant between two groups linked by a line according to Student's T-test, $p \leq 0.05$. When not connected by a line, asterisks designate values determined statistically different from controls (no rosiglitazone and no resveratrol) according to Student's T-test, $p \leq 0.05$. Dollar symbols ($) denote values that were determined statistically significantly different from rosiglitazone conditions (no resveratrol) according to Student's T-test, $p \leq 0.05$. Hash symbols (#) designate significant interaction effects according to two-way ANOVA calculations, $p \leq 0.05$.

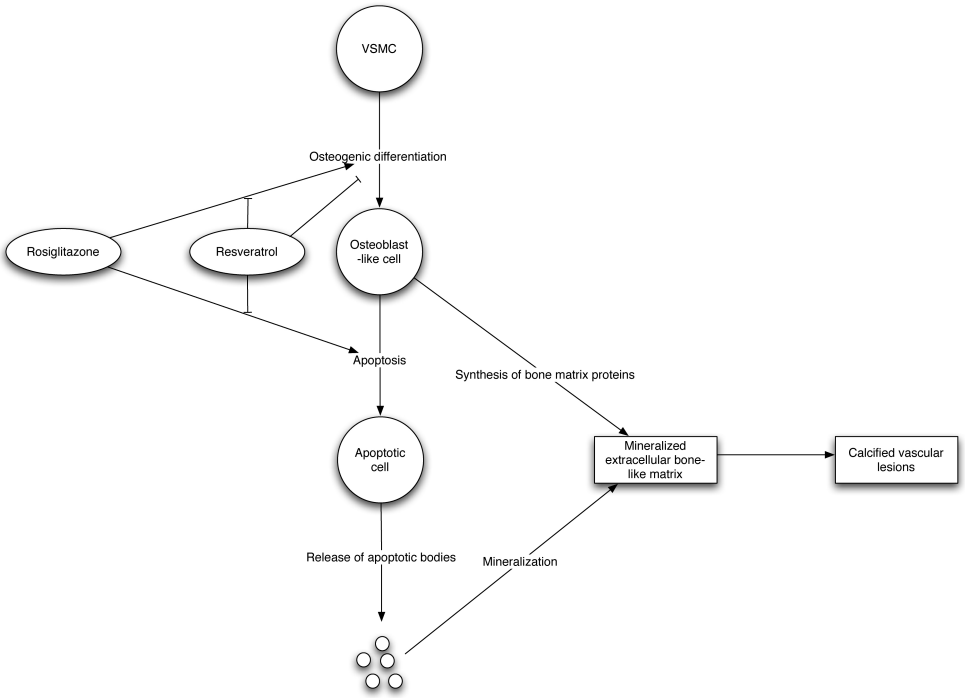

Figure 5.6
Schematic representation of the actions of rosiglitazone and resveratrol on mineralization. The presence of calcified vascular lesions in advanced atherosclerosis is a result of the formation of mineralized bone-like extracellular matrix (ECM) by vascular smooth muscle cells (VSMCs). Under pathological conditions, VSMCs are triggered to differentiate into a bone-like matrix - producing cell with an osteoblast-like phenotype. Apoptosis and the subsequent release of apoptotic bodies initiate ECM mineralization. Rosiglitazone stimulates mineralization by increasing osteoblast-like differentiation and induction of caspase-dependent apoptosis of VSMCs. Resveratrol counteracts rosiglitazone - stimulated mineralization by diminishing osteoblast-like differentiation and apoptosis of VSMCs. Furthermore, resveratrol exhibits direct effects on VSMCs. It reduces alkaline phosphatase activity and oxidative stress.

6 Rosiglitazone - targeted transcriptional networks in mineralization

6.1 Abstract

Clinical studies have recently revealed detrimental skeletal and vascular effects of the insulin sensitizer rosiglitazone. At the cellular level, we have shown earlier that rosiglitazone accelerates osteoblast differentiation from human mesenchymal stem cells (hMSC) at the expense of increased oxidative stress and apoptosis. In calcifying human vascular cells, rosiglitazone stimulates pathological mineralization, an effect that was diminished by the antioxidant resveratrol. In order to elucidate the transcriptional networks underlying the rosiglitazone - enhanced mineralization phenotype, we performed genome-wide transcriptional profiling of osteogenic hMSCs treated with rosiglitazone for short-term periods of 1 up to 48h during the first two days of culture time, a phase that we show is sufficient to

Claudia Bruedigam, Jeroen van de Peppel, Johannes P.T.M. van Leeuwen: *Rosiglitazone-targeted transcriptional networks as gene expression signature of physiological and pathological mineralization - a top-down approach to identify novel targets for bone and vascular health*; submitted

mediate the stimulatory effect of rosiglitazone on mineralization. Microarray-based mRNA expression analysis revealed 190 probes that were differentially expressed in at least one condition compared to vehicle - treated control. This rosiglitazone gene signature contained confirmed primary PPAR targets and was also endogenously regulated during osteogenic differentiation from hMSCs and osteoblast-like differentiation of vascular smooth muscle cells (VSMCs) into calcifying vascular cells (CVCs). Further comparative analysis revealed rosiglitazone targets that were commonly enriched in osteoblasts and CVCs or specifically enriched in either osteoblasts or CVCs. Finally, we compared the expression patterns of CVC - specific genes with patient expression data from carotid plaque *versus* intact adjacent tissue, and identified five rosiglitazone targets that were differentially regulated in CVCs and carotid plaque but not osteoblasts when compared to their respective non-mineralizing counterparts. These targets, i.e PDK4, SDC4, SPRY4, TCF4 (also commonly referred to as 'E2-2'), and DACT1 may specifically control extracellular matrix mineralization in vascular cells and hence provide interesting candidates for further investigations to improve vascular health.

6.2 Introduction

Rosiglitazone is a synthetic peroxisome proliferator-activated receptor γ (PPAR-γ) agonist belonging to the thiazolidinedione class of compounds with insulin - sensitizing, and blood glucose and lipid lowering activities. Despite these beneficial metabolic actions, serious cardiovascular side effects and also detrimental skeletal effects have been reported for rosiglitazone in recent epidemiological studies [40, 72–75]. We have shown earlier that rosiglitazone accelerates osteoblast differentiation from human mesenchymal stem cells (hMSCs) being ultimately followed by increased oxidative stress and apoptosis leading to a reduced number of fully differentiated osteoblasts but increased extracellular matrix mineralization [151].

Moreover, in an *in vitro* model of pathological mineralization we found that rosiglitazone further enhanced extracellular matrix mineralization that was diminishable by the addition of the anti-oxidant resveratrol [159]. Although these observations have revealed novel insights into the relationships between rosiglitazone and cardiovascular events as well as the clinically observed reduced bone quality, the underlying molecular mechanisms have remained elusive.

Human MSCs and also VSMCs follow a well-defined differentiation program *in vitro*. Under the influence of dexamethasone and β-glycerophosphate, hMSCs and VSMCs differentiate into mineralizing osteoblasts or calcifying vascular cells (CVCs), respectively, within a program of two to three weeks. Physiological phases in osteoblast and osteoblast-like differentiation have been described recently: proliferation and basic matrix formation are initiated during phase 1; formation of calcifying matrix occurs during phase 2; apoptosis and mineralization start during phase 3 [119]. Several key transcription factors have been described that are necessary for the occurrence of osteoblast and osteoblast-like differentiation phases [218–223].

In this study, we aimed to 1) investigate whether a specific differentiation phase is critical for initiating the rosiglitazone - accelerated osteoblast differentiation phenotype, 2) identify the molecular networks underlying the observed rosiglitazone - accelerated osteoblast differentiation phenotype, and 3) compare the revealed rosiglitazone - mediated changes in the transcriptome with endogenous osteogenic and osteoblast-like patterns of gene expression. Comprehensive bioinformatics analyses were used to link the obtained results to osteoblast-like differentiation of VSMC and cardiovascular events.

6.3 Materials and Methods

6.3.1 Cell culture

Human bone marrow - derived mesenchymal stem cells (hMSC; Lonza) were cultured as described previously [119]. MSCs were derived from two different donors and passages six and seven were used for the experiments. Adipogenic differentiation was induced by culturing hMSCs (5000 cell/cm2) in differentiation medium that was supplemented with 100 nM dexamethasone, 500 μM 3-isobutyl-1-methylxanthine (IBMX) and 60 μM indomethacin.

6.3.2 Mineralization and DNA assays

Calcium and DNA measurements were performed as described previously [119].

6.3.3 Quantification of mRNA expression

RNA isolation, cDNA synthesis and quantitative RT-PCR (Q-RT-PCR) were carried out as described recently [121].

6.3.4 Illumina gene chip - based gene expression

Illumina HumanHT-12 v3 BeadChip (Illumina, Inc.) human whole-genome expression arrays were used. RNA integrity of isolated RNA was assessed by RNA 6000 Nano assay on a 2100 Bioanalyzer (Agilent Technologies, Santa Clara, CA, USA). The RNA of two biological replicates for each condition was analyzed. The Illumina TotalPrep RNA Amplification Kit (Ambion, Austin, TX, USA) was used for RNA amplification of each sample according to the manufacturer's instructions. In short, T7 oligo(dT) primer was used to generate single stranded cDNA followed by a second strand synthesis to generate double-stranded cDNA. *In vitro* transcription was done to synthesize biotin-labeled cRNA using T7 RNA

polymerase. The cRNA was column purified and checked for quality by RNA 6000 Nano assay. A total of 750 ng of cRNA was hybridized for each array using standard Illumina protocol with streptavidin-Cy3 (GE healthcare) being used for detection. Slides were scanned on an iScan and analyzed using GenomeStudio (both from Illumina, Inc.). Raw data was background subtracted using GenomeStudioV2010.1 (Gene expression module 1.6.0), and processed using the Bioconductor R2.10.0 lumi-package. Data was variance stabilization transformed and quantile normalized. Differentially expressed probes were identified using Bioconductor package 'limma'.

6.3.5 Data analyses

Publicly available gene expression datasets were downloaded from Gene Expression Omnibus (www.ncbi.nlm.nih.gov/geo/) under the accession number GSE37558 for calcifying vascular smooth muscle cells and osteoblasts, and GDS5083 for carotid artery atheroma datasets. The rosiglitazone gene expression dataset has been deposited into GEO under accession number GSE67518. For gene ontology (GO) analysis, selected official gene symbols were analyzed using the Database for Annotation, Visualization and Integrated Discovery (DAVID) 2008 hosted by the National Institute of Allergy and Infectious Diseases (NIAID), NIH (http://david.abcc.ncifcrf.gov/) using $p \leq 0.1$ as cut-off. Unsupervised hierarchical clustering of the log2 fold changes of expression intensities of probes was carried out using Genepattern (http://genepattern.broadinstitute.org/gp/). Dendrograms are displayed next to the respective rows and columns, and data shown by the colours were row-normalized.

Principal component analysis was carried out using Genepattern as well. As input, log2 expression changes of the rosiglitazone signature (190 probes) were used compared to MSC d0 condition.

Genepattern was also used to perform gene set enrichment analysis (GSEA). Normal-

ized gene expression intensities without filtering were used, and each probe was collapsed into a single vector per gene that was then identified by its official gene symbol. For each GSEA, 1000 permutations were performed. Based on PCA analyses [224] for GSEA of osteoblast differentiation, d0 and d2 were grouped (group1, 'undifferentiated') and compared with osteoblasts from all later timepoints (group 2, 'differentiated'). For GSEA of pathological mineralization, VSMCs at d0 (group 1, 'undifferentiated') were compared with CVCs from all timepoints available (group 2, 'differentiated'). An FDR q-value of ≤ 0.1 was used to define statistically significant enrichment.

Ingenuity pathway analysis (IPA) was used to perform upstream regulator analysis, and to generate gene regulatory networks around potential key genes. For upstream regulator analysis, activation z-scores of +2 and -2 were used as cut-offs for predicted activators or inhibitors, respectively. For generated gene regulatory networks, direct up- and downstream connections were generated from an expression data set filtered based on differential expression with $p \leq 0.05$. Quantitative expression changes were overlayed with upregulation shown in red, and downregulation shown in green.

Connectivity map was used as independent compound prediction analysis (CMAP; www.broadinstitute.org/cmap/). This approach uses data from about 6,000 microarray experiments to correlate gene expression levels with about 1,300 different drugs tested in four human cell lines (i.e. HL60, MCF7, SKMEL5, and PC3). The rosiglitazone clusters 1 and 2 were used as UP signature, and clusters 3 and 4 as DOWN signature. The obtained results were filtered based on $p \leq 0.05$.

Hypergeometric probability test was carried out using GeneProf software (www.geneprof.org/). All other statistical analyses were carried out using Graphpad Prism v6. Comparisons with $p \leq 0.05$ determined by Student's t test were defined as statistically significant.

6.4 Results

6.4.1 Rosiglitazone - mediated acceleration of mineralization is initiated during the early osteoblast differentiation phase

We investigated whether a particular osteogenic differentiation phase is important for mediating the stimulatory effect of rosiglitazone on mineralization. Human MSC cultures were supplemented with 10 μM rosiglitazone or respective control for an interval of each three days during different phases of osteogenic differentiation (Figure 6.1 A). ECM mineralization was quantified at day 15 of culture. Interestingly, rosiglitazone treatment during the first three days was already sufficient to stimulate ECM mineralization to a level similar to that observed by continuous treatment (Figure 6.1 B). Rosiglitazone treatment from day 3 until day 6 revealed a similar effect, whereas treatment during any time interval from day 6 until day 15 did not lead to any changes in ECM mineralization (Figure 6.1 B). The increased mineralization levels were not a result of increased cell numbers (Figure 6.1 C). PPARG1 and PPARG2 expression levels were significantly increased upon continuous rosiglitazone treatment, whereas short-term rosiglitazone incubations showed only transient stimulatory effects on PPARG expression (Figures 6.1 D, E).

6.4.2 Rosiglitazone regulates well-characterized PPAR-γ target genes during the early osteoblast differentiation phase

In order to identify rosiglitazone - targeted transcriptional networks, we performed genome wide transcriptional profiling of 10 μM rosiglitazone and control - supplemented hMSC cultures during the initially observed important early (0-3 days) phase. The detailed experimental layout is depicted in Figure 6.2 A. Human MSC cultures were supplemented with rosiglitazone for 1, 3, 6, 24 or 48h directly before harvest during the first 48h of Stage 1 as

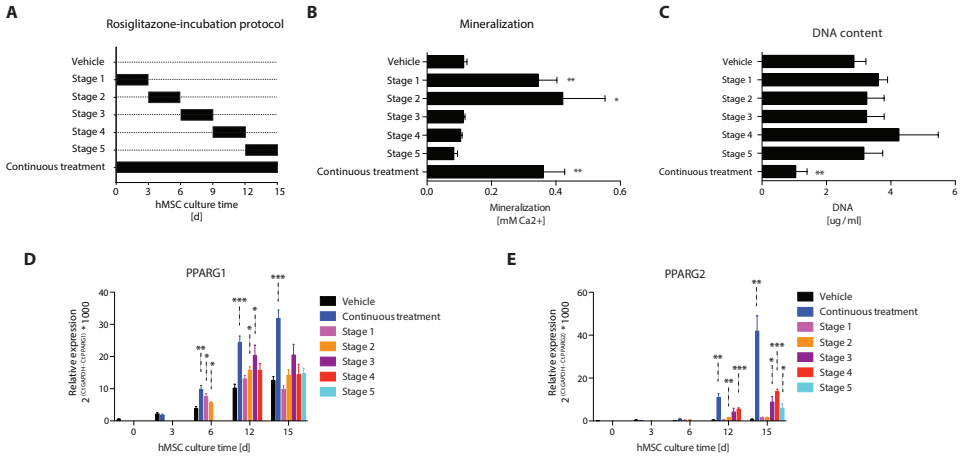

Figure 6.1
The stimulatory effect of rosiglitazone on mineralization is dependent on the early osteoblast differentiation phase. A) Graphical representation of the rosiglitazone incubation protocol. Human bone marrow - derived MSCs were cultured in osteogenic differentiation medium supplemented with 10 μM rosiglitazone during the timepoints as displayed on the x-axis. B) Quantification of mineralization and C) DNA content during the various differentiation stages, continuous or vehicle - treated control conditions as depicted on the y-axis. Quantitative-RT-PCR analysis of D) PPARG1 and E) PPARG2. * $p \leq 0.05$; ** $p \leq 0.01$; *** $p \leq 0.001$; 6 replicates from two independent experiments. Statistics according to Student's T test of the respective rosiglitazone condition compared to vehicle from the same timepoint.

shown in Figure 6.2 A. This narrow time window was already sufficient for rosiglitazone to significantly enhance mineralization (Figure 6.2 B). This stimulation of mineralization was not the result of increased proliferation (Figure 6.2 C). We found that the expression intensities of 190 probes, representing 185 genes, were significantly different from vehicle-treated control ($q \leq 0.05$) during at least one timepoint (Table 6.1). Five genes were represented by two different probes each (PTGS2, IL8, GADD45A, ASS1, ALDH1A3). Thus in total, expression levels of 185 genes were changed significantly upon rosiglitazone treatment. Confirmed primary PPAR target genes were included in this gene signature, and detailed analysis of expression fold changes in the different rosiglitazone versus control conditions re-

vealed distinct PPAR target expression patterns (Figure 6.2 D). The expression levels of fatty acid binding protein 4 (FABP4), stearoyl-CoA desaturase (SCD), aldo-keto reductase family 1 member C2 (AKR1C2), heme oxygenase 1 (HMOX1), and angiopoietin 4 (ANGPTL4) were increased with extended rosiglitazone incubation time compared to vehicle controls, whereas the expression levels of serum / glucocorticoid regulated kinase 1 (SGK1), and prostaglandin-endoperoxide synthase 2 (PTGS2) were reduced upon prolonged incubation time with rosiglitazone (Figure 6.2 D). The observed expression pattern of ANGPTL4 was confirmed by quantitative RT-PCR (Figure 6.2 E). In order to further investigate whether the revealed rosiglitazone gene signature has been associated with stimulated PPAR signaling in a broader range of biological contexts, we applied two different bioinformatics approaches. Firstly, we performed upstream regulator analysis using Ingenuity Pathway Analysis software. We found that rosiglitazone, an additional thiazolidinedione, pioglitazone, and the PPAR agonists fenofibrate and daidzein were amongst the upstream predicted regulatory molecules with the strongest positive activation z-scores (Figure 6.2 F). Most upstream regulators with activation z-scores of 2 or higher included chemicals whereas biomolecules represented only a minor part (Figure 6.2 G). These upstream regulators are mainly annotated as MAPK signaling inhibitors, corticosteroids and insulin sensitizers. In contrast, upstream regulators with negative activation z-scores of less than -2 predicting inhibition are mainly comprised of biomolecules including transcription regulators, cytokines, kinases, and growth factors (Figure 6.2 H). Finally, we compared the revealed rosiglitazone gene signature from the current study with publicly available data sets using 'Connectivity Map'. The identified compounds with $p \leq 0.01$ and positive enrichment included the thiazolidinedione and PPAR agonist troglitazone, as well as compounds from other classes including antihistamines (diphenhydramine), beta blocker (nadalol), serotonin receptor antagonists (quipazine), non-steroidal anti-inflammatories (NSAID; naproxen), antibiotics (benzathine benzylpenicillin, metronidazole), and monoamine oxidase inhibitors (amantadine, iproni-

azid) (Table 6.2). Interestingly, the compound with the strongest negative CMAP score was identified as a potent MAPK activator, and most significant correlations were revealed with MCF7-derived gene expression signatures (Table 6.2).

In summary so far, genome - wide expression profiling of rosiglitazone - treated osteogenic human MSC cultures has revealed a distinct gene signature that contains well - characterized PPAR target genes and is associated with PPAR stimulation in a broad range of biological systems. Furthermore, compounds with high similarity to the effects of rosiglitazone on gene expression were identified although these results were not cross-validated between the two independent bioinformatics approaches used.

Figure 6.2 (following page)
Rosiglitazone regulates well-characterized PPAR-γ target genes during the early osteoblast differentiation phase. A) Graphical display of the rosiglitazone incubation protocol. Osteogenic human bone-marrow derived MSCs were cultured in osteogenic medium and supplemented with 10 μM rosiglitazone during the time as depicted on the x-axis. The control condition was treated with vehicle for 1 h before harvest. B) Mineralization and C) DNA content of the cultures incubated with rosiglitazone for 48 h (d0-2) compared to vehicle control analyzed on day 15. D) Heatmap displaying the microarray-based expression fold changes of well-characterized PPAR target genes in the rosiglitazone treated hMSC conditions compared to controls as described above. E) Quantification of the expression of the confirmed PPAR-γ target gene ANGPTL4 by q-RT-PCR analysis in samples from 2 independent experiments generated similarly as described above. * $p \leq 0.05$. N = 6. Expression levels were calculated relative to GAPDH. F) Upstream regulator analysis of the rosiglitazone - regulated gene signature ($q \leq 0.05$) using Ingenuity Pathway Analysis software (IPA). Heatmap displays activation z-scores. Compound names are displayed on the right of the corresponding heat block. Only compounds with a positive enrichment score (> 2) are shown. Classification and distribution of the identified positive (G) and negative (H) upstream regulators into chemicals (dark blue) and biomolecules (red).

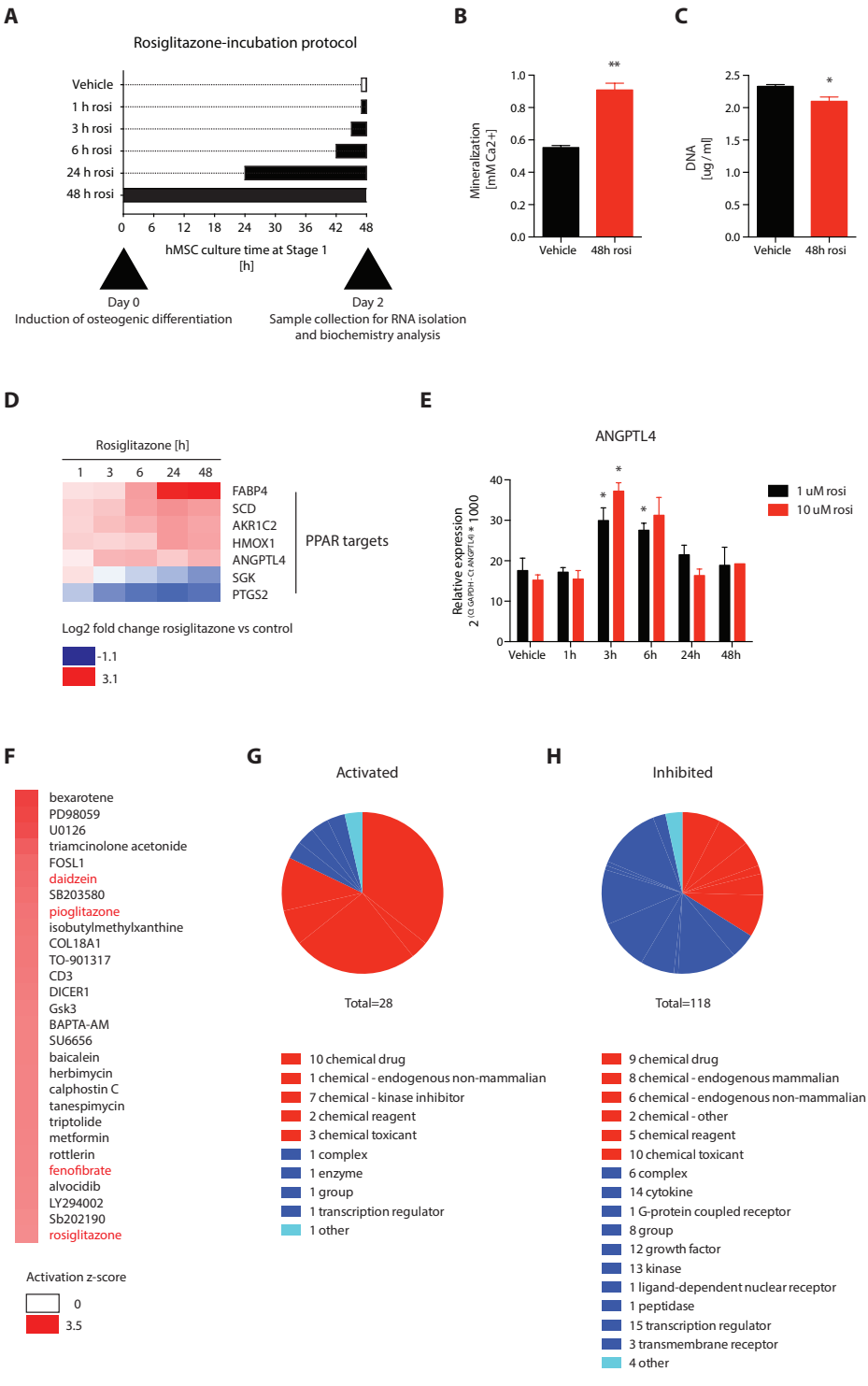
A
Rosiglitazone-incubation protocol
Vehicle
1 h rosi
3 h rosi
6 h rosi
24 h rosi
48 h rosi
0 6 12 18 24 30 36 42 48
hMSC culture time at Stage 1 [h]
Day 0
Induction of osteogenic differentiation
Day 2
Sample collection for RNA isolation and biochemistry analysis
B
Mineralization [mM Ca2+]
1.0 0.8 0.6 0.4 0.2 0.0
**
Vehicle
48h rosi
C
DNA [ug / ml]
2.5 2.0 1.5 1.0 0.5 0.0
*
Vehicle
48h rosi
D
Rosiglitazone [h]
1 3 6 24 48
FABP4
SCD
AKR1C2
HMOX1
ANGPTL4
SGK
PTGS2
PPAR targets
Log2 fold change rosiglitazone vs control
-1.1
3.1
E
ANGPTL4
Relative expression
2^(Ct GAPDH - Ct ANGPTL4) * 1000
40 30 20 10 0
* * * *
Vehicle 1h 3h 6h 24h 48h
1 uM rosi
10 uM rosi
F
bexarotene
PD98059
U0126
triamcinolone acetonide
FOSL1
daidzein
SB203580
pioglitazone
isobutylmethylxanthine
COL18A1
TO-901317
CD3
DICER1
Gsk3
BAPTA-AM
SU6656
baicalein
herbimycin
calphostin C
tanespimycin
triptolide
metformin
rottlerin
fenofibrate
alvocidib
LY294002
Sb202190
rosiglitazone
Activation z-score
0
3.5
G
Activated
Total=28
10 chemical drug
1 chemical - endogenous non-mammalian
7 chemical - kinase inhibitor
2 chemical reagent
3 chemical toxicant
1 complex
1 enzyme
1 group
1 transcription regulator
1 other
H
Inhibited
Total=118
9 chemical drug
8 chemical - endogenous mammalian
6 chemical - endogenous non-mammalian
2 chemical - other
5 chemical reagent
10 chemical toxicant
6 complex
14 cytokine
1 G-protein coupled receptor
8 group
12 growth factor
13 kinase
1 ligand-dependent nuclear receptor
1 peptidase
15 transcription regulator
3 transmembrane receptor
4 other

[h]

6.4.3 Rosiglitazone target genes cluster into separate expression pattern groups that underlie discrete upstream regulatory processes

In order to gain further insights into the nature and dynamics of rosiglitazone - induced changes of the transcriptome in osteogenic human MSCs, we performed hierarchical clustering analysis of the identified rosiglitazone targets based on their fold changes of expression in each rosiglitazone incubation condition compared to vehicle control. We observed great similarity between 3 and 6, or 24 and 48 h time-points, respectively (Figure 6.3 A). Unsupervised hierarchical clustering revealed a separation of expression patterns into four major groups (Figure 6.3 A). Expression patterns of transcripts in cluster 1 were overall increased compared to vehicle controls reaching a plateau during 3 and 6 h of incubation with rosiglitazone (Figure 6.3 B). Transcript expression patterns in cluster 2 revealed an upregulation that was particularly pronounced during 24 and 48 h of incubation with rosiglitazone (Figure 6.3 C). In total, clusters 1 and 2 were comprised of 65 genes. Expression levels of rosiglitazone target genes were reduced compared to control conditions in both clusters 3 and 4 (Figure 6.3 D, E). Expression levels were reduced during 3, 6, 24 and 48 h of rosiglitazone treatment compared to controls in cluster 3 (Figure 6.3 D), whereas transcripts belonging to cluster 4 showed remarkable down-regulation after 48 h of rosiglitazone incubation (Figure 6.3 E). In order to investigate whether clustering of targets according to their expression patterns would reveal cluster-specific transcription factors orchestrating rosiglitazone - initiated responses, we performed upstream regulator prediction analysis using Ingenuity pathway analysis (Figure 6.3 F). Activation of TGF-β signalling and activation of CEBPA, CEBPB, MED1, PGR and TP53 signalling were predicted transcription factors for cluster 1 and cluster 2, respectively (Figure 6.3 F). Cluster 3 containing transcripts down-regulated upon rosiglitazone treatment were predicted to result from the activation of AP-1 signalling and inhibition of a

large number of transcription factors including SMAD, STAT, NfkB, E2F, WNT and FOXO signalling (Figure 6.3 F). Finally, NFAT signalling was predicted to be inhibited resulting in the down-regulation of targets allocated to cluster 4 (Figure 6.3 F). In summary, we identified distinct clusters of rosiglitazone target genes based on their expression patterns that were reflecting distinct gene regulatory modules.

6.4.4 Rosiglitazone target clusters are annotated with distinct cellular compartments, molecular functions and biological processes

In order to investigate whether the revealed gene regulatory modules would also reflect some functional distinction, we performed gene ontology analysis using DAVID functional annotation tool. Regarding cellular compartments, we found that cluster 1 was enriched for insoluble or membrane fraction, and cluster 2 for cytosol and endoplasmic reticulum (Figure 6.4 A). Clusters 3 and 4 were enriched for nucleus-associated compartments, and cytoskeleton or cell junctions, respectively (Figure 6.4 A). Regarding biological processes, we observed strong enrichment of positive regulation of angiogenesis in cluster 1 and metabolic processes including brown fat differentiation in cluster 2 (data not shown). Apoptotic pathways were enriched in cluster 3, and glycoprotein synthesis was strongly enriched in cluster 4 (data not shown). Regarding molecular functions, metabolic activity was remarkably enriched in cluster 2 including 3-alpha hydroxysteroid dehydrogenase (A-specific; AKR1C4) followed by trans-1,2-dihydrobenzene-1,2-diol dehydrogenase activity (dihydrodiol dehydrogenase; DHDH), NAD oxidoreductase, phosphatidylinositol binding and lipid binding (Figure 6.4 B). In cluster 3, gene expression regulatory pathways were mainly enriched including processes involving AU-rich element binding, MAP kinase tyrosine/serine/threonine phosphatase, and double-stranded DNA binding processes (Figure 6.4 B). Cell adhesion

molecule binding was enriched in cluster 4 (Figure 6.4 B). We next investigated whether similar relationships between the individual clusters and their subcellular localization and molecular function described above could be validated by an independent bioinformatics approach using Ingenuity Pathway analysis. Similarly to the results obtained from DAVID, gene products from clusters 1 and 2 were mainly located within the cytosol and cell membrane with a fewer number of gene products located within the extracellular space or nucleus (Figure 6.5). The subcellular localization of the gene products from clusters 3 and 4 showed a great shift towards the nucleus in line with the results obtained from DAVID (Figure 6.6). In summary, we demonstrated that the distinct rosiglitazone target modules were annotated with distinct subcellular localizations and functions demonstrating an overall suppression of gene expression involved in direct transcriptional regulation, and an overall stimulation of gene expression involved in metabolism.

6.4.5 The rosiglitazone gene signature can discriminate differentiating hMSC and VSMC cultures based on their differentiation status

In order to further investigate whether the identified rosiglitazone gene signature would be important for osteogenic and osteoblast-like differentiation processes of hMSC or VSMC cultures, respectively, we performed principal component analysis of the rosiglitazone gene signature on previously published gene expression datasets from hMSC and VSMC cultures differentiating into osteoblasts or calcifying vascular cells (CVCs), respectively [224]. All 185 genes comprising the rosiglitazone signature were found to be present in these hMSC and VSMC datasets. We found that the undifferentiated MSC and VSMC cultures showed a clear difference as indicated by the long distance between them on the two-dimensional PCA plot showing the first and second principal component describing each 67% or 16%,

respectively (Figure 6.7 A). Interestingly, both differentiating osteoblasts and CVCs diverged from their non-mineralizing counterparts into the same direction, and the most differentiated osteoblast and CVC cultures showed greater similarity as indicated by the reduced distance from each other (Figure 6.7 A). The first principal component thus describes the differentiation, and the second principal component describes the cell type. The differentiation of osteoblasts or CVCs results in a more similar profile. We then added GSEA in order to learn about the directionality of gene expression changes of rosiglitazone targets during endogenous osteogenic differentiation. We found that the upregulated genes (clusters 1 and 2; Figures 6.3 B and C) were significantly enriched in osteogenic differentiation (i.e comparing the differentiated osteoblasts with undifferentiated gene expression profiles; Figures 6.7 B, C) whereas no significant enrichment was found for the downregulated genes (clusters 3 and 4; Figures 6.3 D and E; data not shown for enrichment). During osteogenic differentiation of VSMCs into CVCs we found a borderline significant enrichment of rosiglitazone targets from clusters 1 and 2 (Figures 6.7 D, E), and also here no significant enrichment for clusters 3 and 4 was observed (data not shown). In summary, these analyses have provided evidence for the presence of the upregulated rosiglitazone signature during endogenous osteogenic differentiation of MSC and VSMC suggesting that rosiglitazone targets may be important components for the induction of both physiological and pathological mineralization.

6.4.6 Identification of commonly and specifically enriched rosiglitazone targets during physiological and pathological mineralization

In order to investigate whether the rosiglitazone targets may be enriched specifically in either osteoblasts or CVCs, we generated a VENN diagram from the significantly enriched genes determined by GSEA as shown above (Figure 6.8 A). This analysis revealed that the

majority, i.e 30 genes, were found to be commonly enriched in both physiological and pathological mineralization (Figure 6.8 B), whereas only a small number of 14 and 5 genes were found to be specifically enriched in osteoblasts or CVCs, respectively (Figures 6.8 C, D). We finally aimed to investigate whether the identified rosiglitazone gene signature would be detectable in patient-derived carotid plaque tissue [225]. From the 185 genes rosiglitazone signature 148 were present in the carotid artery atheroma datasets. We found that 85 out of these 148 genes from the rosiglitazone signature showed a significant ($p \leq 0.05$) difference in expression in carotid plaque tissue compared to intact adjacent tissue, a number that is well above chance according to hypergeometric probability test ($p \leq$ 1.6e-12; Figure 6.9 A). We next performed unsupervised hierarchical clustering and divided the differentially expressed genes into an upregulated and a downregulated cluster (Figure 6.9 A). Next, comparative analysis of rosiglitazone genes (i.e. carotid plague versus intact tissue; differentiated osteoblasts versus undifferentiated MSCs, and CVCs versus VSMCs) was performed. Comparative analysis of the upregulated cluster revealed that one gene was also enriched specifically in CVCs while 10 genes were also enriched in both osteoblasts and CVCs (Figure 6.9 B). For the downregulated cluster, we identified 4 genes that were also specifically enriched in VSMC, and 4 additional genes that were also enriched in both VSMCs and MSCs (Figure 6.9 C). The gene found to be specifically upregulated in pathological (VSMC) mineralization was identified as PDK4 encoding for pyruvate dehydrogenase kinase isoform 4, and the genes identified to be downregulated exlusively in carotid plaque and CVC but not physiological mineralization were identified as TCF4, SDC4, SPRY4, and DACT1 encoding for transcription factor 4, syndecan 4, sprout homolog 4 (Drosophila), and dishevelled binding antagonist of beta-catenin 1, respectively (Figure 6.9 D). Finally, we investigated whether these five candidate genes identified for rosiglitazone - stimulated pathological mineralization were key components of gene regulatory networks. We therefore performed Ingenuity Pathway Analysis - based generation of gene regulatory networks starting from the 5 key

genes and overlayed the revealed connected up- and downstream molecules with the gene expression data from carotid plaque versus adjacent intact tissue (Figure 6.10). We found overall that the 5 key candidates identified were well connected with differentially regulated genes in carotid plaques and hence may provide promising candidates to develop targeted therapies to improve vascular health.

6.5 Discussion

The current study has revealed three major findings. Firstly, short-term rosiglitazone treatment during the early phase of osteogenic hMSC differentiation is already sufficient to accelerate osteoblast differentiation and bone matrix mineralization that is observed two to three weeks later during culture. Secondly, a rosiglitazone gene signature targeted during the observed important early phase can discriminate osteogenic and osteoblast-like cultures from their undifferentiated hMSC or VSMC counterparts, respectively. And thirdly, a majority of the rosiglitazone gene signature is dysregulated in carotid plaque compared to intact tissue. Comprehensive comparative analyses have revealed 5 rosiglitazone targets that are specifically dysregulated in pathological mineralization providing a rationale for these targets to be validated in further studies to improve vascular health.

The data from the current study demonstrating that rosiglitazone initiates its acceleratory effects on differentiation during the initial phase of osteoblast differentiation are novel and suggest that early proliferation or basic matrix formation processes are particularly susceptible to PPAR stimulation enabling a fine-tuned orchestrated cellular response to environmental conditions during this early stage. In line with this hypothesis, a particularly high susceptibility of the early osteoblast differentiation phase to environmental perturbations has been demonstrated recently in regard to oxygen tension [162, 226], 1α,25-dihydroxyvitamin D3 [102], and interferon-β [227]. Also RUNX2 and WNT effects are time-dependent and

particularly important during the early phase of osteoblast differentiation [211, 228].

The finding that PPARG expression was low during the stages when rosiglitazone treatment initiated the strongest effects demonstrates that the level of receptor expression is not directly correlated with the effects of rosiglitazone on osteoblast differentiation and mineralization. This suggests that a low expression level of PPARG is already sufficient to mediate the rosiglitazone - initiated effects on differentiation and mineralization, or that at least parts of the effects may be mediated PPARG-independently. PPARG independent effects of thiazolidinediones have been described earlier [203] , however, we have shown recently that knockdown of PPARG1 expression diminished, and overexpression of PPARG1 further increased osteoblast differentiation [151]. It is therefore conceivable that a low level of receptor is already sufficient, and that the timing of the rosiglitazone perturbation is of highest importance with early proliferation or basic matrix formation processes being particularly sensitive to environmental inputs during this early differentiation stage. In support of this hypothesis, we have demonstrated by using independent bioinformatics analyses that the gene networks regulated by rosiglitazone during the early osteoblast differentiation stage contain well-characterized PPAR target genes and are also associated with PPAR stimulation in a broad range of other biological systems.

The compounds identified by upstream regulator prediction or connectivity map - based analysis of the rosiglitazone signature include, besides rosiglitazone itself, well-characterized PPAR agonists such as the additional thiazolidinediones pioglitazone and troglitazone, as well as natural PPAR ligands including fenofibrate and daidzein. Hence these data confirm the sanity of the chosen approach to identify novel compounds with potential PPAR agonistic activity or similar working mechanisms, and may provide a starting point for drug repositioning [229]. The identified drugs represent various compound classes derived from natural or synthetic origins, and the large variety of structures and functional annotations is in line with the role of PPARs as low-affinity nuclear receptors orchestrating a wide range of cellular

processes including fatty acid catabolism, inflammatory responses, cell proliferation, apoptosis and differentiation by direct or indirect modes of gene expression regulation [230,231]. Intriguingly, most of the compounds identified by connectivity map - based analysis had been tested in experiments involving the bone metastatic breast cancer cell line MCF-7. We hypothesize that, in the context of PPAR signaling, the response of the MCF-7 transcriptome to rosiglitazone may be most similar to the response of osteogenic MSCs. In support of this, earlier studies have revealed a mimicry of skeletal cellular phenotypes by bone metastasizing breast cancer cells [232–236].

The separate clusters of co-expressed transcripts revealed by hierarchical clustering analysis of rosiglitazone - induced transcript changes are functionally annotated with distinct cellular compartments, molecular functions and biological processes, and are also predicted to underlie discrete upstream regulatory processes. In line with these data, Stuart and coworkers have demonstrated earlier the existence of co-expressed genes forming genetic modules that showed functional relation across the conservation over multiple species [237]. Additional GSEA of the identified rosiglitazone target clusters have revealed that particularly targets from the upregulated clusters are strongly enriched during both osteogenic and osteoblast-like differentiation. One of the major networks (Figure 6.5) includes genes with essential roles in steroid and fatty acid metabolism that are annotated as downstream targets of CCAT/enhancer binding protein (C/EBP) alpha (CEBPA). Moreover, CEPBA itself as well as the glucocorticoid-induced leucine zipper (TSC22D3), aldo-keto reductase family 1 member C3 (AKR1C3), argininosuccinate synthase 1 (ASS1), stearoyl-CoA desaturase (SCD), and phosphoinositide-3-kinase regulatory subunit 1 (PIK3R1) have been described as dexamethasone targets in a broad range of biological systems [238–244]. The identification of a dexamethasone-regulated network associated with enhanced mineralization that is already stimulated endogenously during osteogenic and osteoblast-like differentiation is in line with the essential role of glucocorticoid metabolism for human osteoblast differentiation

and mineralization [119,245,246]. Cortisol triggers the production of a mature extracellular matrix that eventually becomes mineralized upon precipitation and attachment of hydroxyapatite crystals, a process mediated at least partially by alkaline phosphatase (ALPL) [12]. The observed overlap between rosiglitazone- and dexamethasone mediated gene regulation provides further evidence for a role of rosiglitazone - activated PPAR-γ in glucocorticoid - mediated signaling in extracellular matrix mineralization. In support of this, we have shown earlier that PPARG expression is directly induced by dexamethasone in human osteoblasts [121]. The observed additional stimulation of expression of dexamethasone targets by rosiglitazone suggests that osteoblast-, osteoblast-like differentiation - and mineralization processes are susceptible to these environmental inputs in a dose-dependent manner, and that the addition of rosiglitazone to the dexamethasone - containing differentiation condition can further amplify those essential glucocorticoid - regulated processes resulting in an accelerated and enhanced physiological or pathological mineralization phenotype. High pharmacological levels of glucocorticoids for longer periods frequently result in osteoporosis, and metabolic syndrome that is a constellation of metabolic risk factors including insulin resistance, dyslipidemia, hypertension and central obesity that significantly increases the risks of Type 2 diabetes and cardiovascular disease [247]. It is therefore conceivable that rosiglitazone may amplify glucocorticoid signaling above a physiological level causing an accelerated onset of the adverse effects clinically seen by excess glucocorticoid signaling on bone and vascular health.

The fact that differentiated osteoblasts and CVCs show remarkable similarity based on their reduced distance by principal component analysis using the rosiglitazone gene signature is striking as Alves and co-workers found that, despite some similarities, the transcriptomes of osteoblasts and CVCs were overall different, and the degree of difference did not change during the time course of differentiation [224]. The rosiglitazone gene signature can discriminate osteoblasts from MSCs and CVCs from VSMCs based on their differ-

entiation status. Differentiated CVCs and osteoblasts are more similar to each other than undifferentiated MSCs and VSMCs. These results suggest that the rosiglitazone gene signature contains important regulators of extracellular matrix production and mineralization that are common between physiological and pathological conditions. Despite the great overlap identified, we have focused our efforts on the identification of CVC-specific rosiglitazone targets considering the serious cardiovascular side effects that have been reported for rosiglitazone [72, 73, 168] and as those may provide the most promising candidates to target pathological mineralization. We were able to identify five key genes differentially expressed in CVCs compared to VSMCs and also differentially expressed between carotid plaque tissue compared to the respective adjacent intact tissue, showing the same directionality of gene expression change: PDK4, SDC4, SPRY4, TCF4, and DACT1. PDK4 is upregulated in CVCs and also overexpressed in carotid plaques. In line with this finding, the pyruvate dehydrogenase complex has been described as an emerging target for the treatment of metabolic syndrome. To maintain a steady-state level of adenosine triphosphate during the feed-fast cycle, cells need to utilize fatty acid and glucose efficiently that is controlled by the pyruvate dehydrogenase complex. Lee *et al.* have mentioned recently an important role for PDK4 in vascular mineralization including an upregulation of PDK4 and phosphorylation of the pyruvate dehydrogenase complex in cultured VSMCs and calcified vessels of patients with atherosclerosis [248]. In their mentioned unpublished work, PDK4 promoted osteogenic differentiation of VSMCs by phosphorylating SMAD1/5/8 and enhancing bone morphogenic protein 2 signaling [248].

The remaining 4 key genes identified (SDC4, TCF4, DACT1, and SPRY4) are downregulated in CVCs and also under-expressed in carotid plaques. SPRY4 is a member of the Spry protein family that can serve as feedback modulator of receptor tyrosine kinases, PI3K/Akt, and MAPK/ERK signaling mechanisms. Interestingly, SPRY4 has been described recently as a suppressor of VSMC differentiation by antagonizing both MAPK/ERK and Akt signal-

ing *in vitro* [249]. The downregulation of SPRY4 may facilitate the differentiation process of VSMCs that may, together with other stimuli, facilitate the differentiation into CVCs. DACT1 is a member of the Dact protein family of multi-domain adaptor proteins that serve as a nodal point in regulating many cellular activities by regulating Wnt and Tgf-β signaling [250]. However potential roles of DACT1, SDC4 and TCF4 in pathological mineralization have not yet been described.

In conclusion, the current study provides evidence for a particularly high susceptibility to rosiglitazone - mediated perturbation of the osteoblast transcriptome during the early differentiation phase leading to accelerated osteoblast differentiation and mineralization. The identified rosiglitazone gene signature can discriminate non-mineralized VSMC, MSC and early osteoblast cultures from differentiated and mineralized osteoblast and CVC cultures, and is associated with an increased mineralization phenotype. Comprehensive comparative analyses have revealed five rosiglitazone targets that are differentially regulated exclusively in pathological mineralization and hence serve as promising candidates to improve vascular health.

Table 6.1
The rosiglitazone gene signature

Gene symbol	Entrez ID	Gene symbol	Entrez ID	Gene symbol	Entrez ID
ABCA1	19	FOXC2	2303	PPP1R3C	5507
ACADVL	37	FRAT2	23401	PSCD2	9266
AFAP1L1	134265	FTHL2	2497	PTGER2	5732
AGTR1	185	GADD45A	1647	PTGS2	5743
AHNAK	79026	GADD45B	4616	PTPLAD2	401494
AK025332	0	GDE1	51573	PTTG2	10744
AKR1B10	57016	GNAQ	2776	PVRL3	25945
AKR1C2	1646	HBEGF	1839	RASD1	51655
AKR1C3	8644	HES1	3280	RCAN1	1827
ALDH1A3	220	HEYL	26508	RHOB	388
ALG6	29929	HMOX1	3162	RNF13	11342
ANGPTL4	51129	HNRPA1L-2	664709	RRBP1	6238
ANKRD1	27063	HNRPAB	3182	SCD	6319
APOL3	80833	HRASLS3	11145	SDC4	6385
ASS1	445	HSPA1A	3303	SERPINE1	5054
AXUD1	64651	ID1	3397	SERTAD1	29950
BAX	581	ID2	3398	SERTAD4	56256
BCYRN1	618	IER5	51278	SF3B1	23451
BHLHB2	8553	IL10	3586	SGK1	6446
C10orf10	11067	IL8	3576	SHROOM3	57619
C13orf15	28984	ISG20L1	64782	SLC25A25	114789
C14orf24	283635	JUN	3725	SLC2A3	6515
C18orf17	125488	JUNB	3726	SLC40A1	30061
C1QTNF1	114897	KIAA1199	57214	SNAI2	6591
C20orf149	79144	KLF10	7071	SPHK1	8877
C21orf55	54943	KRCC1	51315	SPRY2	10253
C2orf33	56947	KRTAP1-1	81851	SPRY4	81848
CCDC80	151887	KRTAP1-3	81850	STC1	6781
CD276	80381	KRTAP1-5	83895	STK38	11329
CDC14B	8555	LAMA4	3910	SUCLG1	8802
CDC42EP2	10435	LATS2	26524	TCF4	6925
CDC42SE1	56882	LOC134997	134997	TDG	6996
CDKN1A	1026	LOC387763	387763	THBS3	7059
CEBPA	1050	LOC407835	407835	TIPARP	25976
CFD	1675	LOC63920	63920	TKT	7086
CIDEC	63924	LRRC41	10489	TMEM101	84336
CKAP2	26586	LTBR	4055	TMEM135	65084
CLOCK	9575	LYSMD2	256586	TMEM16C	63982
CRYAB	1410	MAFF	23764	TNC	3371
CTNNB1	1499	MANBAL	63905	TOB1	10140
CYGB	114757	MAP3K6	9064	TRIB1	10221
DAB2	1601	MCL1	4170	TRRAP	8295
DACT1	51339	MEF2D	4209	TSC22D3	1831
DBC1	1620	MIDN	90007	UNG	7374
DDIT4	54541	MMD	23531	WRNIP1	56897
DDR2	4921	MYC	4609	XM 371243	na
DEPDC6	64798	MYLIP	29116	XM 375558	na
DHCR7	1717	NFIC	4782	XM 925863	na
DIAPH3	81624	NM 001024646	na	XM 927528	na
DUSP1	1843	NM 032794	na	XM 930284	na
DUSP5	1847	NOV	4856	XM 930995	na
DYRK2	8445	NPSR1	387129	XM 936937	na
EDG3	1903	NR2F1	7025	XM 942223	na
EGFLAM	133584	NUAK1	9891	XM 944429	na
EGR1	1958	OSBPL6	114880	YRDC	79693
EGR2	1959	PANK1	53354	ZC3H12A	80149
EGR3	1960	PDK4	5166	ZFP36	7538
EPHX1	2052	PICALM	8301	ZFP36L1	677
ERP29	10961	PIK3R1	5295	ZNF281	23528
FABP4	2167	PIM1	5292	ZNF581	51545
FAM46B	115572	PPAP2A	8611	ZNF682	91120
FOSB	2354	PPP1R15A	23645		

Table 6.2
Connectivity map analysis of rosiglitazone targets in osteogenic hMSCs

Compound	Cell line	Enrichment	P
diphenhydramine	MCF7	0.99	0.00012
nadolol	MCF7	0.982	0.0006
quipazine	MCF7	0.98	0.0007
benzathine benzylpenicillin	MCF7	0.974	0.00109
amantadine	MCF7	0.967	0.00181
iproniazid	MCF7	0.964	0.00217
methoxamine	MCF7	0.955	0.0035
khellin	MCF7	0.95	0.00455
adiphenine	MCF7	0.937	0.00769
metoprolol	MCF7	0.935	0.00797
trimethobenzamide	MCF7	0.933	0.00849
metronidazole	MCF7	0.928	0.00972
troglitazone	HL60	0.9	0.0001
naproxen	MCF7	0.838	0.00107
CP-320650-01	PC3	0.821	0.00179
PHA-00745360	MCF7	0.802	0.0029
tanespimycin	MCF7	-0.392	0.00006
prochlorperazine	MCF7	-0.518	0.00899
monorden	MCF7	-0.53	0.00118
chlorpromazine	PC3	-0.798	0.00328
fluocinonide	MCF7	-0.833	0.00923
rottlerin	MCF7	-0.836	0.00877
lanatoside C	MCF7	-0.852	0.00647
ethotoin	MCF7	-0.873	0.00409
helveticoside	MCF7	-0.9	0.00192
beta-escin	MCF7	-0.912	0.00118
alsterpaullone	PC3	-0.931	0.00984
parbendazole	MCF7	-0.933	0.00924
azacitidine	MCF7	-0.942	0.0073
papaverine	MCF7	-0.946	0.00634
disulfiram	PC3	-0.954	0.00453
clioquinol	MCF7	-0.957	0.00022
8-azaguanine	MCF7	-0.959	0.00372
benfluorex	MCF7	-0.962	0.00322
camptothecin	MCF7	-0.97	0.00191
methylbenzethonium chloride	PC3	-0.972	0.00161
sulconazole	MCF7	-0.974	0.00139
mebendazole	MCF7	-0.985	0.00048
helveticoside	PC3	-0.985	0.0005
lanatoside C	PC3	-0.989	0.00026
quinisocaine	MCF7	-0.997	0.00004
anisomycin	MCF7	-0.998	0.00004

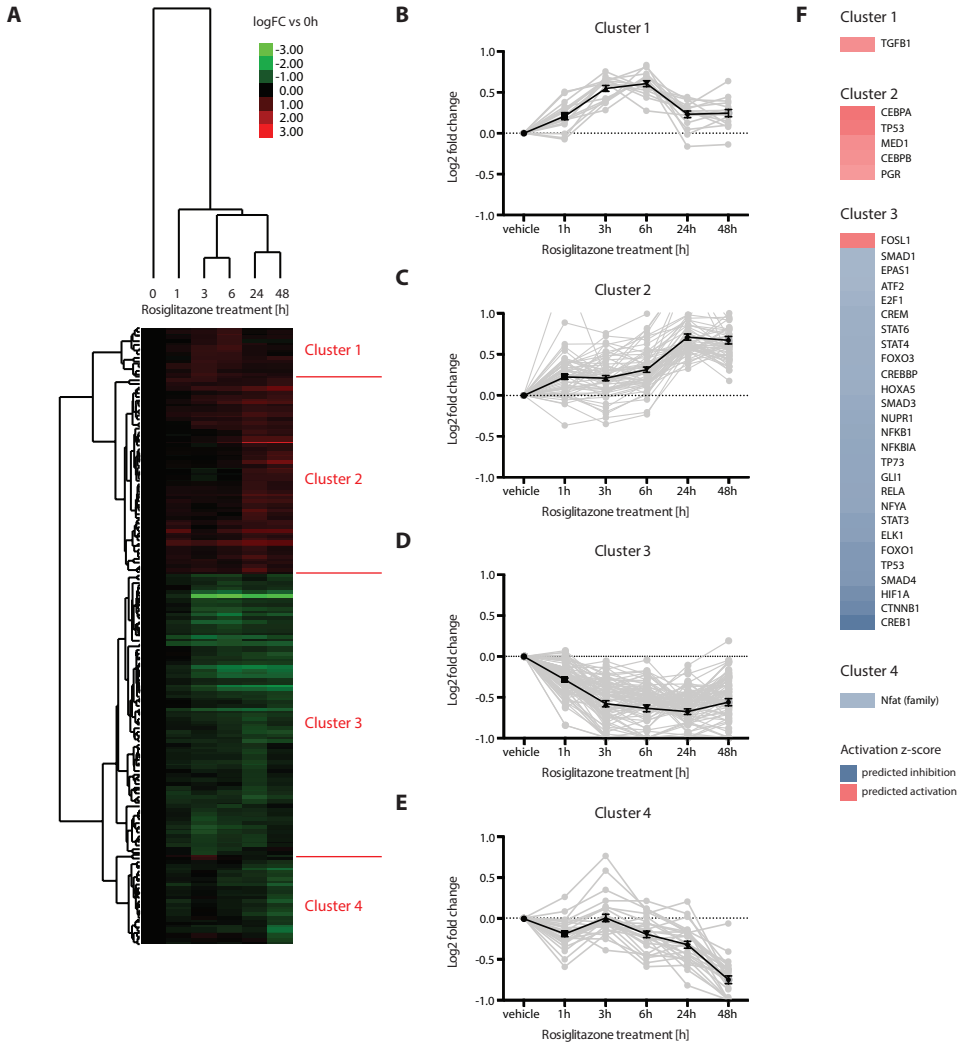

Figure 6.3
Rosiglitazone-target genes cluster into separate expression pattern groups that underlie discrete upstream regulatory processes. A) Heatmap displaying the results obtained from hierarchical clustering analysis. Probesets included were selected based on $q \leq 0.05$ in at least one condition compared to control. Blue: low expression fold change; Red: high expression fold change compared to controls; row-normalized. The data were generated from 3 wells in duplicate for each condition. B - E) Average expression patterns of the four clusters. Data represented are mean $\pm$ S.E. log fold change of each rosiglitazone condition compared to controls. F) Upstream regulator analysis of the four individual clusters using Ingenuity pathway analysis. Transcription regulators were selected; activation and inhibition predication z-score cut-off was +2.00 or -2.00, respectively.

Figure 6.4 (following page)
Rosiglitazone-target clusters are annotated with distinct cellular compartments, molecular functions and biological processes. DAVID gene functional classification tool - based gene ontology analysis of the four individual clusters according to A) cellular compartments, and B) molecular function. Annotations were selected based on $p \leq 0.1$.

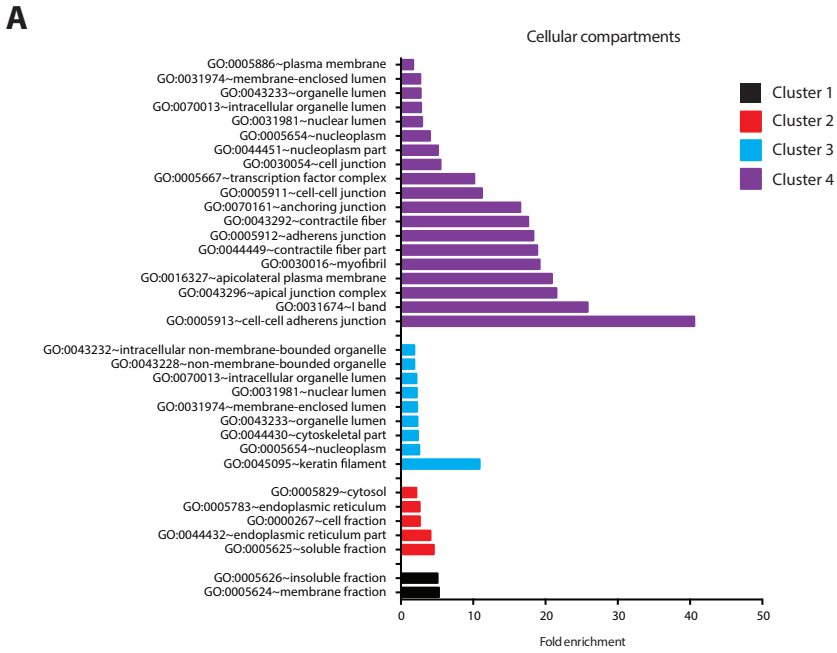
A
Cellular compartments
GO:0005886~plasma membrane
GO:0031974~membrane-enclosed lumen
GO:0043233~organelle lumen
GO:0070013~intracellular organelle lumen
GO:0031981~nuclear lumen
GO:0005654~nucleoplasm
GO:0044451~nucleoplasm part
GO:0030054~cell junction
GO:0005667~transcription factor complex
GO:0005911~cell-cell junction
GO:0070161~anchoring junction
GO:0043292~contractile fiber
GO:0005912~adherens junction
GO:0044449~contractile fiber part
GO:0030016~myofibril
GO:0016327~apicolateral plasma membrane
GO:0043296~apical junction complex
GO:0031674~I band
GO:0005913~cell-cell adherens junction
GO:0043232~intracellular non-membrane-bounded organelle
GO:0043228~non-membrane-bounded organelle
GO:0070013~intracellular organelle lumen
GO:0031981~nuclear lumen
GO:0031974~membrane-enclosed lumen
GO:0043233~organelle lumen
GO:0044430~cytoskeletal part
GO:0005654~nucleoplasm
GO:0045095~keratin filament
GO:0005829~cytosol
GO:0005783~endoplasmic reticulum
GO:0000267~cell fraction
GO:0044432~endoplasmic reticulum part
GO:0005625~soluble fraction
GO:0005626~insoluble fraction
GO:0005624~membrane fraction
0
10
20
30
40
50
Fold enrichment
Cluster 1
Cluster 2
Cluster 3
Cluster 4

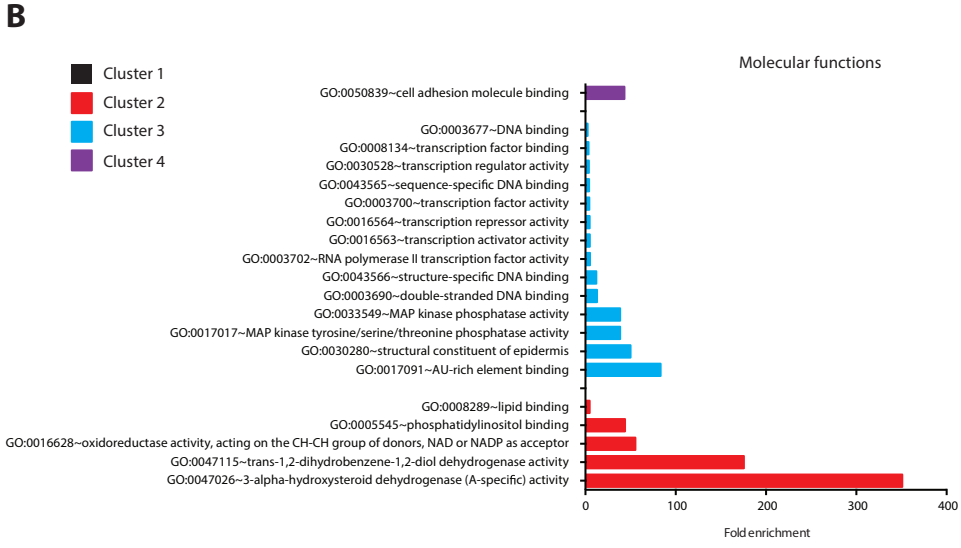
B
Molecular functions
Cluster 1
Cluster 2
Cluster 3
Cluster 4
GO:0050839~cell adhesion molecule binding
GO:0003677~DNA binding
GO:0008134~transcription factor binding
GO:0030528~transcription regulator activity
GO:0043565~sequence-specific DNA binding
GO:0003700~transcription factor activity
GO:0016564~transcription repressor activity
GO:0016563~transcription activator activity
GO:0003702~RNA polymerase II transcription factor activity
GO:0043566~structure-specific DNA binding
GO:0003690~double-stranded DNA binding
GO:0033549~MAP kinase phosphatase activity
GO:0017017~MAP kinase tyrosine/serine/threonine phosphatase activity
GO:0030280~structural constituent of epidermis
GO:0017091~AU-rich element binding
GO:0008289~lipid binding
GO:0005545~phosphatidylinositol binding
GO:0016628~oxidoreductase activity, acting on the CH-CH group of donors, NAD or NADP as acceptor
GO:0047115~trans-1,2-dihydrobenzene-1,2-diol dehydrogenase activity
GO:0047026~3-alpha-hydroxysteroid dehydrogenase (A-specific) activity
0
100
200
300
400
Fold enrichment

[h]

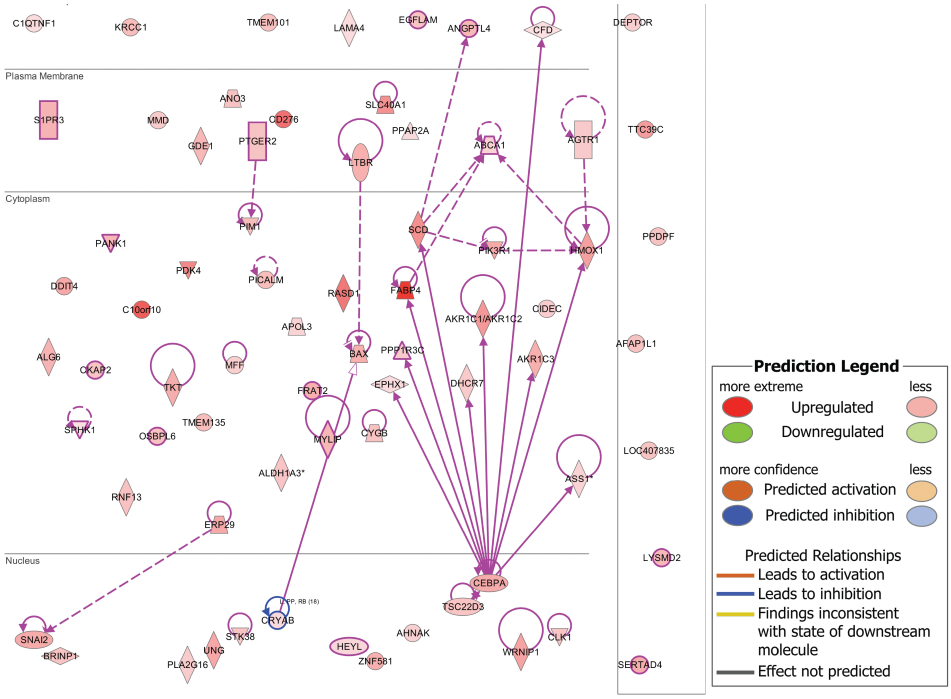

Figure 6.5
Rosiglitazone-target clusters are annotated with distinct cellular compartments, molecular functions and biological processes. Subcellular localization of clusters 1 and 2 by Ingenuity Pathway Analysis. Direct connections were added between the genes with curated regulatory interactions.

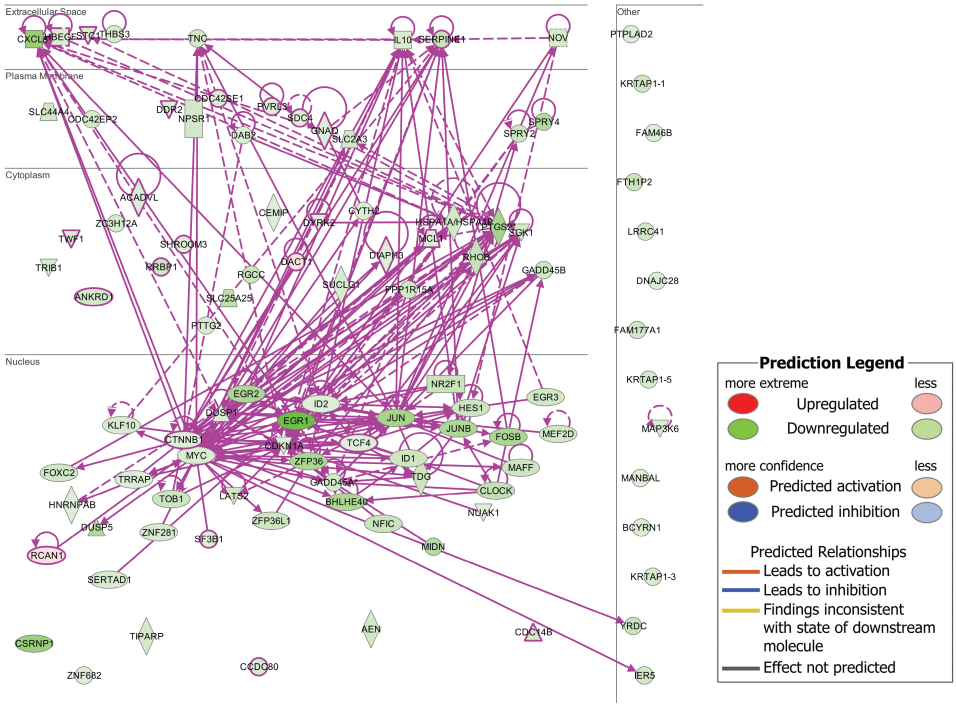

Figure 6.6
Rosiglitazone-target clusters are annotated with distinct cellular compartments, molecular functions and biological processes. Subcellular localization of clusters 3 and 4 by Ingenuity Pathway Analysis. Direct connections were added between the genes with curated regulatory interactions.

Figure 6.7 (following page)
A rosiglitazone-targeted gene signature can discriminate differentiating hMSC and VSMC cultures based on their differentiation status. A) Principal component analysis (PCA) of the rosiglitazone signature in osteoblasts differentiating from hMSCs and CVCs differentiating from VSMC cultures. B-E) GSEA of clusters 1 and 2 from the rosiglitazone signature comparing differentiated osteoblasts with MSC and early (d2) osteoblast cultures (B, C), and comparing CVCs with VSMCs (D, E). Heatmaps in B) and D) show expression changes of the upregulated rosiglitazone targets (i.e cluster 1 and 2 genes) in osteoblasts from different timepoints compared to MSC d0; data were row-normalized. C, and E show GSEA results. The obtained negative enrichment scores indicate an enrichment of the cluster 1 and 2 signature in the differentiated groups in both osteogenic MSC and VSMC-CVC analyses. Statistical parameters for MSC - osteoblast GSEA were determined as the following: normalized enrichment score (-1.266), nominal p-value (0.02), FDR q-value (0.03), FWER p-value (0.03). For VSMC - CVC GSEA, the following statistical parameters were quantified: normalized enrichment score (-1.244), nominal p-value (0.07), FDR q-value (0.058), FWER p-value (0.055).

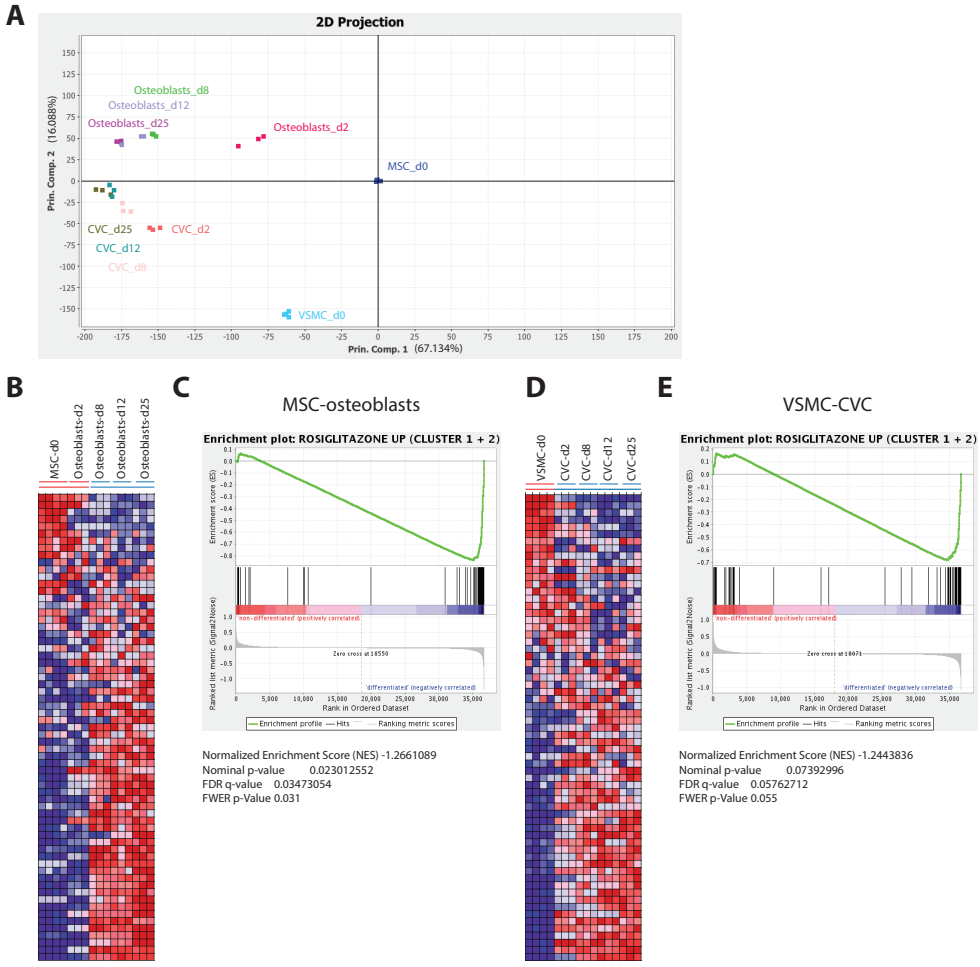
A
2D Projection
Osteoblasts_d8
Osteoblasts_d12
Osteoblasts_d25
Osteoblasts_d2
MSC_d0
CVC_d25
CVC_d2
CVC_d12
CVC_d8
VSMC_d0
Prin. Comp. 2 (16.088%)
Prin. Comp. 1 (67.134%)
B
MSC-d0
Osteoblasts-d2
Osteoblasts-d8
Osteoblasts-d12
Osteoblasts-d25
C
MSC-osteoblasts
Enrichment plot: ROSIGLITAZONE UP (CLUSTER 1 + 2)
Normalized Enrichment Score (NES) -1.2661089
Nominal p-value 0.023012552
FDR q-value 0.03473054
FWER p-Value 0.031
D
VSMC-d0
CVC-d2
CVC-d8
CVC-d12
CVC-d25
E
VSMC-CVC
Enrichment plot: ROSIGLITAZONE UP (CLUSTER 1 + 2)
Normalized Enrichment Score (NES) -1.2443836
Nominal p-value 0.07392996
FDR q-value 0.05762712
FWER p-Value 0.055

[h]

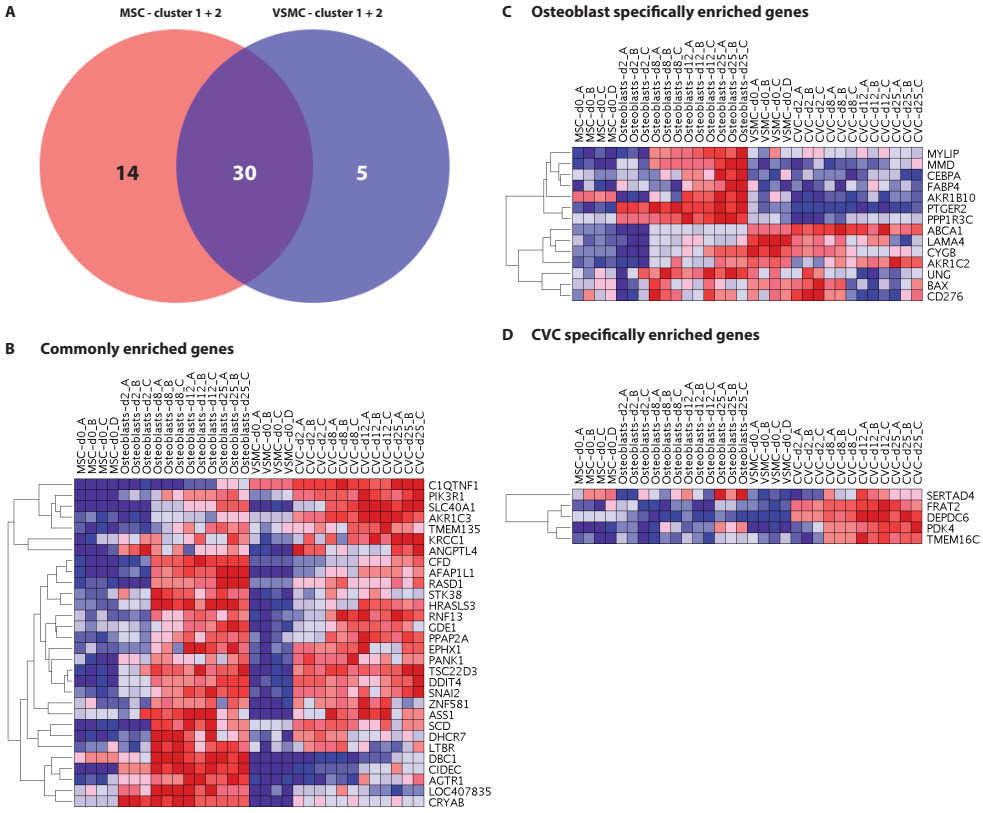

Figure 6.8
Identification of commonly and specifically enriched rosiglitazone targets during physiological and pathological mineralization. A) VENN diagram of cluster 1 and 2 genes identified to be significantly enriched by GSEA analyses of osteoblasts versus MSCs and of CVCs versus VSMCs. Heatmaps displaying expression patterns of the genes identified by GSEA and found to be B) commonly enriched in osteoblasts and CVCs, C) specifically enriched in osteoblasts, and D) specifically enriched in CVCs. All data were row-normalized.

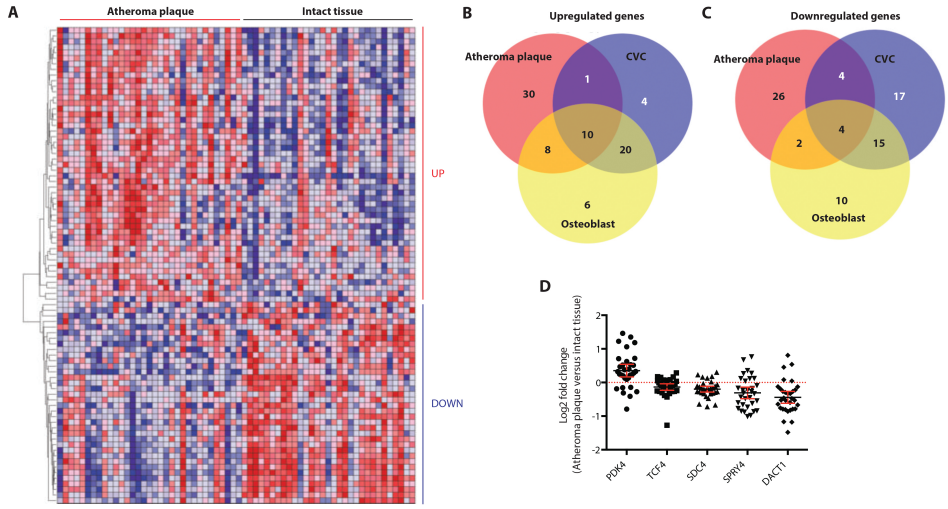

Figure 6.9
Identification of rosiglitazone targets in atherosclerosis. A) Heatmap of the 85 rosiglitazone targets differentially expressed between carotid plaque and intact tissue from atherosclerotic patients. Data were row-normalized. Venn diagrams of the genes from the upregulated carotid plaque cluster, and clusters 1 and 2 in osteoblasts and CVCs (B), and of the genes from the downregulated carotid plaque cluster and clusters 3 and 4 in osteoblasts and CVCs (C). D) Pairwise carotid plaque versus intact tissue expression changes of the identified 5 pathological mineralization - specific rosiglitazone targets PDK4, TCF4, SDC4, SPRY4, and DACT1. Data from each atherosclerotic patient are represented $\pm$ 95% confidence interval. E) Ingenuity pathway analysis generated gene expression regulatory networks around the 5 key targets identified with overlayed expression changes from the patient dataset (carotid plaque versus intact tissue, cut-off $p \leq 0.05$).

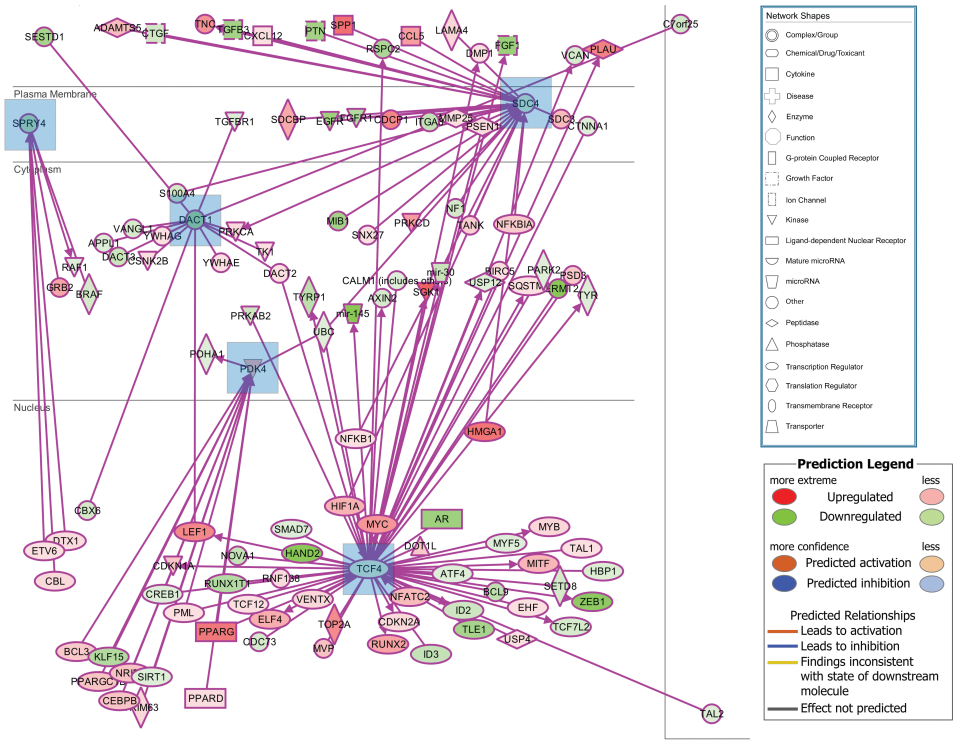

Figure 6.10
Identification of rosiglitazone targets in atherosclerosis. Ingenuity pathway analysis generated gene expression regulatory networks around the 5 key targets identified with overlayed expression changes from the patient dataset (carotid plaque versus intact tissue, cut-off $p \leq 0.05$).

7 General discussion

The PPAR-γ activators of the thiazolidinedione (TZD) class have recently been identified as risk factors for osteoporosis and cardiovascular disease [40, 72–75]. This thesis has aimed to characterize the functional role and consequences of TZD - stimulated PPAR-γ signaling in bone metabolism and pathological mineralization in order to achieve a better understanding that may facilitate the development of strategies to prevent the actions of these risk factors in the future. The studies presented in this thesis have revealed three major findings. Firstly, PPAR-γ signaling is functional and endogenously upregulated in differentiating osteoblast and osteoblast-like cells (Chapter 2) and can operate synergistically with established osteoblast differentiation stimulators such as dexamethasone and 1,25-dihydroxyvitamin D3 (Chapters 2 and 4). Secondly, activation of PPAR-γ signaling by the TZD rosiglitazone accelerates osteoblast differentiation at the expense of increased oxidative stress and apoptosis explaining the widely observed reduction in bone mass and quality in TZD - treated patients (Chapter 3). The adipogenic lineage is protected from this providing an alternative concept of aging - related lineage skewing (Chapter 3). Thirdly, the antioxidant resveratrol diminishes rosiglitazone - mediated actions in osteoblast and osteoblast-like differentiation suggesting that reducing rosiglitazone - stimulated oxidative stress may prevent the detrimental effects of TZDs on bone and cardiovascular health (Chapter 5). Finally, genome-wide expression analyses in human mesenchymal stem cells differentiating into osteoblasts and vascular smooth muscle cells differentiating into calcifying vascular cells revealed five

target gene candidates (PDK4, SDC4, SPRY4, TCF4 (also referred to as E2-2), and DACT1) that may specifically control extracellular matrix mineralization in vascular cells and hence provide interesting candidates for further investigations to improve vascular health (Chapter 6).

7.1 Presence and upregulation of classical 'fat cell' markers in differentiating osteoblasts

The unexpected presence and upregulation of PPAR-γ during osteoblast differentiation was initially discovered by unbiased transcriptome profiling of the human pre-osteoblastic cell line SV-HFO during dexamethasone - induced differentiation *in vitro* (Eijken et al.; data unpublished). The data presented in Chapter 2 have confirmed increasing expression levels of the three PPARG transcripts-1, -3 and -4 giving rise to PPAR-γ1 protein but not PPARG-2 encoding for PPAR-γ2 protein during the differentiation of two human pre-osteoblast cell lines SV-HFO and NHOST, during human MSC differentiation towards the osteoblastic lineage, and finally in a VSMC-based model for vascular calcification that mimics matrix formation and mineralization by the osteoblasts. In the absence of differentiation towards matrix - producing and mineralizing cells, PPARG transcript levels are virtually absent and do not increase during culture time. In addition, transcript levels of three confirmed primary PPARG target genes ANGPTL4, FABP4 and ADFP increase during osteoblast differentiation, which correlates with the changes in expression levels of PPARG transcripts-1, -3 and -4. Together these data demonstrate a clear coupling between PPAR-γ1 expression and extracellular matrix synthesis and mineralization. Alves *et al.* have recently demonstrated high abundance of the PPAR-γ target FABP4 in human trabecular bone samples using large-scale mass spectrometry-based proteomic analyses. FABP4 belonged to the top 20 ranked proteins

according to expression with a higher abundance compared to some of the classical bone proteins BGN, MGP, SPARC, ALPL and SPP1 [251]. Moreover, the transcriptional upregulation of PPAR-γ signaling during osteoblast differentiation has been confirmed recently by Staines and co-workers who performed microarray analyses on murine calvarial osteoblasts cultured under conditions that permit both physiological extracellular matrix mineralization via the formation of discrete nodules and terminal differentiation of osteoblasts into osteocytes [252].

7.2 Molecular cross-talk between PPAR-γ and other nuclear receptors

7.2.1 Glucocorticoid receptor

The short-term dexamethasone incubation studies in Chapter 2 have revealed that PPARG expression is directly stimulated by dexamethasone. Addition of the glucocorticoid receptor antagonist RU-486 blocks the dexamethasone effect demonstrating glucocorticoid receptor dependence. Finally, *in silico* searches for putative glucocorticoid receptor response elements (GRE) in the promoter region of the *PPARG* gene have revealed several hits close to the transcription start sites, and blocking *de novo* protein biosynthesis using cycloheximide does not change the stimulatory action of dexamethasone on *PPARG* expression demonstrating that *PPARG* is a direct glucocorticoid receptor target gene. Despite clear stimulation of bone formation by glucocorticoids *in vitro*, pharmacological levels exceeding the physiological concentrations of glucocorticoids for longer periods can cause detrimental skeletal effects. In support of this, glucocorticoid-treated male Swiss Webster mice exhibit an increase in osteoblast apoptosis in vertebrae and show apoptosis in 28% of the osteocytes in metaphyseal cortical bone [149]. Increased osteoblast and osteocyte apoptosis is also

found in patients with glucocorticoid-induced osteoporosis [149]. These findings suggest that PPAR-γ is a component of the glucocorticoid - mediated apoptosis pathway in bone. We hypothesize that activation of the increased pool of PPAR-γ by its endogenous or synthetic ligands can further amplify the detrimental effects of glucocorticoids on bone.

7.2.2 Vitamin D receptor

The vitamin D receptor (VDR) is important for bone health and osteoblast differentiation, and is expressed in osteoblasts where it interacts directly with the key transcription factor for osteoblast differentiation RUNX2 in the regulation of osteocalcin and osteopontin expression (for review, see [253]). Bosetti and co-workers have revealed recently a stimulatory effect of 1,25-dihydroxyvitamin D3 on proliferation and expression of osteogenic markers as well as human MSC differentiation into osteoblasts demonstrating improved osteoinductivity and osteoconductivity of a poly-L-lactide acid scaffold for bone tissue engineering [254]. A large amount of evidence has accumulated demonstrating extensive molecular cross-talk between VDR and other members of the nuclear receptor superfamily in the control of bone metabolism that is mediated via interaction with a multitude of transcription factors and DNA and histone - modifying proteins (for review, see [255]). In melanoma cells, 1,25-dihydroxyvitamin D3 stimulates PPAR-α/δ expression [104] while in breast cancer cells PPAR-γ binds VDR and represses its transcriptional activity possibly by competing for RXR heterodimerization [256]. Kapil *et al.* have shown recently that molecular cross-talk between PPAR-γ and VDR can improve protection against ischemia reperfusion - induced acute kidney injury *in vivo* [257]. The studies from this thesis in Chapter 4 have revealed a partial suppressive effect of rosiglitazone on 1,25-dihydroxyvitamin D3 - mediated stimulation of the mineralization inhibitor BGLAP that is correlated with excessive mineralization. This mechanism may form an additional component of a molecular cross-talk between VDR

and PPAR-γ signaling in human osteoblast mineralization suggesting that TZD - activated PPAR-γ may partly diminish the regulatory function of VDR in the control of excessive mineralization.

7.3 An alternative model underlying the detrimental consequences of PPAR-γ on bone

The studies from this thesis in Chapter 3 have revealed an acceleration of osteoblast differentiation by activated PPAR-γ that is ultimately followed by mitochondrial dysfunction, oxidative stress and apoptosis. In line with our findings, rosiglitazone was associated with small reductions in femoral neck, total hip and lumbar spine bone mineral density (BMD) and significantly increased bone turnover markers compared with metformin in a recent randomized, double-blinded study in postmenopausal women with type 2 diabetes mellitus [258]. The observed differential susceptibility of adipocytes and osteoblasts to PPAR-γ - induced oxidative stress that favors osteoblast apoptosis but does not derogate adipocyte survival provides a new concept for TZD - induced bone loss and bone marrow adipogenesis that is, unlike earlier models [41, 45, 87, 88, 259], in accordance with uncoupled osteoblast and adipocyte differentiation from their common progenitor, the MSC. In support of this concept, recent studies have provided evidence for an independence of osteoblast from adipocyte differentiation processes and *vice versa*. Rahman *et al.* have recently demonstrated a downstream mechanism of rosiglitazone - activated PPAR-γ2 involving β-catenin. β-catenin signaling is an important stimulator of osteoblast differentiation. In PPAR-γ2 expressing U-33 cells that are primed to differentiate into adipocytes, rosiglitazone treatment lead to a rapid proteolytic degradation of β-catenin. Interestingly, the attempt to rescue this phenotype by stabilizing β-catenin expectedly suppressed the PPAR-γ2 pro-adipogenic

function but to the authors' surprise, osteoblastogenesis was not restored [259]. Moreover, Yoshiko and co-workers have demonstrated that rosiglitazone - enhanced nuclear translocation of PPAR-γ in rat calvaria cells isolated within the osteoblast lineage developmental hierarchy increased CFU-ALP colonies and bone nodule formation despite increasing adipogenesis in these cultures at the same time [260]. Interestingly, in a 14-week prospective, double-blind, randomized, placebo-controlled trial, rosiglitazone treatment has resulted in significantly reduced spine fat besides the expected decreases in femoral neck and lumbar spine BMD [261]. Together these data provide evidence for a new concept on bone health that adds to the explanation of the clinically observed suppressive action of activated PPAR-γ on bone and the widely but not obligatory observed associated phenomenon on bone marrow adipogenesis. This concept is based on a higher susceptibility of the osteogenic than the adipogenic lineage to oxidative stress and apoptosis that is preferentially triggered in the osteoblasts by activated PPAR-γ.

7.4 Rosiglitazone as accelerator of pathological mineralization

In Chapter 5 of this thesis, direct stimulatory effects of rosiglitazone on mineralization of cultured human VSMCs, an *in vitro* model of vascular mineralization, are demonstrated. The stimulatory effect on mineralization is at least partly caused by induction of caspase - dependent apoptosis. In addition, rosiglitazone increases osteoblast-like differentiation that is correlated with the stimulation of oxidative stress and mineralization. The findings presented in Chapter 5 are supported by the studies described in Chapter 6 in which a rosiglitazone gene signature is correlated with osteoblast-like differentiation and mineralization of VSMCs into CVCs. The identified rosiglitazone / differentiation / apoptosis / mineralization

cascade envisions a novel mechanism that may serve as explanatory model for the clinically observed increased risk for myocardial infarction in rosiglitazone - treated diabetic type 2 patients [72, 73]. In support of this, Pro12Ala and C161T loss of function mutations of *PPARG* in humans are associated with a lower incidence of myocardial infarction and angiographically documented atherosclerotic heart disease [182, 183]. Taken together, the findings from this thesis regarding the influence of rosiglitazone on pathological mineralization suggest that, once atherosclerotic plaque has been formed, rosiglitazone accelerates the mineralization process leading to an increase in calcified vascular lesions. We have shown that the caloric restriction mimetic and antioxidant resveratrol diminished rosiglitazone - induced oxidative stress, apoptosis, osteoblast-like differentiation and mineralization. Therefore, improving mitochondrial function and the antioxidant protection system may be a successful strategy to prevent aging - related and TZD - induced bone loss and vascular calcification.

7.5 Preventing the risks of TZDs in bone loss and cardiovascular disease

The novel concept defined in this thesis provides a rationale for using antioxidants or other agents to improve mitochondrial function in order to prevent the clinically observed detrimental effects of TZDs in bone and cardiovascular health. In support of this concept regarding cardiovascular health, the caloric restriction mimetic and antioxidant resveratrol suppresses atherosclerosis in hypercholesterolemic mice (lacking both apolipoprotein E and LDL receptor) on a high fat diet [214] and exerts beneficial effects in male Wistar rats on high-fat diet but not on standard diet (e.g. ox-LDL, decreased serum and hepatic oxidative stress) [215]. In line with the suggested stimulatory action of rosiglitazone on reactive oxygen species being at least partially responsible for the clinically observed detrimental

skeletal effects, Nishikawa and co-workers have demonstrated aging - related bone loss that was associated with ROS and activated PPAR-γ - mediated reduction in Maf expression and rescued by the antioxidant N-acetylcysteine in a murine model *in vivo* [262]. A study conducted by Liu and co-workers has demonstrated protective effects of resveratrol against bone loss induced by estrogen deficiency [263]. Moreover, Hernandez-Vallejo and co-workers have demonstrated improved osteoblastic potential by the antioxidant pravastatin in an *in vitro* study of HIV protease inhibitor treated MSCs [264]. Furthermore, Singh reported an inhibition of collagen type I, osteopontin, and bone sialoprotein formation by 2,3,7,8,-tetrachlorodibenzo-p-dioxin from cigarette smoke, and these effects were antagonized by resveratrol [265]. Also direct stimulatory actions of resveratrol on osteoblastogenesis have been reported previously. Kupisiewicz and co-workers described a resveratrol - mediated activation of osteoblastic activity *in vitro* by transcription of core binding factor α-1 (Cbfa-1; [266]). Su *et al.* reported that resveratrol induces bone morphogenic protein-2 through Src kinase-dependent estrogen receptor activation [267].

7.6 Conclusion

In conclusion, this thesis provides new insights into the relationships between rosiglitazone, adverse cardiovascular events and osteoporosis by providing a new concept that links rosiglitazone - accelerated osteoblast or osteoblast-like differentiation, oxidative stress, and apoptosis with premature mineralization. Reducing rosiglitazone - stimulated oxidative stress may prevent this detrimental cascade. We position PPAR-γ signaling in this model acting downstream of glucocorticoid signaling capable of amplifying the adverse effects of excess glucocorticoids on bone and cardiovascular health.

7.7 Future perspectives

Future studies will be important to evaluate the potential of antioxidant therapy and approaches to improve mitochondrial function in combating the detrimental effects of TZDs on bone and vascular health in diabetic patients. Evidence for the protective effects of antioxidants has been presented in experimental, clinical and epidemiological studies that have demonstrated that antioxidants might be helpful in treating diabetes and its complications (for review, see [268–271]). However, the results of the majority of the prospective randomized controlled antioxidant trials have failed to demonstrate a significant benefit in the prevention of cardiovascular events, of antioxidant supplementation in primary patients without clinical evidence of cardiovascular disease, or in secondary patients with clinical evidence of cardiovascular disease [272–281]. In future studies it will be important to stratify clinical outcomes comparing the effects of antioxidants or agents to improve mitochondrial function on basis of the insulin sensitizer prescribed, and also to adjust for baseline oxidative stress levels. These studies will be necessary to evaluate the potential of antioxidant therapy and approaches to improve mitochondrial function in combating the detrimental effects of TZDs on bone and vascular health in diabetic patients who exhibit insufficient antioxidant systems or impaired mitochondrial function to deal with the metabolic challenge of increased cellular influx of glucose during insulin - sensitizing therapy.

Summary

The general aim of this thesis was to study the role of PPAR-γ signaling in bone formation and pathological mineralization processes. Human mesenchymal stem cells, osteoblast cell lines and vascular smooth muscle cells under osteogenic stimuli served as model systems as described in the **Appendix**. We performed detailed analyses of the expression dynamics of PPAR-γ during the osteoblast differentiation processes in **Chapter 2**. Here we found that PPAR-γ expression levels increased during osteoblast differentiation, and were directly stimulated by the osteogenic differentiation compound dexamethasone, suggesting an involvement of PPAR-γ signaling in osteoblast differentiation. In **Chapter 3**, we investigated the involvement of PPAR-γ signaling in the differentiation of osteoblasts from human mesenchymal stem cells. We found that activation of PPAR-γ signaling caused an acceleration of osteogenic differentiation that was subsequently followed by oxidative stress and a premature onset of apoptosis and mineralization. We also compared the osteogenic and adipogenic lineage regarding their susceptibilities to oxidative stress and found that cells from the adipogenic lineage were protected from oxidative stress and apoptosis that was preferentially induced in cells from the osteogenic lineage by activated PPAR-γ signaling. In **Chapter 4**, we studied a potential cross-talk between PPAR-γ and VDR signaling. We revealed a synergistic effect of rosiglitazone and 1,25-dihydroxyvitamin D3 combination treatment resulting in excessive mineralization that was associated with a suppressive effect of rosiglitazone on 1,25-dihydroxyvitamin D3 - mediated stimulation of the mineralization inhibitor BGLAP. This

may suggest that TZD-activated PPAR-γ diminishes the regulatory function of VDR in the control of excessive mineralization and may provide an additional mechanism underlying the concerning risk of TZDs in bone and cardiovascular disease. In **Chapter 5** of this thesis, direct stimulatory effects of rosiglitazone on mineralization of cultured human vascular smooth muscle cells (VSMCs), an *in vitro* model of vascular mineralization, were demonstrated. The stimulatory effect on mineralization was at least partly caused by the induction of caspase-dependent apoptosis. In addition, rosiglitazone increased osteoblast-like differentiation (i.e. calcifying vascular cells (CVCs)) that was correlated with the stimulation of oxidative stress and mineralization. The identified rosiglitazone / differentiation / apoptosis / mineralization cascade envisions a novel mechanism that may serve as explanatory model for the clinically observed increased risk for myocardial infarction in rosiglitazone-treated diabetic type 2 patients. In addition, we demonstrated that the caloric restriction mimetic and antioxidant resveratrol diminished rosiglitazone-induced oxidative stress, apoptosis, osteoblast-like differentiation and mineralization suggesting that improving mitochondrial function may be a successful strategy to prevent aging-related and TZD-induced bone loss and vascular calcification. Finally, in **Chapter 6**, we performed large-scale transcriptomic profiling in order to identify PPAR-γ - targeted gene regulatory networks underlying the observations from above. The obtained rosiglitazone-regulated networks contained confirmed primary PPAR targets and were also endogenously regulated during osteogenic differentiation from hMSCs and osteoblast-like differentiation of VSMCs into CVCs. Further comparative analysis revealed rosiglitazone targets that were commonly enriched in osteoblasts and CVCs or specifically enriched in either osteoblasts or CVCs. Finally, we compared the expression patterns of CVC-specific genes with patient expression data from carotid plaque versus intact adjacent tissue, and identified five rosiglitazone targets that were differentially regulated in CVCs and carotid plaque but not osteoblasts when compared to their respective non-mineralizing counterparts. These targets, i.e PDK4, SDC4, SPRY4, TCF4 (also commonly referred to as

'E2-2'), and DACT1 may specifically control extracellular matrix mineralization in vascular cells and hence provide interesting candidates for further investigations to improve vascular health. In conclusion, the studies presented in this thesis have elucidated the functional consequences of thiazolidinedione-activated PPAR-γ signaling in bone formation and vascular calcification. Based on the results obtained from these studies, new concepts underlying the detrimental actions of thiazolidinediones on skeletal and vascular health have been formulated. These concepts are based on acceleratory actions of thiazolidinediones on osteoblast and osteoblast-like differentiation processes being ultimatively followed by increased accumulation of reactive oxygen species, apoptosis, and enhanced mineralization. When comparing the osteogenic with the adipogenic lineage that both originate from the same progenitor, the mesenchymal stem cell, we demonstrated a higher susceptibility of the osteogenic than the adipogenic lineage to oxidative stress and apoptosis that was preferentially triggered in the osteoblasts by thiazolidinedione-activated PPAR-γ, providing an alternative explanation for the widely associated bone marrow adipogenesis phenomenon.

Samenvatting

Dit proefschrift beschrijft de rol van de transcriptie factor PPAR-γ in de signaaltransductie tijdens de vorming van bot en pathologische mineralisatie processen. Osteogeen gestimuleerde humane mesenchymale stamcellen, osteoblast cellijnen en vasculaire gladde spiercellen dienden als model systemen en zijn beschreven in **Bijlage 1**. **Hoofdstuk 2** beschrijft een gedetailleerde analyse van PPAR-γ expressie veranderingen tijdens de differentiatie van osteoblasten. Hier hebben we gevonden dat PPAR-γ expressie verhoogd is tijdens de differentiatie van osteoblasten en rechtstreeks gestimuleerd wordt door dexamethason en suggereert dat PPAR-γ signaaltransductie betrokken is tijdens osteogene differentiatie. Vervolgens hebben we in **Hoofdstuk 3** onderzocht of PPAR-γ signaaltransductie betrokken is in de differentiatie van osteoblasten uit menselijke mesenchymale stamcellen. De activatie van PPAR-γ signaaltransductie veroorzaakt een versnelling van osteogene differentiatie. Deze wordt gevolgd door oxidatieve stress en een voortijdig begin van apoptose en mineralisatie. Vervolgens vergelijken we de gevoeligheid voor oxidatieve stress in osteogeen en adipogeen differentiërende cellen. Deze experimenten laten zien dat differentiërende adipocyten beschermd zijn tegen oxidatieve stress en apoptose en geïnduceerd worden in differentiërende osteoblasten door de activatie van PPAR-γ. **In Hoofdstuk 4** onderzoeken we de communicatie tussen PPAR-γ en VDR. Hier laten we zien dat er een synergistisch effect bestaat tussen deze twee transcriptie factoren en een behandeling van zowel rosiglitazon en 1,25-dihydroxyvitamine D3 leidt tot een excessieve mineralisering. Dit was geassocieerd met een

onderdrukkend effect van rosiglitazon op de 1,25-dihydroxyvitamine-D3-gemedieerde stimulatie van de mineralisatie inhibitor BGLAP en suggereert dat de regulerende functie van VDR in de controle van buitensporige mineralisatie verminderd wordt door rosiglitazon-geactiveerde PPAR-γ. In **Hoofdstuk 5** van dit proefschrift demonstreren wij dat rosiglitazon een stimulerend effect heeft op de mineralisatie van gekweekte humane vasculaire gladde spiercellen (VSMC's), een *in vitro model* van vasculaire mineralisatie. Het stimulerende effect op de mineralisatie wordt gedeeltelijk veroorzaakt door de inductie van een caspase-afhankelijke apoptose. Daarnaast verhoogt rosiglitazon een osteoblast-achtige differentiatie (bijvoorbeeld verkalkende vasculaire cellen (CVC)) en is deze gecorreleerd met de stimulatie van oxidatieve stress en mineralisatie. De geïdentificeerde rosiglitazon / differentiatie / apoptose / mineralisatie cascade suggereert een nieuw mechanisme dat een verklaring kan geven voor het verhoogde risico op een myocardinfarct in rosiglitazon behandelde diabetes type 2 patiënten. De antioxidant resveratrol kan de rosiglitazon-geinduceerde oxidatieve stress, apoptose, osteoblast-achtige differentiatie en mineralisatie verminderen en suggereert dat een verbetering van de mitochondriale functie een succesvolle strategie kan zijn voor het TZD-geïnduceerde botverlies en de vasculaire calcificatie. Tenslotte hebben we in **Hoofdstuk 6** genoomwijde expressieprofielen gemaakt van PPAR-γ - gereguleerde signaaltransducties in osteoblast differentiërende mesenchymale stamcellen. De verkregen-rosiglitazon gereguleerde netwerken bevatten bekende PPAR gereguleerde genen die ook gereguleerd worden tijdens de osteogene differentiatie van hMSCs en osteoblast-achtige differentiatie van VSMCs in CVC. In een vergelijkende analyse van differentierende osteoblasten en CVC laten we zien dat rosiglitazon-gereguleerde genen verrijkt zijn. Tenslotte hebben we de expressie van CVC-specifieke genen vergeleken met gen-expressie profielen van arterosclerose patiënten en vinden vijf rosiglitazon targets die differentieel gereguleerd zijn in CVCs en carotis plaque maar niet in osteoblasten in vergelijking met niet-mineraliserende osteoblasten. Deze genen (PDK4, SDC4, SPRY4, TCF4 en DACT1) zijn specifiek voor extracellulaire

matrix mineralisatie in vasculaire cellen en bieden dus interessante kandidaten voor verder onderzoek om de vasculaire gezondheid te verbeteren. De studies in dit proefschrift hebben de functionele gevolgen opgehelderd van thiazolidinedion-geactiveerde PPAR-γ signaaltransductie tijdens de vorming van bot en vasculaire calcificatie. Naar aanleiding van de resultaten van deze studies hebben we nieuwe concepten geformuleerd over de nadelige werking van thiazolidinedionen op de gezondheid van het skelet en vaatstelsel. Deze concepten zijn gebaseerd op de remmende werking van thiazolidinedionen op osteoblast en osteoblast-achtige differentiatieprocessen die worden gevolgd door verhoogde accumulatie van reactieve zuurstof radicalen, apoptose en verbeterde mineralisatie. Bij de vergelijkingen van de osteoblast en adipocyte differentiëren mesenchymale stamcellen, laten we zien dat osteoblast differentiërende cellen gevoeliger zijn voor oxidatieve stress en apoptose die geactiveerd zijn door thiazolidinedion-geactiveerde PPAR-γ. Dit concept levert een alternatieve verklaring voor de vervetting van het beenmerg.

Zusammenfassung

Zielstellung dieser Arbeit war, die Rolle der Peroxisom-Proliferator-Aktivierter-Rezeptor γ (PPAR-γ) - Signaltransduktionskaskade während der Knochenbildung und Gefäßmineralisierung zu untersuchen. Menschliche mesenchymale Stammzellen, Osteoblastzelllinien und glatte Gefäßmuskelzellen unter osteogener Stimulierung dienten als Modellsysteme, wie im **Anhang** beschrieben. Das **zweite Kapitel** beschreibt detaillierte Analysen der Expressionsdynamik von PPAR-γ während des Osteoblastdifferenzierungsprozesses. Die Expression von PPAR-γ war während des Osteoblastendifferenzierungsprozesses erhöht, und wurde direkt durch das Hormon Dexamethason stimuliert. Im **dritten Kapitel** untersuchten wir die Beteiligung der PPAR-γ - Signaltransduktionskaskade während des Differenzierungsprozesses von menschlichen mesenchymalen Stammzellen in Osteoblasten. Wir fanden, dass die Aktivierung der PPAR-γ - Signaltransduktionskaskade eine Beschleunigung der osteogenen Differenzierung bewirkt, die erhöhte oxidative Stresslevel und einen vorzeitigen Beginn der Apoptose und Mineralisierung zur Folge hatte. Wir verglichen auch die osteogene und adipogene Zellreihe in Bezug auf ihre Anfälligkeit für oxidativen Stress und haben festgestellt, dass Zellen der adipogenen Zellreihe vor oxidativem Stress und Apoptose geschützt waren, die vorzugsweise in Zellen der osteogenen Zellreihe von PPAR-γ induziert wurden. Im **vierten Kapitel** untersuchten wir eine potenzielle Kopplung zwischen den PPAR-γ und Vitamin D Rezeptor - Signaltransduktionskaskaden. Wir zeigten eine synergistische Wirkung einer Kombinationsbehandlung mit Rosiglitazon und 1,25-Dihydroxyvitamin D3 die zu ei-

ner übermäßigen Mineralisierung führte. Diese Wirkung war mit einem unterdrückenden Effekt von Rosiglitazon auf die von 1,25-Dihydroxyvitamin D3 vermittelte Stimulierung des Mineralisierungshemmers BGLAP verbunden. Dieses Ergebnis deutet auf eine hemmende Wirkung von Rosiglitazon auf die regulatorische Funktion des VDR in der Kontrolle von übermäßiger Mineralisierung hin, und bildet daher einen zusätzlichen Mechanismus bezüglich des Risikos von Rosiglitazon in Osteoporose und Herz-Kreislauf-Erkrankungen. Im **fünften Kapitel** dieser Arbeit untersuchten wir die direkte stimulierende Wirkung von Rosiglitazon auf die Mineralisierung von kultivierten menschlichen glatten Gefäßmuskelzellen, einem Zellkulturmodell der Gefäßmineralisierung. Die stimulierende Wirkung auf die Mineralisierung wurde zumindest teilweise durch die Induktion von Caspase-abhängiger Apoptose verursacht. Zusätzlich erhöht Rosiglitazon osteoblastenähnliche Differenzierung, die mit der Stimulierung von oxidativem Stress und Mineralisierung korreliert war. Die identifizierte Rosiglitazon- / Differenzierungs- / Apoptose- / Mineralisierungskaskade bildet ein neues Erklärungsmodell für das klinisch beobachtete erhöhte Risiko für Myokardinfarkt in mit Rosiglitazon behandelten Diabetis Mellitus Patienten. Darüber hinaus haben wir gezeigt, dass die Behandlung mit Resveratrol, einem kalorischen restriktionsmimetischen und antioxidativen Molekül, Rosiglitazon-induzierten oxidativen Stress, Apoptose, osteoblastenähnliche Differenzierung und Mineralisierung verhindern kann. Dies deutet darauf hin, dass die Verbesserung der Funktion der Mitochondrien eine erfolgreiche Strategie für die Prävention von alterungsbedingten und Rosiglitazon - induziertem Knochenverlust und Gefäßverkalkung darstellen kann. Schließlich haben wir im **sechsten Kapitel** eine genomweite Transkriptionsanalyse durchgeführt um die Zielgene der PPAR-γ - Signaltransduktionskaskade zu identifizieren. Die erhaltenen Genregulationsnetzwerke bestätigten eine primäre Rolle der PPAR-γ - Signaltransduktionskaskade während der endogenen Osteoblastendifferenzierung und Gefäßmineralisierung. Weitere vergleichende Analysen ergaben Rosiglitazon-Zielgene, die häufig in Osteoblasten und Gefäßmineralisierung angereichert

waren, oder aber spezifisch in entweder Osteoblasten oder Gefäßmineralisierung. Schließlich verglichen wir die Expressionsmuster der erhaltenen gefäßmineralisierungsspezifischen Gene mit Patientenexpressionsdaten von Karotis Plaque und intaktem benachbarten Gewebe. Wir fanden fünf Rosiglitazon-Zielgene, die als spezifische Marker für das Gefäßmineralisierungsmodell und Karotis Plaque dienten. Diese Zielgene (PDK4, SDC4, SPRY4, TCF4 und DACT1) bieten interessante Kandidaten für weitere Untersuchungen, um neue Therapien für Knochenstoffwechsel- und Herz-Kreislauf-Erkrankungen zu schaffen.

Zusammenfassend haben die Untersuchungen in dieser Arbeit zur Aufklärung der funktionellen Konsequenzen der Rosiglitazon-aktivierten PPAR-γ - Signaltransduktionskaskade während der Knochenbildung und Gefäßverkalkung beigetragen. Auf der Basis der aus diesen Untersuchungen erhaltenen Ergebnisse sind neue Konzepte entstanden, welche die nachteiligen Wirkungen von Rosiglitazon auf den Knochenstoffwechsel und das Herz-Kreislauf-System erklären. Diese Konzepte basieren auf einer beschleunigenden Wirkung von Rosiglitazon auf Osteoblasten- und osteoblastenähnliche Differenzierungsprozesse welche anschließend durch erhöhte Akkumulation von reaktiven Sauerstoffspezies, Apoptose und erhöhter Mineralisierung gefolgt werden. Beim Vergleich der osteogenen mit der adipogenen Zellreihe, welche aus dem gleichen Vorläufer, der mesenchymalen Stammzelle, hervorgehen, haben wir gezeigt dass die adipogene Zellreihe weniger anfällig für oxidativen Stress und Apoptose ist, was vorzugsweise in der osteogenen Zellreihe von der Rosiglitazon-aktivierten PPAR-γ - Signaltransduktionskaskade ausgelöst wird. Dieses Konzept liefert eine alternative Erklärung für das häufig beschriebene Phänomen der Knochenmarkadipogenese.

Acknowledgements / Danksagungen

After many years of engagement, I am happy to have put this thesis finally together. This would not have been possible without many people whom I would like to thank.

First of all I would like to thank Prof. Dr. Huib Pols, Rector Magnificus of the Erasmus University Rotterdam, and Prof Dr. Jaap Verweij, Dean of the Erasmus Medical Center Rotterdam, for the opportunity to study and prepare my PhD thesis at this renowned institute. I also acknowledge the financial support from the European Marie Curie Research Training Network NucSys, and its co-ordinator Prof. Dr. Carsten Carlberg, for having me accepted for this generous international and interdisciplinary mobility program.

I am very grateful to the members of the inner committee, Prof. Dr. Gerjo van Osch, Prof. Dr. Danny Huylebroeck, and Prof. Dr. Sander Kersten, for accepting to be part of the examination board, for carefully reading this manuscript, and for all the useful comments that have improved the quality of this thesis.

I am most thankful to my promoter Prof. Dr. Hans van Leeuwen who offered me the opportunity to carry out my PhD studies in his laboratory, under his supervision. Dear Hans, your detailed knowledge about the fascinating world of bone, your support during all the years and guidance helped me to become a researcher, to stand where I am standing now, and to understand what is necessary for being successful in academic science. Thank you very much for mentoring me and at the same time providing me freedom to allow my fascination for scientific research to unleash.

I am also very grateful to my co-promoter, Dr. Jeroen van de Peppel, for his invaluable teaching in microarray and data analysis and beyond. Dear Jeroen, sharing the office with you was one of the best decisions during my PhD. I miss your teasing jokes and shared gadget discoveries. When supervising students now myself, I try to take a leaf out of your book. Thank you for all your support and patience with me, and thank you also for your help with writing the English-Dutch translation of the summary in a very short time.

I would also like to thank Dr. Ksenija Drabek for her support and fruitful discussions throughout the years. Dear Ksenija, you have been a wonderful colleague, and I was very fortunate to have had the luck sharing the office with you.

I am very grateful to Annelies van Amen - Eriks for her invaluable help in organizing my PhD defence. Dear Annelies, thank you very much for your support in making all the arrangements, and also for your help in writing the English-Dutch translation of the summary on a short notice.

I would like to thank Dr. Marco Eijken for all the insightful discussions and teaching of laboratory techniques in the beginning of my PhD. I really appreciated the detailed instructions, and am still benefiting from these on a daily basis. Many thanks also to Dr. Marjolein van Driel and Dr. Bram van der Eerden for teaching and helpful discussions in the lab.

I am also very grateful to Prof. Hans Westerhoff, Dr. Frank Bruggeman, and Dr. Martijn Mone for our comprehensive systems biology sessions. Our meetings were not only very insightful but also always inspiring to start thinking out of the box.

I would also like to thank Marijke and Bianca for their help in keeping the laboratory in order, and their support in setting up cell cultures. Many thanks to the (former) PhD students in the lab: Sander, Martijn, Claudia N, Viola, Rodrigo, and Poom, as well as the (former) NucSys PhD students Tatjana, Aleksandra, Sebastiano, Pedro V, Ellen, Katja, Alexey, Anastasia, Marcin, Carsten, Radu, Fabio, Pedro R, Carole, Thomas, and Gilles. It was great having around many peers all facing the same challenges. Dear Katja, thank you very much

for your friendship over many years, invitations for going out in Amsterdam dancing until late night and comfortable couch. It was great fun, and also thank you very much for all the insightful systems biological discussions that we had. I learned a lot from you. Dear Carsten, getting together and enjoying the cultural wealth of our European NucSys destinations was always a great pleasure, thank you for these great memories.

I am very grateful to my current mentor Dr. Steven Lane at QIMR Berghofer Medical Research Institute, Australia. Thank you very much for your trust and understanding over the past years. It goes without saying that your invaluable support in this new field has provided the final kick to finish this PhD. Thank you very much for your patience and believing in me.

I am most thankful to my dear friends in Brisbane: Motoko, Antiopi, and Carolin. Thank you very much for your support and encouragement over the past years, for our cultural activities, coffees and dinners together. Antiopi, thank you for introducing me to the greek society, and having allowed me to join a real greek wedding! Motoko, thank you so much for our dinner and movie tradition, the sometimes very late dinners after work, the many lovely chats over wine, trips around the countryside, always having time and some good advice and trusting me with your car!

Dear Tina, thank you so much for your friendship. Your visit in Brisbane will always be a great memory for me (of course the ambulance part excluded...), it was such a pleasure having you around in the lab. Thank you for all your good advice, your support, and chats. I am looking forward to catching up with you on many more conferences, and in-between on Skype.

Dear Nadia - if there is one reason why Rotterdam was the right decision for me, it's because I had met you there. It is hard for me to find the right words to express my gratitude for our friendship. It is amazing how synchronized we seem in all aspects of life, and how much more enriched life has become when spending time together. I thank you for sharing so many ideas, listening and giving invaluable advice, being my 'Covey' buddy, introducing

me to the Dutch Salsa community, all those dinners and movies together, shopping weekends and IKEA marathons, and cultural activities. Thank you also for your openness and having included me in your family and Dutch friends circles, I have appreciated this very much. Some of the best parts of my PhD (if not the best at all!) were our wonderful adventure trips together to Africa and Asia, and more recently our tours through Australia. I hope that one day we will be a bit closer geographically again, I miss you very much.

Dear Sabbe, after I had met you for the first time during the Ingenuity course (and you had climbed up those 13 floors by stairs!), I knew you were the smart and strong athlete. Thank you so much for being so persistent and having tolerated my shy behaviour in the beginning, and having introduced me to the international Erasmus MC PhD student crowd. Thank you for the many chats over coffee, listening and advice at Doppio, spending all those nights after the lab at de Witte Aap followed by Surinaams food, and our wonderful trip to the US. These were crazy times, and I will always keep them as a great memory. A highlight of my PhD was our shared living in our amazing apartment at Kop van Zuid in the end. All those dinners together, and tea and chocolates on the couch in the evening, had made my life extremely enjoyable. It is also your fault that, (for a limited amount of time which is my fault), I had considered myself as a runner. I am very grateful to your friendship, and hope we will see each other more often, I miss you! Maarten, thank you so much for your entertaining card game and guitar hero evenings, watching DVDs together, trips to Zealand, and those amazing apple and spek pancakes, these are wonderful memories, and I hope we can catch up very soon again. Many thanks also to Joana for having accepted me as the new flatmate, all that yummy portuguese food, wine, and having introduced me to a lot of fantastic music. Dear Akhgar, thank you so much for your friendship, for sharing enthusiasm for cultural events, cooking all that wonderful Persian food, and the many relaxed brunches and coffees that we had together, I miss you. Melina, thank you so much for still keeping in touch, I am very grateful to have met you, the wonderful brunches and parties at your

place with the 'international crowd' will always be a great memory. Dear Mehrnaz, thank you very much for all your support, the coffees, wonderful barbecues and weekends at the beach together with your family. And Yaser, it was so great having you around - thank you for sharing enthusiasm for the movie evenings together despite being always busy in the lab - I am sure very soon I will need to call you 'Professor'!

Liebe Kristin, ich möchte mich ganz dolle für Deine Freundschaft bedanken, und dafür dass Du mich immer unterstützt hast. Es war für Dich geradezu selbstverständlich dass es alles mit dem Diplom, der Doktorandenstelle, Postdocstelle und schließlich auch der Doktorarbeit klappen wird, so dass ich es dann auch selbst irgendwann geglaubt habe. Vielen Dank für die tolle Zeit in Potsdam zusammen in der WG. Es war eine verrückte Zeit, und ich denke gern daran zurück. Ich danke Dir auch sehr dafür mich immer in Berlin zu empfangen (und für Deine bequeme Couch und die original WG Einkäufe), so dass es sich für mich immer noch wie 'zu Hause' anfühlt. Ich hatte mich sehr gefreut dass Du den weiten Weg nach Australien auf Dich genommen hattest, und denke immer noch gern an unseren gemeinsamen Urlaub zurück.

Lieber Dominik, ich danke Dir sehr für Deine Freundschaft und Unterstützung über viele Jahre, für die vielen bereichernden Gespräche und Erweiterung meiner Musikkenntnisse. Ich danke Dir sehr für Dein allzeit offenes Ohr und Deine aufmunternden Ratschläge. Ich hatte mich sehr gefreut dass Du mich in Australien besucht hattest, es war eine tolle Zeit mit Breaking Bad und den Erkundungsfahrten durch Australien. Tim und Anne, ich möchte mich auch bei Euch ganz doll für die schöne Zeit bedanken, die gemeinsamen Silvesterfeiern, die Immergutfahrten, und natürlich die gemeinsame Zeit in der WG! Ich danke Euch sehr für Euren allzeit positiven Blick auf die Dinge, und hoffe das wir uns bald wiedersehen.

Liebe Dörte, ich musste es eben nachrechnen - wir kennen uns nun schon seit 27 Jahren! Ich danke Dir sehr für unsere lange Freundschaft und Deine Unterstützung. Ich freue mich darauf Dich bald wiederzusehen, und nun auch Deinen zweiten Sohn kennenzulernen. Ich

bin sehr stolz auf Dich! Liebe Christina, es ist immer schön Weihnachten nach Hause nach Schwerin zu kommen und tatsächlich noch Leute zu kennen! Ich danke Dir sehr für unsere Bolero-Abende, und hoffe auf viele mehr!

Schließlich möchte ich mich bei meinen Eltern Brigitte und Michael bedanken, meinem Bruder Daniel, Kornelia, und meinem Cousin Mathias. Es ist fast unmöglich in Worte zu fassen auf wie vielfältige Weise ihr mir in den letzten Jahren beigestanden habt. Lieber Mathias, ich danke Dir sehr für Deine Unterstützung und Besuche in Rotterdam, und dafür dass Du beim Abschied nach Australien für mich da warst. Liebe Mama und lieber Papa - ich danke Euch sehr dafür mich allzeit unterstützt zu haben, Eure Hilfe bei Umzügen, Renoveriungsarbeiten, vielen Besuche und Päckchen - sogar nach Australien. Mama - Deine Weihnachtsplätzchen waren immer das Highlight im Advent, nicht nur für mich sondern auch für meine Kollegen und Freunde in den WGs. Ich danke Euch sehr dafür dass ihr mich immer mein Leben habt selbst bestimmen lassen, dass ihr immer für mich da wart und nie das Vertrauen in mich verloren habt.

Curriculum vitae

Claudia Bruedigam

Personal details

Date of birth	July 25, 1980
Nationality	German

Education

University	*Erasmus University* – Rotterdam, The Netherlands Postgraduate Program in Molecular Medicine	2006 – 2011
	University of Potsdam – Potsdam, Germany Biochemistry MSc Degree equivalent (“Diplom”) BSc Degree equivalent (“Vordiplom”)	1999 – 2005
Upper-track Secondary School	*Goethe Gymnasium* – Schwerin, Germany	1990 – 1999

Work experience

Scientific researcher	*QIMR Berghofer Medical Research Institute* – Brisbane, Australia	2011 – present
	Erasmus Medical Center – Rotterdam, The Netherlands	2006 – 2011
Student worker	*Max Planck Institute for Molecular Plant Physiology* – Potsdam, Germany	2002 – 2004

Publications

Souza-Fonseca-Guimaraes F, Young A, Mittal D, Martinet L, **Bruedigam C**, Takeda K, Andoniou CE, Degli-Esposti MA, Hill GR, Smyth MJ. NK cells require IL-28R for optimal in vivo activity. ***Proc Natl Acad Sci U S A***; 2015 Apr 21. pii: 201424241.

Leveque-El Mouttie L, Vu T, Lineburg KE, Kuns RD, Otzen Bagger F, Teal BE, Lor M, Boyle GM, **Bruedigam C**, Mintern JD, Hill GR, MacDonald KP, Lane SW. Autophagy is required for stem cell mobilization by G-CSF. ***Blood;*** 2015 Mar 18. pii: blood-2014-03-562660.

Bruedigam C, Bagger FO, Heidel FH, Paine Kuhn C, Guignes S, Song A, Austin R, Vu T, Lee E, Riyat S, Moore AS, Lock RB, Bullinger L, Hill GR, Armstrong SA, Williams DA, Lane SW. Telomerase inhibition effectively targets mouse and human AML stem cells and delays relapse following chemotherapy. ***Cell Stem Cell;*** 2014 Dec 4;15(6):775-90.

Mullally A, **Bruedigam C**, Poveromo L, Heidel FH, Purdon A, Vu T, Austin R, Heckl D, Breyfogle LJ, Kuhn CP, Kalaitzidis D, Armstrong SA, Williams DA, Hill GR, Ebert BL, Lane SW. Depletion of Jak2V617F myeloproliferative neoplasm-propagating stem cells by interferion-alpha in a murine model of polycythemia vera. ***Blood;*** 2013 May 2; 121(18):3962-702.

Woeckel VJ, **Bruedigam C**, Koedam M, Chiba H, van der Eerden BC, van Leeuwen JP. 1alpha,25-dihydroxyvitamin D3 and rosiglitazone synergistically enhance osteoblast-mediated mineralization. ***Gene*****;** 2013 Jan 10;512(2):438-43.

Bruedigam C, Koedam M, Eijken M, Chiba H, van Leeuwen JPTM. Opposing actions of rosiglitazone and resveratrol on ectopic mineralization in human vascular smooth muscle cells. ***Journal of Molecular and Cellular Cardiology***; 2011 Nov;51(5):862-71.

Bruedigam C, Koedam M, Eijken M, van de Peppel J, van Leeuwen JPTM. Basic techniques in human mesenchymal stem cell cultures: differentiation into osteogenic and adipogenic lineages, genetic perturbations, and phenotypic analyses. ***Current Protocols in Stem Cell Biology;*** 2011 Jun;Chapter 1:Unit1H.3.

Bruedigam C, Eijken M, Koedam M, van de Peppel J, Drabek K, Chiba H, van Leeuwen JPTM. A new concept underlying stem cell lineage skewing that explains the detrimental effects of thiazolidinediones on bone. ***Stem Cells***; 2010 May;28(5):916-27.

Bruedigam C, Koedam M, Chiba H, Eijken M, van Leeuwen JPTM. Evidence for multiple peroxisome proliferator-activated receptor gamma transcripts in bone: fine-tuning by hormonal regulation and mRNA stability. ***FEBS Letters***; 2008 May;582(11):1618-24.

Schauer N, Semel Y, Roessner U, Gur A, Balbo I, Carrari F, Pleban T, Perez-Melis A, **Bruedigam C**, Kopka J, Willmitzer L, Zamir D, Fernie AR. Comprehensive metabolic profiling and phenotyping of interspecific introgression lines for tomato improvement. ***Nat Biotechnol;*** 2006 Apr;24(4):447-54.

Roessner-Tunali U, Hegemann B, Lytovchenko A, Carrari F, Bruedigam C, Granot D, Fernie AR. Metabolic profiling of transgenic tomato plants overexpressing hexokinase reveals that the influence of hexose phosphorylation diminishes during fruit development. ***Plant Physiol;*** 2003 Sep;133(1):84-99.

PhD portfolio

	Year	Workload (ECTS)
General Academic Skills		
- English Biomedical Writing and Communication (Erasmus MC)	2007	3
- Project Management (Medical University of Vienna, Austria)	2009	1
- The Workshop Writing Successful Grant Proposals V (Erasmus MC)	2010	0.4
Research Skills		
- The Course Biomedical Research Techniques V (Erasmus MC)	2006	1.5
- The Workshop on Basic data analysis on gene expression arrays I (Erasmus MC)	2008	1.5
- Mouse embryonic stem cell culture training course (Max Planck Institute for Molecular Genetics, Berlin, Germany)	2008	5
- TissueFacs (Medical University of Vienna, Austria)	2009	1
- The Basic Course on "R" (Erasmus MC)	2010	1
- The Bioconductor Course (Erasmus MC)	2010	1
- The Photoshop CS3 Workshop for PhD-students and other researchers (Erasmus MC)	2010	0.25
- Biobase: Functional Annotation of Experimental Data using TRANSFAC® Professional, HGMD® Professional, and Genome TraxTM (Erasmus MC)	2011	0.4
In-depth Courses		
- Neuro-Immuno-Endocrinology (Erasmus MC)	2006	2.5
- FEBS Advanced Course in System Biology (Gosau, Austria)	2007	2
- Mechanisms of Gene Expression (University of Kuopio, Finland)	2007	5
- The Course SNPs and Human Diseases (Erasmus MC)	2007	2
Local Seminars and Workshops		
- Internal Medicine Departmental Seminar Series	2006 - 2008	3
- Wetenschapsdagen	2007	1

Conferences		
- Annual Symposium of the Dutch Society for Calcium and Bone Metabolism (NVCB) – oral presentation	2006 – 2008	6
- 34th European Symposium on Calcified Tissues (Copenhagen, Denmark) – poster presentation	2007	2.5
- XV Annual Congress of the European Society of Gene and Cell Therapy (Rotterdam)	2007	2
- 35th European Symposium on Calcified Tissues (Barcelona, Spain) – poster presentation	2008	2.5
- 36th European Symposium on Calcified Tissues (Vienna, Austria) – poster presentation	2009	2.5
- EMBO Meeting 2009 (Amsterdam)	2009	2
- Annual Symposium of the Dutch Society for Stem Cell Research (Utrecht)	2010	1
European Marie Curie Research Training Meetings		
- NucSys Summer Meeting (Kuopio, Finland) *Nuclear receptors and their cofactors; chromatin and nuclear receptor target genes; VDR; PPAR; PXR*	2006	1
- NucSys Winter Meeting (Rotterdam) *Genome-wide high density SNP analysis, proteomic approaches, nuclear receptor imaging, modelling course I*	2007	1
- NucSys Summer Meeting (Birmingham, UK) *Presentation skill course (Peter Evans Associates LTD); modelling course II*	2007	1
- NucSys Winter Meeting (Madrid, Spain) *Nuclear receptors; cancer; modelling course III*	2007	1
- NucSys Summer Meeting (Berlin, Germany) *Modelling; gene regulatory networks in embryogenesis*	2008	1
- NucSys Winter Meeting (Vienna, Austria) *Modelling; human drug metabolism*	2009	1

Appendix

8 Protocol: Basic techniques in human mesenchymal stem cell cultures

8.1 Abstract

This unit describes basic techniques in human mesenchymal stem cell (hMSC) cultures. It includes protocols for the differentiation of hMSCs into osteogenic and adipogenic lineages, genetic perturbations, and phenotypic analyses. hMSCs can be differentiated with dexamethasone and β-glycerophosphate into mineralizing osteoblasts within 2 to 3 weeks, or with dexamethasone, indomethacin, and 3-isobutyl-1-methylxanthine into lipid vesicle-containing adipocytes within 1 to 2 weeks. Phenotypic changes during those highly dynamic differentiation processes can be detected by biochemical and histological assays and gene expression analyses of differentiation markers. In addition, this unit describes an electroporation method that allows the transient genetic perturbation of hMSCs.

Claudia Bruedigam, Marjolein van Driel, Marijke Koedam, Jeroen van de Peppel, Bram C.J. van der Eerden, Marco Eijken, Johannes P.T.M. van Leeuwen: *Basic techniques in human mesenchymal stem cell cultures: differentiation into osteogenic and adipogenic lineages, genetic perturbations, and phenotypic analyses*; 2011; 1H.3.1-1H.3.20; Current Protocols in Stem Cell Biology

8.2 Introduction

This unit describes basic techniques in human mesenchymal stem cell (hMSC) culture. It includes protocols for the differentiation of hMSCs into osteogenic and adipogenic lineages, for the analysis of genetic perturbations, and for phenotypic analyses. hMSCs can be differentiated with dexamethasone and β-glycerophosphate into mineralizing osteoblasts within 2 to 3 weeks [113], or with dexamethasone, indomethacin, and 3-isobutyl-1-methylxanthine into lipid vesicle - containing adipocytes within 1 to 2 weeks [151]. Phenotypic changes during those highly dynamic differentiation processes can be detected by biochemical and histological assays [119] and gene expression analyses of differentiation markers [121, 151]. In addition, this unit describes an electroporation method that allows the transient genetic perturbation of hMSCs [151].

This unit begins with a method for the *in vitro* differentiation of hMSCs into osteogenic and adipogenic lineages (Basic Protocol 1). An electroporation method to transiently transfect hMSCs with expression vector constructs or short hairpin RNAi constructs is provided in Basic Protocol 2. Biochemical assays and histology methods for the analysis of osteoblastic and adipocytic phenotypes are summarized in Basic Protocols 3-7. The method for gene expression analysis of osteogenic and adipogenic differentiation markers is described in Basic Protocol 8.

NOTE: All cell culture incubations are performed in a humidified 37°C, 5% CO_2 incubator unless otherwise specified.

NOTE: All solutions and equipment coming into contact with live cells must be sterile, and proper aseptic technique should be used accordingly.

8.3 Differentiation of hMSCs into osteogenic and adipogenic lineages

This protocol is used for the *in vitro* differentiation of hMSCs into osteogenic and adipogenic lineages. hMSCs are cultured in the presence of dexamethasone and β-glycerophosphate to induce osteogenic differentiation resulting in mineralizing osteoblasts within two to three weeks [113]. hMSC differentiation into lipid vesicle - containing adipocytes is achieved when hMSC cultures are supplemented with

dexamethasone, indomethacin, and 3-isobutyl-1-methylxanthine [151]. The kinetics of osteogenic and adipogenic differentiation can vary between different donors.

Materials

hMSC medium (see recipe), prewarmed (37°C)

Human bone marrow - derived mesenchymal stem cells (tested for surface antigens CD105+, CD166+, CD29+, CD44+, CD14-, CD34-, and CD45-; 750,000 cells per vial; expanded to passage 6; e.g., Lonza)

0.4% (w/v) trypan blue (e.g., Invitrogen)

Phosphate - buffered saline (PBS; pH 7.4; e.g., Invitrogen), prewarmed (37°C)

0.05% (w/v) trypsin (e.g., Invitrogen, cat. no. 15400-054), prewarmed (37°C)

Ethanol, absolute (e.g., Fisher Scientific)

1 mM dexamethasone (see recipe)

2 M β-glycerophosphate (see recipe)

30 mM indomethacin (see recipe)

250 mM 3-isobutyl-1-methylxanthine (IBMX; see recipe)

PBS/Triton (see recipe)

50-ml conical polypropylene centrifuge tubes (e.g., BD Falcon)

Serological pipets (2-ml, 5-ml, 10-ml, and 25-ml volume) with motorized serological pipet filler

Centrifuge with swing-out rotor and adaptors for 50 ml Falcon tubes

Microcentrifuge tubes (0.5 ml volume)

Bright-field microscope

Burker glass slide chamber or electric field multichannel cell counting system, e.g., CASY cell counter (Roche Diagnostics)

175-cm^2 cell culture flasks (preferably with angled neck)

12-well cell culture clusters (22.1 mm diameter) including lids with individual condensation rings

Cell scraper (15-mm, slim blade)

Polypropylene cylindrical test tubes (PP tubes; 3 ml, 4 ml or 5 ml volume), or optionally microcen-

trifuge tubes (2 ml volume)

NOTE: The procedures described in Basic Protocols 1 and 2 are performed in a Class II biological hazard flow hood or a laminar-flow hood.

Expand hMSCs in pre-culture

1. Add 20 ml of hMSC medium to a 50-ml tube using a 25-ml pipet.
2. Draw up 1 ml of preheated hMSC medium into a 2-ml pipet with, then release the medium very slowly into the vial that contains frozen cells and mix by gently pipetting up and down until the cell suspension is thawed.
3. Pipet the cell suspension (1 vial) quickly into the 50-ml tube with hMSC medium prepared in step 1 and mix by gently pipetting up and down 5 times.
4. Add hMSC medium to the tube up to 45 ml with a 25 ml pipet and mix by slowly pipetting up and down ten times.
5. Centrifuge for 5 min at 300 x g, room temperature.
6. Resuspend the cell pellet in 2 ml hMSC medium.

:To do this, remove the supernatant by using the aspiration device first, then rub the bottom side of the tube against the ventilation grid of the clean bench with one quick movement. Add 2 ml hMSC medium with a 2-ml pipet and pipet up and down until no clumps of cells are visible. If the ventilation grid on the bench is not conveniently located, other objects with rough surfaces can be used, e.g., racks for microcentrifuge tubes.

7. Transfer three samples of 10 μl each to a microcentrifuge tube and mix each with 90 μl of 0.4% trypan blue. Count dead (blue stained) and viable (unstained) cells under the microscope in a Burker glass slide chamber. Count at least 100 cells for each replicate and calculate the percentage of viable cells in the total cell suspension.

Optionally, cells can be counted using an automated cell counter according to the manufacturer's instructions. The percentage of viable cells should be at least 65%.

8. Seed 0.75-1 x 10^6 viable cells per 175-cm^2 culture flask in 20 ml hMSC medium.
9. Distribute cells evenly by moving the flask quickly according to a cross-like pattern.

10. Transfer flask into a CO_2 incubator (37°C, 5% CO_2).

11. Replace hMSC medium every 3 to 4 days. Keep the cells in pre-culture for 5 to 7 days until confluency is reached.

Start the hMSC experimental culture

12. Remove medium from flask carefully using the aspiration device.

13. Add 10 ml preheated PBS carefully using a 10-ml pipet. Make sure not to add the solution directly onto the cell layer but instead hold the flask with the side wall down, and drop the PBS there. Gently move the flask back so that the solution will cover the bottom completely.

14. Remove PBS from flask carefully using the aspiration device.

15. Add 1.5 ml 0.05% (1x) trypsin with a 2-ml pipet dropwise on top of the cell layer. Try to distribute the drops over the complete cell layer.

16. Move the flask. Check after 2 min under the microscope whether cells have already detached from the bottom of the flask.

To do this, tap the bottom of the flask once against a surface and subsequently monitor the cell movements under the microscope. All cells should be moving. If not, put the flask into the incubator (37°C) and check again after 2 min.

17. Add 5 ml hMSC medium to the flask, move the flask gently, and transfer the cell suspension to a fresh 50-ml tube. Repeat this with another 5 ml of hMSC medium.

The addition of high amounts of serum proteins in this step is important to protect cells from undesired trypsin-mediated protein digestion that would compromise cell function and viability.

18. Centrifuge for 5 min at 300 x g, room temperature.

19. Resuspend cell pellet in 2 ml hMSC medium.

20. Transfer three samples of 10 μl each to a microcentrifuge tube and mix each with 90 μl of 0.4% (w/v) trypan blue. Count viable (white) and dead (blue stained) cells under the microscope in a Burker glass slide chamber. Count at least 100 cells for each replicate and calculate the percentage of viable cells in the total cell suspension.

Optionally, cells can be counted using an automated cell counter according to the manufacturer's

instructions. The percentage of viable cells should be at least 90%.

21. Fill each well of a 12-well plate with 600 μl of hMSC medium.

22. Dilute the cell suspension with hMSC medium to a final concentration of 2 x 10^5 cells/ml. Resuspend cells thoroughly by pipetting up and down 12 to 20 times.

23. Seed 20,000 cells per well of the 12-well plate by adding 100 μl of cell suspension using a repetitive pipettor. Seed a maximum of four plates each time, working quickly. Then, empty the remaining cells in the pipettor carefully back into the 50-ml tube, mix again by pipetting up and down five times using the same repetitive pipettor, and fill the pipettor up again with the cell suspension. Repeat this step until all plates have been filled.

24. Move the plates in a maximum stack of three plates each according to a crosslike pattern to evenly distribute the cells in each well, and check this under the microscope.

25. Incubate the plates for 2 days in a CO_2 incubator (37°C, 5% CO_2).

Induce osteogenic or adipogenic differentiation

26a. For osteogenic differentiation: Supplement prewarmed hMSC medium by adding 1 mM dexamethasone at a 1:10,000 dilution for a final concentration of 0.1 μM and 2 M β-glycerophosphate at a 1:200 dilution for a final concentration of 10 mM.

26b. For adipogenic differentiation: Supplement prewarmed hMSC medium by adding 1 mM dexamethasone for a final concentration of 0.1 μM, 30 mM indomethacin for a final concentration of 60 μM, and 250 mM IMBX for a final concentration of 0.5 mM. If additional treatments are desired, dilute these compounds in the appropriate solvent.

The final ethanol concentration in the medium should not exceed 1%. Always include control conditions that contain ethanol at an identical concentration to that used under the treatment conditions.

27. Remove medium from wells carefully by using the aspiration device and add 700 μl of osteogenic or adipogenic differentiation medium to each well using a repetitive pipet (preferably automatic).

Carefully add the medium into each well by touching the well's side wall with the pipet. If using an automatic pipet, use a low speed for emptying. Do not let wells get dry. Work quickly and handle a maximum of two plates at a time.

28. Replace the medium every 3 or 4 days.

Prepare cell extracts

29. Wash the wells once with PBS on ice.
30. Add 500 μl PBS/Triton to each well on ice.
31. Scrape the cells and pipet the suspension into a tube (preferably PP tube) on ice.
32. Rinse each well with 500 μl PBS/Triton and add it to the respective tube.
33. Store the cell extracts at - 80°C.

This protocol allows the preculture and differentiation of osteogenic or adipogenic hMSCs in vitro*. One vial (750,000 cells) will yield 2,500,000 cells after expansion that can be seeded into 125 wells in total (12-well format). From each well, cell lysates can be obtained for subsequent biochemical analyses (i.e., DNA content, ALP activity, and quantitative mineralization assays), fixation can be performed for subsequent histological assays (i.e., lipid vesicle staining or mineralization), or RNA can be isolated for subsequent gene-expression analysis.*

8.4 Transient transfection of hMSCs by electroporation

DNA such as expression constructs or vector-based short hairpin constructs can be introduced into hMSCs by electroporation. This is a process that involves the repositioning of plasma membrane lipid molecules, leading to the creation of nanometer-scale waterfilled holes in the plasma membrane, when an electrical field is applied. This increases the electrical conductivity and permeability of the plasma membrane, allowing the introduction of large and highly charged molecules such as DNA that would not cross the hydrophobic bilayer under physiological conditions.

Materials

Plasmid DNA (2 μg of expression vector constructs or shRNAi constructs in a concentration of at least 0.4 μg/ml; e.g., Origene, and MISSION shRNA library, Sigma)
hMSCs in flasks (confluency of 60%; see Basic Protocol 1)

Human MSC Nucleofector Kit (Lonza)

hMSC medium (see recipe), prewarmed (37°C)

Amaxa nucleofector system (Lonza) with Amaxa cuvettes

(http://www.lonzabio.com/)

Additional reagents and equipment for hMSC cell culture (see Basic Protocol 1)

NOTE: The procedures described in Basic Protocols 1 and 2 are performed in a Class II biological hazard flow hood or a laminar-flow hood.

Transient transfection of hMSCs using electroporation

1. Add 2 μg of plasmid DNA (in a maximum volume of 5 μl) per cuvette.
2. Trypsinize hMSCs according to Basic Protocol 1 (steps 13 to 19).
3. Resuspend hMSC pellet in nucleofector solution (from nucleofector kit). Final hMSC concentration in nucleofector solution: 5 x 10^6 cells per 1 ml solution.
4. Pipet 100 μl of resuspended cells into the first cuvette with plasmid DNA.
5. Immediately apply electrical field using Amaxa nucleofector system (U-23 nucleofector program).
6. Add 500 μl of pre-warmed hMSC medium to the cuvette.
7. Transfer the transfected cells into the tube with prewarmed hMSC medium and resuspend carefully.

   Final hMSC concentration in hMSC medium: 3 x 10^4 cells in 700 μl medium.
8. Repeat steps 4 to 7 until all cuvettes have been prepared.
9. Seed cells (i.e., 30,000 cells in 700 μl medium) into each well of a 12-well plate and incubate. Monitor fluorescence and viability of GFP controls under microscope.
10. Refresh medium and induce differentiation 24 hr after transfection according to Basic Protocol 1 (steps 28 to 30).

8.5 Quantification of alkaline phosphatase (ALP) activity

ALP activity can be quantified by the method of Bessey *et al.* in which the rate of the formation of p-nitrophenol (p-NP) produced by hydrolysis of p-nitrophenylphosphate (p-NPP) in alkaline solution

at 37°C is measured spectrophotometrically at 405 nm [282]. ALP activity is expressed as enzyme units (U), which is the amount of enzyme catalyzing the conversion of 1 μmol p-NPP per min at 37°C.

Materials

Cellular extracts of interest (Basic Protocol 1)

10 U/ml alkaline phosphatase (from bovine kidney, e.g., Sigma)

PBS/Triton (see recipe)

p-nitrophenylphosphate (p-NPP; see recipe)

0.1 M sodium hydroxide

Sonicator (e.g., Soniprep 150, Sanyo)

Microcentrifuge tubes (1.5 ml volume)

5-ml polypropylene cylindrical test tubes (PP tubes)

96-well clear polystyrene flat-bottom microtiter plates (e.g., Corning)

Microplate reader (with filter for absorbance detection at 405 nm; e.g., Wallac 1420 Victor 2)

Measure alkaline phosphatase activity

1. Thaw the cellular extracts on ice.

2. Sonicate the samples until they have become homogeneous and all visible precipitates have disappeared.

In the authors' experience, sonication for 10 sec at sonication force 10 (Soniprep 150, Sanyo) is sufficient to achieve homogenous cell lysates. When there is a lot of matrix and calcium in the samples (progressed stage of mineralization), increase duration to 15 sec and sonication force to 15.

3. Prepare a set of standards (diluted in PBS/Triton) in 1.5-ml microcentrifuge tubes according to Table 1.

4. Pipet samples in duplicate into 5-ml PP tubes: For standards: 100 μl each standard dilution For samples: 10 μl sample + 90 μl PBS/Triton.

5. Take one tube and add 100 μl p-NPP. Vortex the tube and incubate in water bath at 37°C. After 10 sec, take the second tube and continue. After exactly 10 min, take the first tube and stop the reaction

by adding 250 µl of 0.1 M sodium hydroxide and place the tube on ice. Then after 10 sec, the second tube and continue.

Table 1
Standards for determining alkaline phosphatase activity

	ALP [µl]	PBS-Triton [µl]	ALP activity [U/ml]
A	15 µl stock (10 U/ml)	1485	0.1
B	250 µl A	250	0.05
C	250 µl B	250	0.025
D	250 µl C	250	0.0125
E	250 µl D	250	0.00625
F	0	500	0

In this way, every tube will have been incubated at 37°C for exactly 10 min.

6. Pipet 200 µl of each standard or sample into a 96-well microtiter plate.

7. Measure the absorbance at 405 nm on a plate reader.

8.6 Quantification of DNA content

DNA content correlates well with the cell number of nonsynchronized hMSC cultures. Thus, it is a suitable parameter to correct ALP activity values in order to establish the ALP activity level per cell. DNA content can be quantified with ethidium bromide after release from its complexes by heparin. Ethidium bromide is an intercalating agent that emits light at 590 nm when excited, with ultraviolet light intensifying about two-fold after binding to double-stranded DNA. Cell lysates need to be initially treated with ribonuclease because ethidium bromide also binds to highly abundant RNA molecules folded into double-stranded secondary structures.

Materials

Cellular extracts of interest (Basic Protocol 1)

DNA standard (see recipe)

Heparin solution (see recipe)

RNase solution (see recipe)

Ethidium bromide solution (see recipe)

Sonicator (e.g., Soniprep 150, Sanyo)

96-well clear polystyrene flat-bottom microtiter plates (e.g., Corning)

Fluorescence microplate reader (e.g., Wallac 1420 Victor 2)

1. Thaw the cellular extracts on ice.

2. Sonicate the samples until they have become homogeneous and all visible precipitates have disappeared.

This step is not necessary if the samples have been sonicated on the same day already. In the authors' experience, sonication for 10 sec at sonication force 10 (Soniprep 150, Sanyo) is sufficient to achieve homogenous cell lysates. When there is a lot of matrix and calcium in the samples (progressed stage of mineralization), increase duration to 15 sec and sonication force to 15.

3. Prepare a set of standards (diluted in PBS/Triton) in a 96-well microtiter plate according to Table 2.

4. Pipet 50 μl of each sample in duplicate into wells of a 96-well microtiter plate.

5. Add 100 μl/well of heparin solution and 50 μl/well of RNase solution to the standards and the samples.

Table 2
Standards for calculation of DNA content

	DNA standard (0.025 mg/ml) [μl]	PBS/Triton [μl]	DNA [μg]
A	0	50	0
B	2.5	47.5	0.0625
C	5	45	0.125
D	10	40	0.25
E	25	25	0.625
F	40	10	1
G	50	0	1.25

6. Incubate 30 min at 37°C.

7. Add 50 μl/well of ethidium bromide solution to each standard and sample.

If you cannot proceed immediately, keep the plate in the dark for a maximum of 30 min.

8. Measure fluorescence on a plate reader.

Use a protocol with an excitation wavelength of 340 nm and an emission wavelength of 590 nm.

8.7 Quantification of mineralization

Mineralization content can be quantified by a modified version of the method of Connerty and Briggs (1966) in which o-cresolphthalein complexone binds to calcium ions to form a chromophore in an alkaline medium that is measured spectrophotometrically around 570 nm. 8-hydroxyquinoline is added to reduce any interference by magnesium.

Materials

Cellular extracts of interest (Basic Protocol 1)

6 M hydrochloric acid

PBS/Triton/HCl (see recipe)

Calcium chloride standard solution in PBS/Triton/HCl (see recipe)

Calcium assay reagent 1 (see recipe)

Calcium assay reagent 2 (see recipe)

Sonicator (e.g., Soniprep 150, Sanyo)

1.5-ml microcentrifuge tubes

96-well clear polystyrene flat-bottom microtiter plates (e.g., Corning)

Microplate reader (with filter for absorbance detection at 595 nm; e.g., Wallac 1420 Victor 2)

Quantify mineralization

1. Thaw the cellular extracts on ice.

2. Sonicate the samples until they have become homogeneous and all visible precipitates have disappeared.

This step is not necessary if the samples have been sonicated on the same day already. In the authors' experience, sonication for 10 sec at sonication force 10 (Soniprep 150, Sanyo) is sufficient to achieve homogenous cell lysates. When there is a lot of matrix and calcium in the samples (progressed

stage of mineralization) increase duration to 15 sec and sonication force to 15.

3. Transfer 95 μl of sample into a 1.5-ml microcentrifuge tube and add 5 μl of 6 M hydrochloric acid.

Table 3
Standards for quantification of mineralization

	$CaCl_2$	PBS/Triton/HCl [μl]	Ca2+ [mM]
A	100 μl stock (3.6 mM)	0	3.6
B	100 μl stock (3.6 mM)	100	1.8
C	100 μl B	100	0.9
D	100 μl C	100	0.45
E	100 μl D	100	0.225
F	100 μl E	100	0.1125
G	0	100	0

4. Vortex and incubate overnight at 4°C.

5. Prepare a set of calcium standards (in PBS/Triton/HCl) in 1.5-ml microcentrifuge tubes according to Table 3.

6. Pipet 10 μl/well of each standard dilution and sample in duplicate into a 96-well microtiter plate.

7. Prepare the calcium assay working solution by mixing equal volumes of reagent 1 and reagent 2.

You will need enough working solution for 100 μl per sample. Overcalculate by one or two samples to allow for pipetting error/variation.

8. Add 100 μl of working solution to each well.

9. Measure the absorbance on a plate reader at 595 nm.

8.8 Histology and semi-quantification of mineralization

Mineralized ECM can be visualized using Alizarin Red S staining. The anthraquinone derivative forms a complex with calcium, manganese, barium, strontium, and iron ions in a chelation process. Under normal hMSC culture conditions, only calcium ions reach a sufficient level for staining.

Materials

Cultures of hMSC in 12-well plates (Basic Protocol 1)

Phosphate-buffered saline (PBS; pH 7.4; e.g., Invitrogen), prewarmed (37°C)

10% (v/v) formalin (1:10 dilution of 37% formaldehyde in PBS)

Alizarin Red S solution (see recipe)

10% (v/v) acetic acid

Ammonium hydroxide

Bright-field microscope with photocamera

Plate shaker

Cell scraper (15 mm slim blade)

85°C heat block

Microcentrifuge for 1.5-ml microcentrifuge tubes allowing 20,000 x g

Microplate reader (with filter for absorbance detection at 405 nm; e.g., Wallac 1420 Victor 2)

Visualize ECM mineralization

1. Wash wells once with PBS.
2. Fix cultures by adding 700 μl of 10% formalin and incubating at room temperature for 15 min.
3. Wash wells twice with Milli-Q water.
4. Stain with 500 μl/well of ARS solution for 20 min.
5. Wash four times, each time for 5 min, with Milli-Q water.

Pipet and aspirate very carefully and slowly when staining samples from the progressed mineralization stage, because the ARS-stained mineralized ECM can become brittle and detach from the bottom of the well.

6. Store in Milli-Q water to take pictures, or proceed with semi-quantification.

Semi-quantify ECM mineralization

7. Remove Milli-Q water and add 400 μl 10% acetic acid per well.

8. Incubate for 30 min at room temperature on a plate shaker.

9. Scrape cells and transfer lysate from each well into a separate 1.5-ml microcentrifuge tube.

10. Vortex the tubes for 30 sec.

11. Incubate tubes for 10 min on a heat block at 85° C.

12. Cool tubes on ice for 5 min.

13. Microcentrifuge 15 min at speed, room temperature.

14. Pipet 100 μl of the supernatant into a 96-well microtiter plate.

15. Add 50 μl ammonium hydroxide to each well in order to neutralize and to bring back the red color.

16. Measure absorbance on a plate reader at 405 nm.

8.9 Histology and semi-quantification of lipid vesicles

Lipid droplets can be visualized with Oil Red O, a lysochrome diazo dye that stains neutral triglycerides, lipids, and lipoproteins.

Materials

Cultures of hMSC in 12-well plates (Basic Protocol 1)

Phosphate-buffered saline (PBS; pH 7.4; e.g., Invitrogen), prewarmed (37°C)

10% (v/v) formalin (1:10 dilution of 37% formaldehyde in PBS)

60% (v/v) 2-propanol in PBS

Oil Red O working solution (see recipe)

Igepal working solution: 4% (v/v) Igepal (Sigma) in 2-propanol

Microscope with photocamera

Plate shaker

96-well clear polystyrene flat bottom microtiter plates (e.g., Corning)

Microtiter plate reader capable of reading at 490 nm)

Stain lipid vesicles

1. Wash wells twice with PBS. 2. Add 700 μl of 10% formalin to each well.

3. Store plates at 4°C overnight or longer.

4. Wash wells once with 60% 2-propanol.

5. Incubate with 500 μl/well Oil Red O working solution for 10 to 30 min.

Check under microscope presence of stained lipid vesicles. Consider an additional, empty plate for background staining from now on.

6. Wash wells three times with water and keep them in water.

7. Take pictures using microscope with photocamera.

8. Store plates at 4°C overnight or longer.

Semi-quantify lipid vesicles

9. Dry wells.

For this, carefully remove water by using an aspiration device and incubate the plates without lid in a dry incubator at 37°C. Check after 1 hr whether the surface of each well is completely dry.

10. Add 250 μl Igepal working solution to each well and shake for 30 min on a plate shaker.

11. Transfer 100 μl of each well into a 96-well microtiter plate.

12. Measure absorbance on a plate reader at 490 nm.

8.10 Gene expression analysis of osteogenic and adipogenic differentiation markers

The expression levels of osteogenic and adipogenic differentiation markers can be determined at transcript level by quantitative reverse transcriptase polymerase chain reaction (quantitative RT-PCR) in which a specific sequence of a complementary DNA (cDNA) molecule is simultaneously amplified and quantified as the number of copies relative to stably and abundantly expressed genes (i.e., 'housekeeping' genes). The detection is based on nonspecific fluorescent dyes that intercalate with any double-stranded DNA, or sequence-specific DNA probes consisting of oligonucleotides that are la-

beled with a fluorescent reporter which permits detection only after hybridization of the probe with its target sequence. cDNA can be synthesized from mature mRNA by reverse transcriptase, which adds pair-wise complementary deoxyribonucleotides onto a free 3' hydroxyl group. The initial free 3' hydroxyl group is provided by hybridization of an oligo-T oligonucleotide primer onto the poly(A) tail of the mature mRNA template, or by random hexamer primers that hybridize to their complementary sequences anywhere else on the mRNA template. The mRNA templates can be obtained from cell lysates by phenolchloroform extraction [283]. The latter is a liquid-liquid extraction technique in which a mixture of equal volumes of an aqueous sample (i.e., cell lysate) and a solution containing water-saturated phenol, chloroform, and a chaotropic denaturing compound (guanidium thiocyanate) is separated into three different phases by centrifugation. While DNA and protein partition in the interphase and organic phase, respectively, RNA accumulates in the upper aqueous phase. RNA is then recovered by precipitation with 2-propanol. An additional purification step with EDTA and lithium chloride becomes necessary when a lot of mineralized ECM is present in the hMSC cultures.

Materials

Cultures of hMSC in 12-well plates (Basic Protocol 1)

Phosphate-buffered saline (PBS; pH 7.4; e.g., Invitrogen), cold TRIzol (Invitrogen) or equivalent

Chloroform

2-propanol

Ethanol, absolute (e.g., Fisher Scientific)

1 M EDTA (RNase-free; e.g., Invitrogen)

8 M lithium chloride (RNase-free; e.g., Ambion)

70% ethanol prepared with RNase-free H2O

RevertAid First Strand cDNA Synthesis Kit (Fermentas)

RNase-and DNase-free water (e.g., Invitrogen)

RT-PCR master mix stock (see recipe)

Primer mix (2.5 μM forward primer + 2.5 μM reverse primer; primer sequences for the detection of osteoblast, adipocyte differentiation and housekeeping genes described in [151]

Cell scraper (15 mm slim blade)

Microcentrifuge tubes (0.5 ml and 1.5 ml volume)

Refrigerated microcentrifuge allowing 20,000 x g

Microvolume spectrophotometer (e.g., NanoDrop)

25°C, 42°C, 65°C, and 70°C water baths or heat blocks 96-well PCR plates (compatible to thermal cycler system; e.g., Bioplastics)

Thermal cycler with fluorescence detection system (excitation wavelength of 495 nm and an emission wavelength of 520 nm; e.g., ABI PRISM 7500 sequence detector, Applied Biosystems)

Note: The solutions and equipment used for the RNA isolation and cDNA synthesis techniques described below need to be RNase-free.

Isolate total RNA from hMSC cultures

1. Wash wells once with cold PBS.
2. Add 400 µl of TRIzol to each well using a repetitive pipettor.
3. Scrape cells from the bottom of each well and transfer into a 1.5-ml microcentrifuge tube.
4. Store samples at -20°C or proceed immediately.
5. Thaw cell lysates on ice.
6. Add 80 µl of chloroform to each tube and mix immediately by inverting the tube 15 times.

Handle a maximum of four tubes at the same time. Do not vortex, or you will shear genomic DNA.

7. Incubate samples for 10 min on ice.
8. Centrifuge samples at maximum speed at 4°C for at least 20 min.

This step leads to the separation of the sample into the pink-colored lower organic phase containing protein, the white interphase containing DNA, and the transparent upper aqueous phase that contains the desired RNA.

9. Transfer the upper phase into a fresh 1.5-ml microcentrifuge tube.

Pipet carefully and do not touch the interphase or lower phase. It is better to not transfer the upper phase completely than to risk any contamination with the interphase or organic phase.

10. To each tube, add a volume of 2-propanol equal to the volume of upper phase solution in the tube

and vortex vigorously.

This volume amounts to 200 to 240 µl.

11. Precipitate samples by incubation at -20°C overnight.

12. Microcentrifuge at least 30 min at 20,000 x g, 4°C.

13. Wash RNA pellet once with absolute ethanol.

For this, add 600 µl ethanol, microcentrifuge 10 min at maximum speed, 4°C, and quickly remove supernatant by decanting. Quickly dry lid of each tube with a clean tissue.

14. Let RNA pellets dry at room temperature.

The pellet dries in about 5 to 15 min. Do not leave pellets at room temperature longer than necessary. The characteristic ethanol odor will have been volatilized when the pellet is dry.

Purify RNA extracts

15. Add 80 µl of 0.1 M EDTA to each tube and dissolve RNA pellets by pipetting up and down 12 times, then vigorously vortexing.

Increase EDTA volume to 160 µl when extracting RNA from cultures of progressed mineralization stage.

16. Add 80 µl of 8 M lithium chloride to each tube and vortex immediately. Handle only one tube each time.

Increase the volume of lithium chloride to 160 µl when extracting RNA from cultures of progressed mineralization stage.

17. Precipitate RNA by incubating tubes at -20°C overnight.

18. Microcentrifuge at least 30 min at maximum speed, 4°C.

19. Wash RNA pellet three times with 600 µl of 70% ethanol.

For this, add 600 µl of ethanol, microcentrifuge 10 min at maximum speed, 4°C, and quickly remove supernatant. It is handy to use an aspiration device for this. Leave centrifuge spinning while handling a maximum number of 10 samples at the same time.

20. Wash RNA pellet once with absolute ethanol.

21. Dry RNA pellet.

22. Resuspend RNA pellet in 12 μl of water.

23. Proceed to RNA quantification or store samples at -80°C.

Quantify RNA

24. Thaw samples on ice.

25. Measure the concentration of RNA in 0.75 μl of each sample using a microvolume spectrophotometer.

The RNA concentration is measured spectrophotometrically at 260 nm, at which single-stranded RNA molecules have an average extinction coefficient of 0.02 $(\mu g/ml)^{-1}$ cm^{-1}. The contamination of RNA extracts with proteins can be estimated by the 260:280 absorption ratio, since the aromatic groups present in aromatic amino acids absorb light at 280 nm. The 260:280 absorption ratio for pure RNA is 2. Contamination with phenol is indicated by absorption of light at 270 nm. The 260:270 absorption ratio for pure RNA is 1.2. Thiocyanates and phenolate ion absorb light at 230 nm, and the 260:230 absorption ratio for pure RNA amounts to 2.

Synthesize cDNA

26. Pipet 1 μg of RNA in a total volume of 10 μl water into a 0.5-ml microcentrifuge tube.

If the concentrations of RNA in the extracts are lower than 100 ng/μl, lower amounts of RNA may be used. It is important that the same amount of RNA be used for all samples that will be comparatively analyzed. In the authors' experience, the lowest possible input of RNA is 150 ng.

27. Add 1 μl of oligo-T oligonucleotide primers (100 μM or 0.5 μg/μl oligo(dT)18 primer stock) and 1 μl of hexamer primers (100 μM or 0.2 μg/μl random hexamer primer stock) to each sample.

These items are provided with the first-strand cDNA synthesis kit from Fermentas.

28. Vortex, and then microcentrifuge briefly to bring solution to the bottom of the tube.

29. Incubate at 65°C for 5 min.

30. Chill on ice, then microcentrifuge briefly to bring solution to the bottom of the tube.

31. Add 4 μl reaction buffer, 2 μl of 10 mM dNTP mix, 1 μl of 20 U/μl RNase inhibitor, and 1 μl of 200 U/μl M-MuLV reverse transcriptase to each tube.

These items are part of the first-strand cDNA synthesis kit from Fermentas. Prepare a master mix instead of pipetting all compounds individually.

32. Vortex, and then microcentrifuge briefly to bring solution to the bottom of the tube.
33. Incubate at 25°C for 5 min, then at 42°C for 60 min, and subsequently at 70°C for 5 min.
34. Chill samples on ice and spin down.
35. Add 230 µl of DNase-free water to each tube.

If the input of RNA was lower than 1 µg, reduce the amount of water to be added in this step accordingly. The lowest possible volume of added water is 130 µl, because too high concentrations of kit components might otherwise interfere with subsequent analyses.

Perform quantitative RT-PCR

36. Prepare RT-PCR master mix according to the following scheme per sample:

9.5 µl RNase-free water
12.5 µl master mix stock
1 µl primer mix.

This recipe is suitable for the analysis of 2 µl of cDNA sample per well. However, if high Ct values (i.e., above 27) are anticipated, it is advisable to use a higher volume of cDNA sample and to reduce the volume of water accordingly. The cDNA input can be increased to a maximum volume of 5% (v/v) of the initial volume of cDNA synthesis product - i.e., if 130 µl of water have been added to the cDNA synthesis product in step 35, a maximum volume of 7.5 µl cDNA sample can be used per RT-PCR reaction (25 µl reaction volume).

37. Pipet 23 µl of RT-PCR master mix per well into a 96-well PCR plate.
38. Add 2 µl of cDNA sample per well.
39. Run quantitative RT-PCR on thermal cycler according to the following protocol:

1 cycle: 2 min 50°C

1 cycle: 10 min 95°C

40 cycles: 15 sec 95°C

1 min 60°C.

The third step is repeated 40 times. For detecting SYBR or FAM, use optical filters that allow an excitation wavelength of 495 nm and an emission wavelength of 520 nm.

When using nonspecific, fluorescent dyes for detection (i.e., SYBR), it is advisable to perform a dissociation run subsequently to each completed RT-PCR run. During the dissociation run, the amplified RT-PCR samples are heated up slowly to 95°C while the fluorescence signal is detected continuously. The fluorescence signal drops when double-stranded DNA molecules separate into single-stranded DNA molecules according to their specific melting temperature. The dissociation curve displays the derivative of fluorescence signal as function of temperature. Thus, the dissociation curve gives rise to a peak at the melting point of the desired PCR product if it has been amplified during the RT-PCR.

8.11 Reagents and solutions

For culture recipes and steps, use sterile tissue culture - grade water. For other purposes, use deionized, distilled water or equivalent in recipes and protocol steps.

Alizarin Red S solution

Dissolve 3 g of Alizarin Red S in 500 ml Milli-Q water and adjust pH to 4.2 with ammonium hydroxide. Store up to 1 year at 4°C.

β-Glycerophosphate (2 M)

Dissolve 100 g of β-glycerophosphate (e.g., Sigma) in 231.5 ml Milli-Q water. Filter-sterilize, aliquot, and store up to 1 year at 4°C.

Calcium assay reagent 1

Dilute 6 ml ethanolamine (e.g., Merck) in 100 ml of Milli-Q water and adjust pH to 10.6 with 6 M HCl. Store reagent at 4°C (stable for 40 days).

Calcium assay reagent 2

Dissolve 22.81 mg o-cresolphthalein purple (e.g., Sigma) and 287.42 mg 8-hydroxyquinoline (e.g., Merck) in 80 ml of Milli-Q water. Add 5 ml of 6 M hydrochloric acid and make up the volume with Milli-Q water to 100 ml. Store at 4°C (stable for 40 days).

Calcium chloride standard solution in PBS/Triton/HCl (3.6 mM)

Dissolve 26.5 mg calcium chloride (e.g., Sigma) in 50 ml PBS/Triton/HCl (see recipe) and store up to 6 months at 4°C.

The resulting solution contains 3.6 mM calcium.

Dexamethasone (1 mM)

Dissolve 100 mg of dexamethasone (e.g., Sigma) in 255 ml absolute ethanol and store in aliquots up to 1 year at -20°C.

Diethanolamine buffer

Dissolve 9.5 ml diethanolamine (e.g., Merck) and 20 mg magnesium chloride in 100 ml Milli-Q water. Adjust pH to 9.8 using 6 M HCl.

DNA standard

Dissolve 1 mg of deoxyribonucleic acid sodium salt (e.g., from calf thymus; Sigma) in 40 ml of PBS/Triton (see recipe). Prepare 0.5-ml aliquots and store up to 1 year at - 20°C.

Ethidium bromide solution

Dissolve 1 g of ethidium bromide (e.g., 95% HPLC, Sigma) in 200 ml of Milli-Q water and store 1-ml stock aliquots up to 5 years at -20°C, protected from light.

Dilute stock aliquot 1:200 in PBS (e.g., Invitrogen) prior to the assay.

Heparin solution

Dilute a 5000 IU/ml stock (e.g., LEO Pharma, http://www.leo-pharma.com/; store up to 6 months at 4°C) 1:600 in PBS (e.g., Invitrogen).

hMSC medium

Combine the following:

440 ml α-MEM (without phenol red and calcium chloride; e.g., Invitrogen)

10 ml penicillin-streptomycin (50,000Uof penicillin and 50,000Uof streptomycin; e.g., utilizing penicillin G sodium salt and streptomycin sulfate in 0.85% saline, Invitrogen)

2.39 g HEPES (molecular biology grade; e.g., Promega)

900 μl of 1 M calcium chloride (CaCl2 .2H2O)

Adjust to pH to 7.5 with 10 M sodium hydroxide

Add 50 ml fetal bovine serum (FBS: Invitrogen; heat-inactivate 1 hr at 56°C)

Sterilize through a 0.2 μm filter

Indomethacin (30 mM)

Dissolve 5 g indomethacin (e.g., Sigma) in 467.3 ml ethanol. Store in aliquots up to 1 year at - 20°C.

3-Isobutyl-1-methylxanthine (IBMX; 250 mM)

Dissolve 100 mg of 3-isobutyl-1-methylxanthine (IBMX; e.g., Sigma) in 1 ml Milli-Q water, then add 50 μl of 5 M sodium hydroxide solution. If solution is not clear yet, add another 10 μl of 5 M sodium

hydroxide solution. Add Milli-Q water up to a volume of 1.8 ml, filter-sterilize, aliquot, and store up to 1 year at - 20°C.

Oil Red O working solution

Mix 3 parts of saturated Oil Red O solution (e.g., Clin-Tech, http://www.clintech.co.uk) with 2 parts of Milli-Q water and filter through 0.2-μm filter or Whatman filter paper. Prepare fresh.

PBS/Triton (0.1%)

Mix 1 ml of Triton X-100 with 1 liter of PBS (e.g., Invitrogen) and store up to 1 month at 4°C

PBS/Triton/HCl

Add 1.6 ml HCl (6 M) to 40 ml PBS/Triton (see recipe) and store up to 1 month at 4°C

p-NPP (20 mM)

Dissolve 742 mg 4-nitrophenylphosphate disodium salt hexahydrate (e.g., Fluka) in 100 ml diethanolamine buffer (see recipe), prepare 50-ml aliquots, and store up to 6 months at - 20°C, protected from light.

RNase solution

Dissolve 100 mg of ribonuclease A (e.g., from bovine pancreas, Sigma) in 20 ml PBS (e.g., Invitrogen) and prepare stock aliquots of 0.5 ml. Store up to 5 years at - 20°C. Dilute stock aliquot 1:100 in PBS prior to the assay.

RT-PCR master mix stock

Combine the following items from the qPCR core kit for SYBR Green I (Eurogentec, cat. no. RT-SN10-05):

7.5 ml 10x reaction buffer (containing KCl, Tris-HCl, and a passive reference)

5.25 ml 50 mM magnesium chloride

3 ml 5 mM dNTP mix

2.25 ml SYBR dye

19.125 ml of DNase-free water

Prepare aliquots of 6.25 ml and store up to 6 months at - 20°C.

To prepare a working stock, thaw the master mix stock prepared above and add 62.5 ml of PCR enzyme (5 U/μl, e.g., HotGoldStar from qPCR core kit for SYBR Green I, Eurogentec).

This RT-PCR master mix working stock can be stored protected from light at 4°C for up to 2 weeks.

8.12 Commentary

Background information

Bone marrow-derived hMSCs are progenitor cells from a rare population in bone marrow that are capable of differentiation into bone, cartilage, fat, muscle, tendon, and marrow stroma [284]. A set of cell surface markers that would characterize a pure hMSC population has not been identified to date. Currently, hMSCs are defined as the nonhematopoietic plastic adherent cells in the bone marrow that are positive for the surface antigens CD105, CD166, CD29, and CD44, and negative for CD34 and CD45. *In vitro*, hMSCs can be induced to differentiate into mineralizing osteoblast cultures and lipid vesicle - containing adipocyte cultures upon stimulation with the respective differentiation compounds. Dexamethasone is essential for proper human osteoblast differentiation and ECM mineralization, and β-glycerophosphate is required as phosphate donor for the mineralization process. Adipogenic differentiation can be induced by supplementation of hMSC cultures with dexamethasone, indomethacin, and 3-isobutyl-1-methylxanthine [151]. Additional adipogenic differentiation compounds include rosiglitazone and insulin. However, although the addition of these compounds can increase the number of lipid vesicles in adipogenic cultures, supplementation with these additional differentiation compounds has not been shown to successfully combat heterogeneity in the cultures. Heterogeneity is a widely observed phenomenon in differentiating hMSC cultures *in vitro* [284–287].With regard to the osteogenic

and adipogenic conditions described in this unit, the extent of ECM mineralization and lipid vesicle accumulation differs between positions within a culture well (Figure 1. A). Intriguingly, the quantitative or semi-quantitative values for mineralization or lipid vesicles from complete wells usually show high similarities (i.e., the differences are within biological variability of less than 10%) when compared with different wells from a specific condition (Figure 1 A). Whether heterogeneity is just an undesired stochastic phenomenon that results from nonoptimal selection due to a current lack of definitive hMSC markers, or whether it even possesses functional significance for differentiation processes, is an important topic of current research.

The osteogenic and adipogenic differentiation process in hMSC cultures can be monitored by histological, biochemical, or gene expression analyses of differentiation markers. Alkaline phosphatase (ALP) is a classical marker for osteoblast differentiation. Its activity levels change dynamically during the osteogenic differentiation process according to a specific pattern. ALP activity is virtually absent in undifferentiated hMSCs; it increases rapidly during osteogenic differentiation until its peak level is reached during mineralization onset, and it subsequently decreases again (Figure 1 B). However, ALP is an important enzyme that is, despite its high expression in bone, present ubiquitously throughout the body. It dephosphorylates nucleotides, proteins, and alkaloids most effectively in an alkaline environment. Recently, ALP activity has been shown to correlate with fat storage during preadipocyte maturation as well [288]. Thus, ALP needs to be considered as a marker of differentiation of hMSCs into both lineages, although its expression and activity patterns are lineage-specific.

ECM mineralization is a process that occurs during bone formation in which calcium-based minerals are formed within cells and tissues. *In vitro*, the formation and deposition of minerals result from a non-physiological process during the late osteoblast differentiation phase in which extracellular ALP releases inorganic phosphate from ester phosphates such as β-glycerophosphate at neutral pH. The local increase in inorganic phosphate then promotes rapid mineral deposition onto a collagen-rich ECM that has been produced by the osteoblasts before. Mineralization content is thus an endpoint marker of the metabolic activity of osteoblasts (i.e., energy metabolism, extracellularmatrix synthesis, and matrix vesicle biogenesis). Mineralization occurs specifically in the osteogenic condition (it remains absent when β-glycerophosphate is added to the adipogenic differentiation cocktail), and is thus considered

as a specific osteoblast differentiation marker (Figure 1 B).

Adipogenic differentiation can be assessed by histology of lipid-containing vesicles. Adipocytes from human bone marrow contain considerable cytoplasm with lipid droplets scattered throughout. The accumulation of lipid droplets starts between 5 and 10 days of adipogenic differentiation, depending on the donor. A negligible number (<0.1%) of lipid droplets occurs sporadically in the osteogenic condition, possibly due to the presence of preadipocytes in the initial heterogeneous hMSC population.

Classical osteogenic and adipogenic differentiation markers include ALPL, RUNX2, COL1A1, and BGLAP for the osteogenic lineage, and PPARG and FABP4 for the adipogenic lineage. Expression levels of these genes change in a specific pattern during the time course of differentiation, and are therefore suitable for phenotyping. However, depending on the time point of analysis, expression levels of osteogenic markers are not always absent in the adipogenic lineage and *vice versa*, although their expression levels follow a specific pattern that is distinct from the other lineage (Figure 1 C).

The kinetics of all differentiation markers (ALP activity, mineralization, lipid vesicles, and gene expression values) are donorspecific, and thus need to be determined in an initial control experiment for each hMSC batch.

Critical parameters and troubleshooting

Transient transfection using electroporation: Too large a size of plasmids, too much salt in plasmid preparations, and too low or too high confluency of cells before trypsinization can lead to poor transfection efficiency.

Mineralization assays: ECM mineralization is strongly influenced by the volume of culture medium used. During incubation, evaporation of medium in culture plates differs between wells, i.e., medium evaporates faster from wells at outer than inner position. In fact, up to 15% of medium can evaporate during 2 days of incubation, and the volume of evaporated medium can differ up to 10% between wells. Therefore, a randomized plate layout or different plate layouts between independent experiments are necessary.

When osteogenic cultures are harvested at a progressed mineralization stage, it can become difficult to scrape the compact mineralized cell layer from the well, and the resulting quantitative mineralization

data may vary strongly. Therefore, it is advisable to incubate each well from this condition with 500 μl of PBS/Triton/HCl overnight at 4°C after scraping, and to subsequently measure mineralization in these samples. The values can then be added to the results obtained from the cell lysates.

Anticipated results

This unit contains protocols for the differentiation of hMSCs into the osteogenic or adipogenic lineage, genetic perturbation, and histological, biochemical, and gene expression analyses of the obtained phenotypes. The differentiation kinetics depend on the hMSC donor, and, thus, need to be determined in an initial pilot experiment for each hMSC batch. In general, osteogenic differentiation of hMSCs results in mature osteoblasts and ECM mineralization after 15 to 25 days in culture. Adipocytes with accumulated lipid vesicles occur earlier in the adipogenic condition, after about 7 to 12 days in culture. With regard to the transient transfection protocol described, transfection efficiencies of about 40% to 60% are expected.

Time Considerations

The expansion of hMSCs should take about 1 week until the required confluency has been reached. Then it should take about 2 to 3weeks to differentiate hMSCs into osteoblast cultures with mineralized ECM, or 1 to 2 weeks to differentiate hMSCs into adipocytes. Histological and biochemical assays can be accomplished within 1 to 3 days, depending on the number of samples. The isolation of RNA, cDNA synthesis, and quantitative RT-PCR for gene expression analyses require approximately 5 to 7 days, also depending on the number of samples. Taken together, the time needed to be considered for the accomplishment of the expansion and differentiation of hMSCs and subsequent phenotypic analyses amounts to approximately 5 to 6 weeks.

Figure 1 (following page)
Histological, biochemical, and gene expression analysis of osteoblast and adipocyte differentiation markers. (A) Alizarin Red S (upper left panel) and Oil RedO staining (lower left panel) of osteogenic and adipogenic hMSCs at day 15 of differentiation. Semi-quantification of Alizarin Red S (upper right panel) and Oil Red O staining (lower right panel). (B) Quantification of ALP activity (left panel) and mineralization (right panel) in osteogenic and adipogenic hMSCs during different time points of differentiation. (C) Quantitative RT-PCR analysis of osteoblast and adipocyte differentiation marker genes in osteogenic and adipogenic hMSCs during different time points of differentiation.

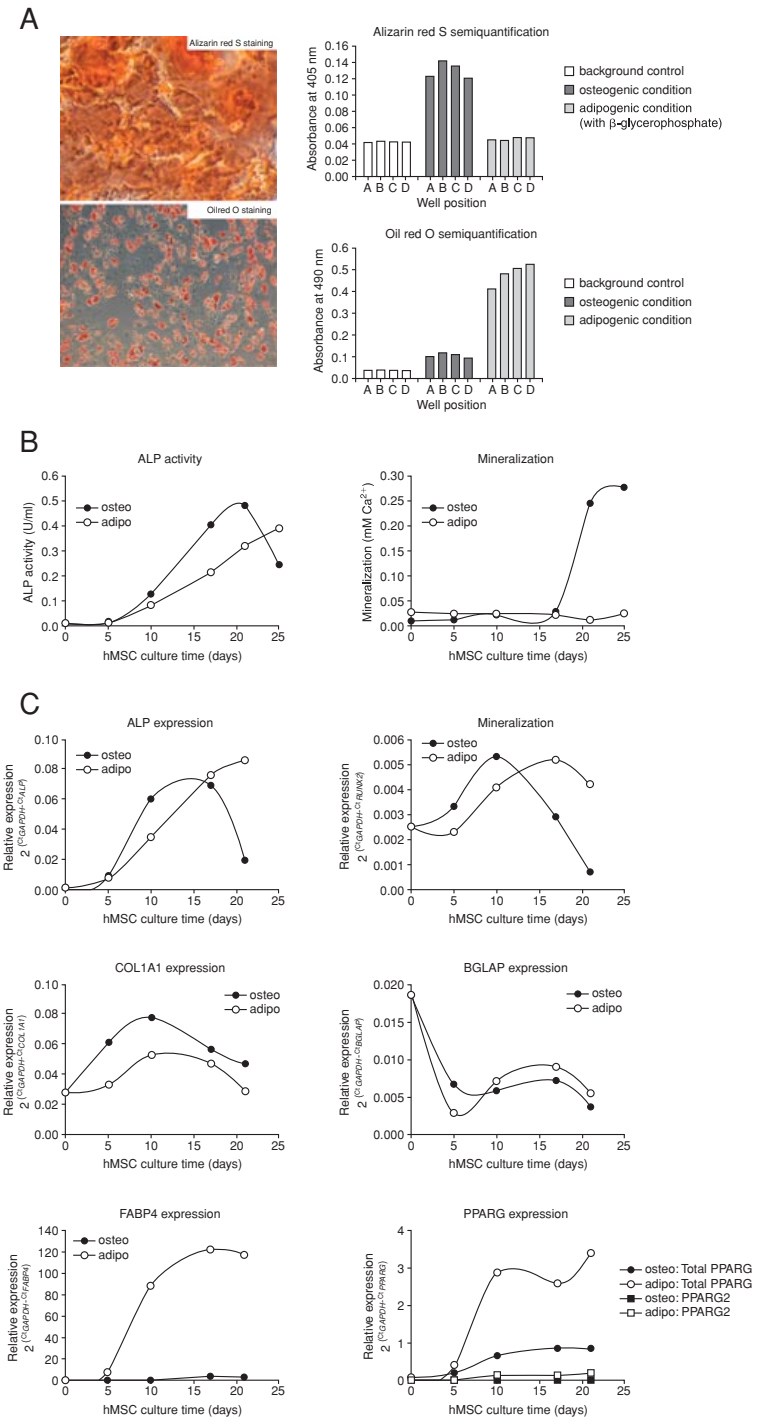
A
Alizarin red S staining
Oilred O staining
Alizarin red S semiquantification
Absorbance at 405 nm
Well position
background control
osteogenic condition
adipogenic condition
(with β-glycerophosphate)
Oil red O semiquantification
Absorbance at 490 nm
B
ALP activity
ALP activity (U/ml)
Mineralization
Mineralization (mM Ca2+)
osteo
adipo
hMSC culture time (days)
C
ALP expression
Mineralization
COL1A1 expression
BGLAP expression
FABP4 expression
PPARG expression
osteo: Total PPARG
adipo: Total PPARG
osteo: PPARG2
adipo: PPARG2

[h]

Bibliography

[1] S C Manolagas and R L Jilka. Bone marrow, cytokines, and bone remodeling. Emerging insights into the pathophysiology of osteoporosis. *New England Journal of Medicine*, 332(5):305–311, February 1995.

[2] G D Roodman. Cell biology of the osteoclast. *Exp Hematol*, 27(8):1229–1241, August 1999.

[3] T Suda, N Takahashi, N Udagawa, E Jimi, M T Gillespie, and T J Martin. Modulation of osteoclast differentiation and function by the new members of the tumor necrosis factor receptor and ligand families. *Endocr Rev*, 20(3):345–357, June 1999.

[4] R T Turner, B L Riggs, and T C Spelsberg. Skeletal effects of estrogen. *Endocr Rev*, 15(3):275–300, June 1994.

[5] G G Teng, J R Curtis, and K G Saag. Mortality and osteoporotic fractures: is the link causal, and is it modifiable? *Clin Exp Rheumatol*, 26(5 Suppl 51):S125–37, September 2008.

[6] H K Genant, C Cooper, G Poor, I Reid, G Ehrlich, J Kanis, B E Nordin, E Barrett-Connor, D Black, J P Bonjour, B Dawson-Hughes, P D Delmas, J Dequeker, S Ragi Eis, C Gennari, O Johnell, C C Jr Johnston, E M Lau, U A Liberman, R Lindsay, T J Martin, B Masri, C A Mautalen, P J Meunier, N Khaltaev, and et al. Interim report and recommendations of the World Health Organization Task-Force for Osteoporosis. *Osteoporosis International*, 10(4):259–264, 1999.

[7] B Perdu and W Van Hul. Sclerosing Bone Disorders: Too Much of a Good Thing. *Critical Reviews in Eukaryotic Gene Expression*, 20(3):195–212, 2010.

[8] M C de Vernejoul. Sclerosing bone disorders. *Best Practice & Research in Clinical Rheumatology*, 22(1):71–83, March 2008.

[9] M C de Vernejoul and U Kornak. Heritable sclerosing bone disorders Presentation and new molecular mechanisms. *Skeletal Biology and Medicine*, 1192:269–277, 2010.

[10] E Seeman and P D Delmas. Bone quality–the material and structural basis of bone strength and fragility. *New England Journal of Medicine*, 354(21):2250–2261, May 2006.

[11] Y Meng, Y X Qin, E DiMasi, X Ba, M Rafailovich, and N Pernodet. Biomineralization of a self-assembled extracellular matrix for bone tissue engineering. *Tissue engineering. Part A*, 15(2):355–366, February 2009.

[12] M Balcerzak, E Hamade, L Zhang, S Pikula, G Azzar, J Radisson, J Bandorowicz-Pikula, and R Buchet. The roles of annexins and alkaline phosphatase in mineralization process. *Acta biochimica Polonica*, 50(4):1019–1038, 2003.

[13] E E Golub, G Harrison, A G Taylor, S Camper, and I M Shapiro. The role of alkaline phosphatase in cartilage mineralization. *Bone and mineral*, 17(2):273–278, May 1992.

[14] W B Valhmu, L N Wu, and R E Wuthier. Effects of Ca/Pi ratio, Ca2+ x Pi ion product, and pH of incubation fluid on accumulation of 45Ca2+ by matrix vesicles in vitro. *Bone and mineral*, 8(3):195–209, March 1990.

[15] R E Wuthier, L N Wu, G R Sauer, B R Genge, T Yoshimori, and Y Ishikawa. Mechanism of matrix vesicle calcification: characterization of ion channels and the nucleational core of growth plate vesicles. *Bone and mineral*, 17(2):290–295, May 1992.

[16] D Harmey, L Hessle, S Narisawa, K A Johnson, R Terkeltaub, and J L Millan. Concerted regulation of inorganic pyrophosphate and osteopontin by akp2, enpp1, and ank: an integrated model of the pathogenesis of mineralization disorders. *The American journal of pathology*, 164(4):1199–1209, April 2004.

[17] D A Towler and L L Demer. Thematic series on the pathobiology of vascular calcification: an introduction. *Circulation Research*, 108(11):1378–1380, May 2011.

[18] T M Doherty, L A Fitzpatrick, D Inoue, J H Qiao, M C Fishbein, R C Detrano, P K Shah, and T B Rajavashisth. Molecular, endocrine, and genetic mechanisms of arterial calcification. *Endocr Rev*, 25(4):629–672, August 2004.

[19] C Maayan, O Peleg, F Eyal, P Mogle, E Rosenmann, and J Bar Ziv. Idiopathic infantile arterial calcification: a case report and review of the literature. *Eur J Pediatr*, 142(3):211–215, August 1984.

[20] E B Singleton and D F Merten. An unusual syndrome of widened medullary cavities of the metacarpals and phalanges, aortic calcification and abnormal dentition. *Pediatr Radiol*, 1(1):2–7, March 1973.

[21] F M Pope. Autosomal dominant pseudoxanthoma elasticum. *J Med Genet*, 11(2):152–157, June 1974.

[22] J L Breslow. Mouse models of atherosclerosis. *Science*, 272(5262):685–688, May 1996.

[23] R C Detrano, N D Wong, T M Doherty, and R Shavelle. Prognostic significance of coronary calcific deposits in asymptomatic high-risk subjects. *Am J Med*, 102(4):344–349, April 1997.

[24] L Wexler, B Brundage, J Crouse, R Detrano, V Fuster, J Maddahi, J Rumberger, W Stanford, R White, and K Taubert. Coronary artery calcification: pathophysiology, epidemiology, imaging methods, and clinical

implications. A statement for health professionals from the American Heart Association. Writing Group. *Circulation*, 94(5):1175–1192, September 1996.

[25] L Zhang, A Zalewski, Y Liu, T Mazurek, S Cowan, J L Martin, S M Hofmann, H Vlassara, and Y Shi. Diabetes-induced oxidative stress and low-grade inflammation in porcine coronary arteries. *Circulation*, 108(4):472–478, July 2003.

[26] Y Tintut, J Patel, M Territo, T Saini, F Parhami, and L L Demer. Monocyte/macrophage regulation of vascular calcification in vitro. *Circulation*, 105(5):650–655, February 2002.

[27] George P Sorescu, Hannah Song, Sarah L Tressel, Jinah Hwang, Sergey Dikalov, Debra A Smith, Nolan L Boyd, Manu O Platt, Bernard Lassègue, Kathy K Griendling, and Hanjoong Jo. Bone morphogenic protein 4 produced in endothelial cells by oscillatory shear stress induces monocyte adhesion by stimulating reactive oxygen species production from a nox1-based nadph oxidase. *Circ Res*, 95(8):773–9, Oct 2004.

[28] N Mody, F Parhami, T A Sarafian, and L L Demer. Oxidative stress modulates osteoblastic differentiation of vascular and bone cells. *Free Radic Biol Med*, 31(4):509–519, August 2001.

[29] T Sutra, M Morena, A S Bargnoux, B Caporiccio, B Canaud, and J P Cristol. Superoxide production: a procalcifying cell signalling event in osteoblastic differentiation of vascular smooth muscle cells exposed to calcification media. *Free Radic Res*, 42(9):789–797, September 2008.

[30] C H Byon, A Javed, Q Dai, J C Kappes, T L Clemens, V M Darley-Usmar, J M McDonald, and Y Chen. Oxidative stress induces vascular calcification through modulation of the osteogenic transcription factor Runx2 by AKT signaling. *The Journal of biological chemistry*, 283(22):15319–15327, May 2008.

[31] H You, H Yang, Q Zhu, M Li, J Xue, Y Gu, S Lin, and F Ding. Advanced oxidation protein products induce vascular calcification by promoting osteoblastic trans-differentiation of smooth muscle cells via oxidative stress and ERK pathway. *Ren Fail*, 31(4):313–319, 2009.

[32] J R Dwyer, N Sever, M Carlson, S F Nelson, P A Beachy, and F Parhami. Oxysterols are novel activators of the hedgehog signaling pathway in pluripotent mesenchymal cells. *The Journal of biological chemistry*, 282(12):8959–8968, March 2007.

[33] H Liu, L Yuan, S Xu, and K Wang. Endothelial cell and macrophage regulation of vascular smooth muscle cell calcification modulated by cholestane-3beta, 5alpha, 6beta-triol. *Cell Biol Int*, 31(9):900–907, September 2007.

[34] M P Lynch, C Capparelli, J L Stein, G S Stein, and J B Lian. Apoptosis during bone-like tissue development in vitro. *Journal of cellular biochemistry*, 68(1):31–49, January 1998.

[35] D Proudfoot, J N Skepper, L Hegyi, M R Bennett, C M Shanahan, and P L Weissberg. Apoptosis regulates human vascular calcification in vitro: evidence for initiation of vascular calcification by apoptotic bodies. *Circ Res*, 87(11):1055–62, Nov 2000.

[36] M Liberman, E Bassi, M K Martinatti, F C Lario, J Jr Wosniak, P M Pomerantzeff, and F R Laurindo. Oxidant generation predominates around calcifying foci and enhances progression of aortic valve calcification. *Arteriosclerosis, Thrombosis, and Vascular Biology*, 28(3):463–470, March 2008.

[37] Murray Clarke and Martin Bennett. The emerging role of vascular smooth muscle cell apoptosis in atherosclerosis and plaque stability. *Am J Nephrol*, 26(6):531–5, 2006.

[38] M C Clarke, T D Littlewood, N Figg, J J Maguire, A P Davenport, M Goddard, and M R Bennett. Chronic apoptosis of vascular smooth muscle cells accelerates atherosclerosis and promotes calcification and medial degeneration. *Circulation Research*, 102(12):1529–1538, June 2008.

[39] X Duan, Y Zhou, X Teng, C Tang, and Y Qi. Endoplasmic reticulum stress-mediated apoptosis is activated in vascular calcification. *Biochem Biophys Res Commun*, 387(4):694–699, October 2009.

[40] A Grey, M Bolland, G Gamble, D Wattie, A Horne, J Davidson, and I R Reid. The peroxisome proliferator-activated receptor-gamma agonist rosiglitazone decreases bone formation and bone mineral density in healthy postmenopausal women: a randomized, controlled trial. *Journal of Clinical Endocrinology & Metabolism*, 92(4):1305–1310, April 2007.

[41] B Lecka-Czernik, I Gubrij, E J Moerman, O Kajkenova, D A Lipschitz, S C Manolagas, and R L Jilka. Inhibition of Osf2/Cbfa1 expression and terminal osteoblast differentiation by PPARgamma2. *Journal of cellular biochemistry*, 74(3):357–371, September 1999.

[42] S Muruganandan, A A Roman, and C J Sinal. Adipocyte differentiation of bone marrow-derived mesenchymal stem cells: cross talk with the osteoblastogenic program. *Cellular and Molecular Life Sciences*, 66(2):236–253, January 2009.

[43] E J Moerman, K Teng, D A Lipschitz, and B Lecka-Czernik. Aging activates adipogenic and suppresses osteogenic programs in mesenchymal marrow stroma/stem cells: the role of PPAR-gamma2 transcription factor and TGF-beta/BMP signaling pathways. *Aging cell*, 3(6):379–389, December 2004.

[44] D Zipori. The stem state: mesenchymal plasticity as a paradigm. *Curr Stem Cell Res Ther*, 1(1):95–102, January 2006.

[45] B Lecka-Czernik, E J Moerman, D F Grant, J M Lehmann, S C Manolagas, and R L Jilka. Divergent effects of selective peroxisome proliferator-activated receptor-gamma 2 ligands on adipocyte versus osteoblast differentiation. *Endocrinology*, 143(6):2376–2384, June 2002.

[46] O P Lazarenko, S O Rzonca, L J Suva, and B Lecka-Czernik. Netoglitazone is a PPAR-gamma ligand with selective effects on bone and fat. *Bone*, 38(1):74–84, January 2006.

[47] A A Ali, R S Weinstein, S A Stewart, A M Parfitt, S C Manolagas, and R L Jilka. Rosiglitazone causes bone loss in mice by suppressing osteoblast differentiation and bone formation. *Endocrinology*, 146(3):1226–1235, March 2005.

[48] S O Rzonca, L J Suva, D Gaddy, D C Montague, and B Lecka-Czernik. Bone is a target for the antidiabetic compound rosiglitazone. *Endocrinology*, 145(1):401–406, January 2004.

[49] T Akune, S Ohba, S Kamekura, M Yamaguchi, U I Chung, N Kubota, Y Terauchi, Y Harada, Y Azuma, K Nakamura, T Kadowaki, and H Kawaguchi. PPARgamma insufficiency enhances osteogenesis through osteoblast formation from bone marrow progenitors. *Journal of Clinical Investigation*, 113(6):846–855, March 2004.

[50] T A Cock, J Back, F Elefteriou, G Karsenty, P Kastner, S Chan, and J Auwerx. Enhanced bone formation in lipodystrophic PPARgamma(hyp/hyp) mice relocates haematopoiesis to the spleen. *EMBO Rep*, 5(10):1007–1012, October 2004.

[51] S Tonna and N A Sims. Talking among ourselves: paracrine control of bone formation within the osteoblast lineage. *Calcified tissue international*, 94(1):35–45, January 2014.

[52] N Qiu, L Cao, V David, L D Quarles, and Z Xiao. Kif3a deficiency reverses the skeletal abnormalities in Pkd1 deficient mice by restoring the balance between osteogenesis and adipogenesis. *PLoS ONE*, 5(12):e15240, 2010.

[53] O Donoso, A M Pino, G Seitz, N Osses, and J P Rodriguez. Osteoporosis-associated alteration in the signalling status of BMP-2 in human MSCs under adipogenic conditions. *Journal of cellular biochemistry*, January 2015.

[54] W N Addison, M M Fu, H X Yang, Z Lin, K Nagano, F Gori, and R Baron. Direct transcriptional repression of Zfp423 by Zfp521 mediates a bone morphogenic protein-dependent osteoblast versus adipocyte lineage commitment switch. *Molecular and Cellular Biology*, 34(16):3076–3085, August 2014.

[55] S Ahdjoudj, F Lasmoles, X Holy, E Zerath, and P J Marie. Transforming growth factor beta2 inhibits adipocyte differentiation induced by skeletal unloading in rat bone marrow stroma. *Journal of Bone and Mineral Research*, 17(4):668–677, April 2002.

[56] D Lozano, L F de Castro, S Dapia, I Andrade-Zapata, F Manzarbeitia, M V Alvarez-Arroyo, E Gomez-Barrena, and P Esbrit. Role of parathyroid hormone-related protein in the decreased osteoblast function in diabetes-related osteopenia. *Endocrinology*, 150(5):2027–2035, May 2009.

[57] G K Chan, D Miao, R Deckelbaum, I Bolivar, A Karaplis, and D Goltzman. Parathyroid hormone-related peptide interacts with bone morphogenetic protein 2 to increase osteoblastogenesis and decrease adipogenesis in pluripotent C3H10T 1/2 mesenchymal cells. *Endocrinology*, 144(12):5511–5520, December 2003.

[58] I D'Alimonte, A Lannutti, C Pipino, P Di Tomo, L Pierdomenico, E Cianci, I Antonucci, M Marchisio, M Romano, L Stuppia, F Caciagli, A Pandolfi, and R Ciccarelli. Wnt signaling behaves as a "master regulator" in the osteogenic and adipogenic commitment of human amniotic fluid mesenchymal stem cells. *Stem cell reviews*, 9(5):642–654, October 2013.

[59] K L Auld, S P Berasi, Y Liu, M Cain, Y Zhang, C Huard, S Fukayama, J Zhang, S Choe, W Zhong, B M Bhat, R A Bhat, E L Brown, and R V Martinez. Estrogen-related receptor alpha regulates osteoblast differentiation via Wnt/beta-catenin signaling. *Journal of molecular endocrinology*, 48(2):177–191, April 2012.

[60] M Suzawa, I Takada, J Yanagisawa, F Ohtake, S Ogawa, T Yamauchi, T Kadowaki, Y Takeuchi, H Shibuya, Y Gotoh, K Matsumoto, and S Kato. Cytokines suppress adipogenesis and PPAR-gamma function through the TAK1/TAB1/NIK cascade. *Nature Cell Biology*, 5(3):224–230, March 2003.

[61] C Janani and B D Ranjitha Kumari. PPAR gamma gene - A review. *Diabetes & metabolic syndrome*, October 2014.

[62] E D Rosen and B M Spiegelman. PPARgamma : a nuclear regulator of metabolism, differentiation, and cell growth. *The Journal of biological chemistry*, 276(41):37731–37734, October 2001.

[63] C Knouff and J Auwerx. Peroxisome proliferator-activated receptor-gamma calls for activation in moderation: lessons from genetics and pharmacology. *Endocr Rev*, 25(6):899–918, December 2004.

[64] M Lehrke and M A Lazar. The many faces of PPARgamma. *Cell*, 123(6):993–999, December 2005.

[65] B M Forman, J Chen, and R M Evans. Hypolipidemic drugs, polyunsaturated fatty acids, and eicosanoids are ligands for peroxisome proliferator-activated receptors alpha and delta. *Proceedings of the National Academy of Sciences of the United States of America*, 94(9):4312–4317, April 1997.

[66] S A Kliewer, S S Sundseth, S A Jones, P J Brown, G B Wisely, C S Koble, P Devchand, W Wahli, T M Willson, J M Lenhard, and J M Lehmann. Fatty acids and eicosanoids regulate gene expression through direct interactions with peroxisome proliferator-activated receptors alpha and gamma. *Proceedings of the National Academy of Sciences of the United States of America*, 94(9):4318–4323, April 1997.

[67] G Krey, O Braissant, F L'Horset, E Kalkhoven, M Perroud, M G Parker, and W Wahli. Fatty acids, eicosanoids, and hypolipidemic agents identified as ligands of peroxisome proliferator-activated receptors by coactivator-dependent receptor ligand assay. *Mol Endocrinol*, 11(6):779–791, June 1997.

[68] F Picard and J Auwerx. PPAR(gamma) and glucose homeostasis. *Annu Rev Nutr*, 22:167–197, 2002.

[69] A Werman, A Hollenberg, G Solanes, C Bjorbaek, A J Vidal-Puig, and J S Flier. Ligand-independent activation domain in the N terminus of peroxisome proliferator-activated receptor gamma (PPARgamma). Differential activity of PPARgamma1 and -2 isoforms and influence of insulin. *The Journal of biological chemistry*, 272(32):20230–20235, August 1997.

[70] P Tontonoz, E Hu, and B M Spiegelman. Stimulation of adipogenesis in fibroblasts by PPAR gamma 2, a lipid-activated transcription factor. *Cell*, 79(7):1147–1156, December 1994.

[71] A J Vidal-Puig, R V Considine, M Jimenez-Linan, A Werman, W J Pories, J F Caro, and J S Flier. Peroxisome proliferator-activated receptor gene expression in human tissues. Effects of obesity, weight loss, and regulation by insulin and glucocorticoids. *Journal of Clinical Investigation*, 99(10):2416–2422, May 1997.

[72] S E Nissen and K Wolski. Effect of rosiglitazone on the risk of myocardial infarction and death from cardiovascular causes. *New England Journal of Medicine*, 356(24):2457–2471, June 2007.

[73] S Singh, Y K Loke, and C D Furberg. Long-term risk of cardiovascular events with rosiglitazone: a meta-analysis. *JAMA : the journal of the American Medical Association*, 298(10):1189–1195, September 2007.

[74] P D Home, S J Pocock, H Beck-Nielsen, P S Curtis, R Gomis, M Hanefeld, N P Jones, M Komajda, and J J McMurray. Rosiglitazone evaluated for cardiovascular outcomes in oral agent combination therapy for type 2 diabetes (RECORD): a multicentre, randomised, open-label trial. *Lancet*, 373(9681):2125–2135, June 2009.

[75] R M Lago, P P Singh, and R W Nesto. Congestive heart failure and cardiovascular death in patients with prediabetes and type 2 diabetes given thiazolidinediones: a meta-analysis of randomised clinical trials. *Lancet*, 370(9593):1129–1136, September 2007.

[76] D Bruemmer, F Yin, J Liu, J P Berger, T Sakai, F Blaschke, E Fleck, A J Van Herle, B M Forman, and R E Law. Regulation of the growth arrest and DNA damage-inducible gene 45 (GADD45) by peroxisome proliferator-activated receptor gamma in vascular smooth muscle cells. *Circulation Research*, 93(4):e38–47, August 2003.

[77] Y Lin, X Zhu, F L McLntee, H Xiao, J Zhang, M Fu, and Y E Chen. Interferon regulatory factor-1 mediates PPARgamma-induced apoptosis in vascular smooth muscle cells. *Arteriosclerosis, Thrombosis, and Vascular Biology*, 24(2):257–263, February 2004.

[78] T Okura, M Nakamura, Y Takata, S Watanabe, Y Kitami, and K Hiwada. Troglitazone induces apoptosis via the p53 and Gadd45 pathway in vascular smooth muscle cells. *Eur J Pharmacol*, 407(3):227–235, November 2000.

[79] S Redondo, E Ruiz, C G Santos-Gallego, E Padilla, and T Tejerina. Pioglitazone induces vascular smooth muscle cell apoptosis through a peroxisome proliferator-activated receptor-gamma, transforming growth factor-beta1, and a Smad2-dependent mechanism. *Diabetes*, 54(3):811–817, March 2005.

[80] E Ruiz, S Redondo, A Gordillo-Moscoso, and T Tejerina. Pioglitazone induces apoptosis in human vascular smooth muscle cells from diabetic patients involving the transforming growth factor-beta/activin receptor-like kinase-4/5/7/Smad2 signaling pathway. *J Pharmacol Exp Ther*, 321(2):431–438, May 2007.

[81] Z A Habib, S L Havstad, K Wells, G Divine, M Pladevall, and L K Williams. Thiazolidinedione use and the longitudinal risk of fractures in patients with type 2 diabetes mellitus. *The Journal of clinical endocrinology and metabolism*, 95(2):592–600.

[82] C R Dormuth, G Carney, B Carleton, K Bassett, and J M Wright. Thiazolidinediones and fractures in men and women. *Arch Intern Med*, 169(15):1395–1402, August 2009.

[83] F Y Hsiao and C D Mullins. The association between thiazolidinediones and hospitalisation for fracture in type 2 diabetic patients: a Taiwanese population-based nested case-control study. *Diabetologia*, 53(3):489–496.

[84] I J Douglas, S J Evans, S Pocock, and L Smeeth. The risk of fractures associated with thiazolidinediones: a self-controlled case-series study. *PLoS Med*, 6(9):e1000154, September 2009.

[85] S G Jones, S R Momin, M W Good, T K Shea, and K Patric. Distal upper and lower limb fractures associated with thiazolidinedione use. *Am J Manag Care*, 15(8):491–496, August 2009.

[86] Y Wan, L W Chong, and R M Evans. PPAR-gamma regulates osteoclastogenesis in mice. *Nature Medicine*, 13(12):1496–1503, December 2007.

[87] Emma Khan and Yousef Abu-Amer. Activation of peroxisome proliferator-activated receptor-gamma inhibits differentiation of preosteoblasts. *J Lab Clin Med*, 142(1):29–34, Jul 2003.

[88] Min Jae Jeon, Jeong Ah Kim, Sung Hee Kwon, Sang Wan Kim, Kyong Soo Park, Sung-Woo Park, Seong Yeon Kim, and Chan Soo Shin. Activation of peroxisome proliferator-activated receptor-gamma inhibits the runx2-mediated transcription of osteocalcin in osteoblasts. *J Biol Chem*, 278(26):23270–7, Jun 2003.

[89] S Watanabe, Y Takeuchi, S Fukumoto, H Fujita, T Nakano, and T Fujita. Decrease in serum leptin by troglitazone is associated with preventing bone loss in type 2 diabetic patients. *Journal of Bone and Mineral Metabolism*, 21(3):166–171, 2003.

[90] J Cornish, K E Callon, A R King, G J Cooper, and I R Reid. Systemic administration of amylin increases bone mass, linear growth, and adiposity in adult male mice. *Am J Physiol*, 275(4 Pt 1):E694–9, October 1998.

[91] J Cornish, K E Callon, and I R Reid. Insulin increases histomorphometric indices of bone formation In vivo. *Calcified tissue international*, 59(6):492–495, December 1996.

[92] B Lecka-Czernik, C Ackert-Bicknell, M L Adamo, V Marmolejos, G A Churchill, K R Shockley, I R Reid, A Grey, and C J Rosen. Activation of peroxisome proliferator-activated receptor gamma (ppargamma) by rosiglitazone suppresses components of the insulin-like growth factor regulatory system in vitro and in vivo. *Endocrinology*, 148(2):903–11, Feb 2007.

[93] G L Rubin, Y Zhao, A M Kalus, and E R Simpson. Peroxisome proliferator-activated receptor gamma ligands inhibit estrogen biosynthesis in human breast adipose tissue: possible implications for breast cancer therapy. *Cancer Res*, 60(6):1604–1608, March 2000.

[94] Bloomberg. Ex-regulator said to testify glaxosmithkline withheld study, 07 2010.

[95] European Medicines Agency. European medicines agency recommends suspension of avandia, avandamet and avaglim, 09 2010.

[96] Fairfax New Zealand Limited. Diabetes drug withdrawn, 02 2011.

[97] S Christakos, P Dhawan, Y Liu, X Peng, and A Porta. New insights into the mechanisms of vitamin D action. *Journal of cellular biochemistry*, 88(4):695–705, March 2003.

[98] M van Driel, M Koedam, C J Buurman, M Hewison, H Chiba, A G Uitterlinden, H A Pols, and J P van Leeuwen. Evidence for auto/paracrine actions of vitamin D in bone: 1alpha-hydroxylase expression and activity in human bone cells. *FASEB J*, 20(13):2417–2419, November 2006.

[99] T Miyahara, T Simoura, N Osahune, Y Uchida, T Sakuma, N Nemoto, A Kozakai, T Takamura, R Yamazaki, S Higuchi, H Chiba, K Iba, and N Sawada. A highly potent 26,27-Hexafluoro-1a,25-dihydroxyvitamin D3 on calcification in SV40-transformed human fetal osteoblastic cells. *Calcified tissue international*, 70(6):488–495, June 2002.

[100] Q Shen and S Christakos. The vitamin D receptor, Runx2, and the Notch signaling pathway cooperate in the transcriptional regulation of osteopontin. *The Journal of biological chemistry*, 280(49):40589–40598, December 2005.

[101] T K Barthel, D R Mathern, G K Whitfield, C A Haussler, H A th Hopper, J C Hsieh, S A Slater, G Hsieh, M Kaczmarska, P W Jurutka, O I Kolek, F K Ghishan, and M R Haussler. 1,25-Dihydroxyvitamin D3/VDR-mediated induction of FGF23 as well as transcriptional control of other bone anabolic and catabolic genes

that orchestrate the regulation of phosphate and calcium mineral metabolism. *J Steroid Biochem Mol Biol*, 103(3-5):381–388, March 2007.

[102] V J Woeckel, R D Alves, S M Swagemakers, M Eijken, H Chiba, B C van der Eerden, and J P van Leeuwen. 1Alpha,25-(OH)2D3 acts in the early phase of osteoblast differentiation to enhance mineralization via accelerated production of mature matrix vesicles. *J Cell Physiol*, 225(2):593–600, November 2010.

[103] G J Atkins, P H Anderson, D M Findlay, K J Welldon, C Vincent, A C Zannettino, P D O'Loughlin, and H A Morris. Metabolism of vitamin D3 in human osteoblasts: evidence for autocrine and paracrine activities of 1 alpha,25-dihydroxyvitamin D3. *Bone*, 40(6):1517–1528, June 2007.

[104] T W Dunlop, S Vaisanen, C Frank, F Molnar, L Sinkkonen, and C Carlberg. The human peroxisome proliferator-activated receptor delta gene is a primary target of 1alpha,25-dihydroxyvitamin D3 and its nuclear receptor. *Journal of molecular biology*, 349(2):248–260, June 2005.

[105] P Sertznig, T Dunlop, M Seifert, W Tilgen, and J Reichrath. Cross-talk between vitamin D receptor (VDR)- and peroxisome proliferator-activated receptor (PPAR)-signaling in melanoma cells. *Anticancer Res*, 29(9):3647–3658, September 2009.

[106] S Heikkinen, J Auwerx, and C A Argmann. PPARgamma in human and mouse physiology. *Biochim Biophys Acta*, 1771(8):999–1013, August 2007.

[107] M Ricote, J Huang, L Fajas, A Li, J Welch, J Najib, J L Witztum, J Auwerx, W Palinski, and C K Glass. Expression of the peroxisome proliferator-activated receptor gamma (PPARgamma) in human atherosclerosis and regulation in macrophages by colony stimulating factors and oxidized low density lipoprotein. *Proceedings of the National Academy of Sciences of the United States of America*, 95(13):7614–7619, June 1998.

[108] L Fajas, J C Fruchart, and J Auwerx. Ppargamma3 mrna: a distinct ppargamma mrna subtype transcribed from an independent promoter. *FEBS Lett*, 438(1-2):55–60, Oct 1998.

[109] German Gaston Leparc and Robi David Mitra. Non-est-based prediction of novel alternatively spliced cassette exons with cell signaling function in caenorhabditis elegans and human. *Nucleic Acids Res*, 35(10):3192–202, 2007.

[110] R Mukherjee, L Jow, G E Croston, and J R Paterniti, Jr. Identification, characterization, and tissue distribution of human peroxisome proliferator-activated receptor (ppar) isoforms ppargamma2 versus ppargamma1 and activation with retinoid x receptor agonists and antagonists. *J Biol Chem*, 272(12):8071–6, Mar 1997.

[111] S M Jackson and L L Demer. Peroxisome proliferator-activated receptor activators modulate the osteoblastic maturation of mc3t3-e1 preosteoblasts. *FEBS Lett*, 471(1):119–24, Apr 2000.

[112] H Chiba, N Sawada, T Ono, S Ishii, and M Mori. Establishment and characterization of a simian virus 40-immortalized osteoblastic cell line from normal human bone. *Jpn J Cancer Res*, 84(3):290–297, March 1993.

[113] M Eijken, S Swagemakers, M Koedam, C Steenbergen, P Derkx, A G Uitterlinden, P J van der Spek, J A Visser, F H de Jong, H A Pols, and J P van Leeuwen. The activin A-follistatin system: potent regulator of human extracellular matrix mineralization. *FASEB J*, 21(11):2949–2960, September 2007.

[114] M Eijken, M Hewison, M S Cooper, F H de Jong, H Chiba, P M Stewart, A G Uitterlinden, H A P Pols, and J P T M van Leeuwen. 11beta-hydroxysteroid dehydrogenase expression and glucocorticoid synthesis are directed by a molecular switch during osteoblast differentiation. *Mol Endocrinol*, 19(3):621–31, Mar 2005.

[115] Stéphane Mandard, Fokko Zandbergen, Nguan Soon Tan, Pascal Escher, David Patsouris, Wolfgang Koenig, Robert Kleemann, Arjen Bakker, Frank Veenman, Walter Wahli, Michael Müller, and Sander Kersten. The direct peroxisome proliferator-activated receptor target fasting-induced adipose factor (fiaf/pgar/angptl4) is present in blood plasma as a truncated protein that is increased by fenofibrate treatment. *J Biol Chem*, 279(33):34411–20, Aug 2004.

[116] Paul Targett-Adams, Marion J McElwee, Ewa Ehrenborg, Mattias C Gustafsson, Colin N Palmer, and John McLauchlan. A ppar response element regulates transcription of the gene for human adipose differentiation-related protein. *Biochim Biophys Acta*, 1728(1-2):95–104, Apr 2005.

[117] Béatrice Desvergne, Liliane Michalik, and Walter Wahli. Be fit or be sick: peroxisome proliferator-activated receptors are down the road. *Mol Endocrinol*, 18(6):1321–32, Jun 2004.

[118] Joseph P Stains and Roberto Civitelli. Genomic approaches to identifying transcriptional regulators of osteoblast differentiation. *Genome Biol*, 4(7):222, 2003.

[119] M Eijken, M Koedam, M van Driel, C J Buurman, H A Pols, and J P van Leeuwen. The essential role of glucocorticoids for proper human osteoblast differentiation and matrix mineralization. *Molecular and Cellular Endocrinology*, 248(1-2):87–93, March 2006.

[120] Osteoporosis prevention, diagnosis, and therapy. *JAMA : the journal of the American Medical Association*, 285(6):785–795, February 2001.

[121] Claudia Bruedigam, Marijke Koedam, Hideki Chiba, Marco Eijken, and Johannes P T M van Leeuwen. Evidence for multiple peroxisome proliferator-activated receptor γ transcripts in bone: Fine-tuning by hormonal regulation and mRNA stability. *FEBS letters*, 582(11):1618–1624, 2008.

[122] R Saladin, L Fajas, S Dana, Y D Halvorsen, J Auwerx, and M Briggs. Differential regulation of peroxisome proliferator activated receptor gamma1 (ppargamma1) and ppargamma2 messenger rna expression in the early stages of adipogenesis. *Cell Growth Differ*, 10(1):43–8, Jan 1999.

[123] D D Patel, B L Knight, D Wiggins, S M Humphreys, and G F Gibbons. Disturbances in the normal regulation of srebp-sensitive genes in ppar alpha-deficient mice. *J Lipid Res*, 42(3):328–37, Mar 2001.

[124] P S Gillies and C J Dunn. Pioglitazone. *Drugs*, 60(2):333–43– discussion 344–5, August 2000.

[125] G L Plosker and D Faulds. Troglitazone: a review of its use in the management of type 2 diabetes mellitus. *Drugs*, 57(3):409–438, March 1999.

[126] Y Kiyota, T Kondo, Y Maeshiba, A Hashimoto, K Yamashita, Y Yoshimura, M Motohashi, and S Tanayama. Studies on the metabolism of the new antidiabetic agent pioglitazone. Identification of metabolites in rats and dogs. *Arzneimittelforschung*, 47(1):22–28, January 1997.

[127] Lisa D Yee, Nita Williams, Ping Wen, Donn C Young, Joanne Lester, Maria V Johnson, William B Farrar, Michael J Walker, Stephen P Povoski, Saul Suster, and Charis Eng. Pilot study of rosiglitazone therapy in women with breast cancer: effects of short-term therapy on tumor tissue and serum markers. *Clin Cancer Res*, 13(1):246–52, Jan 2007.

[128] Luigi A Warren and Derrick J Rossi. Stem cells and aging in the hematopoietic system. *Mech Ageing Dev*, 130(1-2):46–53, 2009.

[129] R Yu, S Mandlekar, W Lei, W E Fahl, T H Tan, and A N Kong. p38 mitogen-activated protein kinase negatively regulates the induction of phase ii drug-metabolizing enzymes that detoxify carcinogens. *J Biol Chem*, 275(4):2322–7, Jan 2000.

[130] Masanobu Kawai, Maureen J Devlin, and Clifford J Rosen. Fat targets for skeletal health. *Nat Rev Rheumatol*, 5(7):365–72, Jul 2009.

[131] H Kobayashi, Y h Gao, C Ueta, A Yamaguchi, and T Komori. Multilineage differentiation of cbfa1-deficient calvarial cells in vitro. *Biochem Biophys Res Commun*, 273(2):630–6, Jul 2000.

[132] W Liu, S Toyosawa, T Furuichi, N Kanatani, C Yoshida, Y Liu, M Himeno, S Narai, A Yamaguchi, and T Komori. Overexpression of cbfa1 in osteoblasts inhibits osteoblast maturation and causes osteopenia with multiple fractures. *J Cell Biol*, 155(1):157–66, Oct 2001.

[133] R F Kletzien, S D Clarke, and R G Ulrich. Enhancement of adipocyte differentiation by an insulin-sensitizing agent. *Mol Pharmacol*, 41(2):393–8, Feb 1992.

[134] J M Gimble, C E Robinson, X Wu, K A Kelly, B R Rodriguez, S A Kliewer, J M Lehmann, and D C Morris. Peroxisome proliferator-activated receptor-gamma activation by thiazolidinediones induces adipogenesis in bone marrow stromal cells. *Mol Pharmacol*, 50(5):1087–94, Nov 1996.

[135] S V Komarova, F I Ataullakhanov, and R K Globus. Bioenergetics and mitochondrial transmembrane potential during differentiation of cultured osteoblasts. *Am J Physiol Cell Physiol*, 279(4):C1220–9, Oct 2000.

[136] Chien-Tsun Chen, Yu-Ru V Shih, Tom K Kuo, Oscar K Lee, and Yau-Huei Wei. Coordinated changes of mitochondrial biogenesis and antioxidant enzymes during osteogenic differentiation of human mesenchymal stem cells. *Stem Cells*, 26(4):960–8, Apr 2008.

[137] T Wenz, F Diaz, B M Spiegelman, and C T Moraes. Activation of the PPAR/PGC-1alpha pathway prevents a bioenergetic deficit and effectively improves a mitochondrial myopathy phenotype. *Cell Metab*, 8(3):249–256, September 2008.

[138] Y L Wang, K A Frauwirth, S M Rangwala, M A Lazar, and C B Thompson. Thiazolidinedione activation of peroxisome proliferator-activated receptor gamma can enhance mitochondrial potential and promote cell survival. *The Journal of biological chemistry*, 277(35):31781–31788, August 2002.

[139] M P Bova, D Tam, G McMahon, and M N Mattson. Troglitazone induces a rapid drop of mitochondrial membrane potential in liver HepG2 cells. *Toxicol Lett*, 155(1):41–50, January 2005.

[140] C Dello Russo, V Gavrilyuk, G Weinberg, A Almeida, J P Bolanos, J Palmer, D Pelligrino, E Galea, and D L Feinstein. Peroxisome proliferator-activated receptor gamma thiazolidinedione agonists increase glucose metabolism in astrocytes. *The Journal of biological chemistry*, 278(8):5828–5836, February 2003.

[141] Leonard Guarente. Sirtuins and ageing–new findings. *EMBO Rep*, 14(9):750, Sep 2013.

[142] Anne Eckert, Uta Keil, Celio A Marques, Astrid Bonert, Claudia Frey, Katrin Schüssel, and Walter E Müller. Mitochondrial dysfunction, apoptotic cell death, and alzheimer's disease. *Biochem Pharmacol*, 66(8):1627–34, Oct 2003.

[143] A Elbaz, X Wu, D Rivas, J M Gimble, and G Duque. Inhibition of Fatty Acid Biosynthesis Prevents Adipocyte Lipotoxicity on Human Osteoblasts In Vitro. *J Cell Mol Med*, March 2009.

[144] J Y Jung, C I Yoo, H T Kim, C H Kwon, J Y Park, and Y K Kim. Role of mitogen-activated protein kinase (MAPK) in troglitazone-induced osteoblastic cell death. *Toxicology*, 234(1-2):73–82, May 2007.

[145] M A Soroceanu, D Miao, X Y Bai, H Su, D Goltzman, and A C Karaplis. Rosiglitazone impacts negatively on bone by promoting osteoblast/osteocyte apoptosis. *The Journal of endocrinology*, 183(1):203–216, October 2004.

[146] Cheryl L Ackert-Bicknell, Keith R Shockley, Lindsay G Horton, Beata Lecka-Czernik, Gary A Churchill, and Clifford J Rosen. Strain-specific effects of rosiglitazone on bone mass, body composition, and serum insulin-like growth factor-i. *Endocrinology*, 150(3):1330–40, Mar 2009.

[147] Maria Almeida, Li Han, Marta Martin-Millan, Lilian I Plotkin, Scott A Stewart, Paula K Roberson, Stavroula Kousteni, Charles A O'Brien, Teresita Bellido, A Michael Parfitt, Robert S Weinstein, Robert L Jilka, and Stavros C Manolagas. Skeletal involution by age-associated oxidative stress and its acceleration by loss of sex steroids. *J Biol Chem*, 282(37):27285–97, Sep 2007.

[148] Maria Almeida, Elena Ambrogini, Li Han, Stavros C Manolagas, and Robert L Jilka. Increased lipid oxidation causes oxidative stress, increased peroxisome proliferator-activated receptor-gamma expression, and diminished pro-osteogenic wnt signaling in the skeleton. *J Biol Chem*, 284(40):27438–48, Oct 2009.

[149] R S Weinstein, R L Jilka, A M Parfitt, and S C Manolagas. Inhibition of osteoblastogenesis and promotion of apoptosis of osteoblasts and osteocytes by glucocorticoids. potential mechanisms of their deleterious effects on bone. *J Clin Invest*, 102(2):274–82, Jul 1998.

[150] M van Driel, M Koedam, C J Buurman, M Roelse, F Weyts, H Chiba, A G Uitterlinden, H A Pols, and J P van Leeuwen. Evidence that both 1alpha,25-dihydroxyvitamin D3 and 24-hydroxylated D3 enhance human osteoblast differentiation and mineralization. *Journal of cellular biochemistry*, 99(3):922–935, October 2006.

[151] Claudia Bruedigam, Marco Eijken, Marijke Koedam, Jeroen van de Peppel, Ksenija Drabek, Hideki Chiba, and Johannes P T M van Leeuwen. A New Concept Underlying Stem Cell Lineage Skewing That Explains the Detrimental Effects of Thiazolidinediones on Bone. *Stem cells (Dayton, Ohio)*, 28(5):N/A–N/A, 2010.

[152] S Lim, C J Jin, M Kim, S S Chung, H S Park, I K Lee, C T Lee, Y M Cho, H K Lee, and K S Park. PPARgamma gene transfer sustains apoptosis, inhibits vascular smooth muscle cell proliferation, and reduces neointima formation after balloon injury in rats. *Arteriosclerosis, Thrombosis, and Vascular Biology*, 26(4):808–813, April 2006.

[153] H M Wain, M Lush, F Ducluzeau, and S Povey. Genew: the human gene nomenclature database. *Nucleic Acids Res*, 30(1):169–171, January 2002.

[154] S Chakreeyarat, S Saetung, L O Chailurkit, S Rattanasiri, S Ditbanjong, N Chitrapazt, S Jaovisidha, and B Ongphiphadhanakul. Elevated vitamin D status in postmenopausal women on thiazolidinediones for type 2 diabetes. *Endocrine*, 39(3):278–282.

[155] A L Boskey, L Spevak, E Paschalis, S B Doty, and M D McKee. Osteopontin deficiency increases mineral content and mineral crystallinity in mouse bone. *Calcif Tissue Int*, 71(2):145–54, Aug 2002.

[156] A L Boskey, M Maresca, W Ullrich, S B Doty, W T Butler, and C W Prince. Osteopontin-hydroxyapatite interactions in vitro: inhibition of hydroxyapatite formation and growth in a gelatin-gel. *Bone Miner*, 22(2):147–59, Aug 1993.

[157] G K Hunter, P V Hauschka, A R Poole, L C Rosenberg, and H A Goldberg. Nucleation and inhibition of hydroxyapatite formation by mineralized tissue proteins. *Biochem J*, 317 (Pt 1):59–64, Jul 1996.

[158] R W Romberg, P G Werness, B L Riggs, and K G Mann. Inhibition of hydroxyapatite crystal growth by bone-specific and other calcium-binding proteins. *Biochemistry*, 25(5):1176–80, Mar 1986.

[159] C Bruedigam, M Eijken, M Koedam, H Chiba, and J P van Leeuwen. Opposing actions of rosiglitazone and resveratrol on mineralization in human vascular smooth muscle cells. *Journal of molecular and cellular cardiology*, 51(5):862–871, November 2011.

[160] J Lian, C Stewart, E Puchacz, S Mackowiak, V Shalhoub, D Collart, G Zambetti, and G Stein. Structure of the rat osteocalcin gene and regulation of vitamin d-dependent expression. *Proc Natl Acad Sci U S A*, 86(4):1143–7, Feb 1989.

[161] P Ducy, C Desbois, B Boyce, G Pinero, B Story, C Dunstan, E Smith, J Bonadio, S Goldstein, C Gundberg, A Bradley, and G Karsenty. Increased bone formation in osteocalcin-deficient mice. *Nature*, 382(6590):448–52, Aug 1996.

[162] C Nicolaije, M Koedam, and J P van Leeuwen. Decreased oxygen tension lowers reactive oxygen species and apoptosis and inhibits osteoblast matrix mineralization through changes in early osteoblast differentiation. *J Cell Physiol*, 227(4):1309–1318, April 2012.

[163] Zhang Xiaoyu, Biswas Payal, Owraghi Melissa, and Laura P Zanello. 1alpha,25(oh)2-vitamin d3 membrane-initiated calcium signaling modulates exocytosis and cell survival. *J Steroid Biochem Mol Biol*, 103(3-5):457–61, Mar 2007.

[164] Xiaoyu Zhang and Laura P Zanello. Vitamin d receptor-dependent 1 alpha,25(oh)2 vitamin d3-induced anti-apoptotic pi3k/akt signaling in osteoblasts. *J Bone Miner Res*, 23(8):1238–48, Aug 2008.

[165] Toshiyuki Sakaki, Norio Kagawa, Keiko Yamamoto, and Kuniyo Inouye. Metabolism of vitamin d3 by cytochromes p450. *Front Biosci*, 10:119–34, Jan 2005.

[166] P Sertznig, M Seifert, W Tilgen, and J Reichrath. Activation of vitamin D receptor (VDR)- and peroxisome proliferator-activated receptor (PPAR)-signaling pathways through 1,25(OH)(2)D(3) in melanoma cell lines and other skin-derived cell lines. *Dermatoendocrinol*, 1(4):232–238, July 2009.

[167] Murray C H Clarke, Nichola Figg, Janet J Maguire, Anthony P Davenport, Martin Goddard, Trevor D Littlewood, and Martin R Bennett. Apoptosis of vascular smooth muscle cells induces features of plaque vulnerability in atherosclerosis. *Nat Med*, 12(9):1075–80, Sep 2006.

[168] Philip D Home, Stuart J Pocock, Henning Beck-Nielsen, Ramón Gomis, Markolf Hanefeld, Nigel P Jones, Michel Komajda, John J V McMurray, and RECORD Study Group. Rosiglitazone evaluated for cardiovascular outcomes–an interim analysis. *N Engl J Med*, 357(1):28–38, Jul 2007.

[169] K Mori, A Shioi, S Jono, Y Nishizawa, and H Morii. Dexamethasone enhances in vitro vascular calcification by promoting osteoblastic differentiation of vascular smooth muscle cells. *Arterioscler Thromb Vasc Biol*, 19(9):2112–8, Sep 1999.

[170] A Shioi, Y Nishizawa, S Jono, H Koyama, M Hosoi, and H Morii. Beta-glycerophosphate accelerates calcification in cultured bovine vascular smooth muscle cells. *Arterioscler Thromb Vasc Biol*, 15(11):2003–2009, November 1995.

[171] Alan Garfinkel, Yin Tintut, Danny Petrasek, Kristina Boström, and Linda L Demer. Pattern formation by vascular mesenchymal cells. *Proc Natl Acad Sci U S A*, 101(25):9247–50, Jun 2004.

[172] K K Griendling, D Sorescu, B Lassegue, and M Ushio-Fukai. Modulation of protein kinase activity and gene expression by reactive oxygen species and their role in vascular physiology and pathophysiology. *Arteriosclerosis, Thrombosis, and Vascular Biology*, 20(10):2175–2183, October 2000.

[173] S H Ellmark, G J Dusting, M N Fui, N Guzzo-Pernell, and G R Drummond. The contribution of Nox4 to NADPH oxidase activity in mouse vascular smooth muscle. *Cardiovasc Res*, 65(2):495–504, February 2005.

[174] S Itoh, S Umemoto, M Hiromoto, Y Toma, Y Tomochika, S Aoyagi, M Tanaka, T Fujii, and M Matsuzaki. Importance of NAD(P)H oxidase-mediated oxidative stress and contractile type smooth muscle myosin heavy chain SM2 at the early stage of atherosclerosis. *Circulation*, 105(19):2288–2295, May 2002.

[175] N Kawada, S Seki, M Inoue, and T Kuroki. Effect of antioxidants, resveratrol, quercetin, and N-acetylcysteine, on the functions of cultured rat hepatic stellate cells and Kupffer cells. *Hepatology*, 27(5):1265–1274, May 1998.

[176] Francine Z Marques, M Andrea Markus, and Brian J Morris. Resveratrol: cellular actions of a potent natural chemical that confers a diversity of health benefits. *Int J Biochem Cell Biol*, 41(11):2125–8, Nov 2009.

[177] Suresh Varma Penumathsa and Nilanjana Maulik. Resveratrol: a promising agent in promoting cardioprotection against coronary heart disease. *Can J Physiol Pharmacol*, 87(4):275–86, Apr 2009.

[178] G J Soleas, E P Diamandis, and D M Goldberg. Resveratrol: a molecule whose time has come? And gone? *Clin Biochem*, 30(2):91–113, March 1997.

[179] K P L Bhat, J W 2nd Kosmeder, and J M Pezzuto. Biological effects of resveratrol. *Antioxid Redox Signal*, 3(6):1041–1064, December 2001.

[180] G Dalfino, S Simone, S Porreca, C Cosola, C Balestra, C Manno, F P Schena, G Grandaliano, and G Pertosa. Bone morphogenetic protein-2 may represent the molecular link between oxidative stress and vascular stiffness in chronic kidney disease. *Atherosclerosis*, 211(2):418–23, Aug 2010.

[181] Alejandra San Martín, Pingfeng Du, Anna Dikalova, Bernard Lassègue, María Aleman, María Carolina Góngora, Kathryn Brown, Giji Joseph, David G Harrison, W Robert Taylor, Hanjoong Jo, and Kathy K Griendling. Reactive oxygen species-selective regulation of aortic inflammatory gene expression in type 2 diabetes. *Am J Physiol Heart Circ Physiol*, 292(5):H2073–82, May 2007.

[182] P M Ridker, N R Cook, S Cheng, H A Erlich, K Lindpaintner, J Plutzky, and R Y Zee. Alanine for proline substitution in the peroxisome proliferator-activated receptor gamma-2 (PPARG2) gene and the risk of incident myocardial infarction. *Arteriosclerosis, Thrombosis, and Vascular Biology*, 23(5):859–863, May 2003.

[183] X L Wang, J Oosterhof, and N Duarte. Peroxisome proliferator-activated receptor gamma C161–>T polymorphism and coronary artery disease. *Cardiovasc Res*, 44(3):588–594, December 1999.

[184] Z Chen, S Ishibashi, S Perrey, Ji Osuga, T Gotoda, T Kitamine, Y Tamura, H Okazaki, N Yahagi, Y Iizuka, F Shionoiri, K Ohashi, K Harada, H Shimano, R Nagai, and N Yamada. Troglitazone inhibits atherosclerosis in apolipoprotein E-knockout mice: pleiotropic effects on CD36 expression and HDL. *Arteriosclerosis, Thrombosis, and Vascular Biology*, 21(3):372–377, March 2001.

[185] Z Levi, A Shaish, N Yacov, H Levkovitz, S Trestman, Y Gerber, H Cohen, A Dvir, R Rhachmani, M Ravid, and D Harats. Rosiglitazone (PPARgamma-agonist) attenuates atherogenesis with no effect on hyperglycaemia in a combined diabetes-atherosclerosis mouse model. *Diabetes Obes Metab*, 5(1):45–50, January 2003.

[186] A C Calkin, J M Forbes, C M Smith, M Lassila, M E Cooper, K A Jandeleit-Dahm, and T J Allen. Rosiglitazone attenuates atherosclerosis in a model of insulin insufficiency independent of its metabolic effects. *Arteriosclerosis, Thrombosis, and Vascular Biology*, 25(9):1903–1909, September 2005.

[187] A C Li, K K Brown, M J Silvestre, T M Willson, W Palinski, and C K Glass. Peroxisome proliferator-activated receptor gamma ligands inhibit development of atherosclerosis in LDL receptor-deficient mice. *Journal of Clinical Investigation*, 106(4):523–531, August 2000.

[188] H Koshiyama, D Shimono, N Kuwamura, J Minamikawa, and Y Nakamura. Rapid communication: in-

hibitory effect of pioglitazone on carotid arterial wall thickness in type 2 diabetes. *Journal of Clinical Endocrinology & Metabolism*, 86(7):3452–3456, July 2001.

[189] J Minamikawa, S Tanaka, M Yamauchi, D Inoue, and H Koshiyama. Potent inhibitory effect of troglitazone on carotid arterial wall thickness in type 2 diabetes. *Journal of Clinical Endocrinology & Metabolism*, 83(5):1818–1820, May 1998.

[190] R C Johnson, J A Leopold, and J Loscalzo. Vascular calcification: pathobiological mechanisms and clinical implications. *Circulation Research*, 99(10):1044–1059, November 2006.

[191] T M Doherty, K Asotra, L A Fitzpatrick, J H Qiao, D J Wilkin, R C Detrano, C R Dunstan, P K Shah, and T B Rajavashisth. Calcification in atherosclerosis: bone biology and chronic inflammation at the arterial crossroads. *Proceedings of the National Academy of Sciences of the United States of America*, 100(20):11201–11206, September 2003.

[192] M J Budoff. Atherosclerosis imaging and calcified plaque: coronary artery disease risk assessment. *Prog Cardiovasc Dis*, 46(2):135–148, September 2003.

[193] M Y Speer and C M Giachelli. Regulation of cardiovascular calcification. *Cardiovasc Pathol*, 13(2):63–70, March 2004.

[194] T Schinke and G Karsenty. Vascular calcification–a passive process in need of inhibitors. *Nephrol Dial Transplant*, 15(9):1272–4, Sep 2000.

[195] P K Narayanan, T Hart, F Elcock, C Zhang, L Hahn, D McFarland, L Schwartz, D G Morgan, and P Bugelski. Troglitazone-induced intracellular oxidative stress in rat hepatoma cells: a flow cytometric assessment. *Cytometry A*, 52(1):28–35, March 2003.

[196] A M Lennon, M Ramauge, A Dessouroux, and M Pierre. MAP kinase cascades are activated in astrocytes and preadipocytes by 15-deoxy-Delta(12-14)-prostaglandin J(2) and the thiazolidinedione ciglitazone through peroxisome proliferator activator receptor gamma-independent mechanisms involving reactive oxygenated species. *The Journal of biological chemistry*, 277(33):29681–29685, August 2002.

[197] W C Huang, C C Chio, K H Chi, H M Wu, and W W Lin. Superoxide anion-dependent Raf/MEK/ERK activation by peroxisome proliferator activated receptor gamma agonists 15-deoxy-delta(12,14)-prostaglandin J(2), ciglitazone, and GW1929. *Experimental cell research*, 277(2):192–200, July 2002.

[198] Maria A Potenza, Sara Gagliardi, Leonarda De Benedictis, Addolorata Zigrino, Edy Tiravanti, Giuseppe Colantuono, Antonio Federici, Loredana Lorusso, Vincenzo Benagiano, Michael J Quon, and Monica Montagnani. Treatment of spontaneously hypertensive rats with rosiglitazone ameliorates cardiovascular patho-

physiology via antioxidant mechanisms in the vasculature. *Am J Physiol Endocrinol Metab*, 297(3):E685–94, Sep 2009.

[199] Jinah Hwang, Dean J Kleinhenz, Heidi L Rupnow, Adam G Campbell, Peter M Thulé, Roy L Sutliff, and C Michael Hart. The ppargamma ligand, rosiglitazone, reduces vascular oxidative stress and nadph oxidase expression in diabetic mice. *Vascul Pharmacol*, 46(6):456–62, Jun 2007.

[200] Ling Gao and Giovanni E Mann. Vascular nad(p)h oxidase activation in diabetes: a double-edged sword in redox signalling. *Cardiovasc Res*, 82(1):9–20, Apr 2009.

[201] Jayesh B Majithiya and R Balaraman. Time-dependent changes in antioxidant enzymes and vascular reactivity of aorta in streptozotocin-induced diabetic rats treated with curcumin. *J Cardiovasc Pharmacol*, 46(5):697–705, Nov 2005.

[202] E C Opara, E Abdel-Rahman, S Soliman, W A Kamel, S Souka, J E Lowe, and S Abdel-Aleem. Depletion of total antioxidant capacity in type 2 diabetes. *Metabolism*, 48(11):1414–7, Nov 1999.

[203] D L Feinstein, A Spagnolo, C Akar, G Weinberg, P Murphy, V Gavrilyuk, and C Dello Russo. Receptor-independent actions of PPAR thiazolidinedione agonists: is mitochondrial function the key? *Biochemical Pharmacology*, 70(2):177–188, July 2005.

[204] Lynda F Bonewald. The amazing osteocyte. *J Bone Miner Res*, 26(2):229–38, Feb 2011.

[205] Wendy Tseng, Lucia S Graham, Yifan Geng, Aneela Reddy, Jinxiu Lu, Rita B Effros, Linda Demer, and Yin Tintut. Pka-induced receptor activator of nf-kappab ligand (rankl) expression in vascular cells mediates osteoclastogenesis but not matrix calcification. *J Biol Chem*, 285(39):29925–31, Sep 2010.

[206] M Jeziorska, C McCollum, and D E Woolley. Calcification in atherosclerotic plaque of human carotid arteries: associations with mast cells and macrophages. *J Pathol*, 185(1):10–7, May 1998.

[207] Haibin Zhou, Linshan Shang, Xi Li, Xiyu Zhang, Guimin Gao, Chenhong Guo, Bingxi Chen, Qiji Liu, Yaoqin Gong, and Changshun Shao. Resveratrol augments the canonical wnt signaling pathway in promoting osteoblastic differentiation of multipotent mesenchymal cells. *Exp Cell Res*, 315(17):2953–62, Oct 2009.

[208] Chung-Lan Kao, Lung-Kuo Tai, Shih-Hwa Chiou, Yi-Jen Chen, Kung-Hsiung Lee, Shih-Jie Chou, Yuh-Lih Chang, Chia-Ming Chang, Shih-Jen Chen, Hung-Hai Ku, and Hsin-Yang Li. Resveratrol promotes osteogenic differentiation and protects against dexamethasone damage in murine induced pluripotent stem cells. *Stem Cells Dev*, 19(2):247–58, Feb 2010.

[209] Z Dai, Y Li, L D Quarles, T Song, W Pan, H Zhou, and Z Xiao. Resveratrol enhances proliferation and osteoblastic differentiation in human mesenchymal stem cells via er-dependent erk1/2 activation. *Phytomedicine*, 14(12):806–14, Dec 2007.

[210] K Mizutani, K Ikeda, Y Kawai, and Y Yamori. Resveratrol stimulates the proliferation and differentiation of osteoblastic mc3t3-e1 cells. *Biochem Biophys Res Commun*, 253(3):859–63, Dec 1998.

[211] M Eijken, I M Meijer, I Westbroek, M Koedam, H Chiba, A G Uitterlinden, H A Pols, and J P van Leeuwen. Wnt signaling acts and is regulated in a human osteoblast differentiation dependent manner. *Journal of cellular biochemistry*, 104(2):568–579, May 2008.

[212] C Siddhivarn, A Banes, C Champagne, E L Riché, W Weerapradist, and S Offenbacher. Mechanical loading and delta12prostaglandin j2 induce bone morphogenetic protein-2, peroxisome proliferator-activated receptor gamma-1, and bone nodule formation in an osteoblastic cell line. *J Periodontal Res*, 42(5):383–92, Oct 2007.

[213] Xiang Zhou, Yanhui Sheng, Rong Yang, and Xiangqing Kong. Nicotine promotes cardiomyocyte apoptosis via oxidative stress and altered apoptosis-related gene expression. *Cardiology*, 115(4):243–50, 2010.

[214] H Fukao, Y Ijiri, M Miura, M Hashimoto, T Yamashita, C Fukunaga, K Oiwa, Y Kawai, M Suwa, and J Yamamoto. Effect of trans-resveratrol on the thrombogenicity and atherogenicity in apolipoprotein E-deficient and low-density lipoprotein receptor-deficient mice. *Blood Coagul Fibrinolysis*, 15(6):441–446, September 2004.

[215] K K Rocha, G A Souza, G X Ebaid, F R Seiva, A C Cataneo, and E L Novelli. Resveratrol toxicity: effects on risk factors for atherosclerosis and hepatic oxidative stress in standard and high-fat diets. *Food Chem Toxicol*, 47(6):1362–1367, June 2009.

[216] David M Goldberg, Joseph Yan, and George J Soleas. Absorption of three wine-related polyphenols in three different matrices by healthy subjects. *Clin Biochem*, 36(1):79–87, Feb 2003.

[217] Thomas Walle, Faye Hsieh, Mark H DeLegge, John E Oatis, Jr, and U Kristina Walle. High absorption but very low bioavailability of oral resveratrol in humans. *Drug Metab Dispos*, 32(12):1377–82, Dec 2004.

[218] G R Jr Beck, B Zerler, and E Moran. Gene array analysis of osteoblast differentiation. *Cell Growth Differ*, 12(2):61–83, February 2001.

[219] H Qi, D J Aguiar, S M Williams, A La Pean, W Pan, and C M Verfaillie. Identification of genes responsible for osteoblast differentiation from human mesodermal progenitor cells. *Proceedings of the National Academy of Sciences of the United States of America*, 100(6):3305–3310, March 2003.

[220] Y Tokuzawa, K Yagi, Y Yamashita, Y Nakachi, I Nikaido, H Bono, Y Ninomiya, Y Kanesaki-Yatsuka, M Akita, H Motegi, S Wakana, T Noda, F Sablitzky, S Arai, R Kurokawa, T Fukuda, T Katagiri, C Schonbach, T Suda, Y Mizuno, and Y Okazaki. Id4, a new candidate gene for senile osteoporosis, acts as a molecular switch promoting osteoblast differentiation. *PLoS Genet*, 6(7):e1001019.

[221] J Tan, J Lu, W Huang, Z Dong, C Kong, L Li, L Gao, J Guo, and B Huang. Genome-wide analysis of histone H3 lysine9 modifications in human mesenchymal stem cell osteogenic differentiation. *PLoS ONE*, 4(8):e6792, 2009.

[222] Y Ishida and J N Heersche. Glucocorticoid-induced osteoporosis: both in vivo and in vitro concentrations of glucocorticoids higher than physiological levels attenuate osteoblast differentiation. *Journal of Bone and Mineral Research*, 13(12):1822–1826, December 1998.

[223] P Liesegang, G Romalo, M Sudmann, L Wolf, and H U Schweikert. Human osteoblast-like cells contain specific, saturable, high-affinity glucocorticoid, androgen, estrogen, and 1 alpha,25-dihydroxycholecalciferol receptors. *Journal of andrology*, 15(3):194–199, May 1994.

[224] R D Alves, M Eijken, J van de Peppel, and J P van Leeuwen. Calcifying vascular smooth muscle cells and osteoblasts: independent cell types exhibiting extracellular matrix and biomineralization-related mimicries. *BMC genomics*, 15:965, 2014.

[225] H Ayari and G Bricca. Identification of two genes potentially associated in iron-heme homeostasis in human carotid plaque using microarray analysis. *Journal of biosciences*, 38(2):311–315, June 2013.

[226] C Nicolaije, J van de Peppel, and J P van Leeuwen. Oxygen-induced transcriptional dynamics in human osteoblasts are most prominent at the onset of mineralization. *J Cell Physiol*, 228(9):1863–1872, September 2013.

[227] V J Woeckel, M Eijken, J van de Peppel, H Chiba, B C van der Eerden, and J P van Leeuwen. IFNbeta impairs extracellular matrix formation leading to inhibition of mineralization by effects in the early stage of human osteoblast differentiation. *J Cell Physiol*, 227(6):2668–2676, June 2012.

[228] T Komori. Regulation of osteoblast differentiation by Runx2. *Advances in experimental medicine and biology*, 658:43–49, 2010.

[229] M Iskar, G Zeller, P Blattmann, M Campillos, M Kuhn, K H Kaminska, H Runz, A C Gavin, R Pepperkok, V van Noort, and P Bork. Characterization of drug-induced transcriptional modules: towards drug repositioning and functional understanding. *Molecular systems biology*, 9:662, 2013.

[230] K Schoonjans, B Staels, and J Auwerx. Role of the peroxisome proliferator-activated receptor (PPAR) in mediating the effects of fibrates and fatty acids on gene expression. *Journal of lipid research*, 37(5):907–925, May 1996.

[231] A K Hihi, L Michalik, and W Wahli. PPARs: transcriptional effectors of fatty acids and their derivatives. *Cellular and Molecular Life Sciences*, 59(5):790–798, May 2002.

[232] G L Barnes, A Javed, S M Waller, M H Kamal, K E Hebert, M Q Hassan, A Bellahcene, A J van Wijnen, M F Young, J B Lian, G S Stein, and L C Gerstenfeld. Osteoblast-related transcription factors Runx2 (Cbfa1/AML3) and MSX2 mediate the expression of bone sialoprotein in human metastatic breast cancer cells. *Cancer Res*, 63(10):2631–2637, May 2003.

[233] N Voorzanger-Rousselot, D Goehrig, F Journe, V Doriath, J J Body, P Clezardin, and P Garnero. Increased Dickkopf-1 expression in breast cancer bone metastases. *British journal of cancer*, 97(7):964–970, October 2007.

[234] J Pratap, A Javed, L R Languino, A J van Wijnen, J L Stein, G S Stein, and J B Lian. The Runx2 osteogenic transcription factor regulates matrix metalloproteinase 9 in bone metastatic cancer cells and controls cell invasion. *Molecular and Cellular Biology*, 25(19):8581–8591, October 2005.

[235] J H Clement, N Marr, A Meissner, M Schwalbe, W Sebald, K O Kliche, K Hoffken, and S Wolfl. Bone morphogenetic protein 2 (BMP-2) induces sequential changes of Id gene expression in the breast cancer cell line MCF-7. *Journal of cancer research and clinical oncology*, 126(5):271–279, May 2000.

[236] G Bu, W Lu, C C Liu, K Selander, T Yoneda, C Hall, E T Keller, and Y Li. Breast cancer-derived Dickkopf1 inhibits osteoblast differentiation and osteoprotegerin expression: implication for breast cancer osteolytic bone metastases. *International journal of cancer. Journal international du cancer*, 123(5):1034–1042, September 2008.

[237] J M Stuart, E Segal, D Koller, and S K Kim. A gene-coexpression network for global discovery of conserved genetic modules. *Science*, 302(5643):249–255, October 2003.

[238] G K Michalopoulos, W C Bowen, K Mule, and J Luo. HGF-, EGF-, and dexamethasone-induced gene expression patterns during formation of tissue in hepatic organoid cultures. *Gene expression*, 11(2):55–75, 2003.

[239] Z D Burke, C N Shen, K L Ralphs, and D Tosh. Characterization of liver function in transdifferentiated hepatocytes. *J Cell Physiol*, 206(1):147–159, January 2006.

[240] J Li, N Zhang, X Huang, J Xu, J C Fernandes, K Dai, and X Zhang. Dexamethasone shifts bone marrow stromal cells from osteoblasts to adipocytes by C/EBPalpha promoter methylation. *Cell death & disease*, 4:e832, 2013.

[241] P E Suarez, E G Rodriguez, R Soundararajan, A M Merillat, J C Stehle, S Rotman, T Roger, M J Voirol, J Wang, O Gross, V Petrilli, K Nadra, A Wilson, F Beermann, F P Pralong, M Maillard, D Pearce, R Chrast, B C Rossier, and E Hummler. The glucocorticoid-induced leucine zipper (gilz/Tsc22d3-2) gene locus plays a crucial role in male fertility. *Molecular Endocrinology*, 26(6):1000–1013, June 2012.

[242] W R Lo, L L Rowlette, M Caballero, P Yang, M R Hernandez, and T Borras. Tissue differential microarray analysis of dexamethasone induction reveals potential mechanisms of steroid glaucoma. *Investigative ophthalmology & visual science*, 44(2):473–485, February 2003.

[243] Y C Kim, F E Gomez, B G Fox, and J M Ntambi. Differential regulation of the stearoyl-CoA desaturase genes by thiazolidinediones in 3T3-L1 adipocytes. *Journal of lipid research*, 41(8):1310–1316, August 2000.

[244] Taiyi Kuo, Tzu-Chieh Chen, and Jen-Chywan Wang. The Role of Pik3r1 in Excess Glucocorticoid-induced Metabolic Disorders. pages SAT–12–SAT–12.

[245] S L Cheng, S F Zhang, and L V Avioli. Expression of bone matrix proteins during dexamethasone-induced mineralization of human bone marrow stromal cells. *Journal of cellular biochemistry*, 61(2):182–193, May 1996.

[246] K Iba, H Chiba, N Sawada, S Hirota, S Ishii, and M Mori. Glucocorticoids induce mineralization coupled with bone protein expression without influence on growth of a human osteoblastic cell line. *Cell structure and function*, 20(5):319–330, October 1995.

[247] R S Weinstein. Glucocorticoid-induced osteoporosis. *Reviews in endocrine & metabolic disorders*, 2(1):65–73, January 2001.

[248] I K Lee. The role of pyruvate dehydrogenase kinase in diabetes and obesity. *Diabetes & metabolism journal*, 38(3):181–186, June 2014.

[249] X Yang, Y Gong, Y Tang, H Li, Q He, L Gower, L Liaw, and R E Friesel. Spry1 and Spry4 differentially regulate human aortic smooth muscle cell phenotype via Akt/FoxO/myocardin signaling. *PLoS ONE*, 8(3):e58746, 2013.

[250] F R Schubert, D R Sobreira, R G Janousek, L E Alvares, and S Dietrich. Dact genes are chordate specific regulators at the intersection of Wnt and Tgf-beta signaling pathways. *BMC evolutionary biology*, 14:157, 2014.

[251] R D Alves, J A Demmers, K Bezstarosti, B C van der Eerden, J A Verhaar, M Eijken, and J P van Leeuwen. Unraveling the human bone microenvironment beyond the classical extracellular matrix proteins: a human bone protein library. *Journal of proteome research*, 10(10):4725–4733, October 2011.

[252] K A Staines, D Zhu, C Farquharson, and V E MacRae. Identification of novel regulators of osteoblast matrix mineralization by time series transcriptional profiling. *Journal of Bone and Mineral Metabolism*, 32(3):240–251, May 2014.

[253] M van Driel and J P van Leeuwen. Vitamin D endocrine system and osteoblasts. *BoneKEy reports*, 3:493, 2014.

[254] M Bosetti, L Fusaro, E Nicoli, A Borrone, S Aprile, and M Cannas. Poly-L-lactide acid-modified scaffolds for osteoinduction and osteoconduction. *Journal of biomedical materials research. Part A*, 102(10):3531–3539, October 2014.

[255] M J Larriba, J M Gonzalez-Sancho, F Bonilla, and A Munoz. Interaction of vitamin D with membrane-based signaling pathways. *Frontiers in physiology*, 5:60, 2014.

[256] F Alimirah, X Peng, L Yuan, R R Mehta, A von Knethen, D Choubey, and R G Mehta. Crosstalk between the peroxisome proliferator-activated receptor gamma (PPARgamma) and the vitamin D receptor (VDR) in human breast cancer cells: PPARgamma binds to VDR and inhibits 1alpha,25-dihydroxyvitamin D3 mediated transactivation. *Experimental cell research*, 318(19):2490–2497, November 2012.

[257] A Kapil, J P Singh, T Kaur, B Singh, and A P Singh. Involvement of peroxisome proliferator-activated receptor gamma in vitamin D-mediated protection against acute kidney injury in rats. *The Journal of surgical research*, 185(2):774–783, December 2013.

[258] J P Bilezikian, R G Josse, R Eastell, E M Lewiecki, C G Miller, M Wooddell, A R Northcutt, B G Kravitz, G Paul, A R Cobitz, A J Nino, and L A Fitzpatrick. Rosiglitazone decreases bone mineral density and increases bone turnover in postmenopausal women with type 2 diabetes mellitus. *The Journal of clinical endocrinology and metabolism*, 98(4):1519–1528, 2013.

[259] S Rahman, P J Czernik, Y Lu, and B Lecka-Czernik. beta-catenin directly sequesters adipocytic and insulin sensitizing activities but not osteoblastic activity of PPARgamma2 in marrow mesenchymal stem cells. *PLoS ONE*, 7(12):e51746, 2012.

[260] Y Yoshiko, K Oizumi, T Hasegawa, T Minamizaki, K Tanne, N Maeda, and J E Aubin. A subset of osteoblasts expressing high endogenous levels of PPARgamma switches fate to adipocytes in the rat calvaria cell culture model. *PLoS ONE*, 5(7):e11782, 2010.

[261] T Harslof, L Wamberg, L Moller, H Stodkilde-Jorgensen, S Ringgaard, S B Pedersen, and B L Langdahl. Rosiglitazone Decreases Bone Mass and Bone Marrow Fat. *Journal of Clinical Endocrinology & Metabolism*, 96(5):1541–1548, May 2011.

[262] K Nishikawa, T Nakashima, S Takeda, M Isogai, M Hamada, A Kimura, T Kodama, A Yamaguchi, M J Owen, S Takahashi, and H Takayanagi. Maf promotes osteoblast differentiation in mice by mediating the age-related switch in mesenchymal cell differentiation. *Journal of Clinical Investigation*, 120(10):3455–3465, October 2010.

[263] Z P Liu, W X Li, B Yu, J Huang, J Sun, J S Huo, and C X Liu. Effects of trans-resveratrol from Polygonum

cuspidatum on bone loss using the ovariectomized rat model. *Journal of medicinal food*, 8(1):14–19, April 2005.

[264] S J Hernandez-Vallejo, C Beaupere, J Larghero, J Capeau, and C Lagathu. HIV protease inhibitors induce senescence and alter osteoblastic potential of human bone marrow mesenchymal stem cells: beneficial effect of pravastatin. *Aging cell*, 12(6):955–965, December 2013.

[265] S U Singh, R F Casper, Fritz, P. C., B Sukhu, B Ganss, B Jr Girard, J F Savouret, and H C Tenenbaum. Inhibition of dioxin effects on bone formation in vitro by a newly described aryl hydrocarbon receptor antagonist, resveratrol. *The Journal of endocrinology*, 167(1):183–195, October 2000.

[266] K Kupisiewicz, P Boissy, B M Abdallah, F D Hansen, R G Erben, J F Savouret, K Soe, T L Andersen, T Plesner, and J M Delaisse. Potential of resveratrol analogues as antagonists of osteoclasts and promoters of osteoblasts. *Calcified tissue international*, 87(5):437–449, November 2010.

[267] J L Su, C Y Yang, M Zhao, M L Kuo, and M L Yen. Forkhead proteins are critical for bone morphogenetic protein-2 regulation and anti-tumor activity of resveratrol. *The Journal of biological chemistry*, 282(27):19385–19398, July 2007.

[268] F A Matough, S B Budin, Z A Hamid, N Alwahaibi, and J Mohamed. The role of oxidative stress and antioxidants in diabetic complications. *Sultan Qaboos University medical journal*, 12(1):5–18, February 2012.

[269] J Garrido-Maraver, M D Cordero, M Oropesa-Avila, A F Vega, M de la Mata, A D Pavon, E Alcocer-Gomez, C P Calero, M V Paz, M Alanis, I de Lavera, D Cotan, and J A Sanchez-Alcazar. Clinical applications of coenzyme Q10. *Frontiers in bioscience*, 19:619–633, 2014.

[270] D Montero, G Walther, C D Stehouwer, A J Houben, J A Beckman, and A Vinet. Effect of antioxidant vitamin supplementation on endothelial function in type 2 diabetes mellitus: a systematic review and meta-analysis of randomized controlled trials. *Obesity reviews : an official journal of the International Association for the Study of Obesity*, 15(2):107–116, February 2014.

[271] A Fardet and Y Boirie. Associations between diet-related diseases and impaired physiological mechanisms: a holistic approach based on meta-analyses to identify targets for preventive nutrition. *Nutrition reviews*, 71(10):643–656, October 2013.

[272] D P Vivekananthan, M S Penn, S K Sapp, A Hsu, and E J Topol. Use of antioxidant vitamins for the prevention of cardiovascular disease: meta-analysis of randomised trials. *Lancet*, 361(9374):2017–2023, June 2003.

[273] Gruppo Italiano per lo Studio della Sopravvivenza nell'Infarto miocardico. Dietary supplementation with n-3 polyunsaturated fatty acids and vitamin E after myocardial infarction: results of the GISSI-Prevenzione trial. Gruppo Italiano per lo Studio della Sopravvivenza nell'Infarto miocardico. *Lancet*, 354(9177):447–455, August 1999.

[274] S Yusuf, G Dagenais, J Pogue, J Bosch, and P Sleight. Vitamin E supplementation and cardiovascular events in high-risk patients. The Heart Outcomes Prevention Evaluation Study Investigators. *New England Journal of Medicine*, 342(3):154–160, January 2000.

[275] S Pruthi, T G Allison, and D D Hensrud. Vitamin E supplementation in the prevention of coronary heart disease. *Mayo Clinic proceedings*, 76(11):1131–1136, November 2001.

[276] L Kritharides and R Stocker. The use of antioxidant supplements in coronary heart disease. *Atherosclerosis*, 164(2):211–219, October 2002.

[277] I M Lee, N R Cook, J M Gaziano, D Gordon, P M Ridker, J E Manson, C H Hennekens, and J E Buring. Vitamin E in the primary prevention of cardiovascular disease and cancer: the Women's Health Study: a randomized controlled trial. *JAMA : the journal of the American Medical Association*, 294(1):56–65, July 2005.

[278] T Costacou, J C Zgibor, R W Evans, Y Y Tyurina, V E Kagan, and T J Orchard. Antioxidants and coronary artery disease among individuals with type 1 diabetes: Findings from the Pittsburgh Epidemiology of Diabetes Complications Study. *Journal of diabetes and its complications*, 20(6):387–394, November 2006.

[279] U Milman, S Blum, C Shapira, D Aronson, R Miller-Lotan, Y Anbinder, J Alshiek, L Bennett, M Kostenko, M Landau, S Keidar, Y Levy, A Khemlin, A Radan, and A P Levy. Vitamin E supplementation reduces cardiovascular events in a subgroup of middle-aged individuals with both type 2 diabetes mellitus and the haptoglobin 2-2 genotype: a prospective double-blinded clinical trial. *Arteriosclerosis, Thrombosis, and Vascular Biology*, 28(2):341–347, February 2008.

[280] H N Hodis, W J Mack, L Dustin, P R Mahrer, S P Azen, R Detrano, J Selhub, P Alaupovic, C R Liu, C H Liu, J Hwang, A G Wilcox, and R H Selzer. High-dose B vitamin supplementation and progression of subclinical atherosclerosis: a randomized controlled trial. *Stroke; a journal of cerebral circulation*, 40(3):730–736, March 2009.

[281] M Shargorodsky, O Debby, Z Matas, and R Zimlichman. Effect of long-term treatment with antioxidants (vitamin C, vitamin E, coenzyme Q10 and selenium) on arterial compliance, humoral factors and inflammatory markers in patients with multiple cardiovascular risk factors. *Nutrition & metabolism*, 7:55, 2010.

[282] O A BESSEY, O H LOWRY, and M J BROCK. A method for the rapid determination of alkaline phosphates with five cubic millimeters of serum. *J Biol Chem*, 164:321–9, Jul 1946.

[283] P Chomczynski and N Sacchi. Single-step method of rna isolation by acid guanidinium thiocyanate-phenol-chloroform extraction. *Anal Biochem*, 162(1):156–9, Apr 1987.

[284] M F Pittenger, A M Mackay, S C Beck, R K Jaiswal, R Douglas, J D Mosca, M A Moorman, D W Simonetti, S Craig, and D R Marshak. Multilineage potential of adult human mesenchymal stem cells. *Science*, 284(5411):143–7, Apr 1999.

[285] Yuehua Jiang, Balkrishna N Jahagirdar, R Lee Reinhardt, Robert E Schwartz, C Dirk Keene, Xilma R Ortiz-Gonzalez, Morayma Reyes, Todd Lenvik, Troy Lund, Mark Blackstad, Jingbo Du, Sara Aldrich, Aaron Lisberg, Walter C Low, David A Largaespada, and Catherine M Verfaillie. Pluripotency of mesenchymal stem cells derived from adult marrow. *Nature*, 418(6893):41–9, Jul 2002.

[286] Karen Bieback, Susanne Kern, Harald Klüter, and Hermann Eichler. Critical parameters for the isolation of mesenchymal stem cells from umbilical cord blood. *Stem Cells*, 22(4):625–34, 2004.

[287] Wolfgang Wagner, Robert E Feldmann, Jr, Anja Seckinger, Martin H Maurer, Frederik Wein, Jonathon Blake, Ulf Krause, Armin Kalenka, Heinrich F Bürgers, Rainer Saffrich, Patrick Wuchter, Wolfgang Kuschinsky, and Anthony D Ho. The heterogeneity of human mesenchymal stem cell preparations–evidence from simultaneous analysis of proteomes and transcriptomes. *Exp Hematol*, 34(4):536–48, Apr 2006.

[288] Aus T Ali, Clem B Penny, Janice E Paiker, George Psaras, Faisel Ikram, and Nigel J Crowther. The relationship between alkaline phosphatase activity and intracellular lipid accumulation in murine 3t3-l1 cells and human preadipocytes. *Anal Biochem*, 354(2):247–54, Jul 2006.